THE UNIVERSITY
of EDINBURGH

Fire Performance of Fibre Reinforced Polymer (FRP) Bars in Reinforced Concrete: An Experimental Approach

Emma R. E. McIntyre

(nee Reid)

For the Degree of Doctor of Philosophy

University of Edinburgh

2019

DECLARATION

I declare that this thesis has been composed solely by myself and that it has not been submitted, in whole or in part, in any previous application for a degree. Except where states otherwise by reference or acknowledgment, the work presented is entirely my own.

Emma Ruth Elizabeth McIntyre

Date: 22/08/2019

ABSTRACT

During the past two decades, Fibre Reinforced Polymer (FRP) bars have been applied as viable alternatives to internal steel reinforcement of concrete, owing to their numerous benefits over steel reinforcement including comparatively high tensile strength and non-corrosive properties. However, there are limitations on the use of FRP as reinforcement, where fire resistance of structures is required, due to a lack of understanding of the behaviour of FRP materials at elevated temperature. This hinders application of FRP materials in many cases.

To understand the complexities of FRP bars' response at elevated temperature, this thesis examines current design guidance and literature to highlight gaps in understanding. The experimental work within the thesis focusses on three commercially available FRP bars; two Glass FRP (GFRP) bars and one Carbon FRP (CFRP) bar. Bench-scale characterisation tests using Dynamic Mechanical analysis (DMA) and Thermogravimetric analysis (TGA) have been performed to understand the deterioration of FRP bars at elevated temperature. The experimental work has defined a glass transition (T_g) and decomposition temperature (T_d) range for each of the FRP bars.

Using the results from the bench-scale characterisation tests and direct tensile tests, a novel predictive model for the reduction in tensile strength of FRP materials at high temperature has been proposed. A study on the bond capacity of fibre reinforced polymer (FRP) bars in concrete at elevated temperature demonstrated the requirement for cold anchorage of the reinforcement.

To further determine the impact of cold anchorage on FRP reinforced concrete (RC) beams, tests were carried out with both continuous and lap spliced FRP at ambient temperature and under sustained load with transient localised heating. Cold anchorage of the reinforcement was maintained throughout testing and confirmed with local temperature measurements. The results demonstrate that cold anchorage (i.e. maintained below the onset of the glass transition range) of FRP bars is necessary

to ensure their safe use as internal reinforcement in concrete, unless unrealistically deep concrete cover is provided. Cold anchorage may be provided in a number of ways; continuity of reinforcement across compartments, bent bars in the anchorage zone or increased concrete cover at anchorage zones. Where this is provided the performance of FRP bars is demonstrated – for the particular conditions of the current study – to be satisfactory under full service loads and at reinforcement temperatures exceeding the decomposition of the polymer matrix (>380°C for the bars in the current study).

The research has identified a minimum suite of tests necessary to characterize thermo-mechanical behaviour of proprietary FRP bars. By understanding the effects of temperature on the polymer resin matrix and on the FRPs' tensile and bond properties, and by rationally optimizing the placement and anchorage of the bars, this thesis has demonstrated FRP reinforcements may be designed as fire-safe alternatives to steel reinforcement for concrete.

LAY SUMMARY

Steel reinforced concrete forms the backbone of our global infrastructure, and has been thoroughly researched in its many forms. Steel reinforced concrete is not corrosion resistant, and can suffer significant degradation as the result of, for example, de-icing salts used on roads. Fibre reinforced polymer (FRP) bars represent a viable alternative to steel reinforcement, owing not only to their corrosion resistance but also due to their high tensile strength. This permits a more efficient and cost effective form, which in turn improves whole life costing.

The FRP bar is a heterogenous material in that it is formed using very thin fibres (such as glass or carbon) and surrounding them with a polymer resin. These materials are pulled through a mould to form a bar. The polymer resin is susceptible to damage at elevated temperature, whereby it softens and then decomposes. This impacts upon the mechanical properties of the FRP and their use in reinforced concrete design. This thesis presents various experimental regimes which have sought to predict strength loss (both bond and tensile) of the FRP bars at elevated temperature. The thesis has presented design recommendations that may lead to realistic and viable approach for the commercial use of FRP bars in reinforced concrete, where structural fire resistance is required.

ACKNOWLEDGEMENTS

I am extremely grateful to my supervisor Luke Bisby for his ongoing support and frequent thought provoking discussions on this topic and structural and fire engineering in general. I also thank Tim Stratford for his technical advice and many discussions over lab experiments and the direction of the thesis. I gratefully acknowledge the huge contribution in technical support given to me by Jim Hutcheson, Kevin Tierney, Michal Krajcovic and the technicians within the School of Engineering. Thank you also to Antonio Bilotta for his input with the tensile pilot testing.

The people of the John Muir building provided many happy memories, and I want to specifically mention Juan Hidalgo Medina and Cristian Maluk for influencing the early days of my PhD, and Holly Smith (Warren), Ieuan Rickard and Martyn MacLaggan for the many conversations as desk buddies in the office. The ethos in this office is hugely influential in the production of great research and I hope this continues!

I gratefully acknowledge the support of the UK Engineering Physical Sciences Research Council (EPSRC) and industrial partners BP Composites and Pultrall Inc.

Lastly, I want to say a huge thank you to my husband David for never letting me give up, and laterally my daughter Winnie for motivating me to get it across the finish line.

TABLE OF CONTENTS

FIGURES

CHAPTER 1 INTRODUCTION

1.1 BACKGROUND

Societal demands on infrastructure are changing. Infrastructure repair, rehabilitation, change of purpose, and service life extension of existing assets is more important than ever, and there are demands for new construction to be more durable and robust. To accommodate these demands requires innovation in the materials and technologies that are used for infrastructure. Various novel composite materials have become popular; harnessing the particular properties of each of their constituents to provide functionality superior to the individual constituents alone. Fibre reinforced polymers (FRP) are one such relatively novel introduction into the built environment, and these are particularly popular – and now widely applied internationally – for structural strengthening applications.

During the past two decades, FRPs have also been applied as viable alternatives to internal steel reinforcement of concrete (e.g. Pultrall 2005), owing to their numerous benefits over steel reinforcement including comparatively high tensile strength and non-corrosive properties. Design guidance is now available internationally for the design and analysis of FRP reinforced concrete structural elements (e.g. CSA s806 2012, ACI 440.1R 2015), and it is evident that FRP reinforcements are likely to become commonplace in construction. However, unanswered questions remain, particularly with respect to their long-term durability within concrete, which has not yet been demonstrated beyond about 20 years. Most importantly, their performance at elevated temperature or in fire is known to be potentially problematic due to their polymeric composition; which is described in the following sections. Researchers understand that the variability of FRP compositions makes it challenging to universally quantify material behaviour at elevated temperature, and current data us

With each innovation in construction materials comes inherent limitations to its use, and these limitations are not always understood prior to application. Brannigan (2008) discusses the concept of *Innovation Risk, which* he defines as "t*he ability to create a product that meets the technical requirement of a regulation but represents a novel hazard".* For example, in fire engineering, when a building product comes on to the market

specifically for fire resistance, it is required to undergo a regulatory test to determine what fire resistance period is and/or surface spread of flame class (amongst other criteria). The outputs from this test then allows designers to know whether this particular product meets the performance requirements for a new building, prior to installation. Whilst this seems logical, the regulatory test may actually not be suitable given the way, for example, the product is to be installed within a building, and as such, the associated hazard may not be adequately understood until demonstrated in-situ (i.e. a fire within a building).

To avoid innovation risk in the application of FRP materials as reinforcement for concrete, it is essential to question whether the design methodologies used for steel reinforced concrete analysis and design are appropriate for designing FRP reinforced concrete.

FRPs meet most of the technical requirements for reinforcement of concrete as steel reinforcing bars; these being strong and stiff in tension, having reasonable shear behaviour, and providing a mechanical bond with concrete. However, the constituent materials of FRP, and FRP materials themselves, are fundamentally different to the essentially homogenous and isotropic nature of mild steel. In addition, FRP materials are not universally produced or specified, according to accepted international standards. This is the case with conventional deformed mild steel reinforcement; company specific manufacturing techniques and source materials remain undisclosed for FRPs in many cases. Bisby and Stratford (2012) point out that the current design frameworks used for steel reinforced concrete are not sufficient where internal FRP reinforcement is used. Internationally leading design guidance (ACI 440.1R-2006) for the use of FRP bars as internal reinforcement of concrete (ACI 2006) previously discouraged the use of FRP bars in applications where fire resistance was required, stating that "The use of FRP reinforcement is not recommended for structures in which fire resistance is essential to maintain structural integrity." The most recent revision of ACI 440.1R-2015 (Section 4.4.5) now acknowledges that FRP reinforced concrete elements can be designed to provide fire resistance, but notes that

a different methodology is required to that used for steel reinforced concrete; this is suggested as being a performance based structural design for fire approach. No clear procedures are currently available to determine or define the fire resistance (or performance) of FRP reinforced concrete. The fundamental motivation of the research presented herein is to present a hypothesis on defining mechanical degradation of FRP at elevated temperature such that they may be useful inputs in determining fire resistance of an FRP reinforced structure.

1.2 Aims & Objectives of the Research

The main aim of this PhD research is to understand the response to fire of FRP reinforcing materials and FRP reinforced concrete in bending, and to determine a simplified approach that allows an evaluation of mechanical degradation of FRP at high temperature. Beyond this research, this approach provides a valuable input to determine the fire resistance of FRP reinforced concrete, such that is can be widely applied as a viable alternative to steel reinforcement in constructing fire-safe concrete infrastructure. The research adopts a multi scale approach and seeks to correlate behaviour from bench scale material testing on FRPs to intermediate scale experiments on reinforced concrete beams in bending. This is accomplished by studying the response of the constituent components of FRP reinforcing bars through bench scale thermo-mechanical testing and analysis, experimental evaluation of the mechanical response (in direct tension and in bond within concrete) of FRPs at elevated temperature, and tests on FRP reinforced concrete beams under sustained loading, exposed to elevated temperature. The above aspects are achieved through the following five objectives:

1. **Review of literature to identify the current understanding of FRP as reinforcement in concrete:** A review of available research to provide a platform of knowledge to build upon, and highlights current gaps in understanding of FRP at elevated temperature and in fire (as is relevant to concrete reinforcing applications).

2. **To identify changes in the thermo-mechanical response of FRP reinforcing bars, bench scale thermomechanical analysis is performed to understand the deterioration of the FRP (in particular its polymer matrix).** Examination of the degradation and decomposition of FRP bars' polymer matrices identifies key thermal responses (and stages) that are significant for their structural responses at high temperature. Most notably, the FRPs' glass transition temperature (T_g) and decomposition temperature (T_d) ranges are characterised with a view to quantifying the decreases they experience in strength.
3. **Identification of bench scale testing methodologies to quantify the tensile and bond strength loss for FRP bars at elevated temperature based on the results of Objective 2 above.** Because there is a range of FRP products available for application globally, all of which will have subtle differences when compared one to another, a specific understanding of each uniquely manufactured FRP product is necessary. Single curves for reductions of tensile strength, bond strength, and elastic moduli with increasing temperature are not applicable to all FRP reinforcing bars. This differs from steel reinforcement, for which standard reduction curves are widely available. Reduction curves for specific FRP reinforcing bars must be tailored based on their specific constituent components. By identifying degradation and decomposition mechanisms using bench scale thermal analysis for respective bar types, a small number of small scale tests on the FRP materials can be used to define and quantify losses of mechanical and bond properties at elevated temperature. A series of such tests on FRPs are used to examine the tensile strength and bond strength (with concrete) reductions at elevated temperature. The fundamental objective of the research is to define the minimum suite of tests necessary to characterise the temperature dependent bond and tensile strength loss curves for a specific FRP reinforcing product. This suite of tests could subsequently be used to develop quantified inputs needed for structural fire design of FRP reinforced concrete elements.

4. **Demonstrating an understanding of the flexural response of FRP reinforced beams at elevated temperature (with and without reinforcing bar splices):** Following the determination of tensile and bond strength loss of reinforcing bars at elevated temperature, it is necessary to identify the consequences of this response for the performance of FRP reinforced concrete elements. The research presented herein includes studies on the structural fire response of intermediate scale FRP reinforced concrete beams under sustained load in bending. These tests also examine the impacts of the presence of a reinforcement splice within the heated zone of the beams on their structural fire response. Previous research (Nigro, Cefarelli, Bilotta, et al., 2011) has shown that maintaining "cold anchorage" of the FRP reinforcement is integral to achieving adequate fire resistance, and this study further examines (and validates) this concept. The experiments were intended to demonstrate the impact of tensile and bond strength loss (as reported on under objective 3) on structural behaviour when FRP is used as internal reinforcement for concrete.
5. **Demonstrating a pragmatic and rational approach to ensure the fire-safe design and use of FRP reinforced concrete in new construction where a fire rating is required:** The experimental work, from bench scale to intermediate scale, is used to demonstrate the simplified approaches that can used to determine mechanical degradation of proprietary FRP bars. These are intended to be used as valuable inputs in achieving a fire safe design of FRP reinforcement, in the hope that it can be demonstrated that FRP reinforced concrete can be a viable alternative to steel reinforced concrete in a building applications for new construction. The research aims to provide practical recommendations for structural fire design of these types of elements.

1.3 CHAPTER OUTLINE

1.3.1 Chapter 1: Introduction

This chapter provides a brief summary of the background and motivation behind the project, highlighting the aims and objectives of the research along with the structure of the thesis.

1.3.2 Chapter 2: Literature Review

Chapter 2 presents a review of the available literature and subsequent motivation behind the research contained within this thesis.

1.3.3 Chapter 3: Bench Scale Thermal Characterisation of FRP bars

This chapter presents and discusses experimental work documenting thermal analysis on small samples taken from three different, commercially available FRP bars; two manufactured from glass fibres and one from carbon fibres. A range of experiments is presented using dynamic mechanical analysis (DMA) and thermogravimetric analysis (TGA). The work presented focuses on defining the glass transition and decomposition temperatures for the materials under consideration, and forms the foundation for examining loss of mechanical properties at elevated temperature and the structural fire behaviour of FRP reinforced concrete.

1.3.4 Chapter 4: Analysis of Tensile Strength Loss of FRP bars with Elevated Temperature

Steady state thermal regime tensile tests are presented on the three different FRP bars at elevated temperature. The selected testing temperatures are based on results from the bench scale thermal characterisation in Chapter 3. Also discussed is an anchorage technique was necessary to allow the FRP bars to be secured in a mechanical testing frame. A novel two-step model for reduction in tensile strength of FRP bars at elevated temperature is presented, linking the bench scale behaviour to the observed tensile strength reductions at elevated temperature, and a minimum suite of tests necessary to define the model for any candidate FRP reinforcing bar is proposed.

1.3.5 Chapter 5: Analysis of Bond Strength Loss of FRP bars in concrete with Elevated Temperature

The bond behaviour of FRP reinforcing bars in concrete, being different to that of deformed steel reinforcing bars, is variable and depends on the surface coating applied to the FRP bars during manufacturing. Bond pullout tests are presented on FRP bars embedded in 150mm cubes of concrete to study and quantify the degradation of concrete FRP bond strength at temperatures within the range of the glass transition temperature. This testing establishes the requirement for cold anchorage of FRP reinforcement, and further links the necessary temperatures to achieve this to the testing presented in Chapter 3.

1.3.6 Chapter 6: Analysis of FRP Reinforced Beams at Elevated Temperature

Tests on 32 FRP reinforced concrete beams tested in four-point bending under sustained load at elevated temperature are presented in this chapter. The testing and analysis seeks study the response of FRP reinforced concrete elements in bending at elevated temperature, and to establish links between the thermal analysis from Chapter 3 and mechanical tests from Chapters 4 and 5. A comparison of bond-critical and non bond-critical applications is made by using both spliced and continuous FRP reinforcement to confirm the importance of cold anchorage of the FRP reinforcement.

1.3.7 Chapter 7: Conclusions and further work

This chapter presents a summary of the work, drawing out the main conclusions. Recommendations for future development of the research into the fire performance of FRP reinforced concrete are also made.

CHAPTER 2 LITERATURE REVIEW

2.1 CHAPTER OVERVIEW

This chapter presents an overview of research carried out to date on Fibre Reinforced Polymer (FRP) as internal reinforcement in concrete, focusing on the FRP composition, mechanical properties and performance at elevated temperature.

2.2 BACKGROUND

A comprehensive review on the application of FRP was carried out by Bakis *et al.* (2002) to mark the 150th Anniversary of the American Society of Civil Engineers (ASCE), and provides a reference for the development and widespread application of FRP. This is briefly summarised in the following paragraph. The introduction of glass fibre reinforced polymers followed the end of the Second World War, with carbon FRP commercialised for the aerospace and defence industries in the 1960s and 1970s to meet the demand for higher strength and stiffness. The cost of these materials remained relatively high and so the focus turned to driving down costs and making FRP more commercial. This was happily met with greater public expectation towards improving functionality and long-term sustainability of infrastructure. FRP in the construction industry was gradually encouraged following research and demonstration projects in the late 1980s and 1990s, with non-metallic rebar such as FRP utilised in the mid-1990s (Hollaway, 2003).

The driving factors for the inclusion of FRP reinforcement in concrete are the relatively high tensile strength (in comparison to that of steel), low specific weight and its non-corrosive properties. However as noted by Bakis *et al.* (2002) the cost of FRP can be prohibitive in its use. Burgoyne and Balafas (2007) determined that GFRP was 6.5 times that of steel in terms of cost per unit force (based on 2004 prices). However, these are material costs only and do not consider whole life cycle costing (LCC); where high performance materials (HPM) such as FRP have been demonstrated to have 8.4% lower life cycle costs than non-HPM alternatives such as steel (when considering sustainability criteria in LCC) (Ilg, Hoehne, & Guenther, 2016).

With cost being a major consideration in any infrastructure investment, FRP, as noted, has been slower than traditional construction materials to become commonplace where its advantages were not immediately obvious. However in addition to re-valuing FRP in terms of whole life cycle costing, FRP's non corrosive properties are invaluable where corrosion of steel in modern bridges has become particularly problematic in the last two decades (Hollaway, 2003) . With a significant backlog arising in the maintenance and repair of these, there is a requirement for resource efficient infrastructure, which can provide a low maintenance long term solution to reduce the backlog (Ilg, Hoehne, & Guenther, 2016). It should be noted that there is currently no guidance on structural fire safety for bridges in existence despite the bridge fires becoming more common and leading to significant economic losses (Garlock, Paya-Zaforteza, Kodur, et al., 2012) .

HPM such as FRP may be the answer to this but there remains a question over how FRP reinforced concrete can perform during a fire. As such, an understanding of the current research in the performance of FRP bars at high temperature is required to allow a considered approach in undertaking further experimental work and subsequently seeking to refine the design process for FRP reinforced concrete (and indeed other FRP applications). The motivation, where supported by current research and that presented within this thesis, is to allow FRP reinforcement to be used with confidence in structural fire design by providing simplified approaches to determining material degradation of FRP reinforcement at elevated temperature.

2.3 Properties of an FRP Bar

With a focus on FRP as internal reinforcement in concrete, the auto-comparison is to that of steel. While this is a necessary comparison to understand where FRP may be beneficial over steel, it is equally this relatively new material's downfall where designers seek to use the same design process. Fundamentally, FRP is very different material in comparison to steel and is a proprietary product of the manufacturer. The vast complexity of the processes surrounding manufacture of FRP bars ensures that no two bars are alike, requiring analysis of each bar to determine its thermal and

mechanical properties. Research (including that discussed within this thesis), is ongoing to make this analysis more efficient and economically viable.

The investigation of any composite material must first begin with an examination of its constituents. The formation of a composite material takes place where individual materials cannot meet the required design criteria, and are therefore combined to create a superior material. The benefits of FRP are (but not limited to) high tensile strength, high stiffness-to-weight ratio, electromagnetically neutral and non-corrosive. In the case of glass fibre reinforced polymer, the use of glass fibres instead of bulk material reduces the likelihood of brittle fracture caused by critical surface flaws (Chapman, 1974; Callister, 2007), thus the tensile capacity of the fibres is much greater than that of the bulk material. While the fibres have high tensile strength, the use of a polymer matrix binds the fibres together and allows stress transfer between the fibres (Robert & Benmokrane, 2010a). In addition, the matrix provides a physical barrier not only to external sources (i.e. chemical and mechanical), but also internally as it separates the fibres' mechanical abrasion. Figure 2-1 Stress-strain relationships for fibrous reinforcement and matrix (ISIS Canada Corporation, 2006) shows the example composite strength of an FRP bar in comparison to that of the fibres and the matrix.

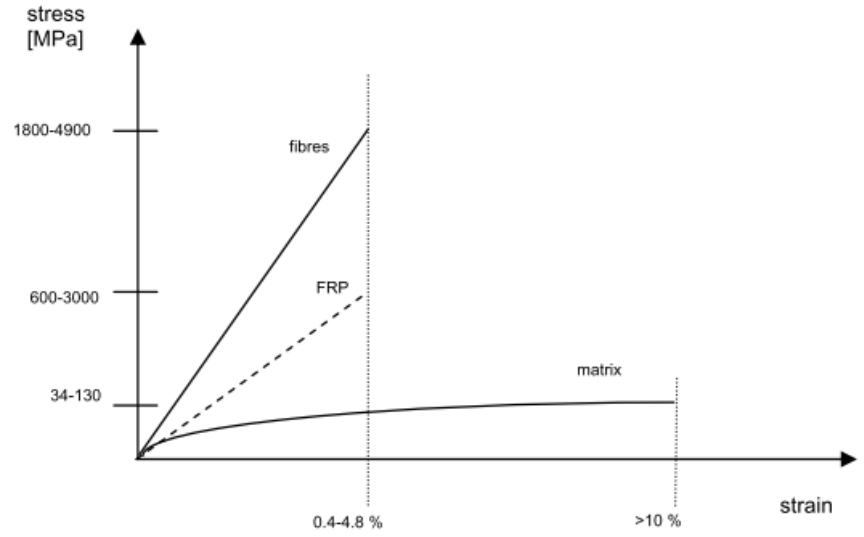

Figure 2-1 Stress-strain relationships for fibrous reinforcement and matrix (ISIS Canada Corporation 2006)

From the same reference (ISIS Canada Corporation, 2006), typical properties of FRP are shown in Table 2-1.

Table 2-1 Typical mechanical properties of FRP reinforcing bars (ISIS Canada Corporation 2006)

Fibre Type	Trade Name	Tensile Strength (MPa)	Modulus of Elasticity (GPa)	Ultimate Tensile Strain
Carbon	V-ROD	1596	120.0	0.013
	Aslan	2068	124.0	0.017
	Leadline	2250	147.0	0.015
	NEFMAC	1200	100.0	0.012
Glass	V-ROD	710	46.4	0.017
	Aslan	690	40.8	0.017
	NEFMAC	600	30.0	0.020

In manufacturing the FRP bars, typically a pultrusion process is used whereby continuous strands of fibres are pulled through a resin tank and cured in a heated die (see Figure 2-2).

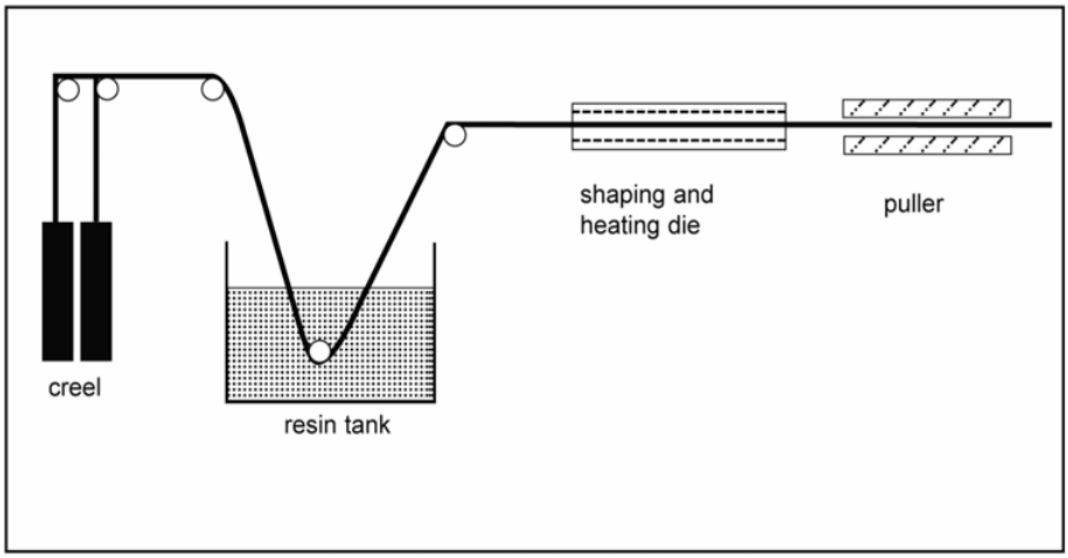

Figure 2-2 Pultrusion Process (ISIS Canada Corporation, 2006)

Following curing of the bars, a coating is applied to the core, which undergoes a secondary curing process. The coating may take the form of:

1. Large deformations moulded onto the FRP bar;
2. Helical braid of fibres (varying thickness) wound around the core of the bar;
3. Sand (varying thickness, may also be used in conjunction with the helical braid);
4. Resin roughening whereby excess polymer resin is not removed from the outside of the bar, which creates a rough texture when cured (may also be used in conjunction with the helical braid).

The application of the coating is necessary to allow the FRP bar to mechanically adhere to the concrete. Type of fibre, type of resin, curing time and coating are proprietary to the manufacturer, which results in significant variability between FRP bars. Research acknowledges this variability though with little additional information of the FRP composition available from manufactures, it is challenging to quantify the variability with accuracy.

The basic make-up of the polymer matrix is complex and highly variable, particularly in the case of vinylester which is less well documented but arguably superior in comparison to its polyester counterpart in terms of strength and improved chemical resistance. As with any organic substrate, the matrix is subject to thermal degradation and decomposition. Specifically, the polymer matrix softens at the material's Glass Transition Temperature (T_g) and decomposes upon reaching the Decomposition Temperature (T_d). These temperatures can be identified using Dynamic Mechanical Analysis (DMA) and Thermogravimetric Analysis (TGA) respectively. T_g is commonly stated as a single value in test reports and material specifications, notably Abbasi and Hogg, (2005) stated that glass transition temperatures for vinyl esters are in the region of 100 °C. Robert, Cousin and Benmokrane (2009) stated the value of the tested FRP with a vinyl ester resin to be 105°C and 134°C (high T_g due to post curing phenomenon), while Maranan *et al.* (2014) stated the T_g of their tested vinylester FRP as 117°C. However as demonstrated by Bakis *et al.* (2014) and discussed by Michels *et al.* (2015), there can be substantial differences between definitions of T_g, varying by as much as 23°C. Katz, Berman and Bank (1999) stated that 60°C to 130°C was the typical

range for thermosetting polymers. The terminology "glass transition" eludes to the fact that the process sees the polymer undergo a transition from a hard material to a soft, rubber like state (Michels, Widmann, Czaderski, et al., 2015), rather than a single temperature-related event. As such, it is uncommon to find a typical set of values of T_g due to the variability of both the FRP matrix and the way in which the value can be defined.

The limiting temperature for 'adequate' performance of FRP materials is commonly taken to be T_g (Bisby & Kodur, 2007; Nigro, Cefarelli, Bilotta, et al., 2011). FRP manufacturers can increase crosslinking of the polymer to improve thermal stability, specifically Saafi (2002) noted that denser netting of the polymer chains would limit the decrease in the mechanical properties of the FRP bars at elevated temperature. However the fibres impede this process, and thus FRP bars may not be as thermally stable as the manufacturers intended (Regnier & Mortaigne, 1995). It should be noted that degradation of mechanical properties is observed even before T_g, since in reality the transition occurs over a range of temperatures. The anisotropy of unidirectional FRP materials means that transverse strength, shear strength and stiffness, and bond strength are more severely affected by elevated temperatures, decreasing rapidly in the range of T_g (Foster & Bisby, 2008). This is due to the polymer matrix providing the only interaction between fibres in the transverse direction.

Due to the perception of the FRPs being limited in their use by T_g, there is limited research and discussion on the decomposition and oxidation temperatures of the FRP. For example Correia *et al.* (2013) state the decomposition temperature of the FRP they are investigating, as determined from Differential Scanning Calorimetry (DSC) and Thermo-gravimetric Analysis (TGA), but yet none of the experimental program includes this temperature as part of the test matrix. The research presented later in the thesis is motivated to present a fuller picture of FRP behaviour at elevated temperature such that it can be evaluated more coherently in structural fire design.

2.4 TENSILE BEHAVIOUR OF FRP

It should be noted in the first instance, testing the tensile capacity of FRP bars is a challenge as traditional grip systems for steel cannot be used due to the low shear strength of the polymer matrix, i.e. the grip will crush the FRP bar. A standardized test method, ASTM D3916 (American Society for Testing and Materials (ASTM), 2008) has been developed for GFRP, however as acknowledged by researchers (Micelli & Nanni, 2003) the methodology was difficult to apply and did not reference testing of Carbon FRP bars. As a result, many researchers have had to develop their own testing methodologies (Micelli & Nanni, 2003) which is time consuming and inefficient long-term. Notably Maranan *et al.* (2014) stated the high cost of developing such methodologies and used flexural strength testing of GFRP to investigate tensile performance as a cheaper and simpler alternative. While as expected, they established that flexural strength and stiffness of GFRP would decrease with increasing temperature, the author acknowledged that further work was required to predict tensile strength loss from these types of experiments.

Researchers have also evidenced failure within the grips as a result of elevated temperatures within the anchorage zones heating and subsequently the FRP suffering a shear failure with the clamp (Bai & Keller, 2009). This has typically been overcome in subsequent research by ensuring that the anchorage remains at ambient temperature during testing (Correia, Gomes, Pires, et al., 2013).

Bisby *et al.* (2005) assembled data available from literature and produced models to fit the data, to show the temperature-dependent ultimate tensile strength of bare glass and carbon fibres (Figure 2-3), and the ultimate tensile strength of various GFRP and CFRP bars (Figure 2-4 and Figure 2-5 respectively). Note, the numbers in the legends for Figure 2-3, Figure 2-4 and Figure 2-5 correspond to the references stated following Figure 2-5.

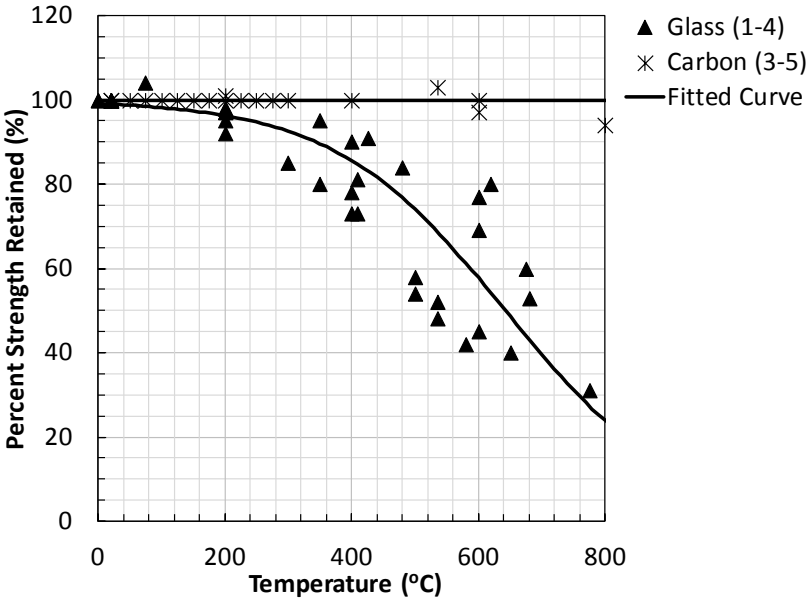

Figure 2-3 Variation in tensile strength of fibres with temperature

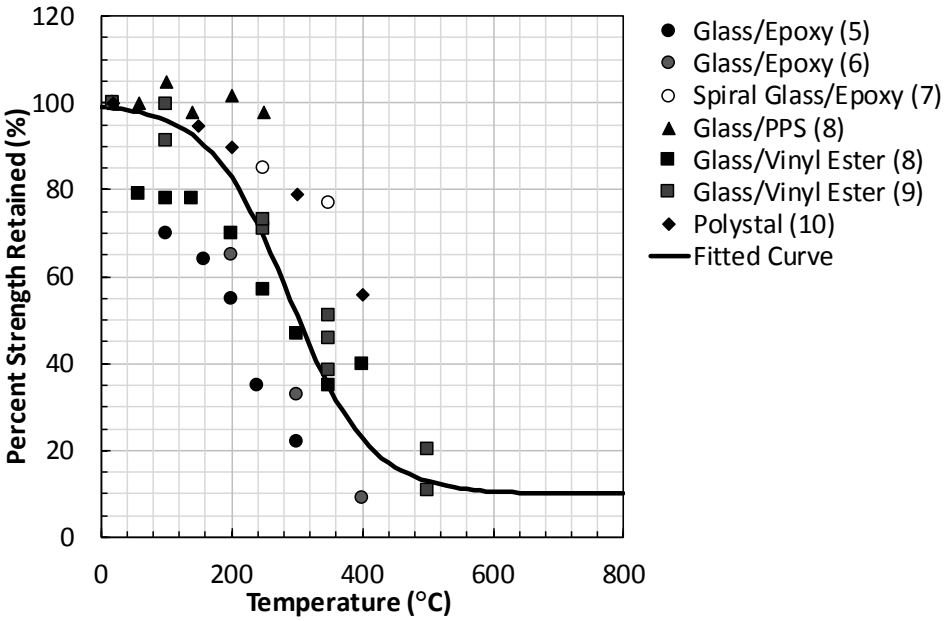

Figure 2-4 Variation in tensile strength of various glass FRPS with temperature

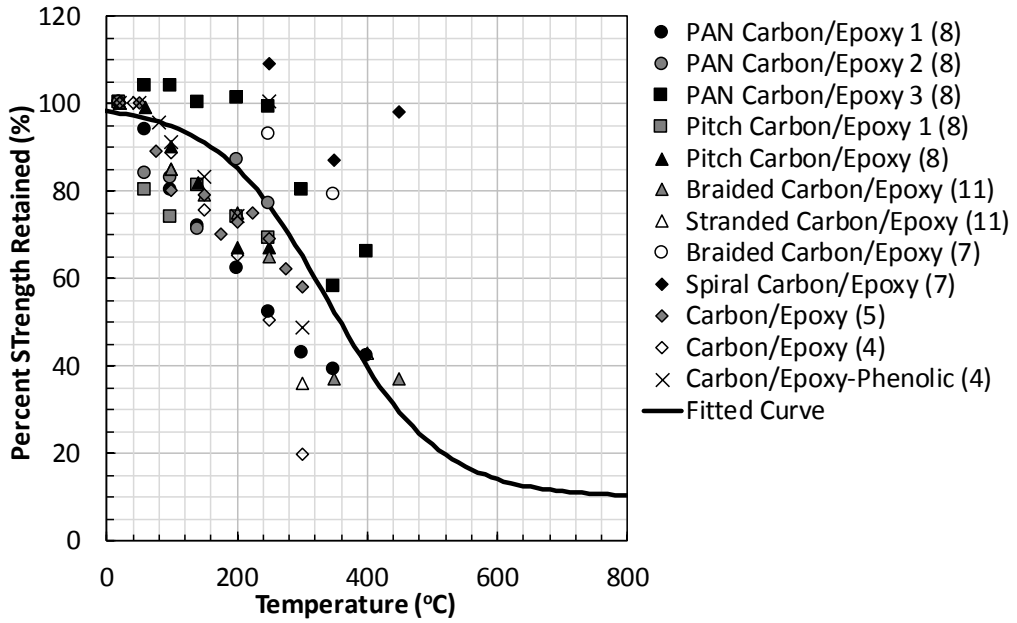

Figure 2-5 Variation in tensile strength of various carbon FRPs with temperature

(1) (Rehm & Franke, 1979)

(2) (Sen, Mariscal, & Shahawy, 1993)

(3) (Rostasy, 1992)

(4) (Dimitrienko, 1999)

(5) (Sumida, Fujisaki, Watanabe, et al., 2001)

(6) (Dimitrienko, 1997)

(7) (Tanano, Masuda, Kage, et al., 1995)

(8) (Kumahara, Masuda, Tanano, et al., 1993)

(9) (Wang, Wong, & Kodur, 2003)

(10) (Clarke, 1993)

(11) (Tanano, Masuda, Sakashita, et al., 1997)

In Figure 2-3, Figure 2-4 and Figure 2-5 the model shows a residual tensile strength of 10% of ambient capacity. This residual capacity was chosen based on a test carried out on a specific epoxy resin and the author acknowledged that in the development of this model, further tests would need to be carried out to determine residual capacity for specific FRP resins, however in this instance residual strength values were not critical (Bisby, 2003).

This work demonstrated that both bare glass fibres and GFRP bars are sensitive to elevated temperature; however, the FRPs are considerably more sensitive than the bare fibres themselves, with losses in tensile strength evident even at 100°C. By

comparison, Figure 2-6 shows that there is zero tensile strength loss for hot rolled steel at 100˚C and only 2% loss for prestressing steel (EN1992-1-2, European Committee for Standardization 2010). It should be noted here that although FRP seems in comparison much weaker than that of steel at elevated temperature, the absolute strength values of FRP are higher than that of steel. For example, VROD (see Table 2-1) glass FRP tensile strength is 710MPa in comparison to the yield strength of mild streel typically in the region of 350MPa (MatWeb, 2019).

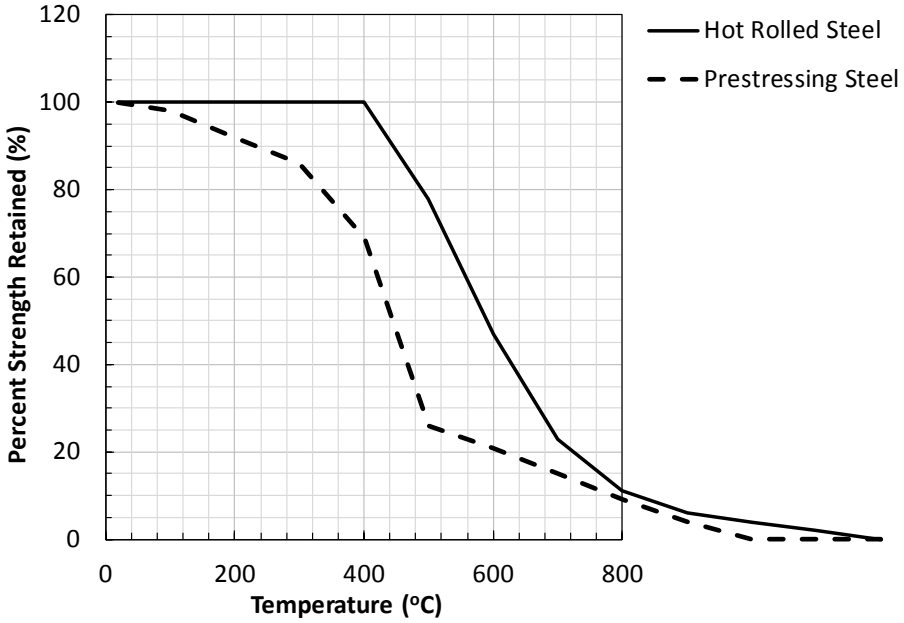

Figure 2-6 Variation in tensile strength of steel with temperature according to EN1992-1-2

It is also evident from Figure 2-4 and Figure 2-5 that there is variation in the data points dependent on the type of polymer matrix; such is the criticality of the resin in determining the performance of FRP at elevated temperature. From the literature (and as shown in Figure 2-3), it would appear than the carbon fibres are relatively unaffected by elevated temperature but like GFRP, CFRP is also sensitive to changes in temperature. This is because load sharing between the fibres is reduced at temperatures in the range of T_g due to loss of the resin's ability to transfer loads through shear stresses, resulting in loss of bulk strength for the FRP bars in comparison to individual fibres. Furthermore, as the fibres are not continuous within the bar, researchers have typically found tensile tests at higher temperatures to be less repeatable, i.e. greater variability in the residual tensile strength. As noted by Wang,

Wong and Kodur (2007) the mechanical behaviour of the FRP is more greatly affected by the bond behaviour between the fibres as the resin decomposes with increasing temperature.

Though not included within the literature discussed above, Abbasi and Hogg (2005) tested the tensile strength of GFRP bars both unexposed and in Alkaline environments. While the tests concluded a linear decrease in tensile strength at elevated temperature (in both environments), in reality they were only tested at ambient, 80 °C and 120 °C, which was concluded as likely to be around the bars glass transition temperature. The decrease in tensile strength was assumed to continue linearly, and thus extrapolated to determine the temperature at which the FRP bars would have zero strength; calculated as being between 264°C and 420°C, though there was no experimental data to validate the extrapolation. More recently Kashwani and Al-Tamimi (2014) conducted a small set of tensile strength tests on GFRP bars. They concluded that tensile strength decrease at high temperature was "almost linear" and indicated that 350°C is critical for FRP composite bars but they have not evidenced why this specific temperature is critical other than the fact they have chosen to heat the bars to this temperature prior to performing the tensile test. In reviewing this work, it was challenging to draw conclusions on the experiments carried out due to the limited information on the specifics of the test method used for the high temperature tests.

In addition to determining the absolute tensile strength at elevated temperature, researchers have also sought to observe the behaviour of the FRP bars themselves as they reach failure. Whilst FRP typically failed in a brittle manner with clear rupture of fibres, it was observed that the softening of the polymer matrix led to an uneven stress distribution within the fibres themselves, with ruptured fibres observed prior to complete failure of the bar at and above tests at 200°C (Correia, Gomes, Pires, et al., 2013). Furthermore, it was noted that the inability of the softened polymer resin to transfer stress between the fibres meant the tensile capacity of the FRP was more greatly affected by elevated temperature in comparison to the stiffness of the FRP.

As with the literature summarised by Bisby, Green and Kodur (2005), subsequent research has indicated tensile strength reduces at elevated temperature specifically upon reaching a stated glass transition temperature. However the literature has typically had little regard for correlating the specific formulation of the FRP bar to tensile behaviour at elevated temperatures nor to specifying how the stated glass transition temperature has been defined (as discussed previously in section 2.3). Furthermore, the research is limited in the range of temperatures tested around the glass transition of the polymer matrix given the range of ways that can be used to define it. This is the motivation to understand the contribution of the FRP's matrix resin at high temperature with particular emphasis on defining behaviour within and above the T_g range.

2.5 FRP Reinforced Concrete

Until recently the use of FRP reinforced concrete was limited to structures where fire resistance for load bearing capacity was not required (ACI 2006) . However the guidance of ACI 440.1R-15 (ACI, 2015) has been updated to reflect the research that has been carried out implying that FRP can be used to produce a fire safe structural design. No prescriptive method is provided and thus the approach requires a performance based analysis with recommended fire resistance testing in accordance with ASTM E119 (ASTM, 2018). The guidance highlights that due to the serviceability limit state criteria governing the design (i.e. deflection), FRP reinforcement will be under-utilised in terms of strength and therefore have additional capacity in the event of a fire (Bisby & Kodur, 2007). Creep rupture limits may also apply to reinforcement limiting the permissible stress level to 20% for GFRP and 55% for CFRP (ACI 440.1R-15). Furthermore there is reference to ensuring that bond strength loss due to elevated temperature is considered (especially given this is not necessary in steel reinforced concrete design), though there is no method provided to determine this. The criteria highlighted within the guidance show a considered and holistic response to design though placed significant emphasis on the designer fully understanding the *"structural fire endurance criteria"*. This author acknowledges the progress in

permitting performance-based design however, the guidance raises the interesting issue of competence in structural fire design in an area where much research is still ongoing. While the criteria highlighted in the guidance is important in ensuring the success of using of FRP as reinforcement, this author believes it is necessary to quantify these to holistically understand the behaviour of FRP reinforced concrete in fire, with reference to the proprietary nature of the FRP bars. Specifically tensile and bond strength losses with respect to each tested FRP bar will be experimentally evaluated within this thesis.

In contrast to the ACI guidance, Canadian guidance CAN/CSA S806-12 (Canadian Standards Association, 2012), provides tables based on the work of Kodur & Baingo (1998) to determine fire resistance of a FRP reinforced concrete slab. Fire resistance is determined based on slab thickness, concrete cover, aggregate type and critical temperature. An example of this is shown in Figure 2-7 for 150mm slab thickness with siliceous aggregate.

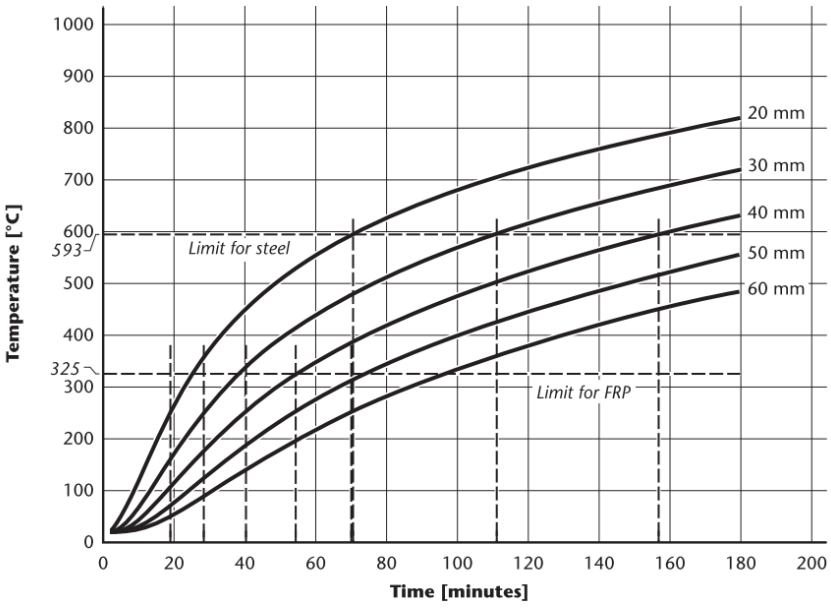

Figure 2-7 Fire Resistance of 150mm Concrete Slabs (Siliceous Aggregate);(Canadian Standards Association, 2012)

The standard states that the critical temperature, for any specific formulation of FRP bar, shall be provided by the manufacturer, where it is determined based on tensile tests at elevated temperature. While these tables are useful in principle, this author

acknowledges that critical temperatures are typically not provided by a manufacturer, and furthermore consideration is not given to other temperature-influenced factors such as bond.

2.5.1 FRP-Concrete Bond

Where concrete is to be used with a reinforcing material, the bond between concrete and the reinforcement is essential to the integrity of the structural element. Where the bond between rebar and concrete fails, particularly in the region of a lap splice, this can lead to premature collapse of structure and is of a particular concern for FRP rebar (Abbasi & Hogg, 2006). In contrast to steel which relies on mechanical interlock (via "ribs" which are cast into the steel) and friction at the concrete-rebar interface, the bond of an FRP is also influenced by a third component; chemical adhesion of the surface layer of the bar (Robert, Cousin, & Benmokrane, 2009). This surface layer is typically responsible for failure of the bond, as result of interfacial debonding, i.e. shearing of the resin coating (Chang, Yue, Lin, et al., 2010; Galati, Nanni, Dharani, et al., 2006). There are multiple surface preparations that can be added to FRP e.g. tows of fibres wrapped along the length of the bar or the use of an aggregate bonded to the surface of the bar or a combination of both. This is a secondary process to the pultrusion of the FRP bar, bonded to the polymer matrix protecting the fibres. As a result, the resin matrix of the FRP bars is significant in the degradation of bond at the reinforcement-concrete interface (Bank, Puterman, & Katz, 1998). Thus it is more susceptible to damage at elevated temperature (A. Katz, 1999) where the softening of the polymer matrix alters the stress transfer between fibres and concrete, ultimately causing the bond to fail (Saafi, 2002).

The concrete strength typically has little impact on the bond performance of the FRP reinforcement (Bakis, Bank, Brown, et al., 2002) due to the bond failure mechanism of the FRP bar being predominantly as a result of separation of the FRP coating from the core of the bar (Katz, Berman, & Bank, 1999). Abbasi and Hogg (2005) hypothesized that at lower temperatures (<80°C) the FRP-concrete bond was actually dominated by concrete strength and beyond 80°C bond failure was due to the FRP bar. By contrast

failure of the bond in steel reinforced concrete is largely due to the concrete regardless of temperature (Katz, 1999). It was suggested by Nanni (1993) that in fact some debonding of the reinforcement upon reaching the serviceability limit state may aid redistribution of strains thus providing some "pseudo-ductility" within the reinforced concrete element, though more research is required to understand this.

In flexural FRP reinforced concrete design it is necessary to have an effective embedment length of the reinforcement to achieve equilibrium such that the tensile force in the bar is resisted by surface of the bar, i.e. the average bond stress, and thus can transfer stress to the surrounding concrete. This is significant in considering bond in the design. Eligehausen, Popov, et al (1982) identified that that bond stress was *approximately proportional* to the compressive strength of concrete ($\sqrt{f_c'}$). In steel reinforced concrete, research carried out by Orangun, Jirsa, et al. (1977) underpins the development length equation in ACI 318, also using the bond-compressive strength relationship. Wambeke & Shield (2006) adopted a similar approach for FRP, which relates average bond stress, compressive strength of concrete, normalized cover and normalised embedment length using linear regression:

$$\frac{u}{0.083\sqrt{f_c'}} = 4.0 + 0.3\frac{C}{d_b} + 100\frac{d_b}{l_e} \qquad [2\text{-}1]$$

While previous researchers have shown that concrete strength has little impact on bond strength of FRP (specifically above 80°C), Equation [2-1] is used in ACI 440.1R-15 (American Concrete Institute (ACI), 2015) for determining appropriate splice lengths in ambient FRP reinforced concrete design.

Research into the bond behaviour of FRP reinforced concrete is typically in the form of an FRP bar embedded into a concrete cylinder or cube, which is pulled out of the concrete to determine bond strength (Canadian Standards Association, 2012). Some of the earliest research into bond behaviour of FRP reinforced concrete highlighted that, while bond strength was important in designing reinforced concrete, bond stiffness was likely to be a critical factor in the case of FRP reinforcement. This is due to the comparatively low modulus of the resin used to create the external coating of

the bars (that which permits a mechanical bond with concrete) (Bank, Puterman, & Katz, 1998). Furthermore, experimentally this research by Bank, Puterman and Katz (1998) identified splitting failures during the pullout test, advising that the dimensions of the concrete should be increased to a minimum of 150mm to ensure bond failure. Further research by Katz (1999) introduced a bond breaker at the pull out surface (following recommendation RC6; RILEM-CEB, 1983) and increased the dimensions of the concrete as per the previous findings. Debonding of the external coating from the core of the bars was evident in these tests for various types of surface treatment. It was evident that due to the debonding of the coating, a phenomenon known as slip hardening can occur where the concrete becomes stuck between the coating and the main fibre bundle thus increasing the resistance to the bar being pulled out from the concrete (Katz, 1999). While this ultimately improves the bond strength of the FRP in the concrete, the occurrence of slip hardening and quantifiable increase to the bond strength will be inconsistent due to the variable nature of the concrete.

Chang, Yue, et al. (2010) very clearly describe the mechanics of bond failure at ambient; with failure first occurring at the loaded end of the bar "critical point A", the boundary between the debonding and bond zone (see Figure 2-8). The bond then continues to fail along the embedded length of bar, with maximum shear stress always occurring at critical point A. Prior to complete failure of the bond, the maximum pullout load will be typically be observed.

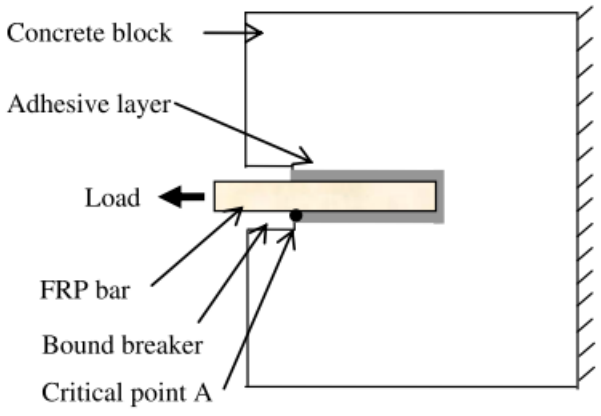

Figure 2-8 Pullout bar model sketch (Chang, Yue, Lin, et al., 2010)*)*

While the bond failure mechanism is typically as result of separation of the coating of the FRP from the core of the bars, failure can also occur due to splitting failure of the concrete. Some researchers observed micro cracking within the concrete, especially where concrete cover was lower (i.e. ~20mm) due to the bursting stresses caused by the differential between the transverse coefficient of thermal expansion of the bars and the concrete (Galati, Nanni, Dharani, et al., 2006). While these are unlikely to present in typical bond pull out tests due to cover in excess of 70mm, it is expected that micro-cracking would be observed in FRP reinforced elements such as beams. Masmoudi, Zaidi and Gérard (2005) determined that concrete cover should be at least double the GFRP reinforcing bar diameter to avoid cracking of concrete, though this was only validated up to 80°C.

Katz, Berman and Bank (1999) found that by 200°C (assumed to be above the glass transition temperature of the bars), there was between 80% and 90% reduction in bond strength in comparison to a 40% loss of bond strength in steel. The ambient bond strength and subsequent bond strength loss varied dependent on the type of coating on the FRP bars. With the exception of one of the FRP bars, the ambient bond strength was comparable to that of steel and in some cases greater, i.e. bars with the large deformations, and the helix and sand coating bars. The authors also determined that certain combinations of coating type improved bond performance, specifically helical wrapping which moderated the post peak loss of bond strength (Katz, Berman, & Bank, 1999).

In later research, Abbasi and Hogg (2005) established an equation [2-2] to determine the bond strength reduction factor (k_u) at elevated temperature (T), though this was based on tests where the GFRP bars were preconditioned in water or an alkaline solution, and tested to a maximum of 120°C.

$$k_u = 1 - 0.000004T - 0.000003T^2 \qquad [2\text{-}2]$$

By using this equation, it is calculated that the FRP bars would retain 57% of their strength at 120°C and 0% at 200°C (in comparison to 10-20%, Katz, Berman and Bank, 1999), though there were no experiments to verify the equation beyond 120°C. The

authors did acknowledge that fundamentally bond strength loss was dependent upon test temperature

Given the loss of bond strength at within the glass transition temperature range, cold anchorage is proposed for the FRP reinforcement such that sufficient stress can be developed in the bar outside the zone exposed to fire. While localized debonding may occur in the fire exposed zone, the fibres will retain tensile capacity (though less than ambient capacity). Consideration therefore must be given to the way in which cold anchorage can be achieved. In designing a structure for fire, it is common to work on the principle of a single compartment fire. In the first instance, the risk of fire must be reduced, however in the event that a fire does occur, the building is designed to inhibit growth and spread of fire to preserve life safety (Scottish Government, 2017). As such cold anchorage may be possible where reinforcement is continuous across more than one compartment. Additionally increasing the concrete cover depth in the anchorage zone would to limit the temperature of the reinforcement, though based on current literature the temperature limit may be less than 120°C, and thus require unattainable concrete covers. The use of bent FRP bars in the anchorage zone may limit the anchorage length and cover depth required(Nigro, Cefarelli, Bilotta, et al., 2013).

While it is expected that cold anchorage will support the use of the reinforcement within the concrete, it has been noted that debonding within the midspan of a slab results in larger cracks within the concrete, leading to the possibility of the reinforcement being directly exposed to the fire (Nigro, Cefarelli, Bilotta, et al., 2011).

While the bond pullout test discussed previously is the simplest to execute, it is acknowledged that this test method is not realistic of reinforced concrete due to the concrete being in compression and no additional effects of shear, flexural and tensile forces (Chana, 1990). Alternative methods such as the *Direct Tension Pullout Bond Test* and *Eccentric Pullout Test* have been used to simulate a more realistic scenario, though the former accounts only for concrete in tension. These tests will, by contrast to the typical bond pullout test, produce lower bound values of bond strength (Tastani &

Pantazopoulou, 2006). However, at this time, there is no evidence in the literature that any of these tests have been undertaken at elevated temperature.

Vinylester resin matrices were shown to be superior following environmental conditioning in comparison to polyester resins (Bank, Puterman, & Katz, 1998), in that vinylester was less likely to undergo degradation around the circumference of the bar and lead to subsequent debonding of the surface substrate from the core of the bar.

Despite substantial research by Bank, Puterman and Katz (1998); Katz, Berman and Bank (1999); Katz and Berman (2000) there has been limited research since on the bond properties of FRP bars in concrete at elevated temperature (Rosa, Firmo, Granadeiro, et al., 2018).

Rosa, Firmo, Granadeiro, et al. (2018) has shown an unmodified DMA storage modulus curve against data from pullout curves, as shown in Figure 2-9.

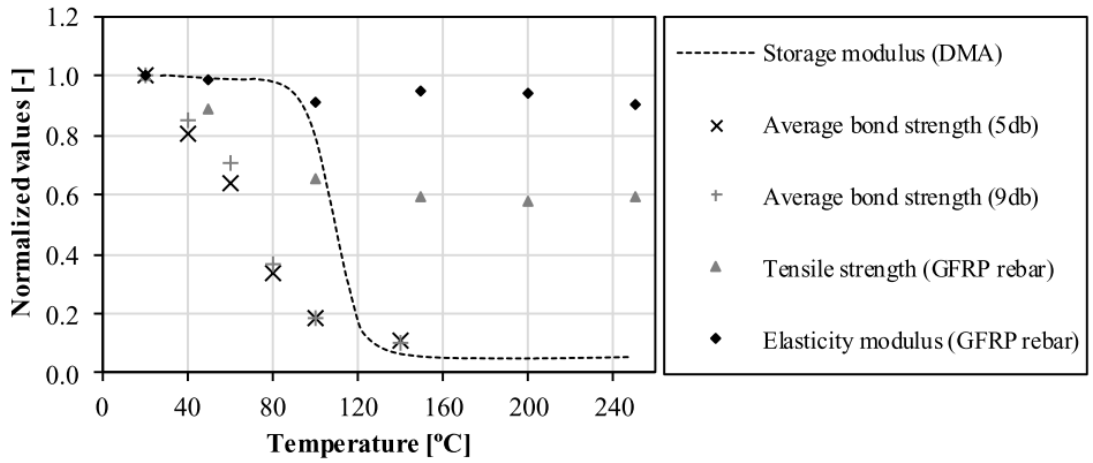

Figure 2-9 Normalized average values of bond strength, tensile strength, elasticity and storage modulus of the GFRP rebars, all as a function of temperature (Rosa, Firmo, Granadeiro, et al., 2018)

Whilst not an analytical bond model, this figure indicates that bond strength loss at higher temperatures (>120°C) is similar to the loss encountered by the storage modulus as measured by DMA.

The bond model produced by Katz & Berman (2000) was founded on the basis of a tanh function modified to account for the FRP bar physical properties, with

parametric analysis to determine the coefficients. This is based on the degree of crosslinking and glass transition temperature, as shown in Equation [2-3].

$$\tau^* = 0.5\left(1 - \tau_r^*\right) \tanh\left\{ -\frac{0.02}{\mathrm{Cr}}\left[T - k_1\left(T_g + \frac{k_1}{0.02}\mathrm{Cr}\right)\right]\right\} + 0.5\left(1 + \tau_r^*\right), \quad (10) \qquad [2\text{-}3]$$

where

$$k_1 = \begin{cases} 1, & T_g \leqslant 80, \\ 1 - 0.025(T_g - 80), & 80 < T_g < 120, \\ 0, & T_g \geqslant 120. \end{cases}$$

While this model shows good agreement with the data from the associated bond pullout tests as shown in Figure 2-10, it requires the degree of crosslinking to be known, which can be challenging to determine with an FRP bar, where some test methods can only be used on a homogenous material, i.e. polymer only, no fibres.

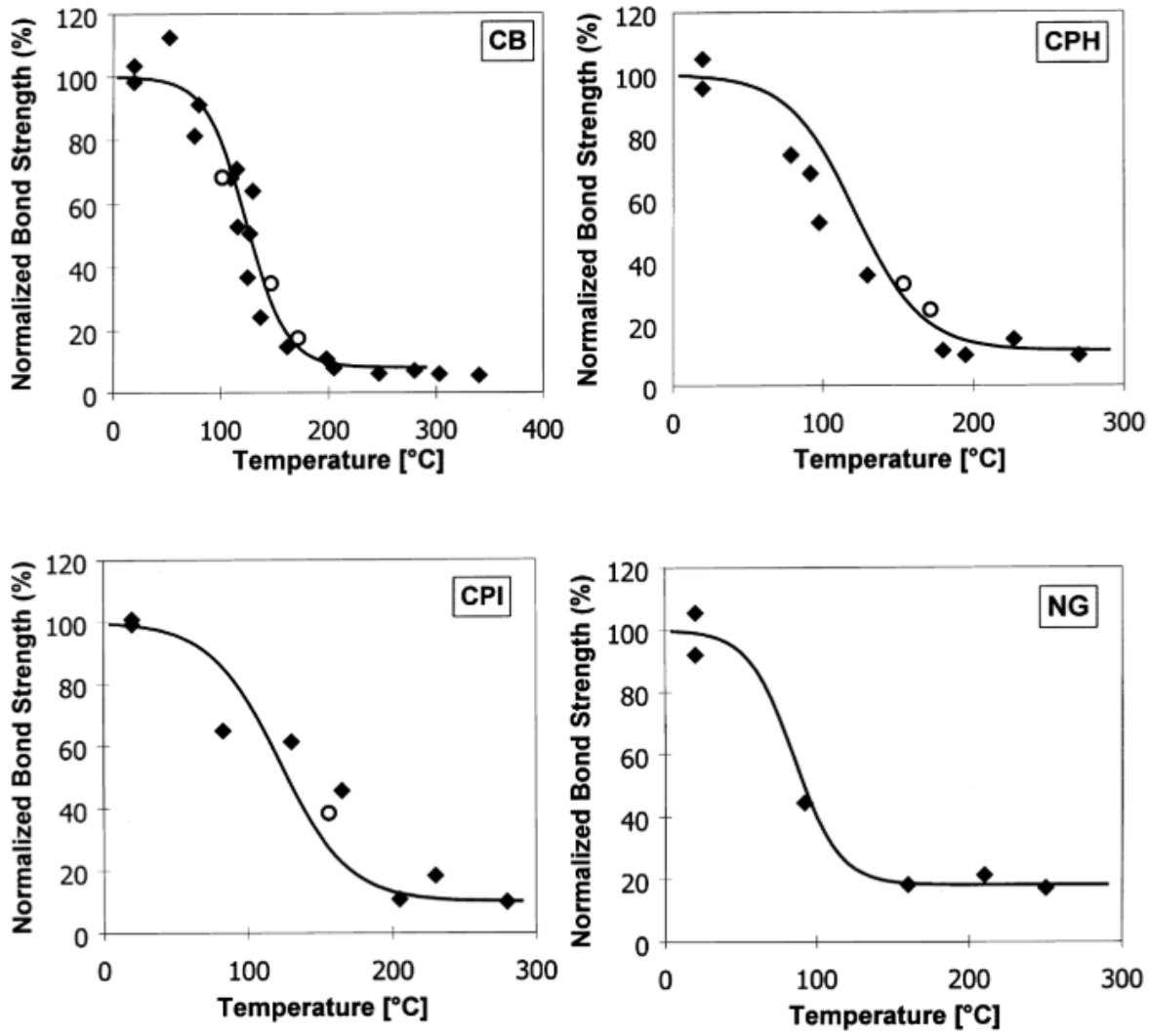

Figure 2-10 Comparison of experimental vs predicted results for bond strength loss (A. Katz & Berman, 2000)

The model has been related to the glass transition temperature though the author has not specified the method used to define this, which could ultimately lead to more variability in the predicted results.

The research carried out within this thesis investigates three FRP reinforcing bars, and therefore it is not an aim of this work to investigate in-depth the bond properties of FRP bars in general. The author acknowledges the great variability in the composition of the FRP bars, and therefore will carry out common bond pull out tests (Katz, Berman, & Bank, 1999), within the glass transition temperature range with the aim of providing qualitative outcomes related to bench scale thermal characterisation. These outcomes will likely present an opportunity to be further investigated beyond

this body of work and will provide valuable inputs into other parts of research carried out within the thesis.

2.5.2 Flexural behaviour of FRP reinforced Concrete at Elevated Temperature

At present, when FRP bars are used as tensile flexural reinforcement for concrete elements the limiting temperature in case of fire is typically assumed to be defined by the FRP's glass transition temperature (T_g) ACI440.1R-2015 (American Concrete Institute (ACI), 2015); this can discourage or prevent FRP from being efficiently used in most structures that require fire resistance ratings.

In conventional steel-reinforced concrete structures, the critical temperature of the reinforcing bars, when exposed to fire, is typically defined by a 50% reduction in yield strength of the reinforcement (Bisby & Kodur, 2007). This definition is used because a steel-reinforced (under-reinforced) flexural concrete element, designed in accordance with typical limit-state design codes, can be expected to be close to collapse, under full service loads, when the steel loses about half of its tensile strength. If critical temperatures for FRP reinforcing bars in flexural reinforcement applications are defined on a similar basis (as has been previously suggested in the literature (Wang, Wong, & Kodur, 2007)), their critical temperatures can be expected to be lower than for steel. This is due to complex softening (degradation) and pyrolysis (decomposition) of the polymer resins used in their manufacture; this occurs at comparatively low temperatures.

Degradation of mechanical properties of FRP bars is of a concern, with critical temperatures for tensile and bond strength being significant in the design (Weber, 2008a). Kodur and Bisby (2005) identified that while slab thickness was influential in the case of steel reinforced concrete due to fire resistance being determined by a critical temperature being reached at the unexposed face, this was not the case for FRP reinforced concrete. For the same reason they also determined that concrete cover did have a significant impact on the thermal behaviour of the GFRP reinforcement as shown in Figure 2-11 (Kodur & Bisby, 2005), noting that siliceous aggregate is the least compatible with fire resistance.

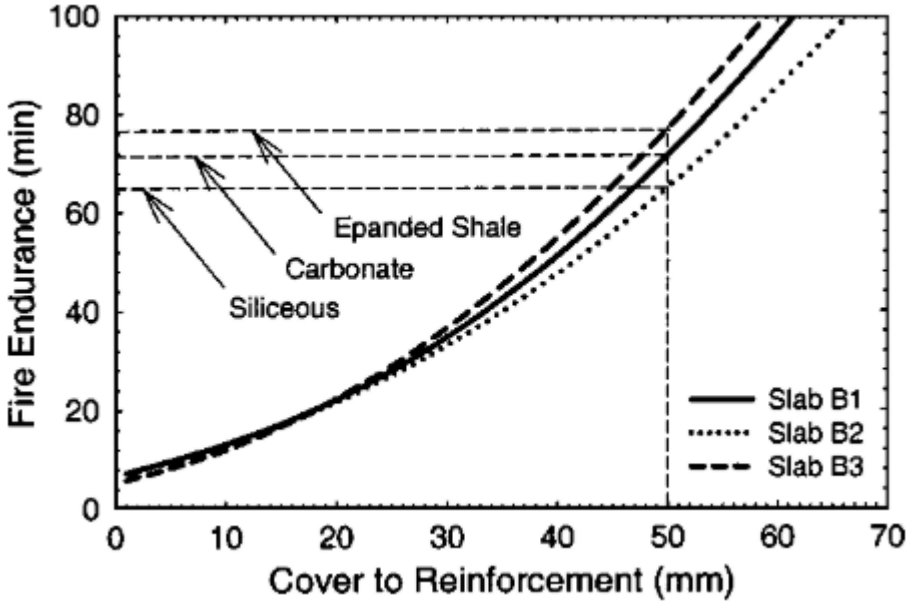

Figure 2-11 Effect of concrete cover thickness and aggregate type on fire resistance of reinforced concrete slabs (Kodur & Bisby, 2005)

This is due to the criticality of the FRP reinforced concrete element ultimately being determined by the reinforcement reaching a critical temperature. Critical temperature, in this case, was defined based on tensile tests carried out by Wang, Wong and Kodur (2003) where the FRP bars were shown to still retain a high percentage (~90%) of their ambient stiffness below ~325°C for GFRP and 250°C for CFRP.

Experimental research of six GFRP reinforced concrete slabs further reinforced the influence of concrete cover on fire endurance and the necessity for cold anchorage of the reinforcement to prevent pull out (Nigro, Cefarelli, Bilotta, et al., 2011). The elastic stiffness of GFRP and CFRP is typically less than that of steel and as such deflection (i.e. serviceability limit) governs the design of reinforced concrete (C. E. Bakis, Bank, Brown, et al., 2002). Though FRP rupture is permitted by ACI 440.1R-15 (ACI, 2015), FRP reinforced concrete may be designed to fail by concrete crushing, requiring over-reinforcement. To improve the efficiency and maximize the potential of the FRP reinforced concrete, the flexural strength of the reinforced concrete can be increased through the use of high strength concrete (Nanni, 1993). While much research has

been undertaken in the area of high strength concrete (HSC), caution should be noted as HSC has demonstrated a propensity to spall during a fire event. Further research is currently underway at the University of Edinburgh developing a novel testing method for spalling to allow reliable and readily repeatable testing on high strength concrete mixes. It is acknowledged by researchers that pre-stressing of the FRP would ensure the reinforcement achieves its potential but by contrast this is the more expensive option (Ibell, Darby, & Denton, 2009; Nanni, 1993). Even in the instance where a reinforced concrete section is design to fail by FRP rupture, crack control serviceability criteria will require to be met ultimately leading to more reinforcement being included within the concrete. As tensile strength of FRP is typically much greater than that of steel, this means that the FRP reinforcement (provided anchorage is kept cold, i.e. less than T_g) will be able to maintain structural stability for temperatures much greater than T_g (Bisby & Kodur, 2007; Robert & Benmokrane, 2010).

Due to the high temperature vulnerability of the FRP bars, researchers have noted the influence of cracking on fire resistance of FRP reinforced concrete. In GFRP reinforced beams at elevated temperature longitudinal cracking along the base of the beams has been observed, which then allowed flames to directly impinge upon the FRP reinforcement (rather than heat conducted through the concrete). This ultimately leads to failure of the beams due to the decomposition of the FRP matrix and subsequent debonding of the rebar from the concrete (Abbasi & Hogg, 2006). Elbadry and Elzaroug (2004) developed design charts to determine the minimum reinforcement ratio to control cracking of the concrete, though these were only validated for CFRP. Furthermore, while the experimental research by A. Abbasi & Hogg (2006) observed crack widths of 2mm, the current ACI guidance limits crack width openings to 0.4 to 0.7mm.

In bending tests on GFRP reinforcement (Maranan, Manalo, Karunasena, et al., 2014), interlaminar shear failure was observed during tests at temperatures up to 150°C,

however this would not be expected to happen in FRP reinforced concrete due to the confinement of the bars within the concrete.

There have been limited studies carried out to date on FRP reinforced concrete at elevated temperature (Rosa, Firmo, Santos, et al., 2018). The research contained herein seeks to add to the current pool of knowledge with by provided a comparative study for both GFRP and CFRP reinforcements with a focus on bond critical and non-bond critical applications.

2.6 Scope Limitations

The literature review set out in this chapter highlights the pre-cursor research to the work undertaken within this thesis; however, it is important to acknowledge the limitations of this work.

Spalling is a notable problem for concrete at elevated temperature, and as discussed in section 2.5.2, can be particularly problematic for high strength concrete, which may be used with FRP reinforcement. The complexity of spalling has limited knowledge in this area, and much research is underway to increase understanding. As such spalling is not part of this body of research.

Toxicity of polymers has been discussed in multiple publications; notably producing dense, sooty, black smoke in the event of a fire (Neale & Labossiere, 1991). The formulation of the polymer dictates the amount and toxicity of the smoke produced. In the instance of FRP used as internal reinforcement in concrete, smoke production may be limited due to concrete cover and subject to the presence of cracks in the concrete (Bisby, 2005). While this author acknowledges the importance of researching toxicity, the focus of this thesis is on three specific FRP bars, which would limit the research outcomes, given that toxicity is dependent on the polymer formulation. Therefore, toxicity is not a research focus within this thesis.

In holistic structural fire design, full structural frame analysis defines how a structure might behave in the event of a fire. To achieve this multiple inputs are required to understand structural interaction, including bond, tensile and shear strength loss at

elevated temperature. As discussed in the literature review, the proprietary formulation of the FRP matrix makes for a considerable amount of variables in determining strength loss models. A large data set would be required across multiple types of FRP bar to carry out a statistical analysis and provide valid inputs to a finite element model. The research carried out within this thesis ultimately adds to the data pool but given the lack of prior research on FRP reinforcement at elevated temperature, more data is required. Therefore full frame analysis is out with the scope of this thesis.

2.7 CHAPTER SUMMARY

By the 1970s, FRP had become commercialised though material cost remained relatively high. Consideration of long-term sustainable infrastructure saw investment into research of FRPs, with whole life cycle costing demonstrated as lower than steel. Primarily though, high tensile strength and non-corrosive properties make FRP an attractive alternative to steel.

FRP reinforcement is produced using a pultrusion process to combine fibres (e.g. glass, carbon, aramid) with a polymer matrix, followed by a secondary curing process for the addition of the surface coating, which is necessary to promote mechanical adhesion with concrete. Herein lies the challenge of FRP; a polymer matrix, which softens at the material's Glass Transition Temperature (T_g) and decomposes upon reaching the Decomposition Temperature (T_d), and a surface treatment, which is also susceptible to elevated temperature but is crucial for the development of the bond. T_g can be determined using a number of methods and it is uncommon for the specific definition to be evident within the literature. Furthermore, T_g is commonly interpreted as a limiting temperature for FRP and as such, there is little discussion on decomposition and oxidation temperatures. This is the motivation to consider FRP behaviour at elevated temperature as a key influencer in structural design.

Experimental determination of tensile strength loss at elevated temperature has typically been an inefficient and costly process with researchers developing their own

testing methodologies. As such they have sought to develop models to predict this loss, with the most commonly used model produced by Bisby (2005). Some further research on tensile behaviour of FRP at elevated temperature has been carried out to date, but it has been limited. Furthermore, the literature typically does not consider the proprietary nature of FRP bars, but rather generalizes dependent on fibre and polymer type, which motivates this author to research the behaviour of specific FRP formulations and the subsequent influence on tensile strength.

While tensile strength is a key component of FRP reinforced concrete, ACI 440-1R-15 highlights the importance of considering bond strength loss at elevated temperature, though no prescriptive method is provided. Where FRP reinforced concrete must provide fire resistance for load bearing, it is necessary to undertake a performance based analysis. As an alternative Canadian guidance CAN/CSA S806-12, provides tables based on the work of Kodur & Baingo (1998) to determine fire resistance of a FRP reinforced concrete slab. Multiple researchers have considered the influence of concrete cover and aggregate type. In the consideration of bond strength, the susceptibility of the FRP coating, typically results in very little residual bond strength beyond the glass transition range. The typical and most simple experiment to examine bond is the bond pullout test. The large reduction in bond strength has determined that cold anchorage of the reinforcement is necessary if it is to be used where a fire may occur. Few bond models have been produced to predict bond strength loss.

Research has demonstrated the viable use of FRP as reinforcement in concrete but with a limited view on the boundary conditions necessary for its practical use. A review of the standards for structural design of FRP reinforced concrete sets out two fundamentally different approaches; holistic performance based design (to which there are few valuable inputs currently available), and prescriptive fire resistance periods determined based on slab thickness, concrete cover, aggregate type and a critical temperature. A critical temperature, which should be defined by the FRP manufacturer, but is not in practice. Nor is there any basis for defining this critical temperature, or reference to the requirement for cold anchorage.

In conclusion, the literature review demonstrates FRP is a material that is fundamentally different to that of steel reinforcement and as such structural fire design cannot follow the same rules as for steel. In order to undertake a performance based design to permit the use of FRP reinforced concrete in a fire scenario, thermo-mechanical elemental behaviour must be understood. Experimentation and modelling has been undertaken for tensile strength loss at elevated temperature but with little regard to the specifics of the test temperatures and the range of test temperatures, which is considered by the research contained in this thesis, specific to the formulation of the FRP bar. To form an improved understanding of high temperature bond behaviour, more data is required considering different FRP fibre and coating types (set out experimentally in Chapter 5). The FRP reinforced concrete beam tests presented in Chapter 6 establish a link between thermal and mechanical behaviour of the bars research in the preceding chapters. This provides a clearer outline of the parameters to be considered in structural fire design rather than simply a critical temperature for the reinforcement.

CHAPTER 3 THERMO-MECHANICAL CHARACTERISATION OF FIBRE REINFORCED POLYMER BARS

3.1 CHAPTER OVERVIEW

This chapter presents bench scale testing of proprietary glass and carbon fibre reinforced polymer bars using thermal analysis techniques; Dynamic Mechanical Analysis (DMA) and Thermo-gravimetric Analysis (TGA). The overarching goal of the research presented is to identify key stages in the materials thermal behaviour, specifically critical temperatures for degradation (i.e. glass transition, T_g) and decomposition (T_d) of the polymer matrix. These key temperatures form the basis of the mechanical testing of FRP components to quantify strength loss at elevated temperature (presented in Chapter 4&5). Furthermore, the impact of elevated temperature on FRP reinforced concrete beam tests is presented in Chapter 6.

As discussed, the degradation and decomposition of the polymer matrix used to manufacture and apply the surface coating to FRP is integral to properly understanding the mechanical response of the bars in concrete at elevated temperature, and hence the fire performance of FRP reinforced concrete.

3.2 TESTING MATERIALS

Two FRP manufacturers provided three FRP bars, namely two commercially available GFRP bars (separate manufacturers) and one commercially available CFRP bar. The respective bars are shown in Figure 3-1 and are denoted as BPG, PTG, and PTC from top to bottom in the figure. Selected manufacturer specified properties for all three bars are given in Table 3-1.

Figure 3-1: Photo of the FRP bars studied in the current project (from top denoted as: BPG, PTG, PTC)

Table 3-1: Manufacturer Specified Properties

	BPG	PTG	PTC
Manufacturer	BP Composites Inc.*	Pultrall Inc.**	Pultrall Inc.
Bar #	3	3	3
Nominal Diameter (mm)	10	9.5	9.5
Fibre Type	Glass	Glass	Carbon
Fibre Content (% Wt.)	83.6	83	*-Not Specified-*
Resin	Vinyl Ester	Modified Vinyl Ester	Modified Vinyl Ester
Min. Tensile Strength (MPa)	1126	889	1431
Modulus of Elasticity (GPa)	63.2	53.4	120
Tensile Strain at Failure (%)	2.07	1.66	1.33

* BP Composites - http://www.bpcomposites.com/products/tuf-bar/

** Pultrall - http://www.pultrall.com/en/index.asp

In addition to the manufacturer specified properties noted in Table 3-1, the surface treatment of the bars is different between manufacturers. The carbon and glass FRP bar, which have been supplied by the same manufacturer (i.e. PTG and PTC), have a coarse sand coating which is adhered to the bars' surface after the pultrusion process. The bars are coating with resin and sand is broadcast into the resin, which is followed by post-pultrusion curing (most likely at a somewhat lower temperature than that used during manufacture of the bars). The BPG glass fibre reinforced bar has a thin double helical wrap of FRP applied to the exterior of the pultruded bar, with a finer sand coating then applied using the same technique as described previously for the PTG and PTC bars. This provides some additional confinement to the longitudinal fibres in the bar. It should be noted that in both cases these coatings are applied in a secondary coating and curing process.

In the ideal case in addition to testing of the FRP bars, the components of the bar (i.e. the fibres and the resin) would be tested separately, however this was not possible. In the first instance, the manufacturer was unable to provide the raw fibres, and the composition of the resin would not be the same as the polymer matrix in the reinforcement bars as it would like undergo a different curing process. Secondly it is not possibly to physically separate the fibres from the polymer matrix as the components are chemically bonded.

3.3 DYNAMIC MECHANICAL ANALYSIS

Dynamic mechanical analysis (DMA) is an oscillatory physical experimental method designed to evaluate the viscoelastic response of materials, and to determine the variation in the stiffness of polymeric materials in particular. Dynamic mechanical analysis can be performed as either a frequency sweep (i.e. oscillating loads of different frequencies at constant temperature with time) or a temperature sweep (i.e. where typically a linear heating rate is used at a constant loading oscillation frequency). Temperature sweep was used in the current set of experiments in accordance with ASTM D7028 (ASTM, 2007).

The stress (σ_a) and strain (ε_a) response under oscillatory loading define the stiffness of the material with increasing temperature; the complex modulus (E^*), which is composed of two vectors denoted as the storage modulus (E') and the loss modulus (E''). These are defined by equations [3-1]-[3-5] (and with reference to Figure 3-2) (PerkinElmer, 2008).

$$\sigma = \sigma_a \sin(\omega t + \delta) \quad [3\text{-}1]$$

$$\varepsilon = \varepsilon_a \sin(\omega t) \quad [3\text{-}2]$$

$$E^* = \frac{\sigma_a}{\varepsilon_a} \quad [3\text{-}3]$$

$$E'(\omega) = E^* \cos(\delta) \quad [3\text{-}4]$$

$$E''(\omega) = E^* \sin(\delta) \quad [3\text{-}5]$$

$$tan\delta = \frac{E''(\omega)}{E'(\omega)} \quad [3\text{-}6]$$

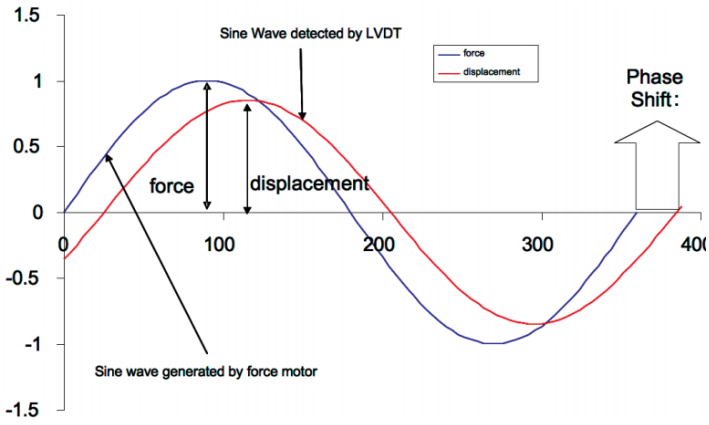

Figure 3-2: Schematic depicting the phase shift between the applied force and the measured displacement in a DMA test (PerkinElmer, 2008)

These two moduli indicate key areas of interest in the material's behaviour, and are related by the measured phase shift angle (δ) (again with reference to Figure 3-2). In polymer-based materials, tracking the variation in Loss and Storage moduli, and the variation in the phase shift angle, allows multiple means of assessing the glass transition temperature of the polymer involved (T_g). One of the widely applied definitions for T_g (noted at T_t in ASTM D7028) uses the peak value of tanδ according to Equation [3-6] which indicates the peak phase shift between the material's elastic and viscous response; i.e. the temperature at which the deformation response of the material lags most significantly behind the oscillatory applied stress. These and other specific definitions used to define T_g are discussed in more detail in Section 3.3.2.

3.3.1 Testing Methodology

A dynamic mechanical analyser (DMAr) manufactured by Triton Technology was used to carry out DMA experiments. This is shown in Figure 3-3.

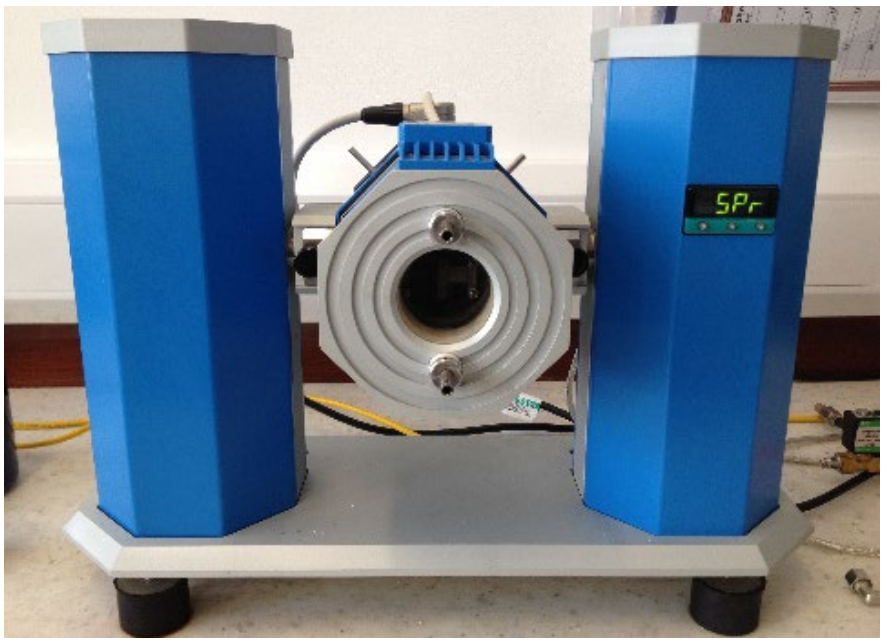

Figure 3-3: Triton Technology Dynamic Mechanical Analyser (DMAr) used in the current study

To perform DMA on FRP bars, it was necessary to obtain prismatic samples of cured FRP bar material. This was accomplished by splitting the bars longitudinally to obtain a prismatic sample of the required size from the core of the respective bars, as shown in Figure 3-4 and Figure 3-5. Typical dimensions of the samples required for DMA testing are approximately 20mm length, 8mm width, and 2mm thickness. The sand/polymer coatings of the bars were also removed prior to DMA testing, and the surface of the DMA samples lightly abraded (to minimise temperature increase) to ensure continuity of fibres in the samples and to obtain orthogonal sample facets. It is not anticipated that any additional stresses or strains were placed on the sample due to the unidirectional fibres and heterogeneous nature of the FRP bars. The samples were dried using desiccant, at ambient temperature (i.e. 20°C), to ensure that they were not affected by moisture resulting from absorption of ambient relative humidity. While the test standard (ASTM D7028) does not reference the use of dessicant, this was a comparable option in lieu of oven drying or storage in a dessicator post lamination (both of which were not possible in the lab).

Figure 3-4: DMA sample preparation by longitudinal splitting with a flat blade

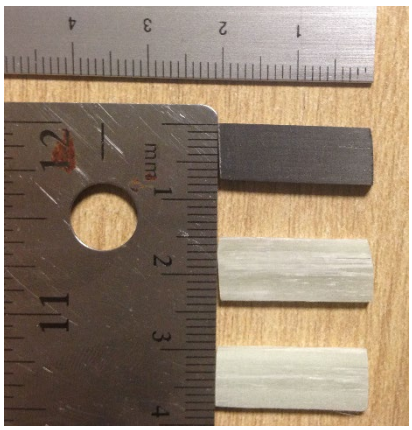

Figure 3-5: Typical DMA samples cut from FRP reinforcing bars

The DMA experiments were performed in accordance with ASTM D7028; at a low constant frequency of 1Hz, with a temperature ramp rate of 2˚C per minute (i.e. temperature sweep), and up to a maximum chamber temperature of 180˚C-200˚C, depending on the sample and run. While ASTM D7028 recommends a standard heating rate of 5 ˚C/minute, the comparatively low heating rate was chosen for precision, to allow the sample to exhibit the glass transition phase at its lowest T_g range (as discussed in ASTM D7028). As discussed in the literature review, the T_g range for thermosetting polymers is typically in the region of 60˚C to 130 ˚C (Katz, Berman, & Bank, 1999), therefore the maximum temperatures used ensured that the T_g phase was observed and concluded before cooling the sample. Air was used as the purge gas as typically there is little decomposition occurring below temperatures in the range of 200˚C, and therefore an inert (Nitrogen) atmosphere was not necessary. Furthermore, a single cantilever-bending configuration was used as the testing setup to minimise any secondary stiffening effects due to thermal expansion or contraction of the samples during heating. While a three point bending configuration would also be appropriate for investigating the samples, unfortunately this was not possible at the time of testing. A minimum of three repeat tests were performed per bar type to verify repeatability and reliability of the results obtained. In the instance where

sample results were not repeatable additional tests would have been undertaken to determine if the results were an anomaly.

3.3.2 Determining the Glass Transition Temperature Range(s)

As discussed in the literature review, there can be variation in the values of T_g for a single FRP bar dependent on the way in which it is defined (Charles E. Bakis, Lopez, & Witt, 2014) and it is often not clear from research which definition has been used when stating the T_g value. From a review of the literature, it is evident that glass transitioning in polymers occurs over a range of temperatures, rather than being a binary criterion based on pre- and post-transition mechanical (or chemical) properties. From this point forward in the current thesis, T_g is considered as a range rather than a single point value; however, point values are necessarily quoted to highlight observations from testing in Chapter 4 through 5.

Figure 3-6 shows selected data obtained from a DMA test on a sample of PTG FRP reinforcing bar, namely storage and loss moduli and tan delta during heating up to 200°C. Figure 3-6 to Figure 3-9 schematically show the various methods that have been used in determining the T_g range for any given polymeric or FRP material. Five methods have been used to determine a single point value of glass transition, which cover the range of glass transition temperatures, and are discussed below:

3.3.2.1 T_g Onset

One of the lowest values in the T_g range is typically identified based on a T_g value determined from the *onset* of the loss of elastic stiffness (storage modulus) of the FRP material; i.e. the onset of storage modulus reduction (German Institue for Standardization, 1999). This temperature can be established based on the intersection of tangent lines approximated from (1) the initial storage modulus loss plateau and (2) the slope of the storage modulus at maximum negative slope, as shown in Figure 3-7. This value is denoted as T_g *Onset*, and it should be noted that its determination can be somewhat subjective due to the visual interpretation of the two tangent lines (refer to Figure 1-7). Qualitative guidance is provided in ASTM D7028 on how to draw the tangent lines; (1) using a temperature that occurs prior to the transition but not

too close or too far away from it, (2) temperature at the inflection point of the modulus drop. ASTM D7028 recommends plotting the storage modulus on a logarithmic scale to determine T_g *Onset* (referred to in the standard as DMA T_g), however the standard acknowledges that by using a linear plot this produces a lower value of T_g, and it is a goal of this research to capture the full range of the glass transition.

3.3.2.2 T_g 2% Offset

The *offset* method identifies T_g based on a two percent loss of storage modulus (E') (German Institue for Standardization, 1999) at a temperature of T_g *Onset* - 50˚C, denoted as T_g *Offset (2%)* in Figure 3-7 . From the initial tangent, as found for determining T_g *Onset*, a line is drawn parallel such that the storage modulus at T_g *Onset* - 50˚C is two percent less than that measured in the test. T_g *Offset (2%)* can therefore be found where this parallel line intersects the storage modulus curve, defining the initial softening of the polymer matrix.

3.3.2.3 T_g Modulus

A third method identifies T_g as the peak rate of loss (i.e. maximum negative slope) in the Storage Modulus (E') curve. Whilst this can be estimated visually, plotting the derivative of the Storage Modulus curve provides a more accurate assessment. This derivative can be rather noisy in practice, so smoothing the derivative using a LOESS function aides the data analysis. This is identified as "USM Deriv. (x)" in Figure 3-9, where x indicates the alpha (α) value used in the LOESS function. In addition, the process was repeated using a smoothed modulus and recalculating the derivative, identified as "SM Deriv. (x)" in Figure 1-9. In most cases, the unsmoothed modulus with the highest α value was used to determine the T_g*Modulus* value (see Figure 3-7). However, it is important to visually assess the data to ensure that the lowest point in the derivative is not due to a lone outlier. This can lead to subjectivity in the assessment of the T_g range,

3.3.2.4 T_g Loss Modulus

The Loss Modulus (E'') curve also provides useful information on the FRP material, and the temperature at the peak Loss Modulus value indicates the point at which the

lost energy is being dissipated from the material i.e. the most significant loss of stiffness in the material with increasing temperature, as shown in Figure 3-8.

3.3.2.5 T_g Tanδ

While the T_g range is largely defined based on the reduction in elastic stiffness of the material, it can also be defined using the interaction between the polymer's elastic and viscous responses. As discussed previously, this interaction occurs most significantly when the phase between the elastic and viscous responses (i.e. the phase angle) peaks. This occurs when the direct response of the material to force is delayed by the softening of the polymer matrix, and thus the deformation lags behind the sinusoidal loading. This maximum phase shift is defined by the temperature of *peak Tanδ*, and is shown in Figure 3-8. *Peak tanδ* is also widely used as a definition of T_g for polymer materials.

3.3.2.6 Analysis of DMA Results

Each of the above-noted T_g determination methods was used to define the respective T_g values for the three FRP bars examined in the current project. Table 3-2, Table 3-3 and Table 3-4 show the glass transition temperatures and their standard deviations for PTC, BPG and PTG bars, respectively. The ranges are similar to that discussed within the literature review. Figure 3-7 and Figure 3-8 depict the results for PTGi. The figures for the other samples tested are included within appendix A. The BPG and PTG bars have four sample results instead of three and pilot tests were undertaken to practice the procedure and check the DMA was operating correctly. The values determined for T_g Loss Modulus have not been included as a test temperature in the elemental tests discussed in chapters 4 and 5, as the loss modulus curves typically did not have a clear peak to determine the value.

Figure 3-10 shows the ranges of T_g for each of the three FRP bar types, with the error bars in the plot defined as ± 3 standard deviations from the mean values determined from three identical repeat tests, to give an indication of the variability in the data.

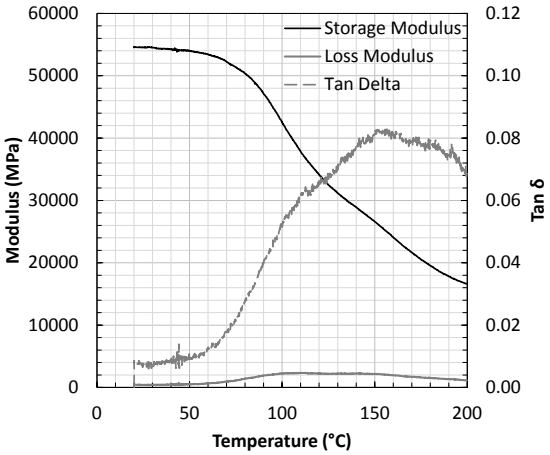

Figure 3-6: Typical DMA measured data for a representative sample of PTG FRP bar

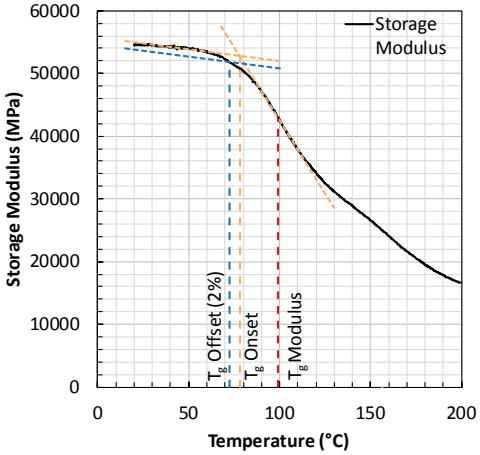

Figure 3-7: Schematic showing how to identify T_g from the Storage and Loss Modulus curves

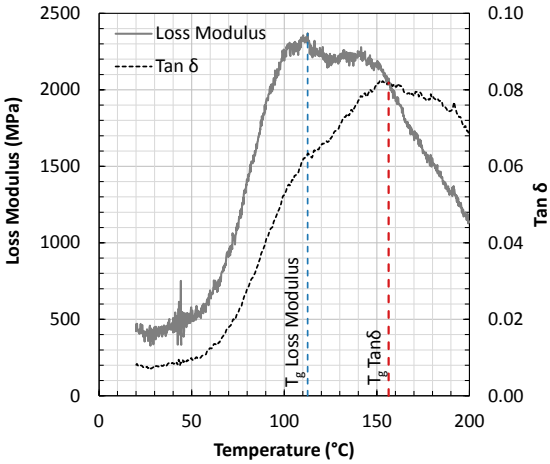

Figure 3-8: Schematic showing how to identify T_g Loss Modulus and T_g Tanδ from DMA curves

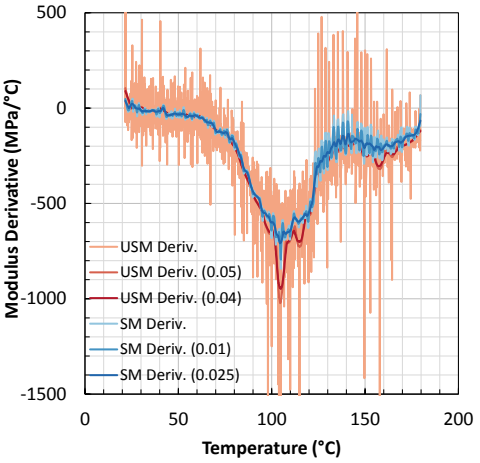

Figure 3-9:Schematic showing how to identify T_g Modulus from derivatives of the Storage Modulus curve

Table 3-2: PTC Glass Transition Temperature values based on various definitions for T_g

	Glass Transition Temperature (˚C)				Standard Deviation	
	i	ii	iii	Avg	σ	3σ
T_g 2% Offset	50.77	54.30	55.10	53.39	1.63	4.89
T_g Onset	60.85	66.08	65.07	64.00	1.96	5.89
T_g Modulus	79.74	89.10	89.35	86.06	3.87	11.62
T_g Loss Modulus	84.53	93.10	92.08	89.90	3.31	9.93
T_g Tan δ	110.84	105.88	107.13	107.95	1.83	5.48

Table 3-3: BPG Glass Transition Temperature values based on various definitions for T_g

	Glass Transition Temperature (˚C)					Standard Deviation	
	i	ii	iii	iv	Avg.	σ	3σ
T_g 2% Offset	84.87	73.11	72.63	82.24	78.21	5.43	16.28
T_g Onset	89.33	83.13	84.38	87.87	86.18	2.51	7.54
T_g Modulus	109.75	104.90	109.75	109.70	108.53	2.09	6.28
T_g Loss Modulus	138.68*	111.19	111.60	119.10	113.96	3.64	10.91
T_g Tan δ	149.24*	134.90	134.70	137.80	135.80	1.42	4.25

*These values have not been included in the calculation of the average as they are anomalous results.

Table 3-4: PTG Glass Transition Temperature values based on various definitions for T_g

	Glass Transition Temperature (˚C)					Standard Deviation	
	i	ii	iii	iv	Avg.	σ	3σ
T_g 2% Offset	72.62	75.58	81.25	78.81	77.07	3.26	9.78
T_g Onset	78.11	83.79	84.12	84.37	82.60	2.60	7.80
T_g Modulus	99.20	113.80	103.44	104.84	105.32	5.32	15.96
T_g Loss Modulus	112.60	130.58	144.71	123.20	127.77	11.68	35.05
T_g Tanδ	156.30	154.14	156.33	149.70	154.12	2.70	8.10

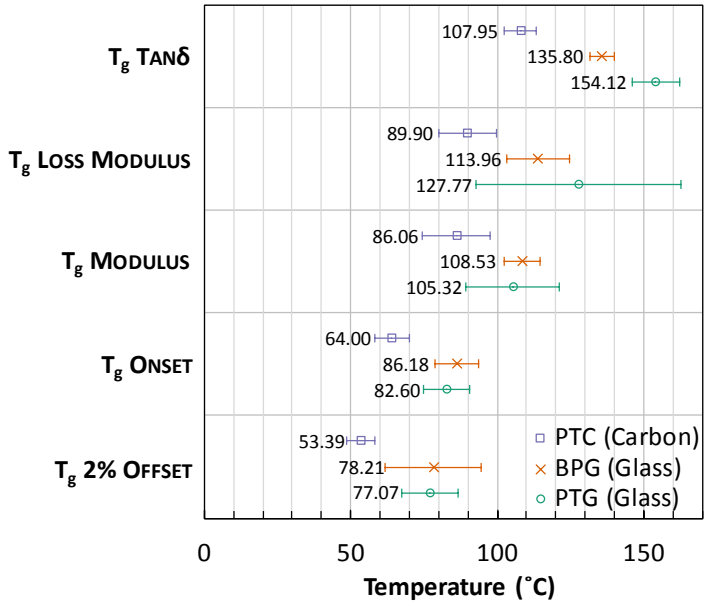

Figure 3-10: Measured T_g ranges for FRP Bars

(error bars show 3 standard deviations from the sample mean values)

While calculating *T_g Onset* relies on consideration of the transition point and subsequent placement of the tangents, the error bars for this value are smaller than for *T_g 2% Offset*, and due to the values differing by only 5-11˚C from *T_gOnset*, *T_g 2% Offset* has not been included in any further analysis. This is also the same for *T_g Modulus* and *T_g Loss Modulus*, therefore only *T_g Modulus* has been used in further analysis.

Figure 3-11, Figure 3-12, and Figure 3-13, and Figure 3-14, Figure 3-15, and Figure 3-16 shows the non-normalised and normalised storage modulus curves for the FRP bars respectively. The quantitative value of the storage modulus measured for the various DMA samples tests at ambient temperature varied by as much as 43% from the maximum value (BPGii, Figure 3-12) in some cases. In theory, all of the normalised curves (Figure 3-14, Figure 3-15 and Figure 3-16) should yield approximately the same values at a given temperature, though it is evident from the figures that this is not always the case. Figure 3-11, Figure 3-12 and Figure 3-13 show the variability in the absolute DMA curve values for the respective samples at ambient temperature. This

might be due to small inaccuracies in sample dimension measurements, slightly variable fibre volume fractions in the respective samples, the fact that samples may have come from different portions of the FRP core of the bars (i.e. close to the core or closer to the edge), or even slight changes in curing of the samples during the manufacturing processes.

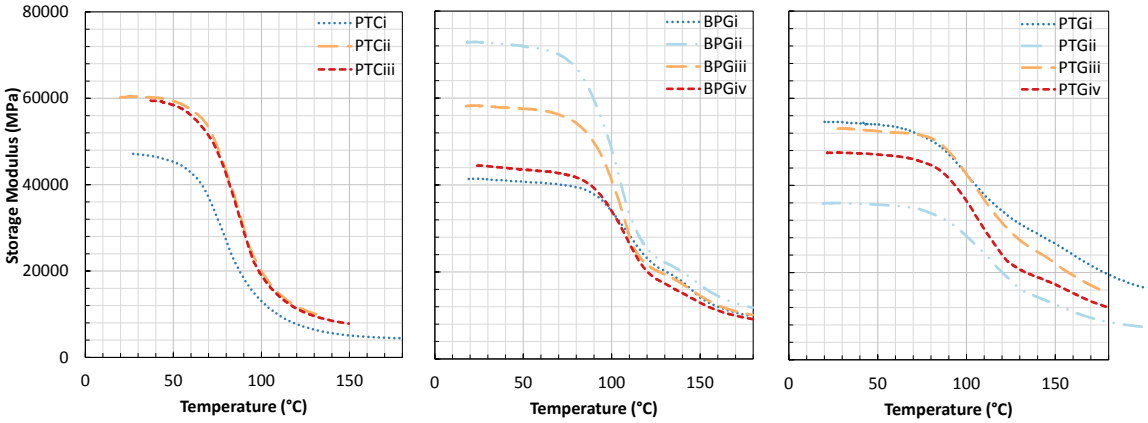

Figure 3-11: Non-normalised PTC Storage Modulus curves

Figure 3-12: Non-normalised BPG Storage Modulus curves

Figure 3-13: Non-normalised PTG Storage Modulus curves

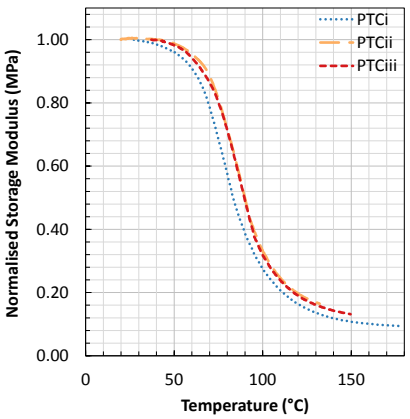

Figure 3-14: Normalised PTC Storage Modulus curves

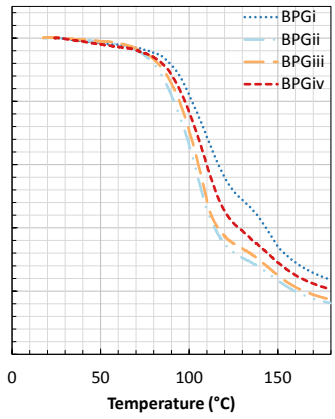

Figure 3-15: Normalised BPG Storage Modulus curves

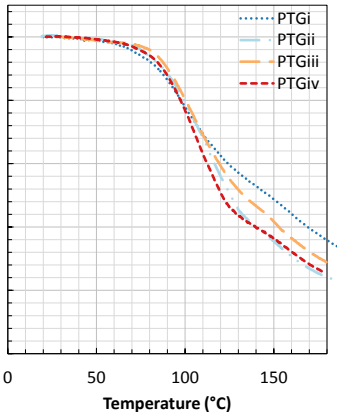

Figure 3-16: Normalised PTG Storage Modulus curves

While this might indicate a source of error in the measurement of the stiffness, it should be noted that definitions of T_g are typically based on the form of the curve rather than specific values. It can be seen from the PTG storage modulus curves that they form similar profiles, and thus indicate similar T_g values. The definitions used throughout this thesis identify key areas of interest in the material's thermo-mechanical behaviour.

3.4 THERMOGRAVIMETRIC ANALYSIS

Thermogravimetric analysis is a technique used to measure mass loss with increasing temperature to define key thermal events in the samples behaviour at elevated temperature. Specifically, for FRP this is useful because the organic polymer matrix undergoes degradation and decomposition leaving only the fibres behind. This influences the mechanical response of the FRP bar in concrete by inhibiting the stress transfer between fibres, subsequently can affect the bond, tensile and flexural capacity of the reinforcement.

3.4.1 Testing Methodology

A combined thermogravimetric and differential scanning calorimetry analyser (TGA/DSC 1), manufactured by Mettler Toldeo has been used for TGA experiments, as shown in Figure 3-17 and Figure 3-18.

Figure 3-17: Mettler Toledo TGA/DSC 1

Figure 3-18 FRP samples in TGA/DSC 1

Fragment samples were prepared as for DMA testing as described in section 3.3.1, with typical dimensions of approximately 5mm length, 5mm width, 3mm thickness with a weight ranging from 30-100 mg for GFRP and 20-60 mg for CFRP (see Figure 3-19 and Figure 3-20). These dimensions were required to allow the sample to fit into the testing crucibles (Figure 3-20). The samples were dried using desiccant, at ambient temperature (i.e. 20˚C), to ensure that they were not affected by moisture resulting from absorption of ambient relative humidity.

Due to the heterogeneous nature of the FRP samples, only fragment samples were prepared, as it would be difficult to ensure that powder samples were representative of the FRP bar. While powder samples may yield a more conservative decomposition temperature due to the size of the particles and subsequent increase surface area for decomposition (Lattimer & Ouellette, 2006), the fragment samples were sufficiently small to assume the reference (gas) temperature was equal to that of the sample temperature.

Figure 3-19 GFRP Sample Preparation for TGA

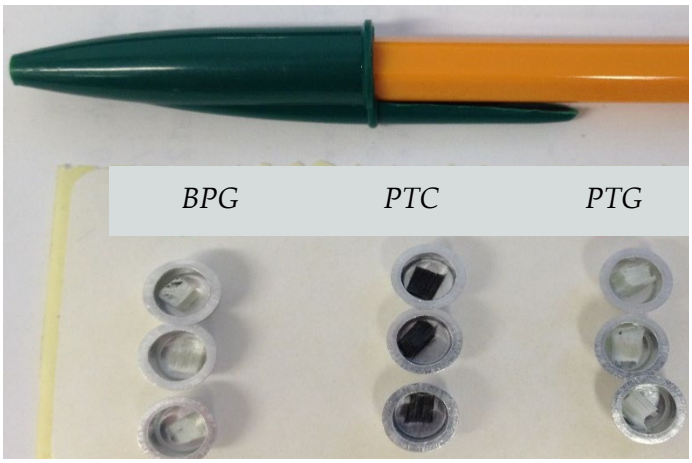

Figure 3-20 FRP TGA Samples in Aluminium Crucibles

Using a purge gas of nitrogen or air, samples were heated to a peak temperature of 800˚C (some tests were carried out at 600˚C where only aluminium crucibles were available). Heating rates of 5 and 10˚C/min were used where typical heating rates for TGA are between 2.5˚C/min and 20˚C/min. The variation in heating rates and in particular the use of lower heating rates allows greater clarity in understanding thermal reactions. A higher heating rate will cause reactions to overlap and overstate the temperatures at which decomposition of the polymer matrix occurs. In addition, 3 tests were performed for the glass FRP bars (BPG & PTG) where they were tested initially in nitrogen up to 800˚C and at a later date re-tested in air up to 800˚C. The test matrix for the TGA tests is shown in Table 3-5.

Blank crucibles were run for each set of variables to allow buoyancy corrections to be made to the sample data. This is required due to variation in density of the purge gas with temperature and the subsequent buoyancy force this applies to the sample (Wagner, 2009).

The gas temperature near the sample has been used to determine critical temperatures as the sample temperature is affected by the thermal conductivity of the polymer, and is subsequently dependent on the heating rate and decomposition of the sample itself.

Table 3-5 TGA Test Matrix

Specimen ID for each FRP Type			**Purge Gas**	**Max. Temperature**	**Heating Rate**
PTC	**BPG**	**PTG**		**˚C**	**˚C/min**
PTC8A5i	BPG8A5i*	PTG8A5i	Air	800	5
PTC8A5ii	BPG8A5ii*	PTG8A5ii			
PTC8A5iii	BPG8A5iii*	PTG8A5iii			
PTC8A10i	BPG8A10i	PTG8A10i			10
PTC8A10ii	BPG8A10ii	PTG8A10ii			
PTC8A10iii	BPG8A10iii	PTG8A10iii			
PTC8A10iv*	BPG8A10iv*	PTG8A10iv*			
PTC8A10v*	BPG8A10v*	PTG8A10v*			
PTC8A10vi*	BPG8A10vi*	PTG8A10vi*			
PTC8A10vii**	BPG8A10vii**	PTG8A10vii**			
PTC8A10viii**	BPG8A10viii**	PTG8A10viii**			
PTC8A10ix*	BPG8A10ix**	PTG8A10ix**			
PTC6N10i	BPG6N10i	PTG6N10i	Nitrogen	600	
PTC6N10ii	BPG6N10ii	PTG6N10ii			
-	BPG6N10iii	PTG6N10iii			
PTC8N10i*	BPG8N10i*	PTG8N10i*		800	
PTC8N10ii*	BPG8N10ii*	PTG8N10ii*			
PTC8N10iii*	BPG8N10iii*	PTG8N10iii*			

* Buoyancy corrections were made after the test was carried out.

**Samples were initially run in Nitrogen to 800°C and then re-tested in Air to 800°C (both tests were carried out at the same heating rate of 10°C per minute)

The unique identification for each test specimen is given herein in the form XXXTPHi, where:

- "XXX" indicates the FRP type, i.e. BPG, PTG, PTC,
- T indicates the maximum testing temperature (°C) (i.e. 6 for 600°C and 8 for 800°C)
- P indicates the purge gas
- "i" indicates the test repeat number for each set of variables in roman numerals.

For example, BPG6N10iii is the third TGA test carried out in Nitrogen, up to a maximum temperature of 600°C temperature on FRP type BPG.

One of the factors, which can affect the TGA measurement, is buoyancy, whereby the surrounding atmosphere produces an upward force on the sample. A blank crucible is used to quantify the buoyancy effect, and subsequently deducted from the mass measured in the FRP tests. This is necessary as gas density varies with temperature and thus the effect is not constant.

3.4.2 Determining the Decomposition Temperatures

Similar to the process for determining T_g there are various methods determining the critical temperatures for the decomposition of the FRP bars. In defining an approach to estimate the temperature for onset of mass loss and thus decomposition (T_d *Onset)* of the polymer matrix in the samples, a temperature at which a specific percentage of the normalised mass was lost was determined based on where the mass loss of the sample became linear. This was set as two percent for the GFRP bars (BPG & PTG) and three percent for the CFRP bar (PTC) on observation of the mass loss curves. An example of T_d *Onset* is shown in Figure 3-21. The value in this case is arbitrary other than to provide a meaningful comparison between tests for each FRP type.

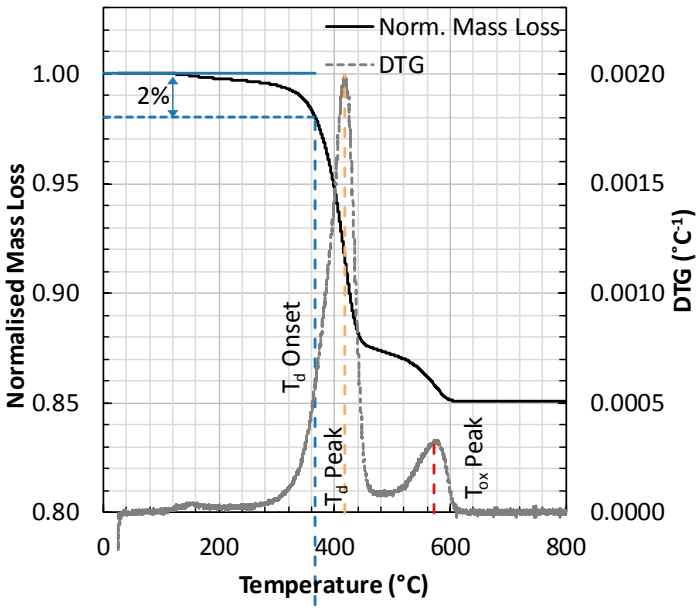

Figure 3-21: Schematic showing how to identify T_d and T_{ox} Peak from the Normalised Mass Loss and DTG curves (Test Specimen BPG8A10i)

To determine the peak decomposition temperature (T_d *Peak*) of the polymer matrix, the Derivative thermo-gravimetric (DTG) equation [3-7] was used for each sample, where the difference in the normalised mass (m^*) and the reference temperature (T_r) was used to calculate the derivative:

$$DTG = \frac{\Delta m^*}{\Delta T_r} \quad [3\text{-}7]$$

The peak of the derivative curve indicates the temperature at which the rate of mass loss (with respect to temperature) is greatest. An example of the determination of T_d *Peak* is shown in Figure 3-21.

Using the data collected from the samples tested twice, first in Nitrogen and then Air, the onset of oxidation (T_{ox} *Onset*) could be determined. An example of this analysis is shown in Figure 3-22, where the intersection of initial tangent and slope tangent on the mass curve defines T_{ox} *Onset*.

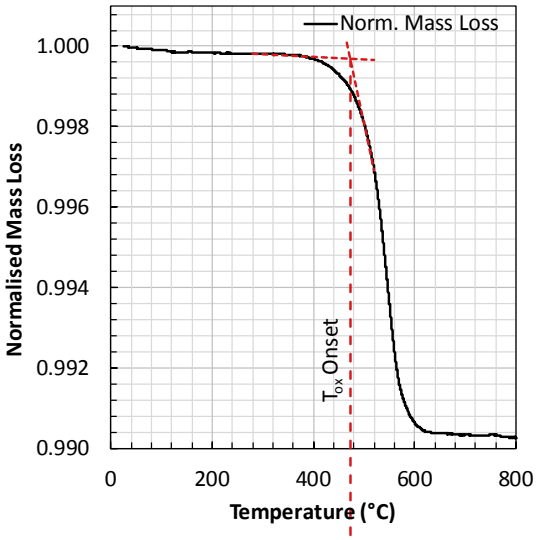

Figure 3-22: Schematic showing how to identify T_{ox} Onset from the Normalised Mass Loss Curve (Test Specimen BPG8A10vii)

To define the peak oxidation temperature (T_{ox} *Peak*), as with T_{ox} *Onset*, only samples tested in air can be analysed. On observation of the DTG curves, it can be seen that there is a difference between the samples tested in Air and those tested in Nitrogen, as shown in Figure 3-23 (Samples BPG8A10i vs BPG8N10i).

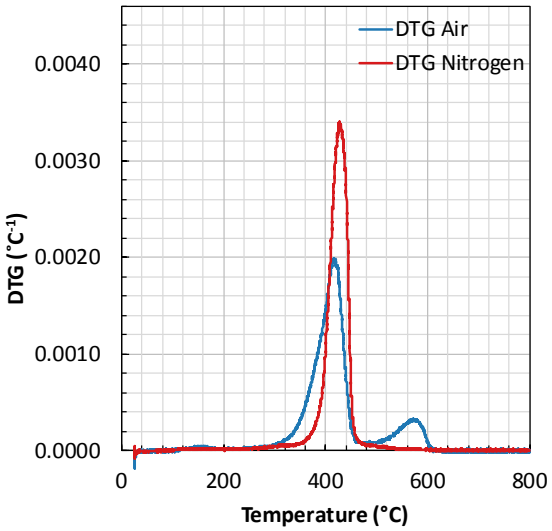

Figure 3-23 DTG Comparison of Purge Gases Air & Nitrogen

Unlike the nitrogen curve, the Air DTG curve has a second peak indicating a second thermal event where the oxidation of the polymer char occurs. An example of T_{ox} *Peak* is shown in Figure 3-21.

3.4.3 Analysis of TGA Results

3.4.3.1 Average TGA data

Figure 3-24 to Figure 3-26 shows the average normalised TGA values obtained for each set of test variables and FRP type. The yellow and red lines indicate the samples tested in nitrogen (note the "N" in the sample identifier), while the blue and black lines indicate samples tested in air ("A" in the sample identifier).

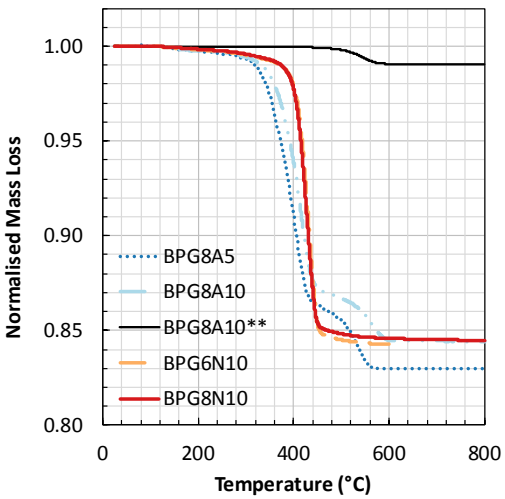

Figure 3-24: Average TGA Normalised Test Data for BPG

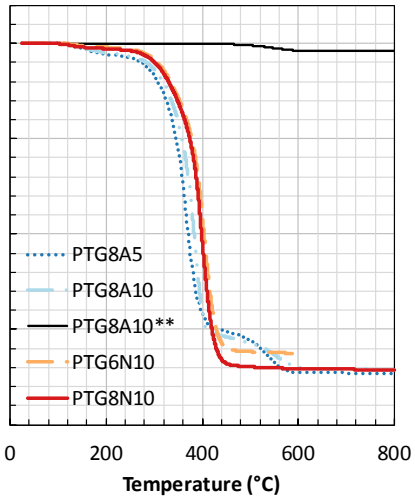

Figure 3-25: Average TGA Normalised Test Data for PTG

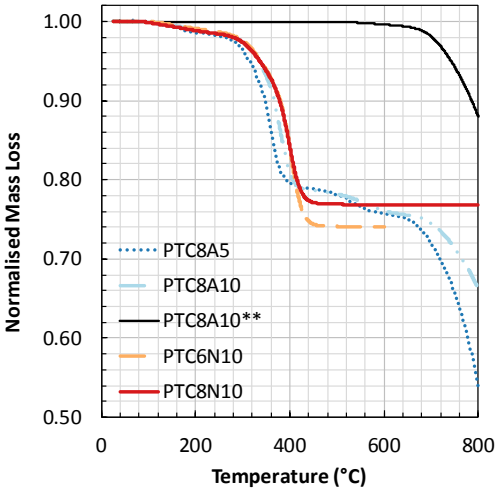

Figure 3-26: Average TGA Normalised Test Data for PTC

With the exception of the samples re-tested in air, there is a significant loss of mass in the samples which represents to the decomposition of the polymer matrix. In all of the bars tested this typically ends after 400˚C, where the mass then remains constant.

However in the case of the samples tested in air, there is a secondary event, where the decomposed polymer char oxidises. This oxidation is also evident by a small mass loss observed in the samples first run in nitrogen and then air. In contrast to the glass FRP bars, the carbon FRP samples are characterised by a third event. At this stage, the polymer matrix has decomposed and the char has oxidised, therefore this indicates, that the carbon fibres (note that this third event does not occur in the samples tested in nitrogen).

3.4.3.2 Decomposition and Oxidation Temperatures

The following tables (Table 3-6, Table 3-7 and Table 3-8) display the calculated decomposition and oxidation temperatures for BPG, PTG and PTC FRP bars respectively. As in Table 3-5, * denotes specimens where buoyancy corrections were made after the test was carried out and ** denotes specimens which were first tested in Nitrogen up to 800°C and then retested in Air to 800°C. Averages have been calculated for each set of test variables. On observation of the data sets for bar PTC, it was not possible to determine T_{ox} *Onset*. This is implies that very little polymer char remained on the fibres, prior to the samples being re-tested in air, and therefore there was no mass to lose in this case.

Table 3-6: BPG TGA Decomposition & Oxidation Temperatures

Specimen ID	T_d Onset (˚C)		T_d Peak (˚C)		T_{ox} Onset (˚C)		T_{ox} Peak (˚C)	
		Avg.		Avg.		Avg.		Avg.
BPG8A5i*	343.33	342.72	404.75	407.69			533.83	537.42
BPG8A5ii*	344.67		415.25				541.83	
BPG8A5iii*	340.17		403.08		-		536.58	
BPG8A10i	366.67	364.94	388.67	407.61	-	-	571.50	570.39
BPG8A10ii	364.83		416.83		-		573.83	
BPG8A10iii	363.33		417.33		-		565.83	
BPG8A10iv*	352.17	355.11	413.33	414.00	-	-	557.67	565.06
BPG8A10v*	358.50		413.33		-		568.33	
BPG8A10vi*	354.67		415.33		-		569.17	
BPG8A10vii**	-	-	-	-	472.22	474.22	546.00	545.33
BPG8A10viii**	-		-		477.69		546.50	
BPG8A10ix**	-		-		472.74		543.50	
BPG6N10i	397.67	398.28	429.33	430.00	-	-	-	-
BPG6N10ii	400.50		430.33		-		-	
BPG6N10iii	396.67		430.33		-		-	
BPG8N10i*	397.67	397.39	427.33	427.33	-	-	-	-
BPG8N10ii*	396.83		427.83		-		-	
BPG8N10iii*	397.67		426.83		-		-	

* Bouyancy corrections were made after the test was carried out.

**Samples were initially run in Nitrogen to 800˚C and then re-tested in Air to 800˚C (both tests were carried out at the same heating rate of 10˚C per minute)

Table 3-7: PTG TGA Decomposition & Oxidation Temperatures

Specimen ID	T_d Onset (˚C)		T_d Peak (˚C)		T_{ox} Onset (˚C)		T_{ox} Peak (˚C)	
		Avg.		Avg.		Avg.		Avg.
PTG8A5i	309.25	308.38	369.00	367.22	-	-	533.83	536.64
PTG8A5ii	305.13		365.58		-		536.33	
PTG8A5iii	310.75		367.08		-		539.75	
PTG8A10i	323.83	326.00	388.67	389.94	-	-	570.17	564.89
PTG8A10ii	326.00		389.33		-		564.83	
PTG8A10iii	328.17		391.83		-		559.67	
PTG8A10iv*	312.00	310.00	383.33	384.00	-	-	552.50	554.17
PTG8A10v*	306.83		387.33		-		557.00	
PTG8A10vi*	311.17		381.33		-		553.00	
PTG8A10vii**	-	-	-	-	460.38	460.38	556.50	551.22
PTG8A10viii**	-		-		463.74		541.17	
PTG8A10ix**	-		-		457.04		556.00	
PTG6N10i	337.83	333.78	401.83	400.33	-	-	-	-
PTG6N10ii	329.00		399.83		-		-	
PTG6N10iii	334.50		399.33		-		-	
PTG8N10i*	329.50	329.61	396.33	396.83	-	-	-	-
PTG8N10ii*	330.33		396.33		-		-	
PTG8N10iii*	329.00		397.83					

* Buoyancy corrections were made after the test was carried out.

**Samples were initially run in Nitrogen to 800˚C and then re-tested in Air to 800˚C (both tests were carried out at the same heating rate of 10˚C per minute)

Table 3-8: PTC TGA Decomposition & Oxidation Temperatures

Specimen ID	T_d Onset (˚C)		T_d Peak (˚C)		T_{ox} Peak (˚C)	
		Avg.		Avg.		Avg.
PTC8A5i	297.17	291.11	365.33	364.06	527.00	528.28
PTC8A5ii	296.58		363.58		527.08	
PTC8A5iii	279.58		363.25		530.75	
PTC8A10i	314.67	314.33	388.83	387.06	568.33	568.72
PTC8A10ii	314.17		383.50		570.00	
PTC8A10iii	314.17		388.83		567.83	
PTC8A10iv*	304.33	301.89	377.83	377.39	554.83	555.89
PTC8A10v*	299.67		378.00		560.50	
PTC8A10vi*	301.67		376.33		552.33	
PTC8A10vii**	-	-	-	-	-	-
PTC8A10viii**	-		-		-	
PTC8A10ix*	-		-		-	
PTC6N10i	310.17	309.40	399.83	400.83	-	-
PTC6N10ii	313.00		401.83		-	-
PTC8N10i*	304.17	307.94	399.83	400.50	-	
PTC8N10ii*	310.67		400.83		-	
PTC8N10iii*	309.00		400.83		-	

* Buoyancy corrections were made after the test was carried out.

**Samples were initially run in Nitrogen to 800˚C and then re-tested in Air to 800˚C (both tests were carried out at the same heating rate of 10˚C per minute)

For the tensile testing as described in chapter 4, the values determined from the samples tested up to 800˚C in air at a heating rate of 10˚C per minute have been used. Furthermore only the samples were buoyancy corrections were made after the test have been used. Figure 3-27 and Figure 3-28 shows the range of the decomposition and oxidation temperatures for each of the three FRP bar types tested in air, with the error bars in the plot defined as ± 3 standard deviations from the mean values determined from three identical repeat tests, to give an indication of the variability in the data.

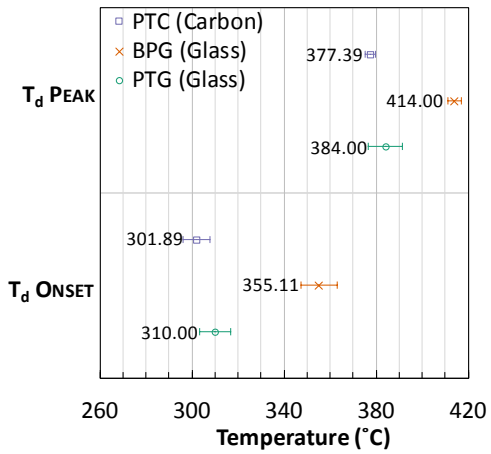

Figure 3-27: Measured T_d ranges for FRP Bars (error bars show 3 standard deviations from the sample mean values)

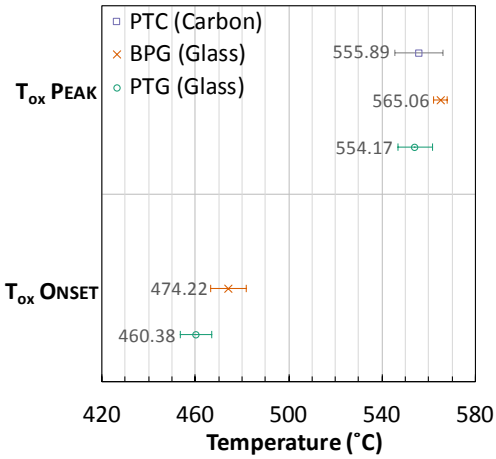

Figure 3-28: Measured T_{ox} ranges for FRP Bars (error bars show 3 standard deviations from the sample mean values)

3.4.3.3 Further analysis

As discussed in section 3.4.2, the percentage mass loss for *T_d Onset* was chosen on observation of the mass loss curves for each FRP type. If there were significant differences in the mass loss profiles for each bar type due to variances in the fibre volume fraction, this method would not be appropriate. Figure 3-29 to Figure 3-32 show the variability in the tested samples for the normalised mass loss for bar BPG. In Figure 3-29, where samples were tested in Air at a rate of 10˚C per minute up to 800˚C, they were relatively small differences in the sample mass below 400˚C and a maximum of 1% difference, to the average value, up to 800˚C. Additionally the response of the bar for each set of test variables is consistent at the onset of decomposition, and during peak decomposition. It is only at the end of the decomposition process where the variability in results occur.

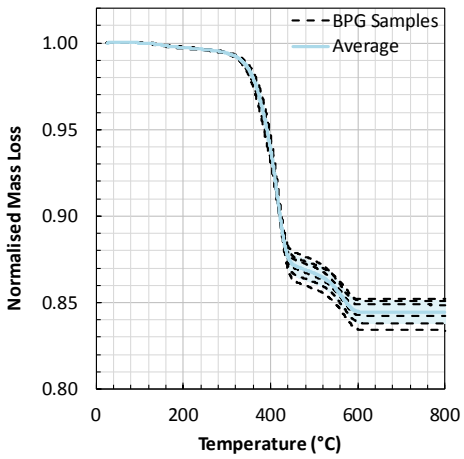

Figure 3-29: BPG TGA Samples (Air, 800˚C, 10˚C/min)

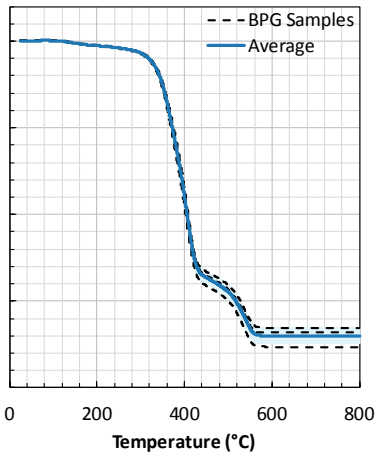

Figure 3-30: BPG TGA Samples (Air, 800˚C, 5˚C/min)

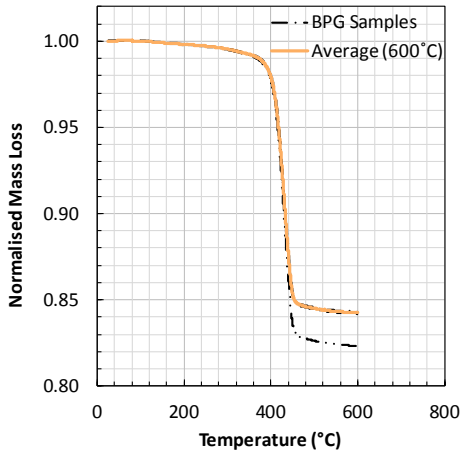

Figure 3-31: BPG TGA Samples (Nitrogen, 600˚C, 10˚C/min)

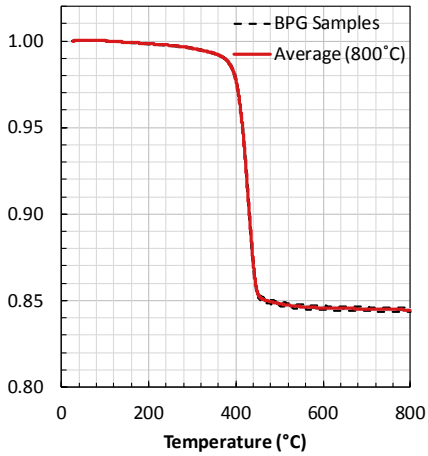

Figure 3-32: BPG TGA Samples (Nitrogen, 800˚C, 10˚C/min)

The glass FRP results highlight two key thermal events when tested in Air; decomposition (pyrolysis) of the organic polymer matrix, and oxidation of the remaining carbonaceous char, leaving the remaining inorganic glass fibres. While the CFRP (PTC) also experienced these events, the further thermal events occur after 600˚C, whereby the organic carbon fibres themselves begin to oxidise and decompose. A comparison of the GFRP samples (BPG, PTG) and CFRP (PTC) is shown in Figure 3-33. Unlike the BPG & PTG DTG curves which reduce to zero approaching 600˚C, the PTC DTG curve increases beyond 600˚C indicating the rate of mass loss with respect to temperature is increasing.

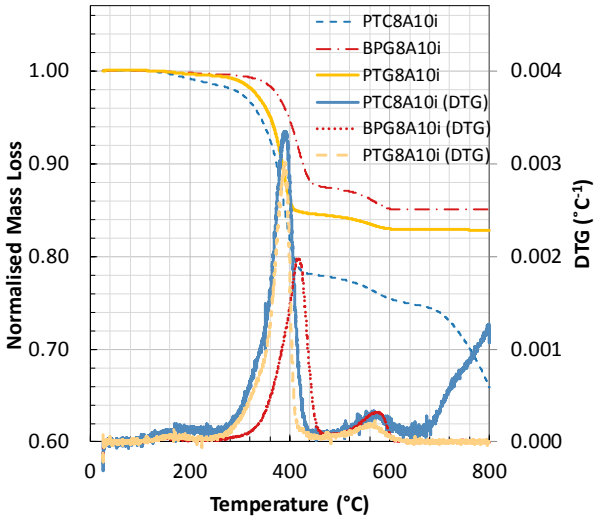

Figure 3-33: Comparison of TGA Data and Analysis for GFRP (BPG) & CFRP (PTC)

Table 3-9 shows the normalised mass retained for each FRP bar, averaged for each set of test variables. The mass loss is approximately as expected of the GFRP bars as the percentage fibre content (by weight) is 83.6% and 83% (Table 3-1) for bars BPG and PTG respectively, the average values recorded in Table 3-9 are in good agreement with these.

Unfortunately, there is no manufacturer specified value for the percentage fibre content for PTC, however the average from Table 3-9 indicates this is approximately 75.7%. The values of mass retained have been taken at 600˚C due to the oxidation of the carbon fibres, as discussed previously. It is acknowledged however, that there may be some overlap in thermal events/reactions and the percentage fibre content indicated by the results is not definitive.

Table 3-9: Normalised Mass Retained for each FRP type

FRP Type	800˚C 10˚C/min Air	800˚C 5˚C/min Air	600˚C 10˚C/min Nitrogen	800˚C 10˚C/min Nitrogen	Average
BPG	0.844	0.830	0.843	0.845	0.840
PTG	0.829	0.827	0.837	0.829	0.830
PTC*	0.761	0.758	0.740	0.768	0.757

* Average values have been taken at 600˚C.

As the FRP bars are used as a reinforcing material and are thus embedded in concrete the oxygen supply to the bars is restricted by crack widths and therefore the onset of decomposition of the polymer matrix can be delayed. This can be seen in Figure 3-24 and Figure 3-25 where the rate of mass loss for the GFRP samples tested in nitrogen compared to air is initially lower, with peak decomposition in nitrogen tests occurring a minimum of 16 °C higher (up to 23 °C) than the samples tested in air. Correia, Gomes, Pires, & Branco (2013) also observed a higher decomposition temperature for FRP samples tested in air in comparison to those tested in nitrogen; however, without the data this cannot be quantified. There are limited examples of TGA tests on FRP samples carried out in both air and nitrogen atmospheres to provide further meaningful comparisons.

Based on the experimental data included herein, the referenced literature, a preliminary conclusion can be drawn that the samples tested in air may be comparatively conservative in the determination of the decomposition temperatures.

While the analysis presented is indicative of the thermal range of application and criticality of the bars, the analysis does not include a determination of the thermal properties of the sand coating. The coating is applied during a secondary curing process, and thus while the degradation and decomposition of the matrix might be characterised, the critical component of the bars may be heavily reliant upon the performance and susceptibility of the mechanical bond of the FRP bars. Further discussion on the implications of elevated temperature on the bond behaviour of the FRP bars in concrete is discussed in chapter 5.

3.5 Further Work

As previously discussed, the test and calculation method used to define T_g and T_d is rarely stated in literature, despite the clear significant difference in the values that might be quoted on the basis of the various available test methods and T_g definitions available in the literature. Researchers must be clearer about the method chosen, the associated standard or reference for this. More research is needed to demonstrate the

variability in the glass transition temperature values, similar to the work carried out by Bakis et al. (2014).

During sample preparation, care was taken to ensure specimens were extracted from the core of the bar, to ensure uniformity. However, it is suggested that in a larger sample set, it would be prudent to take samples from various locations within the bar. This author anticipates that there may be more variability in the results with larger bar diameters as the bars are cured from the outside. It is recommended that research is undertaken to investigate this.

In the DMA testing, it is recommended that a comparable analysis is undertaken for samples tested in three point bending to better understand the influence of the testing setup on the results from the bars.

3.6 CHAPTER SUMMARY

Three FRP bars (2 glass and 1 carbon) have undergone thermomechanical procedures using Dynamic Mechanical Analysis and Thermogravimetric Analysis. In contrast to typical reporting on glass transition of FRP bars, this author has presented the case for T_g to be considered as a range rather than a single value. More importantly, emphasis is placing on clearly stating the method used to define a single point value within this range. Five methods following DMA have been used to identify T_g, based on those available in literature and active standards, with three of the five methods as testing temperatures in Chapter 4 and Chapter 5. *Tg Offset* and T_g *Loss Modulus* have been discounted due to larger error bars and proximal values to other T_g definitions. The results from the DMA showed good repeatability and the glass transition ranges identified for the bars showed good correlation with those presented in the literature review.

To determine decomposition temperatures, Thermogravimetric Analysis has been used with samples varied by bar type, purge gas, heating rate and maximum test temperature. Some samples were re-tested to determine the impact of nitrogen vs air. Similarly to DMA, the results of the TGA were repeatable. The behaviour of the bars

was typically characterised by two events, mass loss associated with the decomposition of the polymer matrix and oxidation of the polymer char (only samples tested in air). In addition carbon samples underwent a third event, whereby oxidation of the carbon fibres occurred (only samples tested in air). There was good agreement between the fibre volume fraction determined from the tests, and those reported by the manufacturers, for the Glass FRPs. Critical temperatures established based on the decomposition of FRP in air, are considered to be more conservative than those tested in nitrogen. The results from the samples tested in air will be provide valuable inputs to the experiments discussed later in the thesis. While no analysis of the sand coating was possible in either DMA or TGA, the impact of the sand coating on bond will be considered in Chapter 5.

Ultimately, the research carried out recognises that FRP bars are proprietary products and in order to identify trends in their thermo-mechanical behaviour, bench-scale characterisation tests, i.e. DMA and TGA, must be undertaken for each product. The information gathered from these tests is invaluable and importantly it is relatively simplistic to obtain, once samples have been prepared. There is no reason why this could not be undertaken for all FRP bars with both test machines commercially available, therefore enabling a test programme to be commissioned in house or externally. This would allow the user to set conservative temperature limits (e.g. T_g *Onset*) where no other information is available with regard to structural behaviour at elevated temperature or conduct a more informed performance based analysis using models developed through research. Crucially the temperatures assessed using these methods, are used as test temperatures for the tensile and bond experiments in the following chapters, which permits the determination of a relationship between bench scale analysis and elemental behaviour of FRP reinforcing bars, provide a valuable input to performance based design

CHAPTER 4 REDUCTIONS IN TENSILE PROPERTIES OF FRP BARS AT ELEVATED TEMPERATURE

4.1.1 Chapter Overview

The ambient tensile capacity of FRP bars is typically much greater than that of steel making FRP an attractive option for reinforcement in concrete. However, the negative influence of temperature on the tensile capacity is well documented, but challenging to quantify due to the great variability of FRP. The ability of FRP reinforcement to maintain tensile capacity is a factor in determining the fire resistance of reinforced concrete. As demonstrated previously in Chapter 3, the softening of the polymer matrix on heating, in the glass transition temperature range (T_g *Onset* to $T_g Tan\delta$), reduces the shear stiffness of the polymer matrix of the FRP, and the onset of thermal decomposition of the polymer matrix can inhibit stress transfer between fibres and thus load carrying ability.

The proprietary nature of the FRP bars relies on individual characterisation, requiring a significant investment in testing which is ultimately expensive, inefficient and time consuming. Whilst models currently exist to predict tensile strength loss with temperature of FRP reinforcement, more research, that is experimental, is required to validate them. The research presented in this chapter seeks to minimise the minimum suite of tests required to understand tensile strength loss with temperature for a specific FRP bar using a novel predictive model directly related to the bench scale thermomechanical analysis testing carried out in Chapter 3. This simplified approach to understanding of tensile strength loss with temperature of specific FRP reinforcement can then be used as an input into structural fire design of FRP reinforced concrete. Current guidance (ACI 440.1R-15) permits a performance based design methodology.

In order to validate the model steady state direct tensile tests were performance on each of the three FRP bars at glass transition and decomposition temperatures determined using thermomechanical analysis in Chapter 3.

4.2 TENSILE TESTING METHODOLOGY

4.2.1 Tensile Testing Apparatus

The tensile testing of FRP reinforcing bars was carried out at the University of Edinburgh using an Instron 600LX materials testing frame. In addition, this testing frame has a bespoke in-built environmental chamber that can be used to heat the specimens to temperatures in the range of 600°C (refer to Figure 4-1, Figure 4-7 and Figure 4-8). The full testing matrix of materials tested, temperatures studied, etc., is presented in Section 4.2.3.1.

Figure 4-1: Instron 600LX with wedge action grips and built-in environmental chamber

Typical wedge action grips were not suitable for testing. It was therefore necessary to develop a special anchorage system, the development of which, is discussed in the following sections.

Due to the high tensile capacity of the CFRP (PTC) bars used in the current study (with a manufacturer-specified tensile capacity of 1431MPa), the ambient temperature tensile tests for these bars were not possible at the University of Edinburgh. These were performed by the author using an Amsler Universal Testing Machine at the Swiss Federal Research Institute for Materials Science and Technology (EMPA) in Zurich, Switzerland using a proprietary set of conical grips developed by

Professor Giovanni Terrasi. With the exception of the grips, the test set-up were very similar to those carried out at the University of Edinburgh.

4.2.2 Development of Anchorage System(s)

Steel reinforcing bars are typically anchored and successfully tested using mechanical wedge action grips with serrated v-notch grip faces (Micelli and Nanni, 2003). The differences in lateral strength and stiffness of FRP bars, as well as the propensity of FRP materials to fail prematurely when pinched, make this technique unsuitable for FRP bars.

Two approaches can be used to overcome this and to provide anchorage so that FRP bars can be tested to failure in tension;

(1) using a full diameter (i.e. 360°) wedge action, similar to a prestressing steel anchor (Bakis *et al.*, 1996), or
(2) relying on mechanical interlocking and/or adhesion of the bar's surface coating within a potting material in a cylindrical tube (Erki and Rizkalla, 1993).

The latter of these two options was chosen in the current study due to the specific geometry of the testing machine (i.e. maximum crosshead spacing) and the large number of samples being tested. The anchorage setup was modified to accommodate a pin connection with the instron 600LX.

Whilst circumferential wedge action can be preferable for high strength FRP bars, it is necessary to carefully optimise the correct geometry of the wedge and the stiffness of the wedge materials for each specific FRP formulation. This is to ensure that localised crushing or pinching of the bar does not occur; this was beyond the scope of the research presented in this thesis.

To create the potting tubes, 275mm lengths of 38mm diameter stainless steel solid round bar was cored to provide a central bore with an internal diameter of 22mm. The internal diameter at one end of the bar was reduced to 13mm, over a length of 25mm, to prevent the potting material from pulling out of the anchorage tube (refer

to Figure 4-2). In addition, an 18mm transverse hole was drilled out at one end to allow the anchors to be secured within the testing frame.

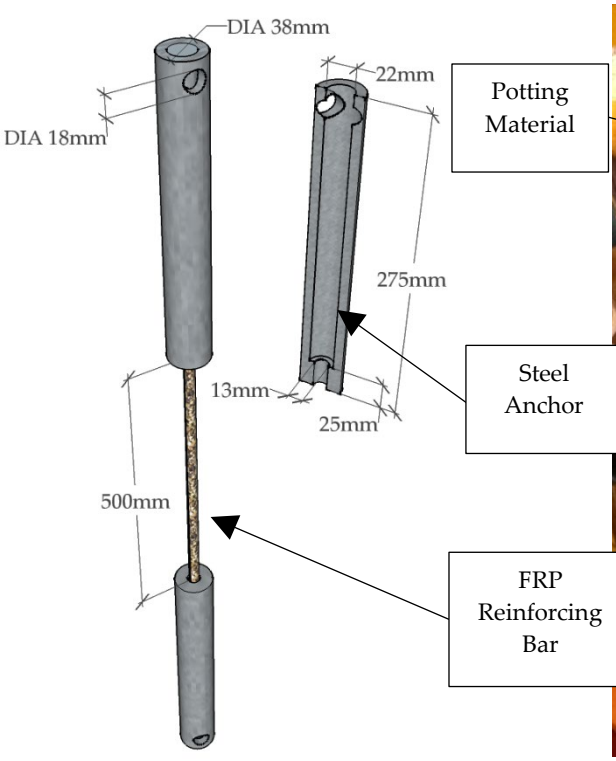

Figure 4-2: Potting anchor details and dimensions

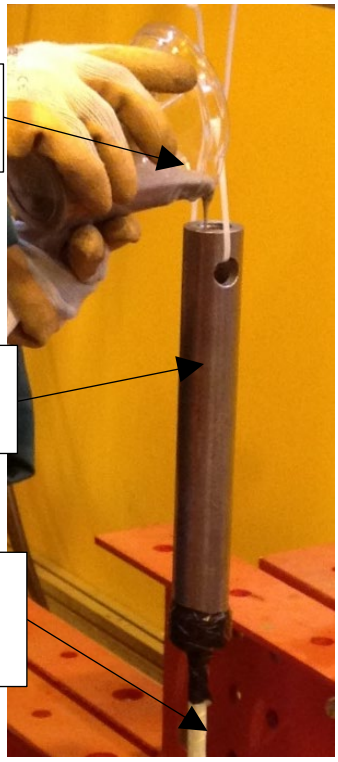

Figure 4-3: Pouring potting material into anchor tubes

In preparing the samples, each FRP bar type was cut into test specimens of one metre length. To pot the FRP bars within the anchor tubes, the FRP bars were inserted into the metal anchors up to the underside of the transverse hole. A plastic cap was secured at the bottom end of the anchor tube, and securely taped to hold the FRP bar concentrically in place. The anchor and bar were then hung from the transverse hole in the anchor, using gravity to naturally align the specimens vertically while the potting material set (see Figure 4-3).

A range of anchorage problems were experienced during the subsequent tests, and alterations were made throughout the testing programme. Two potting materials were used in the current study; (1) a microsilica-filled epoxy system (Gurit SP106 & Fillite filler) and (2) an expanding cementitious grout (Dexpan, typically used for non-explosive demolition purposes). Researchers have demonstrated that expansive grout

is typically the most reliable method for gripping FRP bars (Wang, Wong, & Kodur, 2007). The potting materials were prepared and poured into the anchors (Figure 4-3). Each anchor assembly was left to cure for at least 24 hours based on manufacturer instructions, and this process was repeated for the opposite end of the test specimen.

During initial testing, it was observed that, for the ambient and lower temperature tests, the shear strength of the microsilica epoxy system, and in some cases the coating of the bars, was insufficient to develop the full tensile strength of the bar before failure of the anchorage system and pull-out of the bar from the anchorage tube. Thus, the expanding grout system (similar to that documented by Wang *et al.* 2003) was used for some of the subsequent tensile tests to better ensure that the bar could be anchored up to tensile rupture of the bar (which was a challenge to achieve, as discussed below). Due to limitations of the total clearance between crossheads in the Instron 600LX testing frame, it was not possible to extend the anchorage tubes and obtain a stronger anchorage.

For the ambient temperature tests on the CFRP (PTC) bars, which were never successfully tested to failure at the University of Edinburgh using the anchorage system described above, a specialist anchorage was developed at EMPA, through a collaborative effort with Dr Giovanni Terrasi who is a specialist in this area. The bars were potted using an epoxy resin cast in a conical shape, and the steel anchors were wedge shaped internally (see Figure 4-4 and Figure 4-5). Unlike the tests carried out at the University of Edinburgh, the anchors were screwed into bespoke connectors (Figure 4-6) to attach to the testing apparatus. Whilst this was an effective approach, such anchors could not be implemented at Edinburgh due to temporal, geometric, and financial constraints.

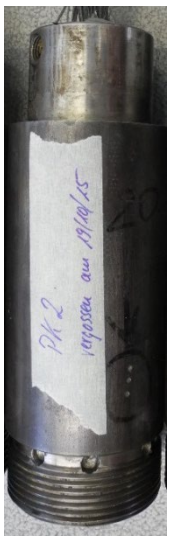

Figure 4-4: Steel anchors with conical internal bores for ambient temperature tests on CFRP (PTC) bars

Figure 4-5: Conical resin wedge cast around CFRP (PTC) bar and placed inside the steel anchor of Figure 1-4

Figure 4-6: Amsler test machine connectors at EMPA

4.2.3 Tensile Testing Procedure

In preparation for the direct tensile tests, samples were inserted into the Instron 600LX in such a manner that only the FRP bar was within the environmental chamber, and the metal anchor tubes were maintained outside the chamber to ensure cold anchorage of the reinforcement. The anchors were secured using bespoke connectors that were manufactured in-house for the Instron 600LX, using an 18mm stainless steel pin as shown in Figure 4-7 and Figure 4-8. This approach ensured that these tests focused on the tensile strength of well-anchored FRP bars, rather than also being affected by bond strength.

The top and bottom of the environmental chamber within the Instron 600LX testing frame have holes through which the sample can pass, therefore the FRP bar was wrapped in loose ceramic fibre insulation within these holes to minimise thermal losses from inside the chamber (see Figure 4-9). In addition this minimised the effect of hot gasses on the metal anchorage tubes. The environmental chamber is fitted with a fan to ensure a uniform internal gas temperature during heating of the samples.

A thermocouple within the chamber was used to provide feedback for controlling the oven temperature, though these control temperature data could not be directly recorded, due to the hardware configuration. However, for the majority of the samples tested four thermocouples (TCs) were placed within the testing chamber; two of which were placed directly in contact with the surface of the FRP bar, as shown in Figure 4-10

To gain an accurate reading of the surface temperature of the bar, a small piece of insulation (3mm x 3mm x 1mm) was placed over the top of the tip of the thermocouple and then attached to the bar using aluminium adhesive tape. A short length of 20mm diameter wire was then used to secure the thermocouple firmly in place. If the thermocouple were not secured to the bar, the TC would measure the temperature of the air within the chamber (since the small diameter of the TC tip would be dominated by convective heat transfer from the turbulent gases within the chamber). Whilst the inclusion of the fan within the oven is intended to evenly distribute the temperature, it is acknowledged that localised heat/cooling effects from the currents within the chamber could occur. As such, one of the two thermocouples on the FRP bars' surface was placed to the side, to capture any obvious effect. Further details of the thermocouple locations are provided in Figure 4-10 and Table 4-1.

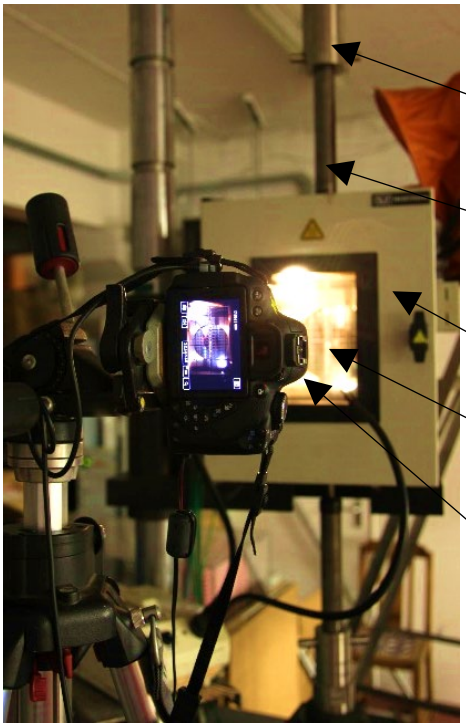

Figure 4-7: Photo of typical direct tensile test setup

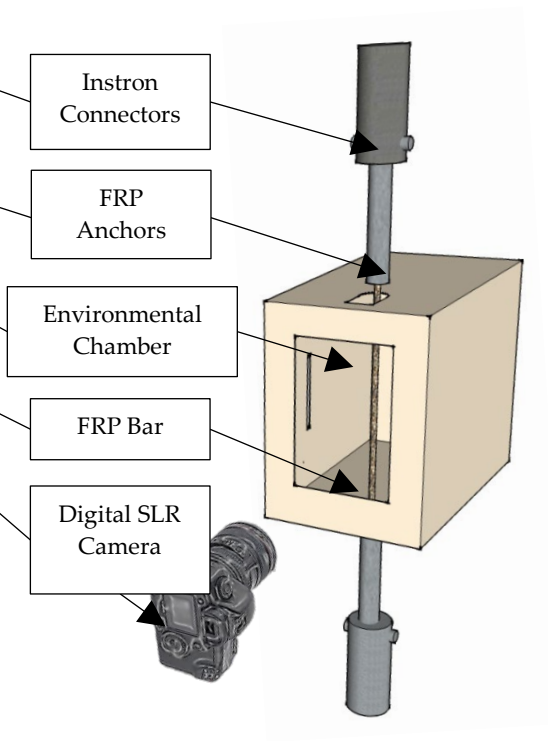

Figure 4-8: Schematic showing various components of direct tensile test setup

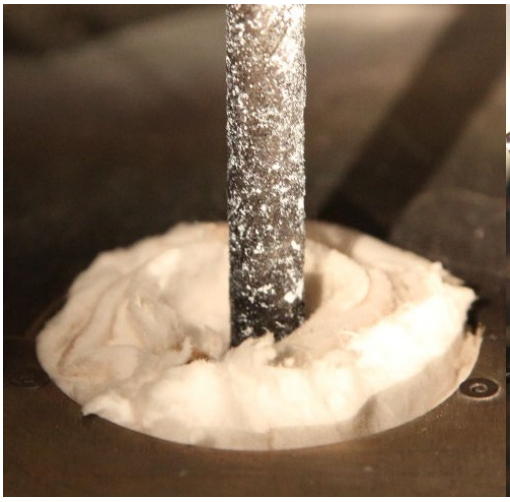

Figure 4-9: Insulation wrapped around FRP as it exits the top hole in the environmental chamber to maintain steady internal temperature

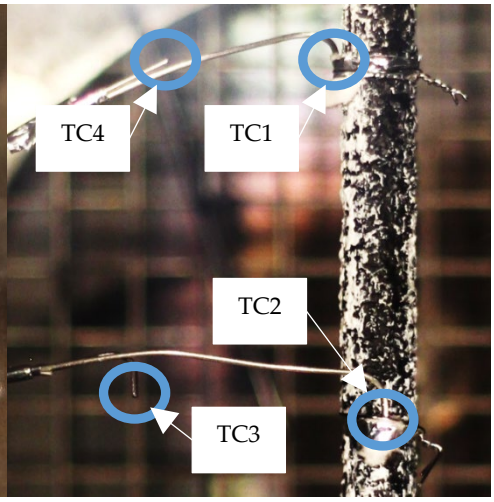

Figure 4-10: Thermocouple placement on the FRP bar (monitoring bar temp.) and within the environmental chamber (monitoring air temperature)

Table 4-1: Thermocouple locations on the FRP bars and within the environmental chamber during testing

Thermocouple Name	**Location** *(see Figure 4-10)*
TC1	• Attached to the FRP bar • 100mm below the top inside surface of the environmental chamber • Placed on the left side of the bar
TC2	• Attached to the FRP bar • 155mm below the top inside surface of the environmental chamber • Placed on the front side of the bar (i.e. visible through the window in the environmental chamber)
TC3	• Exposed to chamber air temperature • 155mm below the top inside surface of the chamber • Approximately 50mm from the FRP bar's surface
TC4	• Exposed to chamber temperature • 100mm below the top inside surface of the chamber • Approximately 50mm from the FRP bar's surface

In general, tensile tests were performed under steady-state thermal conditions wherein the bars were heated up to their test temperature, at a rate of 5°C per minute until the target test temperature was reached. The sample was then held at the target temperature for between 20 and 60 minutes (longer for higher temperatures) to allow the samples to reach uniform internal temperature and to minimise any thermal gradients in the samples that could affect the results. By using steady state as the primary mode of testing, this provides a more conservative approach to determining tensile strength loss with temperature.

The bars were stressed to a sustained low stress level of 10 MPa during heating (under load control) to account for thermal expansion during heating (Hajiloo, Gales, Noël,

et al., 2015). After reaching isothermal conditions, the samples were tested in direct tension, under displacement control at a crosshead stroke rate of 2mm per minute, until failure. Digital image correlation (DIC) analysis was also used to measure the bars' deformations so as to approximately determine the bars' tensile elastic modulus; images were acquired at a frame rate of 0.2 Hz, using a Canon EOS 5D Mark II digital single lens reflex camera with a remote trigger timer. The FRP bars were spray-painted black using high temperature spray paint, and a white speckle pattern was applied by hand to aid in the DIC analysis. While the data for the digital image analysis was collected, the analysis of this data to determine tensile strain was beyond the scope of the thesis, and it is intended that analysis will take place at a later date to further reinforce the outcomes from these experiments.

In addition, two transient thermal regime tests were performed at 20% of the ambient temperature tensile capacity for each of the GFRP bars (BPG & PTG), and a single transient test was carried out for the CFRP bar (PTC) at 25% of the bar's ambient capacity. In these tests, the samples were loaded to a sustained tensile load, and this load was held constant while the ambient temperature in the environmental chamber was increased at a rate of 5^{o}C per minute until failure occurred. This small number of transient thermal regime tests were performed to:

(1) check that a similar response was observed in both transient and steady-state thermal regime conditions at similar loading levels (although note that transient thermal regime tests involve a thermal gradient over the FRP bars' cross-section, and so a somewhat higher tensile strength and stiffness would be expected in these cases), and
(2) check the critical temperature for each of the bars under a realistic heating rate for an FRP bar embedded within concrete, when the bar is loaded to a sustained level equal to the maximum permissible service stress in an FRP bar as dictated by available design codes, i.e. 20% of ultimate for GFRP (ACI 440.1R-15).

While this was the intention for the CFRP bar also, it was determined during testing that the maximum stress achievable during a high temperature steady state tensile

test was around 50% of the ultimate tensile capacity of the CFRP. As such the CFRP tests were carried out at 25% of ultimate capacity to ensure the bars could fail by rupture of the fibres during a transient test. It is acknowledged this may not be representative of the strength utilisation in practice for FRP reinforced concrete.

4.2.3.1 Tensile Testing Matrix

Test temperatures for the steady state thermal regime tests varied from room temperature up to 580˚C. The test matrix for both steady state and transient thermal regime testing is shown in Table 4-2. Variations in the number of specimens tested were due to pilot testing and adaptation of the anchorage system. In some cases, the actual bar surface temperatures achieved during tensile tests on the FRP bars varied slightly from the nominal test temperatures noted in Table 4-2, typically due to the thermal inertia of the environmental chamber during heating. This does not have a negative impact on the results however, as tensile test results are plotted against the measured temperature.

Table 4-2 Tensile Testing Matrix

Temperature Definition*	**BPG**		**PTG**		**PTC**	
	Temp. (˚C)	**No.**	**Temp. (˚C)**	**No.**	**Temp. (˚C)**	**No.**
Ambient **	20	4	20	3	20	4
T_g *Onset*	86	3	83	3	-	
T_g *Modulus*	109	4	105	2	-	
	-	-	136	2	-	
T_g *Tan δ*	136	3	154	3	-	
	149	2	-	-	-	
	225	2	225	2	-	
	300	2	275	2	-	
T_d *Onset*	355	3	310	3	302	3
T_d *Peak*	415	3	384	3	377	3
	-	-			400	1
T_{ox} *Onset*	-	-	460	3	-	
T_{ox} *Peak*	565	3	550	1	556	3
	-	-	570	1	580	3
	Load Level (%)	**No.**	**Load Level (%)**	**No.**	**Load Level (%)**	
Transient	20	2	20	2	25	1

*As defined in Chapter 3.

**Ambient temperature of the lab typically fluctuated seasonally between 10˚C and 25˚C, and this is not considered significant for the tensile performance of the FRP bars.

The unique identification for each test specimen is given herein in the form XXX_YYYi, where "XXX" indicates the FRP type, i.e. BPG, PTG, PTC, YYY indicates the testing temperature (˚C) or load level (as a percentage of ambient) and "i" indicates the test repeat number for each set of variables in roman numerals. For example, BPG_20iii is third steady state test carried out at ambient temperature on

FRP type BPG, and PTC_trans25i is the first transient test carried out at 25% of the ambient load capacity on FRP type PTC.

Data recorded during testing included temperatures (as described previously), tensile load and crosshead stroke.

4.2.4 Pilot Testing

In order to determine the feasibility of tensile tests in the Instron 600LX and anchoring technique as outlined in section 4.2.2 and 4.2.3, a pilot study was carried out on an alternate GFRP bar. The bar and selected manufacturer properties are shown in Figure 4-11 and Table 4-3, respectively.

Figure 4-11: Picture of Sireg Duraglass Bar[1]

Table 4-3 Manufacturer Specified Properties

	SRG
Manufacturer	Sireg
Bar #	Duraglass FL12
Nominal Diameter (mm)	12
Fibre Type	Glass
Fibre Content (% Wt.)	70
Resin	Ortophtalic Polyester
Min. Tensile Strength (MPa)	~1000
Modulus of Elasticity (GPa)	~40

To determine test temperatures, a limited thermal characterisation study was undertaken to determine glass transition and decomposition temperatures, following the same methodologies as outlined in section 3.3 and 3.4. Glass transition temperatures were determined as shown in Table 4-4.

[1] https://www.sireggeotech.it

Table 4-4 SRG Glass Transition Temperature values based on various definitions for T_g

	Glass Transition Temperature (°C)				Standard Deviation	
	i	ii	iii	Avg.	σ	3σ
T_g Onset	56.72	61.89	57.84	58.82	2.22	6.66
T_g Modulus	69.10	78.84	73.98	73.97	3.98	11.93
T_g Tanδ	100.00	103.50	96.75	100.08	2.76	8.27

An example of the DMA test data for the SRG FRP bars is shown in Figure 4-12.

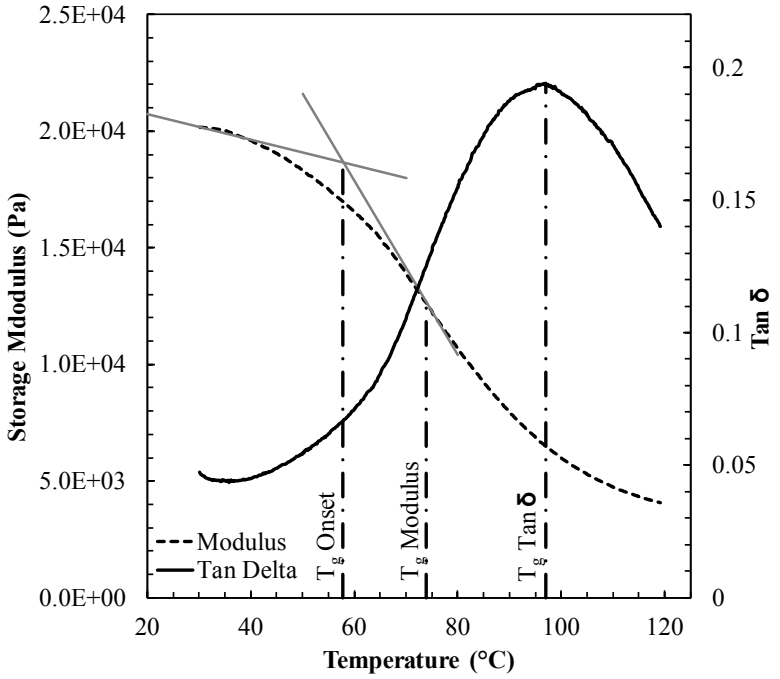

Figure 4-12: Typical DMA measured data for a representative sample of SRG FRP bar

Decomposition and oxidation temperatures are shown in Table 4-5

Table 4-5 SRG TGA Decomposition & Oxidation Temperatures

Specimen ID	T_d Onset (˚C)		T_d Peak (˚C)		T_{ox} Onset (˚C)		T_{ox} Peak (˚C)	
		Avg.		Avg.		Avg.		Avg.
SRG8A10i	319.17	316.06	390.83	390.67	511.70	512.68	542.67	552.94
SRG8A10ii	317.67		391.83		513.21		560.33	
SRG8A10iii	311.33		389.33		513.12		555.83	
SRG8N10i	322.50	318.78	396.33	395.17	-	-	-	-
SRG8N10ii	310.67		392.83		-		-	
SRG8N10iii	323.17		396.33		-		-	

An example of the TGA test data for the SRG FRP bars is shown in Figure 4-12.

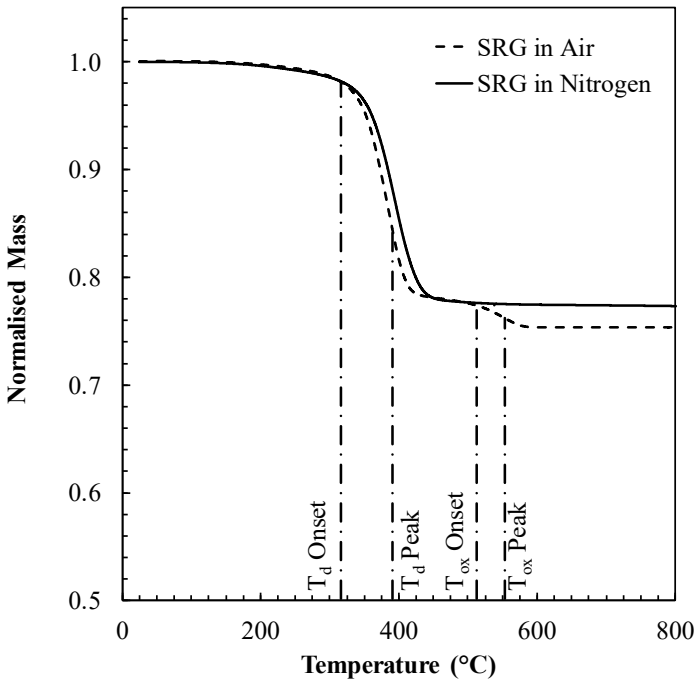

Figure 4-13: Typical TGA measured data for a representative sample of SRG FRP bar

In consideration of the glass transition and decomposition temperatures, the testing matrix for the pilot bars was set out as shown in Table 4-6

Table 4-6 SRG Tensile Testing Matrix

Temperature Definition	**SRG**	
	Temp. (˚C)	**No.**
Ambient *	20	3
T_g Onset	59	2
T_g Modulus	74	2
T_g Tan δ	100	2
	111	3
	150	1
	200	1
*~T_d Onset***	315	2
	375	2
	440	2
	495	2

*Ambient temperature of the lab typically fluctuated seasonally between 10˚C and 25˚C, and this is not considered significant for the tensile performance of the FRP bars.

**Test carried out at 315°C, which is marginally lower than T_d Onset.

4.3 TEST RESULTS AND OBSERVATIONS

4.3.1 Pilot Study Results

Key results from the pilot study direct tensile tests are shown in Table 4-7 and are outlined in greater detail in McIntyre, Bilotta, et al. (2014).

Table 4-7 Bar SRG Tensile Test Results

Specimen ID	Bar Temp. (˚C)	Peak Load (kN)	Tensile Strength (MPa)	Norm. Strength	Failure Mode
SRG_20i	20	86.40	764	0.72	Anchor Failure
SRG_20ii	20	101.44	897	0.85	Coating Failure
SRG_20iii	20	119.58	1057	1.00	Bar Rupture
SRG_59i	59	100.82	891	0.84	Bar Rupture
SRG_59ii	59	101.60	898	0.85	Bar Rupture
SRG_74i	74	92.33	816	0.77	Bar Rupture
SRG_74ii	74	93.72	829	0.78	Bar Rupture
SRG_100i	100	90.58	801	0.76	Bar Rupture
SRG_100ii	100	84.43	747	0.71	Bar Rupture
SRG_111i	111	85.28	754	0.71	Bar Rupture
SRG_111ii	111	72.45	641	0.61	Anchor Failure
SRG_111iii	111	87.27	772	0.73	Bar Rupture
SRG_150i	150	78.11	691	0.65	Bar Rupture
SRG_200i	200	79.91	707	0.67	Bar Rupture
SRG_315i	315	79.61149	704	0.67	Bar Rupture
SRG_315ii	315	79.05534	699	0.66	Bar Rupture
SRG_375i	375	36.49071	323	0.31	Bar Rupture
SRG_375ii	375	38.62978	342	0.32	Bar Rupture
SRG_440i	440	55.12048	487	0.46	Bar Rupture
SRG_440ii	440	44.26141	391	0.37	Bar Rupture
SRG_495i	495	16.9186	150	0.14	Bar Rupture
SRG_495ii	495	15.1431	134	0.13	Bar Rupture

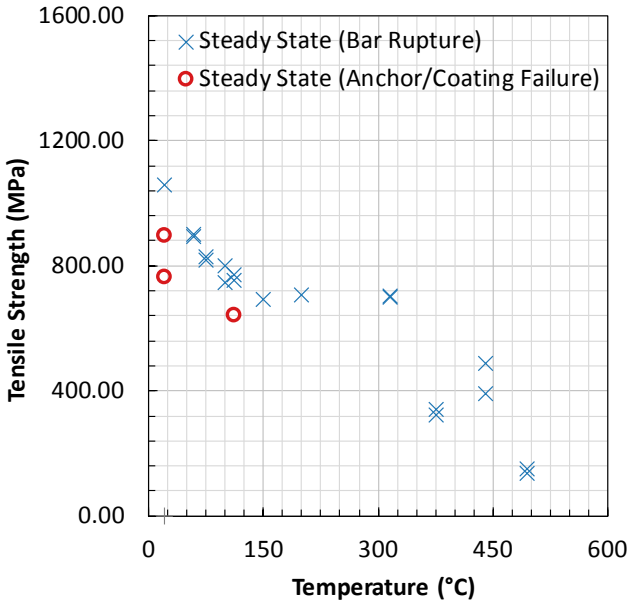

Figure 4-14 Tensile Strength vs Temperature for SRG Bars

As shown in Table 4-7, two of the bars suffered failures within the steel anchor at one end. This was due to an early iteration of the anchorage technique, which was subsequently revised, as outlined in section 4.2.2. The coating failure was due to a bar defect near the anchorage zone.

Even at T_g Onset, >15% loss of tensile strength loss was observed, with up to 35% strength loss at the first plateau, and approximately 70% at peak decomposition of the polymer matrix. It is predicted that if further tests had been undertaken within the oxidation range (see Table 4-5), this would have determined zero tensile strength due to the full decomposition of the matrix at the onset of oxidation.

It is unclear why the tests at 440°C yielded higher tensile strengths than those carried out at 375°C. Additional tests would be required to determine if this is an anomaly or a phenomenon of the SRG GFRP bars.

Figure 4-15 demonstrates load vs cross head displacement for all tests within the loading phase (post heating). With increasing temperature, the stiffness of the FRP SRG bars is observed to decrease, which, during the experiments, coincided with a visually more ductile failure.

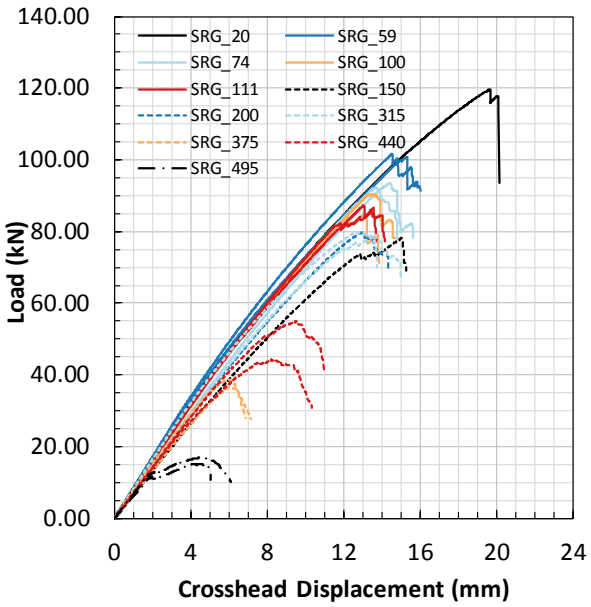

Figure 4-15 Load vs Crosshead Displacement for Bar SRG

By conducting these pilot tests, it was possible to improve on the testing techniques, including anchorage of the bars and the testing methodology. Following this pilot study, the 3 FRP, which are the focus of this thesis, underwent tensile testing across a larger range of temperatures (i.e. at T_d Peak) with additional repeat tests at each temperature.

4.3.2 Main Results

Key results of the direct tensile tests on the GFRP and CFRP bars are given in Table 4-8, Table 4-9 and Table 4-10, with the. The surface temperatures of the tested FRP bars represent the average temperature measured by TC1 and TC2 (see Figure 4-10) during the isothermal stages of the experiments.

Table 4-8: Bar BPG Tensile Test Results

Specimen ID	Bar Temp. (˚C)	Avg. Temp. (˚C)	Peak Load (kN)	Tensile Strength (MPa)	Norm. Strength	Failure Mode
BPG_20i	Ambient	Ambient	115.28	1467.78	1.00	Bar Rupture
BPG_20ii	Ambient		112.39	1430.96	0.97	Coating Failure[2]
BPG_20iii	Ambient		109.67	1396.36	0.95	Coating Failure
BPG_20iv	Ambient		108.86	1386.11	0.94	Coating Failure
BPG_86i	87	87	84.36	1074.08	0.73	Bar Rupture
BPG_86ii	87		87.02	1107.98	0.75	Bar Rupture
BPG_86iii	87		83.40	1061.92	0.72	Bar Rupture
BPG_109i	110	110	77.78	990.31	0.67	Bar Rupture
BPG_109ii	110		76.60	975.30	0.66	Bar Rupture
BPG_109iii	110		72.40	921.85	0.63	Bar Rupture
BPG_109iv	109		77.12	981.96	0.67	Bar Rupture
BPG_136i	138	137	74.79	952.22	0.65	Bar Rupture
BPG_136ii	137		80.33	1022.79	0.70	Bar Rupture
BPG_136iii	137		75.19	957.35	0.65	Bar Rupture
BPG_149i	150	150	76.06	968.40	0.66	Bar Rupture
BPG_149ii	151		78.50	999.53	0.68	Bar Rupture
BPG_225i	228	227	75.69	963.69	0.66	Bar Rupture
BPG_225ii	227		76.43	973.18	0.66	Bar Rupture
BPG_300i	301	302	74.65	950.42	0.65	Bar Rupture
BPG_300ii	303		68.40	870.89	0.59	Bar Rupture
BPG_355i	358	358	51.82	659.77	0.45	Bar Rupture
BPG_355ii	356		47.32	602.55	0.41	Bar Rupture
BPG_355iii	358		40.78	519.26	0.35	Bar Rupture
BPG_415i	415	416	26.15	332.97	0.23	Bar Rupture
BPG_415ii	417		30.57	389.28	0.27	Bar Rupture
BPG_415iii	416		29.34	373.60	0.25	Bar Rupture
BPG_565i	574	570	4.66	59.35	0.04	Bar Rupture
BPG_565ii	567		8.03	102.20	0.07	Bar Rupture
BPG_565iii	570		7.69	97.89	0.07	Bar Rupture
BPG_trans20i	543	556	23.10	294.16	0.20	Bar Rupture
BPG_trans20ii	570		23.10	294.16	0.20	Bar Rupture

[2] within the anchorage zone at the bond between the interface of the potting material and the bar

Table 4-9: Bar PTG Tensile Test Results

Specimen ID	Bar Temp. (˚C)	Avg. Temp. (˚C)	Peak Load (kN)	Tensile Strength (MPa)	Norm. Strength	Failure Mode
PTG_20i	Ambient	Ambient	77.41	1092.03	1.00	Bar Rupture
PTG_20ii	Ambient		81.23	1145.93	1.05	Bar Rupture
PTG_20iii	Ambient		73.99	1043.80	0.95	Bar Rupture
PTG_83i	84	84	72.59	1024.04	0.94	Bar Rupture
PTG_83ii	84		70.10	988.99	0.90	Bar Rupture
PTG_83iii	85		67.81	956.60	0.87	Bar Rupture
PTG_105i	107	108	69.66	982.74	0.90	Bar Rupture
PTG_105ii	108		68.73	969.68	0.89	Bar Rupture
PTG_136i	137	137	59.25	835.89	0.76	Bar Rupture
PTG_136ii	137		60.59	854.85	0.78	Bar Rupture
PTG_154i	152	153	53.88	760.08	0.69	Bar Rupture
PTG_154ii	151		54.79	773.01	0.71	Bar Rupture
PTG_154iii	155		54.76	772.56	0.71	Bar Rupture
PTG_225i	227	227	52.94	746.93	0.68	Bar Rupture
PTG_225ii	227		50.41	711.22	0.65	Bar Rupture
PTG_275i	278	279	52.85	745.60	0.68	Bar Rupture
PTG_275ii	280		54.25	765.35	0.70	Bar Rupture
PTG_310i	312	312	44.09	621.99	0.57	Bar Rupture
PTG_310ii	312		43.47	613.29	0.56	Bar Rupture
PTG_310iii	311		45.14	636.84	0.58	Bar Rupture
PTG_384i	400	401	38.18	538.63	0.49	Bar Rupture
PTG_384ii	401		32.11	453.03	0.41	Bar Rupture
PTG_384iii	401		32.61	460.04	0.42	Bar Rupture
PTG_460i	465	463	7.53	106.16	0.10	Bar Rupture
PTG_460ii	463		9.17	129.40	0.12	Bar Rupture
PTG_460iii	460		0.72	10.11	0.01	Bar Rupture
PTG_550i	533	533	0.72	10.10	0.01	Bar Rupture*
PTG_570i	568	568	0.71	10.05	0.01	Bar Rupture*
PTG_trans20i	527	534	15.48	218.44	0.20	Bar Rupture
PTG_trans20ii	541		15.55	219.33	0.20	Bar Rupture

*Bars ruptured during the heating phase

Table 4-10: Bar PTC Tensile Test Results

Specimen ID	Bar Temp. (˚C)	Avg. Temp. (˚C)	Peak Load (kN)	Tensile Strength (MPa)	Norm. Strength	Failure Mode
PTC_20i	20	20.00	138.68	1956.48	1.00	Bar Rupture
PTC_20ii	20.00		137.41	1938.62	0.99	Bar Rupture
PTC_20iii	20.00		140.06	1975.94	1.01	Bar Rupture
PTC_20iv	20.00		137.06	1933.58	0.99	Bar Rupture
PTC_302i	305	305	45.03	635.26	0.33	Coating Failure[2]
PTC_302ii	304		65.23	920.29	0.47	Bar Rupture
PTC_302iii	306		71.98	1015.48	0.52	Bar Rupture
PTC_377i	385	382	66.85	943.18	0.48	Bar Rupture
PTC_377ii	379		65.12	918.75	0.47	Bar Rupture
PTC_377iii	380		67.47	951.91	0.49	Bar Rupture
PTC_400i	408	408	43.32	611.22	0.31	Coating Failure[2]
PTC_556i	550	554	46.90	661.69	0.34	Coating Failure[2]
PTC_556ii	556		43.64	615.66	0.32	Bar Rupture
PTC_556iii	556		48.37	682.42	0.35	Bar Rupture
PTC_580i	583	590	0.48	6.72	0.00	Bar Rupture
PTC_580ii	592		28.38	400.44	0.21	Bar Rupture
PTC_580iii	595		2.79	39.37	0.02	Bar Rupture
PTC_trans25i	581	581	34.61	488.28	0.25	Bar Rupture

[2]See footnote for Table 4-8

Figure 4-16, Figure 4-17 and Figure 4-18 show the observed relationships between ultimate tensile strength and temperature for bars BPG, PTG and PTC, respectively, as established from the direct tensile tests noted in the tables above.

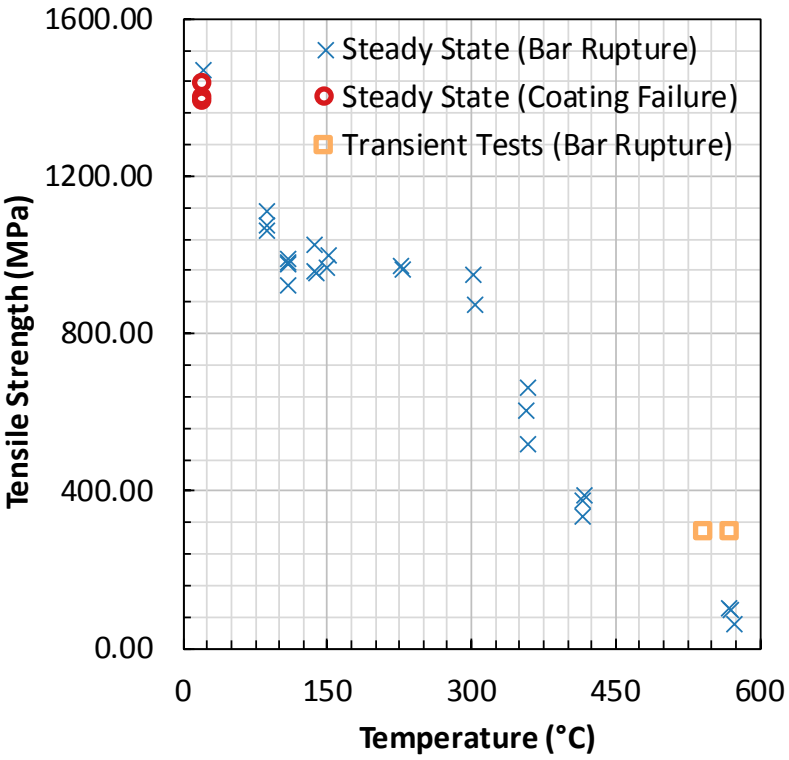

Figure 4-16: Tensile Strength versus Temperature for BPG Bars

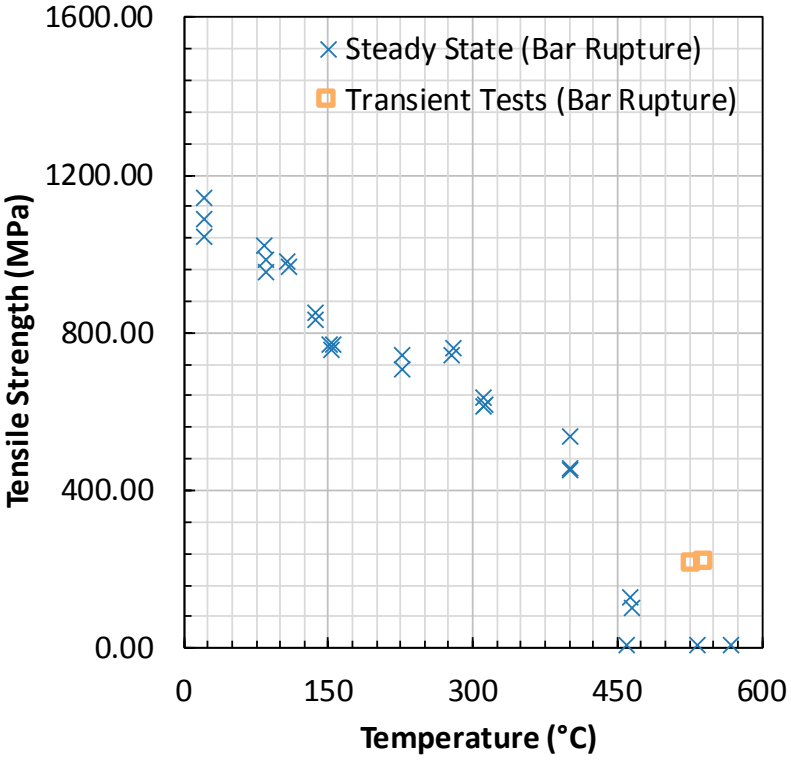

Figure 4-17: Tensile Strength versus Temperature for PTG Bars

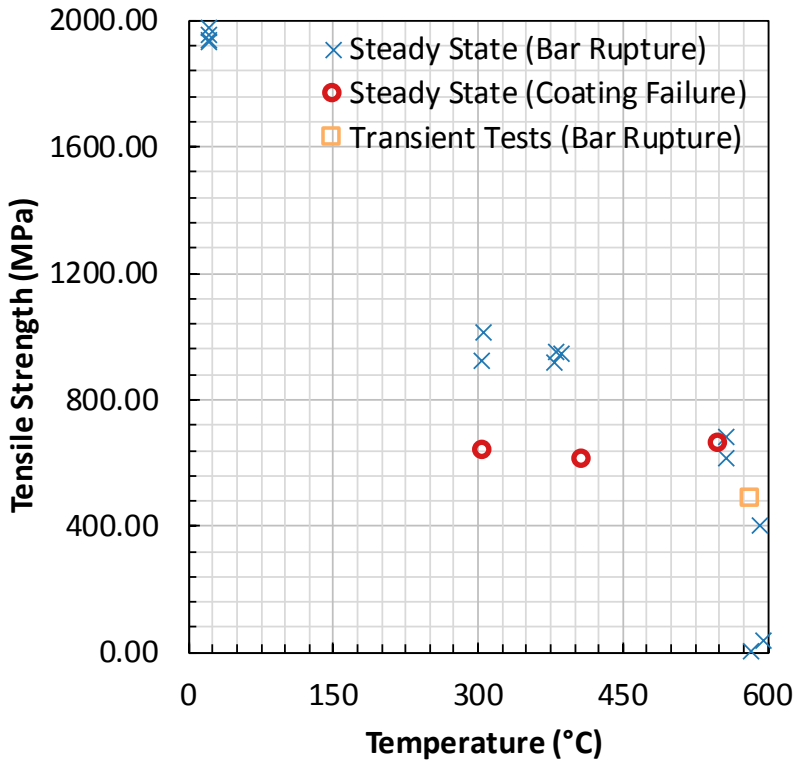

Figure 4-18: Tensile Strength versus Temperature for PTC Bars

The data given in Table 4-8, Table 4-9, and Table 4-10, along with Figure 4-16, Figure 4-17 and Figure 4-18, confirm that both GFRP and CFRP bars suffer considerable losses in tensile strength at elevated temperatures, with reductions manifesting at temperature approaching the T_g of the polymer resin used in the FRP bars' manufacture. It is also evident that the reductions in tensile capacity for the GFRP bars appear to follow a two-step reduction, with a plateau between approximately 150˚C and 300˚C. This observation is used later in this chapter (Section 4.4) to propose an empirical based model for tensile strength reductions of FRP bars based on testing of the types performed in Chapter 3, along with a small number of additional direct tension tests on FRP bars. On the limited data for CFRP tensile tests, it appears there is a plateau between 300˚C and 375˚C though it is unclear on the trend of the strength loss prior to 300˚C.

For the GFRP bar tension tests (i.e. tests on BPG and PTG), the steady state thermal regime tests demonstrated a noticeably lower tensile capacity in comparison to those measured in the transient thermal regime tests, likely due to sustained heating prior

to loading. The transient tests represent a more 'realistic' scenario, the transient scenario is a better – however still imperfect – representation of the conditions likely to be experienced by FRP bars embedded within a concrete structural element during a building fire. The steady state tests can therefore be considered conservative for the purposes of defining high temperature tensile properties for application to practical design of FRP reinforced concrete elements. This permits the development of a failure envelope.

It should be noted that considerably fewer tests were performed on the CFRP bars due to the difficulties encountered ensuring anchorage of the bars. As discussed in the methodology, the ambient tests were carried out at an alternate testing facility to ensure the ultimate capacity of the bar could be achieved. Pilot tests were carried out to determine the maximum capacity that could be achieved during an elevated temperature test for CFRP, and as such the minimum temperature for a steady state thermal test was set as T_d *Onset* for the PTC bars (302°C).

For the majority of the direct tensile tests performed, the FRP bars ruptured within their heated portions within the environmental chamber. However, a small number of tests resulted in a failure of the bars' coating within the anchorage tubes; this occurred at ambient temperature for the BPG bars and at temperatures in the range of decomposition for the PTC bars. This observation highlights a potentially key issue for the FRP bars studied herein. Specifically, the GFRP bar BPG, for which it was demonstrated that the bar may not be able to achieve its full tensile capacity due to a coating/anchorage failure, when there is insufficient anchorage length or radial pressure at the anchorage.

For the CFRP bar PTC, it is unclear why the coating failed in three of the tensile tests performed at three different elevated temperatures (refer to Table 4-10). An additional test was carried out, using additional TCs placed at the core of the FRP bar just inside the upper steel anchor, to determine if longitudinal heat transfer within CFRP bars, from the heated portion of the bars within the environmental chamber, caused conduction along the bars and into the anchorage zones outside the chamber.

This was suspected as a possible cause due to the comparatively high thermal conductivity of carbon fibres along their longitudinal axis, as compared with the comparatively low thermal conductivity of glass fibres (and noting that similar failures were not observed for either of the GFRP bars).

Figure 4-19 shows that the temperature of the anchorage did increase during testing, and that some of this temperature increase may be attributed heat transfer along the PTC bar into the anchorage zone. However, the temperature rise is minor (120˚C) in comparison to the oven and bar surface temperatures (in excess of 580˚C in this case), and so is not thought to be the critical factor. The onset of decomposition of the polymer matrix reduces the bond capacity of the FRP bar with the potting material in the steel anchors. It should be noted here that this figure shows the bar surface temperature exceeding the oven temperature; this is due to an exothermic reaction during decomposition of the polymer resin and is discussed later in the chapter.

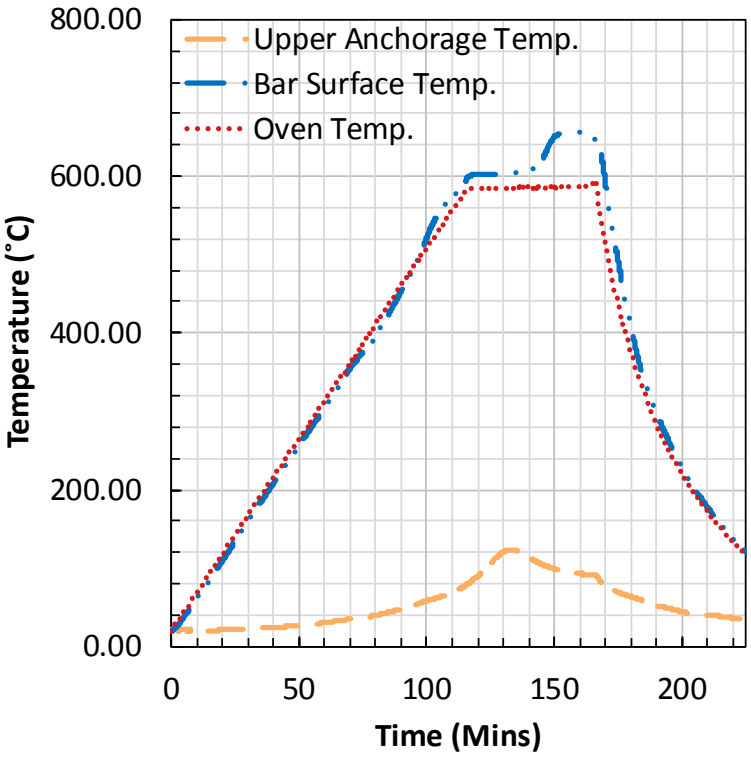

Figure 4-19: Bar PTC, Thermal Conductivity Test

In all of the tensile tests, crosshead displacement was measured as a way of indicating changes in stiffness of the bars at varying temperature. Load versus crosshead

displacement for BPG, PTG and PTC bars is shown in Figure 4-20, Figure 4-21, and Figure 4-22. By comparison BPG is the stiffer of the two GFRP bars tested, with a modulus of elasticity of 63.2 GPa (as shown in Table 3-1), and this is apparent when comparing the load vs crosshead graphs for BPG and PTG. Additionally the spread of the results is observed to be greater for PTG than BPG, indicating a greater loss of stiffness for the PTG bars across the glass transition and decomposition ranges.

For PTC (Figure 4-22), it is observed that the CFRP bar is significantly stiffer than the GFRP bars, with an ambient stiffness of 120 GPa. It is also observed that there is a gap between the ambient tests and the heated tests, this is due to the absence of tests in the glass transition range.

In all cases, the stiffness of the bars was observed to decrease with increasing temperature, though for the glass FRP bars (Figure 4-15, Figure 4-20 and Figure 4-21) it can be see that at lower T_g temperatures (i.e. T_g Onset and T_g Modulus), the stiffness actually increases in some cases . It is unknown why this was the case without carrying out additional tests. However it is hypothesised that there may be post curing of the core polymer, whereby crosslinking of the polymer chains increases ultimately leading to increased stiffness.

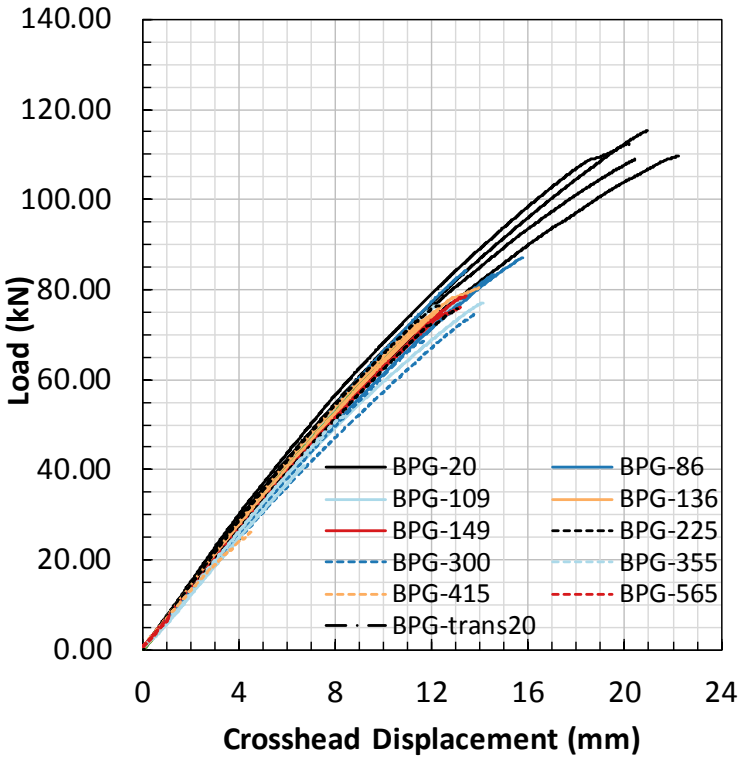

Figure 4-20 Load vs Crosshead Stroke for BPG Bars

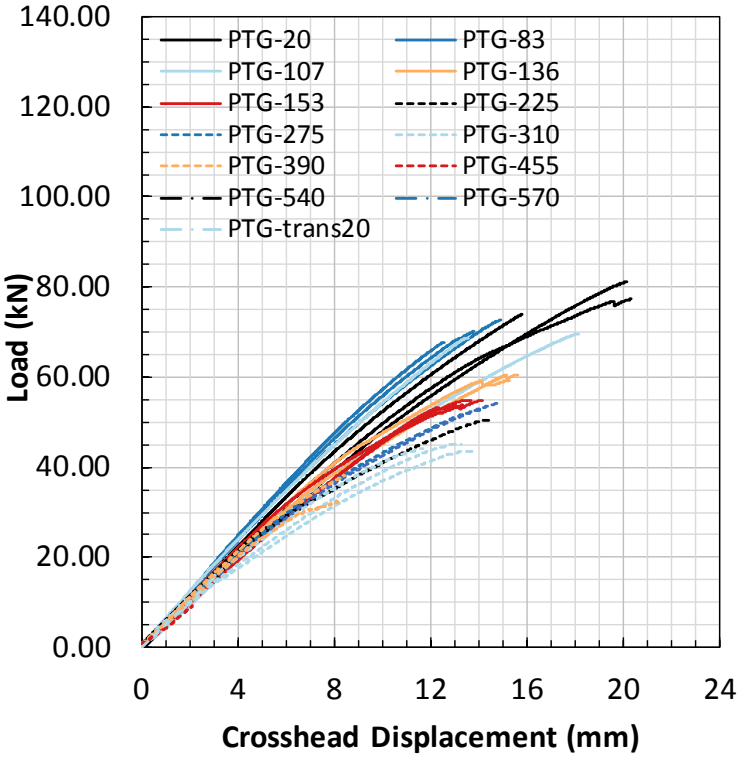

Figure 4-21 Load vs Crosshead Stroke for PTG Bars

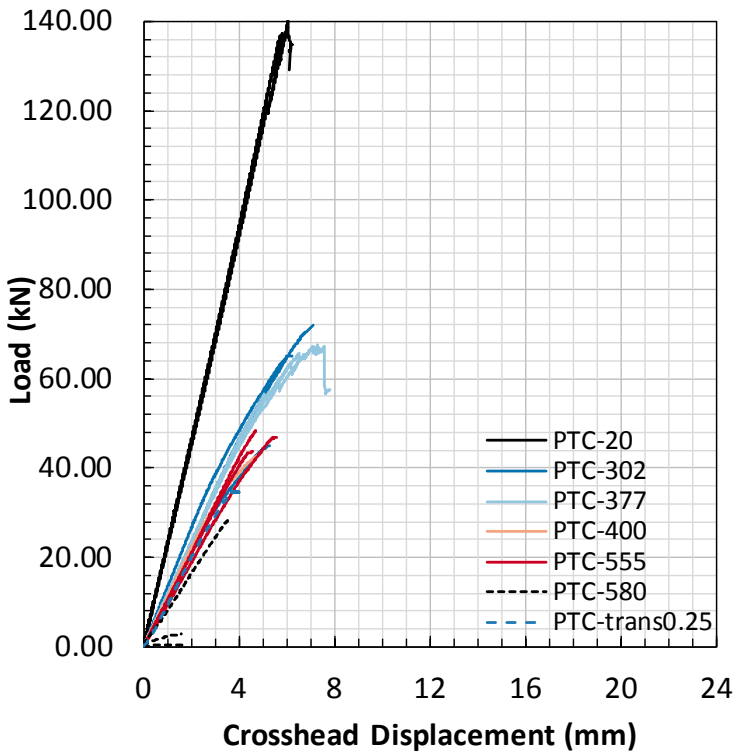

Figure 4-22 Load vs Crosshead Stroke for PTC Bars

Significant visual changes in the FRP bars were also observed both during heating and after the tests had been completed. Figure 4-23 documents the visual impacts of increasing temperature exposures on samples of BPG bar. At ambient temperature and during heating up to temperatures in the range of T_g, the helical glass fibre wrap around this bar type ruptured, and the fibres within the bar splintered. At temperatures between T_g *Tanδ* and T_d *Onset*, the fine sand coating fell off the bars' surface, and bundles of the longitudinal glass fibres became visible within the bar. At temperatures in the range of T_d *Onset* the colour of the bars changed as the polymer matrix began to decompose, and individual fibre bundles were exposed with the resin from the bars observed to "bleed" from the bar during heating (as shown in Figure 4-24). It is hypothesised that the helical wrap of the bar applied radial pressure during heating, under the initial stress (of 10MPa) during heating, and as such that it squeezed this resin from the bar as it decomposed and thermally expanded laterally. At T_{ox} *Peak,* the colour of the bars again changed significantly, indicating oxidation of the polymer matrix (see Chapter 3), such that only the light-coloured glass fibres remained.

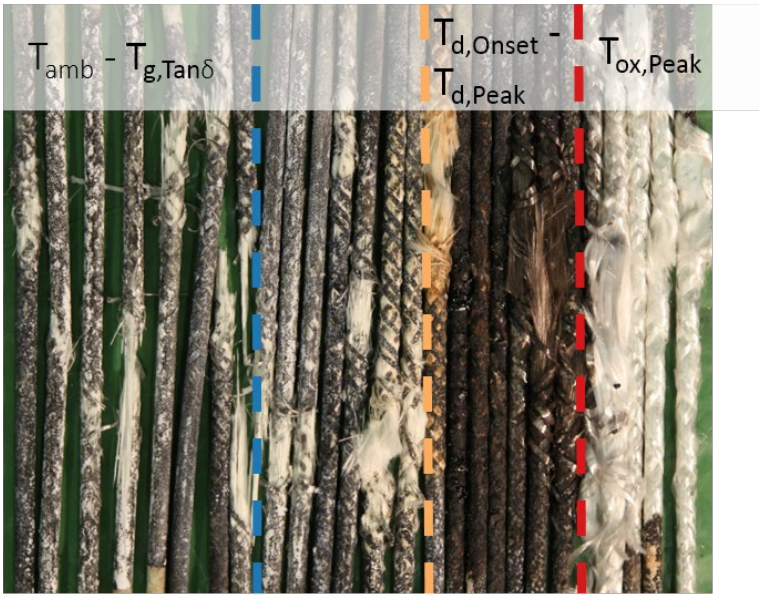

Figure 4-23: Photos Showing the Visual Changes in BPG Bars with Increasing Temperature

Figure 4-24: "Bleeding" Resin from a BPG Bar at the Onset of Decomposition

Figure 4-26 documents the visual impacts of increasing temperature exposures on samples of PTG bar. At ambient temperature and at temperatures up to T_g, the glass fibres ruptured in sections, wherein multiple popping noises could be heard as the bar failed progressively. The resultant appearance of the bar after failure showed the bars' coarse sand surface coating to have split, and bundles of the fibres to have splintered away from one another. In contrast to the BPG bar, PTG bar has no helical fibre wrap on its exterior surface, and therefore there appeared to be more transverse expansion of these bars on heating; this was evidenced by the sand coating splitting around T_g *Modulus* (Figure 4-25) due to the absence of radial pressure applied to compact and contain the fibres. Due to the anisotropic nature of the FRP bars, the longitudinal thermal expansion is low in comparison to the transverse thermal expansion which is 3-6 times that of concrete (Galati, Nanni, Dharani, et al., 2006). At temperatures between T_g *Tanδ* and T_d *Onset* the sand coating also split, however the radial expansion of the bar was less than for BPG bars. Similarly to the BPG bars, the PTG bars changed colour at temperatures in the range of T_d *Onset*, and the fibres became exposed, though some small sections of the sand coating remained attached to the surface of the bars. At temperatures as high as T_{ox} *Onset* the sand coating was

completely removed and the polymer char was also reduced as it oxidised up until T_{ox} *Peak*, above which only the glass fibres remained.

Figure 4-27 shows that some small cracks were observed in the outer sand coating of bar PTC at T_d *Onset*, and it should also be noted that the failure mode was less violent than that observed for these bars at ambient temperature. Due to the dark colour of the carbon fibres at ambient temperature, the decomposition, charring, and oxidation of the polymer char is not clearly apparent, as for the two GFRP bar types (see Figure 4-28).

Figure 4-25 Splitting of sand coating on bar PTG at T_g Modulus, due to transverse thermal expansion of the FRP

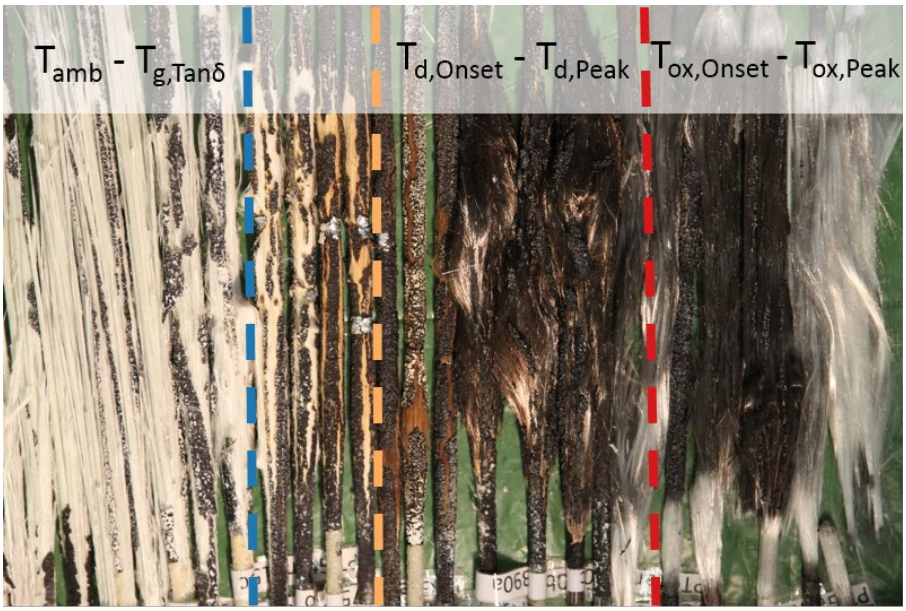

Figure 4-26: Photos Showing the Visual Changes in PTG Bars with Increasing Temperature

Figure 4-27 Splitting of the sand coating on bar PTC at T_d Onset, due to transverse thermal expansion of the FRP

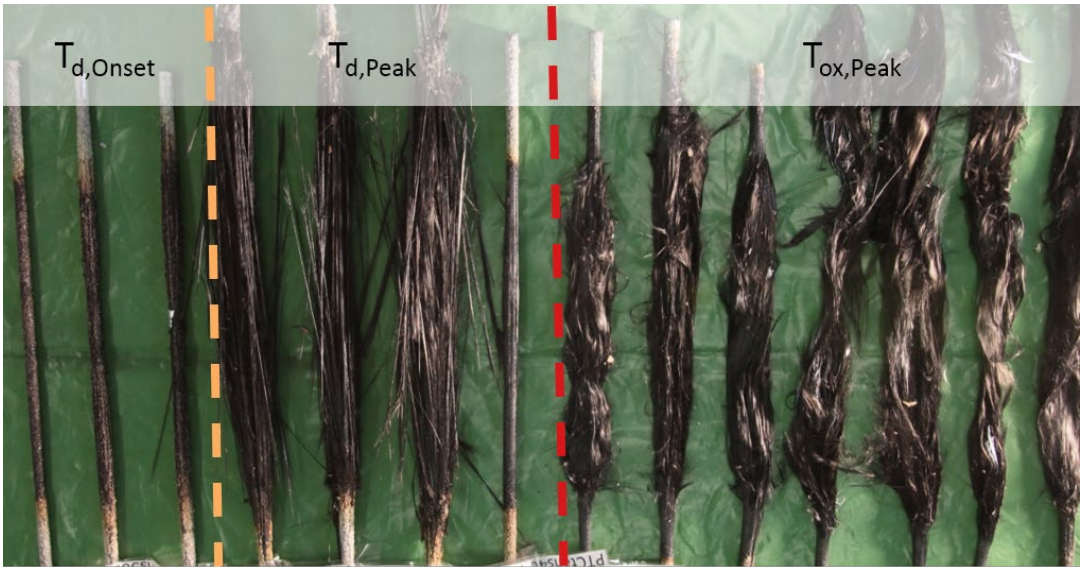

Figure 4-28: Photos Showing the Visual Changes in PTC Bars with Increasing Temperature (note that the three leftmost bars in this image failed by anchorage failure rather than bar rupture)

As previously demonstrated in Chapter 3, the CFRP (bar PTC) experiences oxidation of the carbon fibres at elevated temperature leading to considerable mass loss of the bar at high temperatures that is not observed for the GFRP bars. This oxidation process is an exothermic reaction that, under the right conditions including ample oxygen supply, can cause the temperature of the bar to actually rise significantly above that of the surrounding air flow. This effect was shown in Figure 4-19 earlier in this chapter, where the bar temperature is observed to increase above the air temperature within the environmental chamber during the intended steady-state bar temperature phase of the heating regime. Figure 4-29 shows that some of the carbon fibres within the PTC bar for sample PTC_580i turned white during and after heating, indicating oxidation of the carbon fibres. This is also evident in Figure 4-30 where the

sample was observed to glow red during heating due to the exothermic reaction. The actual test temperature therefore, within the CFRP bars, may have been considerably above the recorded test temperature, though it is difficult to quantify this as a thermocouple cannot be placed at the core of the bar. Whilst this is not ideal, it at least makes the results presented in Table 4-10 and Figure 4-18 conservative for design.

Figure 4-29: Post-test photo showing the aftermath of oxidation of carbon fibres in sample PTC_580i

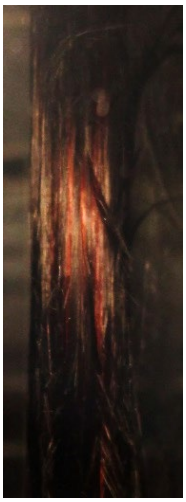

Figure 4-30: Sample PTC_580i glowing red during heating due to exothermic oxidation of the carbon fibres in the bar

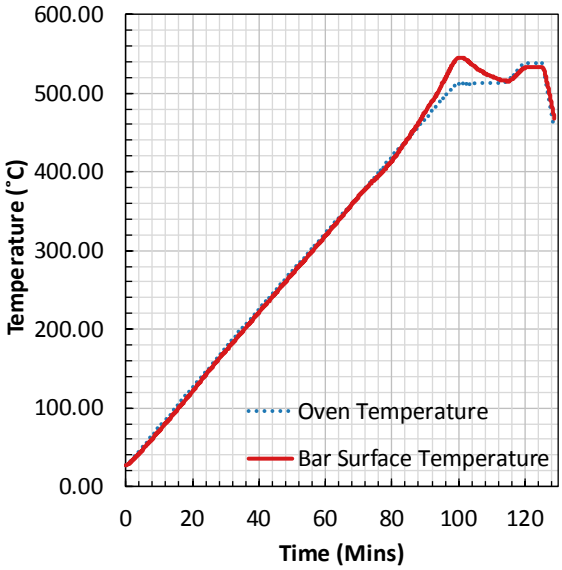

Figure 4-31: Comparison of oven (i.e. Internal Air) and bar surface temperatures for Specimen PTG_540i, where exothermic self-heating is evident from approximately 460°C

Exothermic reactions were also apparent for the GFRP bars, suggesting exothermic oxidation of the polymer resin char at temperatures of about 460°C; Figure 4-31 gives a comparison of oven air temperature (measured 100mm from the top of the oven, TC4) and bar surface temperature for sample PTG_540i. It is evident at approximately 460°C, the surface temperature of bar PTG increases beyond that of the surrounding air temperature within the chamber.

4.4 Semi-Empirical Tensile Strength Loss Model for FRP Bars

Visual examination of the tensile capacity reduction curves for the GFRP bars with exposure to elevated temperature suggests the existence of a two-step reduction in tensile capacity of the bars; this appears to correlate with (1) the thermal degradation (i.e. T_g response) and (2) decomposition (i.e. T_d response) of the bars' polymer matrix during heating. On this basis, a semi-empirical model and a minimum suite of tests is proposed in this section to predict the expected tensile strength losses of essentially any pultruded FRP bar at elevated temperature to limit the time and financial investment in carrying out a full set of tensile tests. The proposed minimum suite of tests is as follows:

1. DMA testing to determine the storage modulus reduction for the FRP bars with temperature, up to a temperature of twice the T_g *Modulus* value.
2. TGA testing to determine the FRP bar's mass loss curve with temperature, up to temperatures well above T_d (taken as 800°C in the current study due to the limits of temperature than could be achieved within the available equipment at the University of Edinburgh).
3. A minimum of two (preferably more) direct tension steady state thermal regime tests on the FRP bar in question, at a temperature in the range of (T_g *Modulus* + T_d *Onset*)/2; these are needed to define the first plateau in the model.
4. A minimum of two (preferably more) direct tension steady state thermal regime tests on the FRP bar in question at a temperature in the range of T_{ox} *Peak*; these are needed to define the second plateau in the model.

5. Where manufacturer specified ultimate tensile strength values are not provided, a minimum of two (preferably more) direct tension tests will also need to be carried out at room temperature.

Note that the first plateau is evident in the test results for BPG and PTG between 150˚C and 300˚C (see Figure 4-16 and Figure 4-17). Furthermore, the prediction of tensile strength will be conservative due to the use of steady state testing as opposed to transient.

Based on the above tests, a semi-empirical model for the tensile strength loss of FRP reinforcement with temperature is proposed according to the following equation (refer to Figure 4-32 and Figure 4-33 for an illustration of the overall shape of the proposed model):

$$f_T^* = \frac{f_T}{f_{amb}} = \alpha_g + k_1 \cdot (1 - \alpha_g) \cdot \alpha_d + k_2 \cdot (1 - \alpha_g) \cdot (1 - \alpha_d) \qquad [4\text{-}1]$$

Where f_T is the FRP ultimate tensile strength at temperature T and f_{amb} is the ultimate tensile strength at ambient temperature. The first step in the reduction of tensile strength is proposed to be defined by the DMA storage modulus loss curve, and is given by:

$$\alpha_g\,(T) = \frac{E_T^* - E_g^*}{1 - E_g^*}\ for\ 20^{\circ}C < T \leq 2 \cdot T_g Modulus$$
$$\alpha_g\,(T) = 0\ for\ T > 2 \cdot T_g Modulus \qquad [4\text{-}2]$$

Where E_T^* and E_g^* are the normalised storage modulus values at temperatures T and twice T_g *Modulus*. The second step in the reduction of the tensile strength is proposed to be defined by the TGA (mass loss) curve and is given by:

$$\alpha_d\,(T) = 1\ for\ 20^{\circ}C < T \leq 2 \cdot T_g Modulus$$
$$\alpha_d\,(T) = \frac{m_T^* - m_{ox}^*}{m_g^* - m_{ox}^*}\ for\ 2 \cdot T_g Modulus < T \leq T_{ox} Onset \qquad [4\text{-}3]$$
$$\alpha_d\,(T) = 0\ for\ T > T_{ox}\ Onset$$

Where m_T^*, m_g^*, and m_{ox}^* are the normalised mass loss values at temperature T, twice T_g *Modulus* and T_{ox} *Onset*. The coefficients k_1 and k_2 represent the percentage of mass loss that defines the two plateaus in the proposed model, and are given by:

$$k_1 = \frac{f_{T_1}}{f_{amb}}\ and\ k_2 = \frac{f_{T_2}}{f_{amb}}\ \ where\ T_1 = \frac{T_g Tan\delta + T_d Onset}{2}\ and\ T_2 = T_{ox} peak \qquad [4\text{-}4]$$

Where f_{T_1} and f_{T_2} are the tensile strengths of the bar at the first and second plateaus, as defined at temperatures T_1 and T_2 (defined in Equation [4-4]). By defining the second plateau at T_{ox} *Peak* rather than T_{ox} *Onset*, the model better captures the mass loss resulting from oxidation of the polymer char, and provides a slightly more conservative prediction.

In the initial iteration of this model as outlined in McIntyre, Bilotta, et al. (2014), tensile strength was determined as zero at T_d. However, on review of the main study of tests and consideration of the physical and chemical degradation of the FRP, T_{ox} Onset is appropriate to represent zero tensile strength, as at this point the polymer matrix will be fully decomposed with only residual char left around the fibres.

Figure 4-32 and Figure 4-33 show comparisons of the proposed model against the test data obtained in the current study, for the BPG and PTG base, respectively, and show reasonable agreement between the tested data and the proposed model for both of these GFRP bar types. Indeed, the new proposed two-step model captures the observed response much better than any of the other models previously proposed in the literature e.g.(L. a. Bisby, Green, & Kodur, 2005), is physically based, and can be developed specifically for any new FRP bar product with a limited number of tests that are relatively easy to perform. A comparison of the proposed model against other models is presented later in this chapter in Section 4.5.

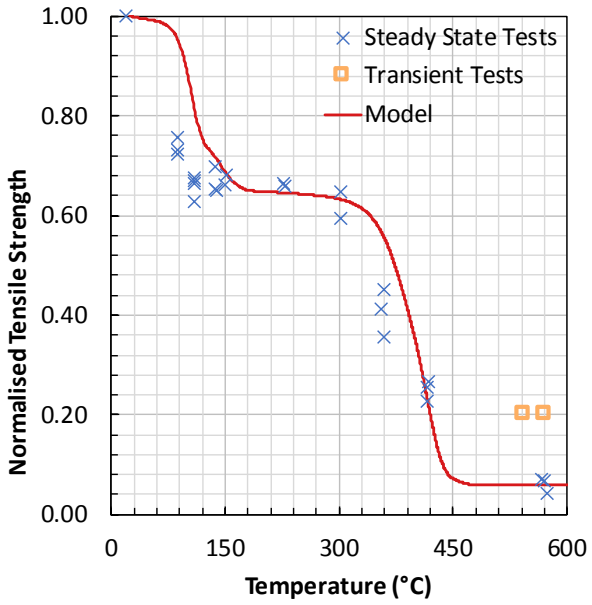

Figure 4-32: Comparison of model with direct tensile data for Bar BPG

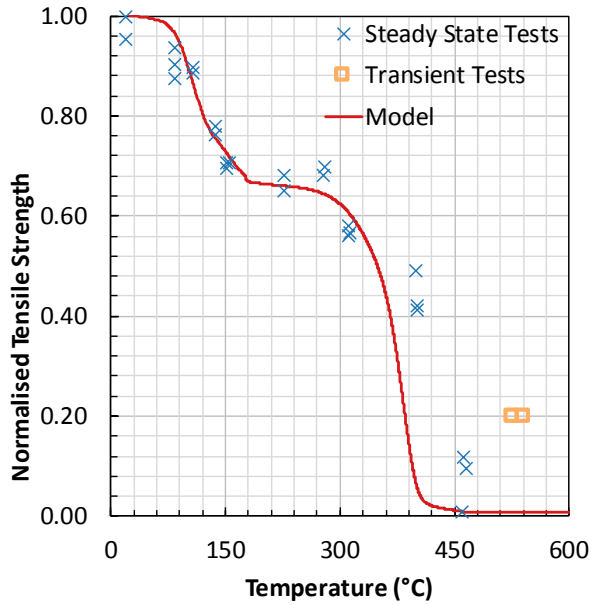

Figure 4-33: Comparison of model with direct tensile data for Bar PTG

On observation of tensile tests results for bar PTC, it is evident that the oxidation of the resin char, and subsequently the hypothesized oxidation of the carbon fibres themselves further reduces the tensile capacity of the bars. On this basis and due to the lack of data prior to the first plateau, the proposed model cannot be validated for

CFRP at this time. Further work is also required to modify the strength loss model to account for the oxidation of the carbon fibres at temperatures above about 550°C.

The proposed model for the GFRP bars has demonstrated that it can be applied to FRP materials from different manufacturers to predict tensile strength loss with temperature. As discussed, a pilot study was carried out on another GFRP bar, SRG (see section 4.2.4). It showed reasonable correlation with the proposed model and the tests presented herein. This parallel work is described in detail by (McIntyre, Bilotta, Bisby, et al., 2014) and the model vs experimental data is shown.

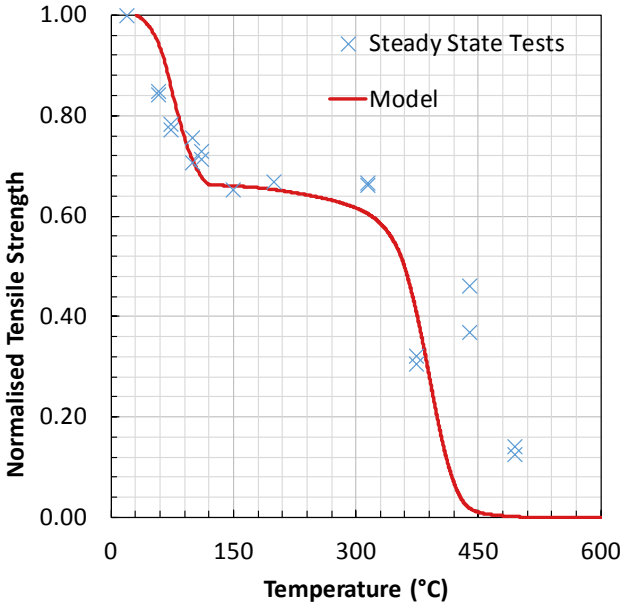

Figure 4-34 Comparison of model with test data for normalised tensile strength vs temperature for Bar SRG (revised from McIntyre, Bilotta, et al., 2014)

4.5 COMPARISON AGAINST LITERATURE

As discussed in Chapter 2, Bisby *et al.*, 2005 assembled data from literature and produced a fitted curve, using a least squares regression technique, to compare the trend in tensile loss at elevated temperature. The models presented herein show a two-step model and as shown in Figure 4-35, show reasonably good correlation with the other glass/vinylester GFRP bar data (see Figure 4-36), accounting for the initial tensile loss within the glass transition temperature (T_g) range. However the model is designed to be unique to each FRP bar, therefore it is not surprising that the model

does not show good correlation with glass FRPs with alternate resins as in Figure 4-35.

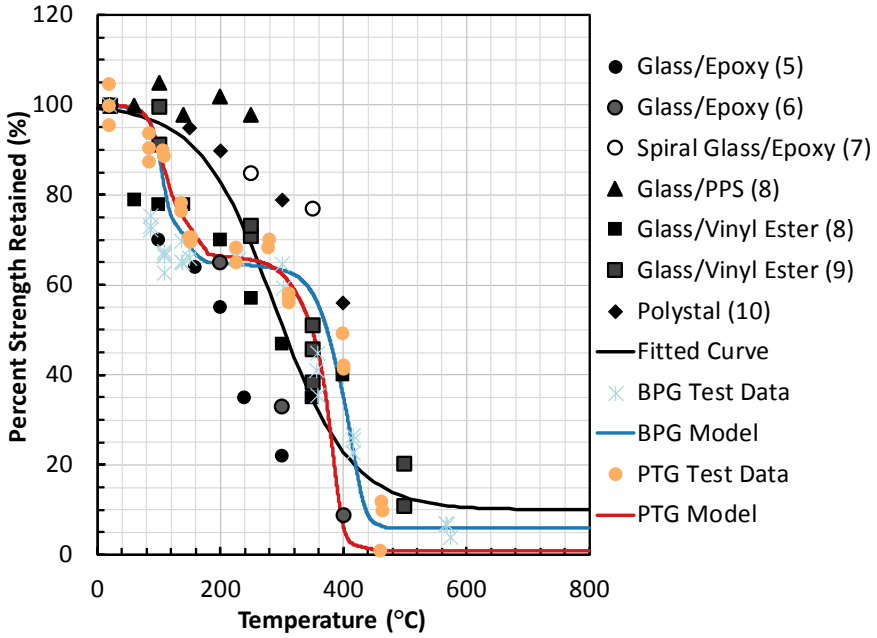

Figure 4-35 Comparison with literature data (L. a. Bisby, Green, & Kodur, 2005) *and fitted curves for tensile loss in GFRP bars*

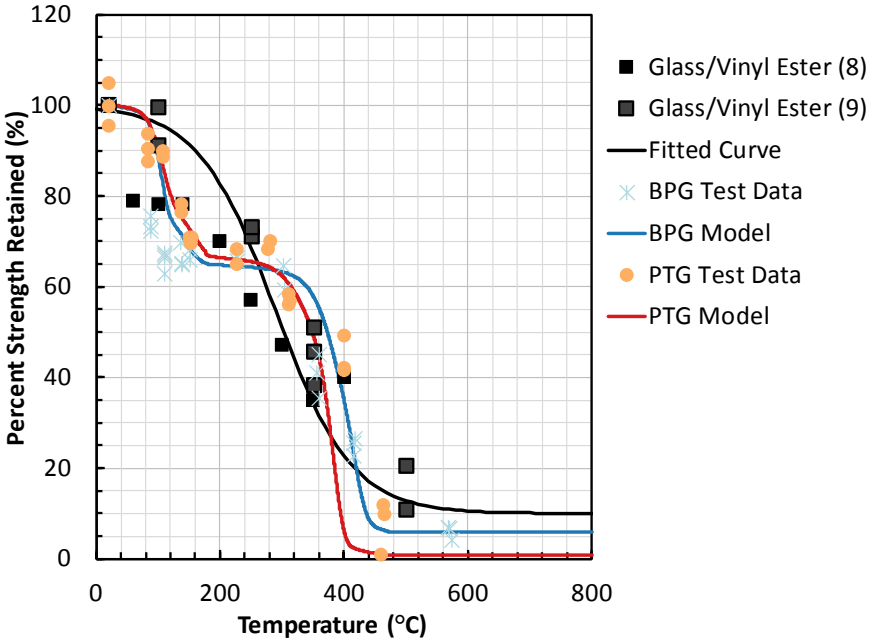

Figure 4-36 Comparison with literature data (Vinylester bars only)(Bisby, Green, & Kodur, 2005) *and fitted curves for tensile loss in GFRP bars*

4.6 COMPARISON OF GFRP AGAINST HOT-ROLLED

As discussed in Chapter 2, the use of FRP as internal reinforcement is benchmarked against steel reinforcement whereby FRP's susceptibility to damage at elevated temperature is seen to be prohibitive in its use in reinforced concrete. Figure 4-37 shows the comparison of normalised tensile strength for the GFRP bars with that of hot rolled and pre-stressing steel using EN1992-1-2 (European Committee for Standardization, 2010). By comparison GFRP shows a lower failure envelope with respect to steel and is also characterised by a two-step loss.

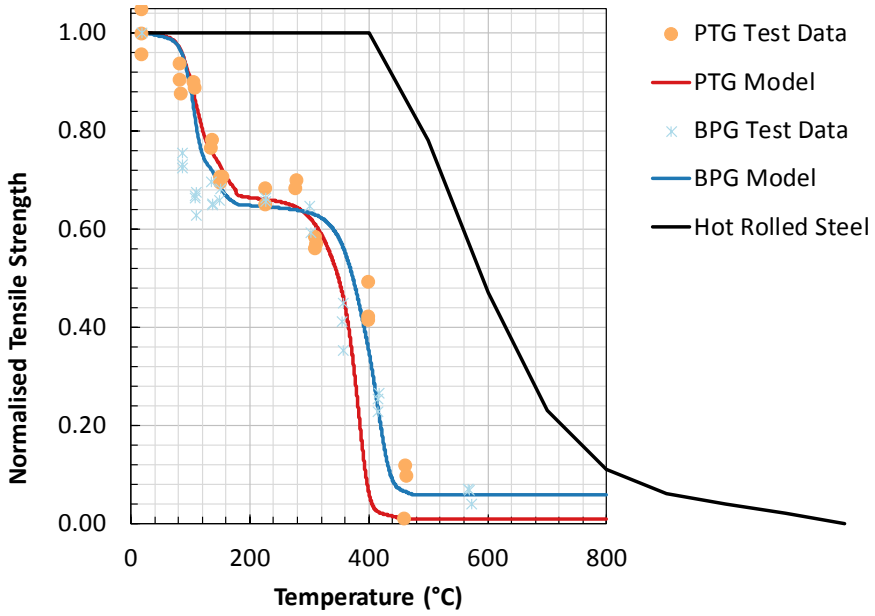

Figure 4-37 Normalised strength comparison for GFRP vs steel

However, when compared with the actual values of tensile strength assuming a yield stress, σ_y = 500MPa, then the FRP can be demonstrated to be superior (see Figure 4-38). It is only at 350˚C-400˚C where the strength of FRP reduces to the equivalent of that of steel at its ambient capacity. Whilst the loss of tensile strength at this point may seem extreme, consideration of the design principles for FRP reinforced concrete must be undertaken. In order to meet serviceability limit requirements (e.g. deflection and creep rupture), the capacity of the FRP reinforcement is typically underutilised (e.g. limited to 20% for creep rupture for GFRP in ACI 440.1R-15) and loss of tensile strength up to 400 ˚C may actually have little impact on the reinforced concrete. The

critical temperature for FRP in reinforced concrete therefore may depend upon the percentage utilisation of the FRP reinforcement in the ambient condition.

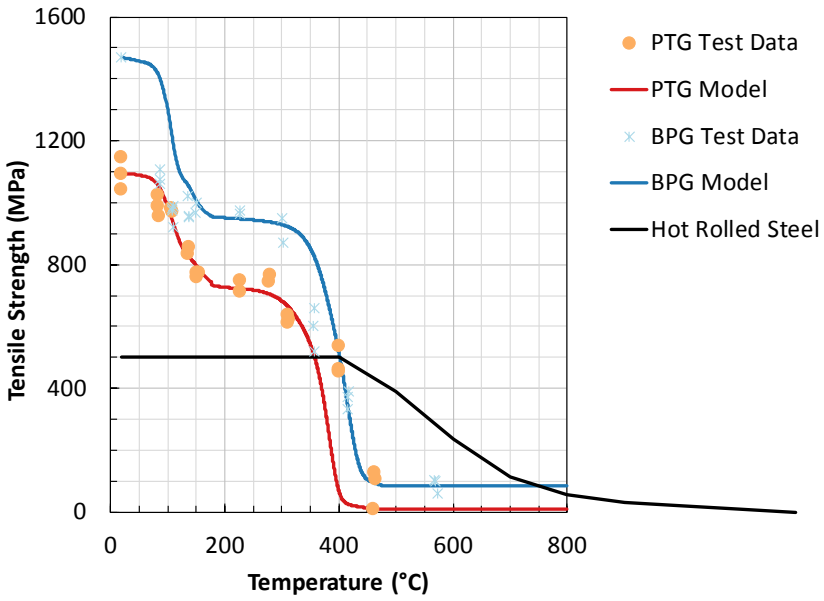

Figure 4-38 Tensile strength comparison for GFRP vs steel

4.7 Further Work

Further test data (including transient testing) are required to fully validate the proposed model in its application to other FRP materials from various manufacturers and with various fibre and resin types, which will also help to understand the sensitivity of the model. It is acknowledged that the application of the model to CFRP bars is limited in the current study. A more in depth study is required into the separate processes that occur when the CFRP bar is heated, to identify trends in the materials behaviour that need to be accounted for in any definable model for tensile strength loss at elevated temperature.

The anchorage technique developed for the suite of testing presented in this chapter was suitable for lower tensile strength bars, i.e. capacity less than 1200MPa. While providing full anchorage to FRP bars tested in tension was clearly not the focus of the current thesis, improvements could be made to the anchorage used to ensure that the shear capacity of the coating does not affect the results, specifically at ambient temperature but also at elevated temperature for the CFRP bars.

4.8 CHAPTER SUMMARY

This chapter has presented results and analysis from a comprehensive study on the tensile capacity of one CFRP and two GFRP commercially available FRP reinforcing bars, for use in reinforced concrete construction. An alternative anchorage technique was developed to allow the FRP bars to be gripped in the testing apparatus without causing premature failure. The characterisation tests of Chapter 3 were used to define the testing temperatures to be interrogated. The use of thermocouples inside the oven and on the surface of the bars verified that these temperatures were reached.

A pilot study on an additional GFRP bar, provided a platform to inform the experimental programme for the 3 main FRP bars to be tested.

Initial tests on the CFRP reinforcement determined that alternative apparatus would be required to find out the ambient tensile capacity of the bars. In conjunction with Professor Giovanni Terrasi, these bars were tested successfully at EMPA using a novel conical anchorage system. The remainder of the CFRP tests were carried out at the University of Edinburgh though, tests below T_d *Onset* (i.e. within the glass transition range) were not possible.

Results from the GFRP tests showed a 2 step reduction in tensile strength with temperature, with a plateau typically around 150°C to 300°C. Unfortunately the limited data on the CFRP bars restricted strong conclusions from being made. Exothermic reactions were also observed, particularly in the case of the CFRP, where during a steady state test to 580°C, the bar was observed to glow red. The carbon fibres oxidised and visually changed from black to white. Visually inspection of the bars after failure was useful in showing the impact of transverse thermal expansion, whereby the helical wrap on bar BPG was observed to resist this expansion.

A novel predictive semi-empirical model for tensile loss with temperature was presented, proposing a minimum suite of tests (DMA/TGA/limited tensile tests) for any specific FRP bar. This limits both the financial and time investment required to experimentally validate tensile strength loss of any FRP bar with temperature. The

model showed good correlation with the GFRP bars, and also with other vinylester GFRP data presented in the literature. The model is, however, unique to each FRP bar and therefore it is not expected that GFRP data sets in general should fit any curve particularly where the resin is different. The proposed model takes a step forward in understanding FRP behaviour at elevated temperature, and provides a valuable input for performance based design of FRP reinforced concrete

In absolute strength terms the GFRP data and models was demonstrated to be superior to that of steel up to 350°C to 400°C, demonstrating GFRP's viability in reinforced concrete. The percentage utilisation of the FRP reinforcement may determine the critical temperature of the reinforcement by understanding how much of the ambient tensile capacity can be compromised before risking failing of the reinforced concrete.

In conclusion, this chapter has set out a comprehensive set of tensile tests on four FRP bars, which have been used to produce and validate a model based on a minimum suite of tests. This sets out a time and cost effective method for determining tensile strength loss for any GFRP bar, though it is acknowledged that additional tensile testing programs would allow for further validation of the model. While a model could not knowingly be produced for CFRP, valuable outcomes where produced; specifically recognizing a third stage of decomposition, oxidation of carbon fibres.

The following chapter examines the bond strength loss of FRP bars at elevated temperature, and thus treats the critical case of the fire safety of FRP reinforcing applications where cool anchorage (or cool reinforcement splices) cannot be assured.

CHAPTER 5 BOND OF FRP BARS IN CONCRETE AT ELEVATED TEMPERATURE

5.1 CHAPTER OVERVIEW

Chapter 4 presented test results and a semi-empirical model for tensile strength loss in pultruded uniaxial FRP reinforcing bars (for glass fibres) at elevated temperatures up to 580°C. In internal reinforcement applications, whilst the tensile capacity of the reinforcing material is a key consideration, it is also necessary for the reinforcing bars to bond with the concrete to allow stress to be developed and transferred effectively. With steel reinforcement, the reinforcing bar bonds mechanically to the concrete, whereby deformations (sand coating/wrapped fibres/combination) on the bar's surface interlock with the concrete. The FRP reinforcing bars studied in the current thesis also bond with concrete mechanically; however the surface of the bars (e.g. the sand coating) is applied in a secondary manufacturing and curing process. For FRP bars the bond strength therefore relies on the performance of the resin matrix at the surface of the bar (into which the sand coating is applied during manufacturing (see section 2.3). Because the polymeric resin is well known to be diminished at temperatures approaching its T_g, the bond of the FRP bars is much more susceptible to damage at elevated temperature than is the case for deformed steel reinforcement (A. Katz, 1999). Furthermore ACI 440.1R-15 mentions that temperature induced bond strength reductions must be considered in the performance based design of FRP reinforced concrete (American Concrete Institute (ACI), 2015), though no method is defined to determine this.

Using the testing and analysis from the thermo-mechanical characterisation tests presented in Chapter 3 to define the glass transition range, bond pullout tests (based on CSA S806-12) are presented in this chapter at ambient temperature and up to $T_g Tan\delta$, as established for each FRP bar. Testing beyond this temperature is irrelevant as bond strength is likely to be close to zero due to the softening of the polymer matrix.

This chapter presents the data from these tests to establish the bond strength reductions at elevated temperature. Finally, as in the previous chapter, consideration is given to the use of a semi-empirical model to predict reductions in bond performance based on the thermo-mechanical testing presented in Chapter 3.

5.2 TESTING METHODOLOGY

5.2.1 Testing Apparatus

The bond pullout testing of FRP bars was performed using an Instron 600LX materials testing frame (also used for the tensile testing presented in Chapter 4). The built-in environmental chamber described in Chapter 4 was also used to heat the specimens.

5.2.2 Sample Preparation

To perform the bond pullout tests, the FRP reinforcing bars were cast inside 150mm concrete cubes with a mean 28-day cylinder compressive strength of 27.5MPa (standard deviation 3.5MPa). All samples were cast form the same batch of ready-mix concrete, which contained a siliceous aggregate. The test specimens were designed using guidance on vertically embedded FRP bars presented by CSA S806-12 Annex G (CSA 2012), although samples were cast horizontally to ensure central placement. Minor adjustments to the sample geometry and dimensions had to be made due to space limitations within the testing apparatus (i.e. the restricted testing height and the dimensions of the environmental heating chamber). Whilst alternative bond pullout tests such as the eccentric pullout test (Chana, 1990) and the direct tension pullout bond test (Tastani & Pantazopoulou, 2006) create a more realistic scenario for determining bond strength, the required specimen dimensions and geometry of the environmental chamber at the University of Edinburgh made these experiments impractical to undertake.

A bond breaker with a length of 55mm was applied to the embedded FRP bars so that the bond length (40mm) was limited to being within the central portion of the embedded length (see Figure 5-1). Electrical (PVC) adhesive tape was applied to the bars' exterior, in two layers, to create the bond breaking surface. Between one and

three thermocouples were attached along the bonded length at the surface of the FRP bar, to verify the surface temperature of the bar during heating and to check (and monitor) that the bond reached the desired temperature during heating and prior to loading of the samples. These were attached with fine wire and were considered to have a minimal impact on the bond strength. Testing was generally performed under a steady-state thermal regime (testing matrix is shown in Table 5-1).

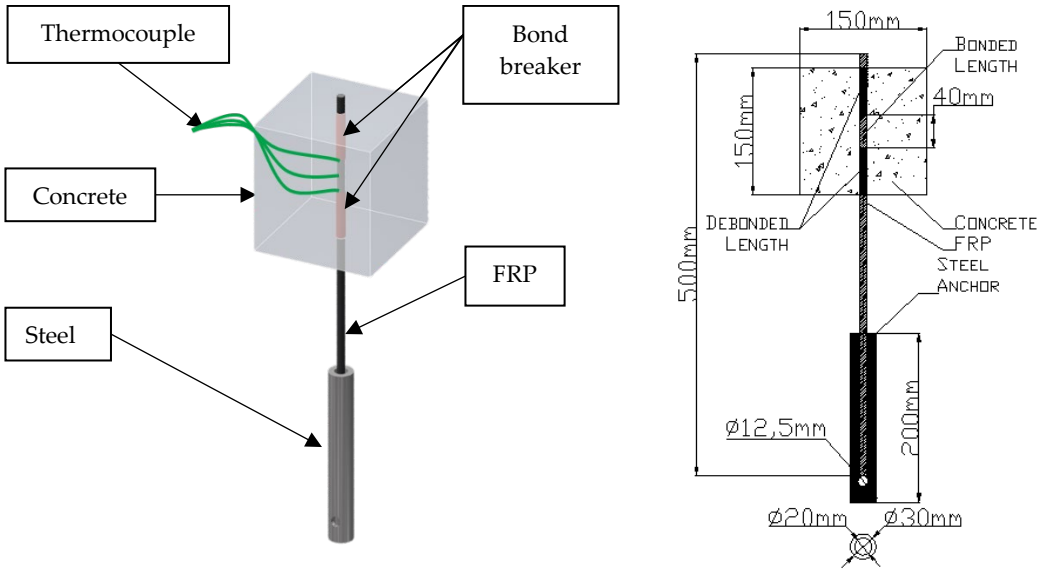

Figure 5-1: Schematic of bond pullout sample showing overall configuration and instrumentation

Concrete samples were cast on their side, with the FRP bar held in place by the surrounding formwork. Samples were left to cure in the structures testing hall at the University of Edinburgh under ambient temperature (10°C-15°C) for a minimum of 28 days prior to testing. Though as discussed in the literature review, concrete strength has minimal impact of the bond strength of the FRP (Bakis, Bank, Brown, et al., 2002).

5.2.3 Development of Tension Loading Anchorage

The development of the tension loading anchorage required to apply tensile loads to the free end of the embedded FRP bars was covered in Chapter 4; a similar tension anchorage was used for the pullout tests of the current chapter. The anchors used for the bond testing were, however, somewhat shorter than those used for the tensile testing in Chapter 4, with a length of 200mm and an external diameter of 30mm. They

were fabricated from stainless steel and were cored to provide an internal diameter of 20mm over a length of 100mm, which again reduced to 18mm for a length of 50mm and finally reduced to 16mm for the final 50mm. This stepped internal coring was used in an attempt to enhance the anchoring capacity, due to undesirable failures of some of the samples during initial trial testing.

The steel anchor tubes were secured to the FRP bar using a plastic cap and adhesive tape, as already described for the tensile testing in Chapter 4. However, due to the weight of the concrete pullout blocks, the samples could not be hung in the same manner as in Chapter 4 for potting and curing. Once the anchors had been attached these were secured to a portable frame and the concrete blocks were manoeuvred until the bar was centrally located within the anchor, as shown in Figure 5-2. A microsilica epoxy system (Gurit SP106 resin and hardener with Fillite filler) was used to pot the bars in the anchors, the same method as described in Chapter 4.

Figure 5-2: Potting technique used for Bond Pullout Specimens

5.2.4 Testing Procedure

A steel testing and restraining rig was used to support the concrete end block at one end (i.e. the upper end) of the bond pullout specimens within the environmental chamber during testing. This was connected within the Instron 600LX testing frame

using the wedge action tensile grips, as shown in Figure 5-3. The free end (i.e. the lower end) of the bond pullout specimens was connected into the Instron 600LX frame using a bespoke pin and shaft connector, similar to that used for the tensile testing presented in Chapter 4. The testing setup used for the bond pullout tests is shown in Figure 5-3 and Figure 5-4.

In general, the bond pullout tests were performed under steady-state thermal conditions wherein the bond pullout blocks were heated within the environmental chamber up to their test temperature. The blocks were heated at a rate of 5°C per minute, until the target test temperature was reached at the bondline surface of the embedded FRP bars – this being confirmed using the internal thermocouples that were placed during casting of the concrete anchor blocks.

During heating the bars were stressed to a sustained level of 10 MPa under load control to account for thermal expansion and/or contraction during heating and so as to avoid seating effects when loading was applied once the samples had reached the target test temperatures.

Due to the influence of elevated temperature it was not possible to use strain gauges or LVDT to determine slip. A digital SLR camera was used to quantify slip through digital image correlation, however interpreting this vast quantity of data was beyond the scope of this thesis

All samples were held at the target test temperature for 15 minutes prior to loading to failure, in order to promote uniform temperatures along the FRP's bonded length and minimise thermal gradients, both within the concrete block and along the bonded surface. The bond pullout specimens were then loaded under displacement control, at a crosshead stroke rate of 2mm per minute (arbitrary rate), until bond failure.

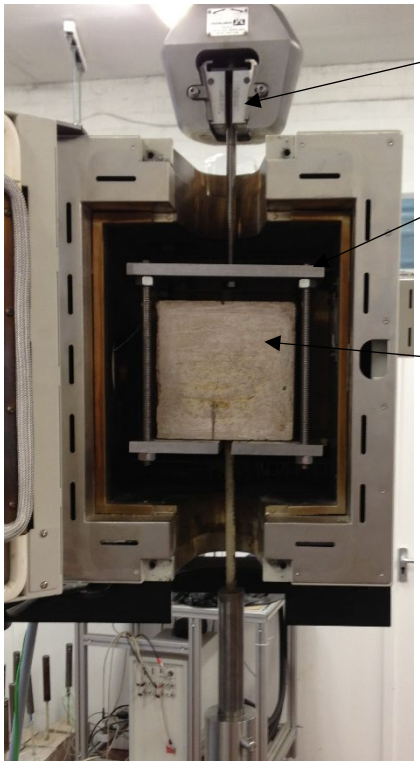

Figure 5-3: Photo of a Typical Bond Pullout Specimen within the Environmental Chamber and ready for testing

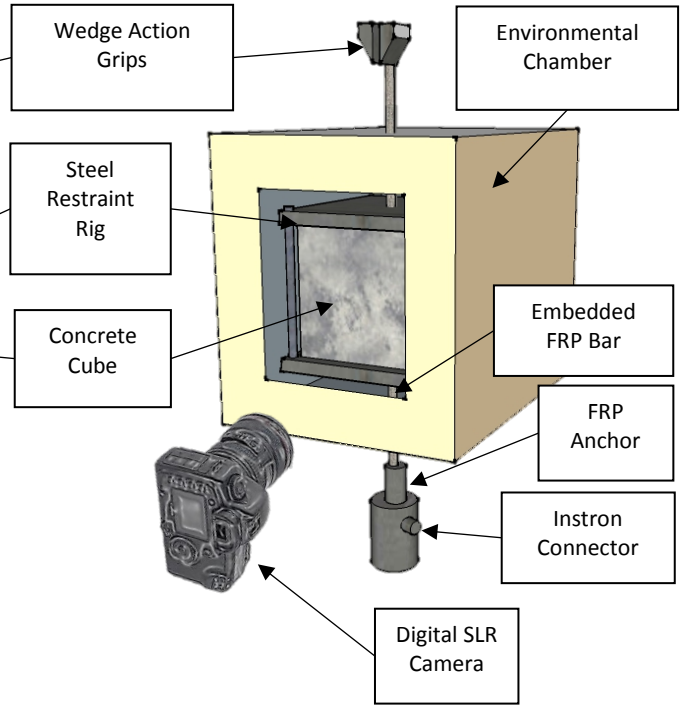

Figure 5-4: Schematic Showing Key Components of the Bond Pullout Test Setup

5.2.5 Bond Testing Matrix

Temperatures within the environmental chamber, for the steady state bond pullout tests, varied from ambient temperature up to 157˚C. The test matrix for the bond pullout tests is given in Table 5-1. In some cases, the actual bar surface temperatures achieved during tensile tests on the FRP bars varied slightly from the nominal test temperatures (these discrepancies are noted in tables 5-2 through 5-4).

Table 5-1: Bond Pullout Testing Matrix

Temperature Definition*	BPG		PTG		PTC	
	Temp. (˚C)	No.	Temp. (˚C)	No.	Temp. (˚C)	No.
Ambient **	20	3	20	3	20	3
Intermediate 1	65	3	66	2	-***	-
T_g Onset	86	3	83	3	64	3
T_g Modulus	109	3	105	3	86	3
Intermediate 2	-	-	133	3	-***	-
T_g Tan δ	136	3	154	3	108	3
Intermediate 3	149	3	-	-***	133	1
Intermediate 4	-	-	-	-***	157	4

*As defined in Chapter 3.

**Ambient temperature of the lab typically fluctuated between 10˚C and 25˚C, although this is not considered to have influenced the test results.

Tests were not undertaken for all bars at all temperatures listed, due to the number of samples available to test.

The unique identification nomenclature for each test specimen is given in the form XXX_BYYYi, where "XXX" indicates the FRP type, i.e. BPG, PTG, PTC, YYY indicates the testing temperature (˚C) and "i" indicates the test number for each set of variables in roman numerals. For example, BPG_B20iii is the third steady state bond pullout test carried out at ambient temperature on FRP bars of type BPG.

5.3 Bond Test Results and Discussion

The results of the bond pullout tests are shown in Table 5-2, Table 5-3 and Table 5-4 for FRP bars BPG, PTG, and PTC, respectively. The surface temperature of the tested FRP bars represents the average temperature of the three thermocouples placed on the bond line during the isothermal phase of the heating. The average bond strength has been calculated using the peak tensile load (P_{max}), the bond embedment length (l

= 40mm), with the FRP bars' nominal diameter (d) as shown in Equation [5-1] (Ammon Katz, Berman, & Bank, 1999):

$$\tau = \frac{P_{max}}{\pi \cdot d \cdot l} \qquad [5\text{-}1]$$

Table 5-2: Bar BPG Bond Pullout Results

Specimen ID	Bar Temp. (˚C)	Avg. Temp. (˚C)	St. Deviation (˚C)		Peak Load (kN)	Bond Strength (MPa)	Avg. Bond Strength (MPa)	St. Deviation		Norm. Strength
			σ	3σ				σ	3σ	
BPG_B20i	Ambient	Ambient	-		13.01	10.35	9.68	0.74	2.22	1.07
BPG_B20ii	Ambient				12.61	10.04				1.04
BPG_B20iii	Ambient				10.87	8.65				0.89
BPG_B65i	72	69	2.39	7.18	10.95	8.71	8.68	2.06	6.17	0.90
BPG_B65ii	70				7.73	6.15				0.64
BPG_B65iii	66				14.06	11.19				1.16
BPG_B86i	71	79	5.96	17.87	11.26	8.96	6.40	1.82	5.45	0.93
BPG_B86ii	80				6.69	5.32				0.55
BPG_B86iii	86*				6.19	4.92				0.51
BPG_B109i	107	108	0.86	2.57	9.31	7.41	6.27	0.86	2.58	0.77
BPG_ B109ii	109*				6.71	5.34				0.55
BPG_B109iii	108				7.61	6.06				0.63
BPG_B136i	136*	136	1.10	3.31	5.93	4.72	4.03	0.50	1.50	0.49
BPG_B136ii	135				4.45	3.54				0.37
BPG_B136iii	137				4.82	3.84				0.40
BPG_B149i	148	148	0.31	0.94	3.63	2.89	3.37	0.39	1.16	0.30
BPG_B149ii	148				4.82	3.84				0.40
BPG_B149iii	148				4.26	3.39				0.35

*No heating data available for these experiments due to damaged thermocouples, nominal test temperatures used.

Table 5-3: Bar PTG Bond Pullout Results

Specimen ID	Bar Temp. (˚C)	Avg. Temp. (˚C)	Standard Deviation (˚C)		Peak Load (kN)	Bond Strength (MPa)	Avg. Bond Strength (MPa)	Standard Deviation		Norm. Strength
			σ	3σ				σ	3σ	
PTG_B20i	Ambient	Ambient	-		22.93	19.21	21.51	1.56	4.67	0.89
PTG_B20i	Ambient				25.42	21.29				0.99
PTG_B20i	Ambient				28.11	23.55				1.09
PTG_B20i	Ambient				26.24	21.98				1.02
PTG_B66i	68	67	1.05	3.14	15.14	12.69	13.69	1.01	3.02	0.59
PTG_B66ii	66				17.55	14.70				0.68
PTG_B83i	84	84	1.32	3.95	12.41	10.39	9.31	0.80	2.40	0.48
PTG_B83ii	83				10.82	9.06				0.42
PTG_B83iii	86				10.13	8.49				0.39
PTG_B105i	109	109	0.97	2.92	9.22	7.72	10.73	3.04	9.13	0.36
PTG_B105ii	107				17.79	14.90				0.69
PTG_B105iii	109				11.44	9.58				0.45
PTG_B133i	128	133	3.71	11.12	9.95	8.34	6.17	1.03	3.10	0.39
PTG_B133ii	132				7.59	6.36				0.30
PTG_B133iii	138				7.13	5.97				0.28
PTG_B154i	153	159	5.42	16.25	4.81	4.03	3.75	0.28	0.84	0.19
PTG_B154ii	164				4.14	3.47				0.16

Table 5-4: Bar PTC Bond Pullout Results

Specimen ID	Bar Temp. (˚C)	Avg. Temp. (˚C)	Standard Deviation (˚C)		Peak Load (kN)	Bond Strength (MPa)	Avg. Bond Strength (MPa)	Standard Deviation		Norm. Strength
			σ	3σ				σ	3σ	
PTC_B20i	20.00	20	-		9.14	7.65	8.70	1.49	4.46	0.88
PTC_B20i	20.00				9.13	7.65				0.88
PTC_B20i	20.00				12.89	10.80				1.24
PTC_B64i	70	67	1.60	4.81	7.32	6.13	6.80	0.48	1.43	0.70
PTC_B64ii	66				8.51	7.12				0.82
PTC_B64iii	66				8.55	7.16				0.82
PTC_B86i	87	87	0.56	1.68	5.82	4.87	5.11	0.20	0.59	0.56
PTC_B86i	87				6.39	5.35				0.62
PTC_B86i	86				6.11	5.12				0.59
PTC_B108i	108	108	1.05	3.14	7.37	6.18	5.25	0.74	2.23	0.71
PTC_B108i	107				5.21	4.36				0.50
PTC_B108i	110				6.23	5.22				0.60
PTC_B133i	133	133	-		4.96	4.15	4.15	-		0.48
PTC_B157i	160	158	3.69	11.08	3.11	2.60	2.57	0.45	1.35	0.30
PTC_B157ii	162				2.18	1.83				0.21
PTC_B157iii	160				3.42	2.87				0.33
PTC_B157iv	152				3.56	2.98				0.34

It is evident from the bond pullout test results that there is variability in the peak bond strength. Particularly in the case of the BPG bars, where a bond pull out test performed at a nominal temperature of 65˚C, resulted in a higher bond strength than the ambient tests. It is hypothesised that the variability in the performance of the bond is due to the surface treatment, which is applied to the bar in a secondary curing process, and there is likely to be inconsistencies in the sand coating. Unfortunately, at this time, there is insufficient data to validate this hypothesis. Tests carried out on a greater number of samples would allow of better understanding of the variability.

Figure 5-5, Figure 5-6 and Figure 5-7 show the relationships between bond strength and temperature for bars BPG, PTG, and PTC, respectively, as established from the bond pullout tests. It is noteworthy that the y-axis data are non-normalised in these figures, so that the bond strength at ambient temperature for bar PTG was about twice that determined for bar BPG and PTC. A comparison of all normalised bond test data is shown in Figure 5-8.

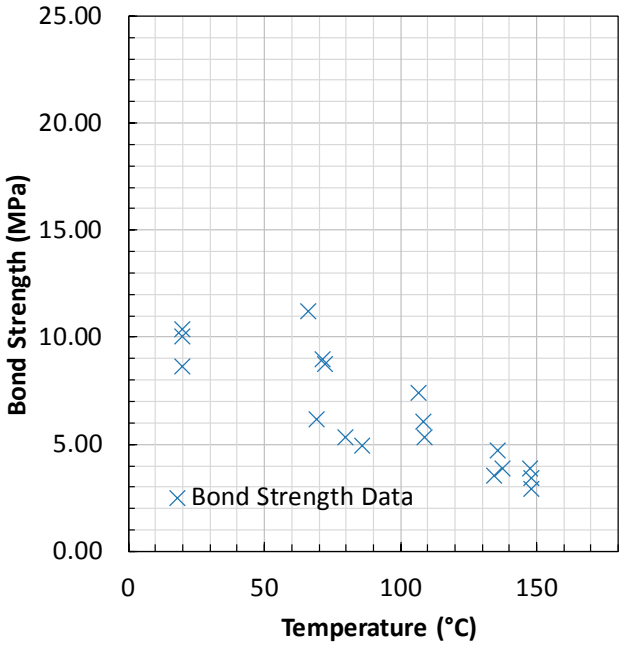

Figure 5-5: Bond Strength versus Test Temperature for BPG Bars

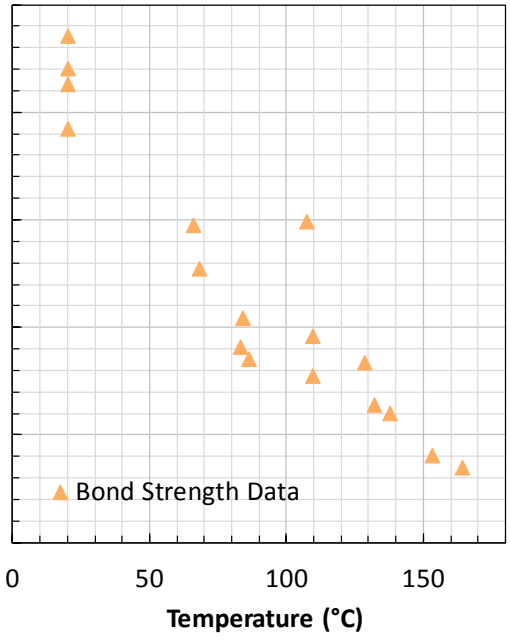

Figure 5-6: Bond Strength versus Test Temperature for PTG Bars

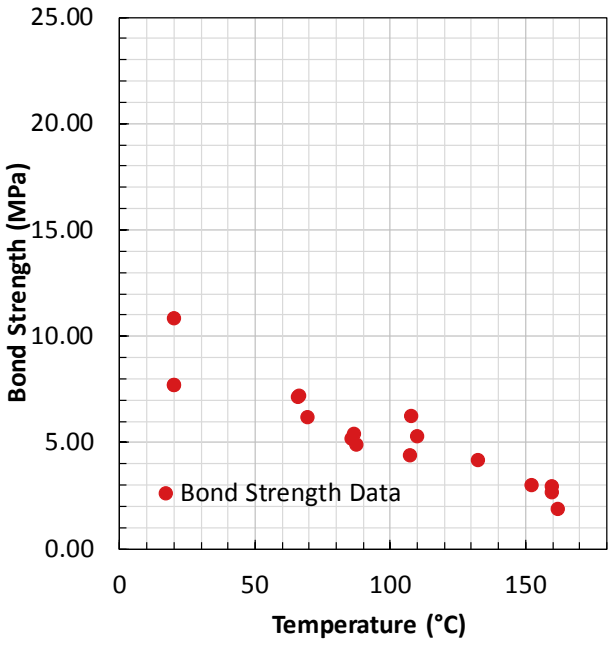

Figure 5-7: Bond Strength versus Test Temperature for PTC Bars

sh

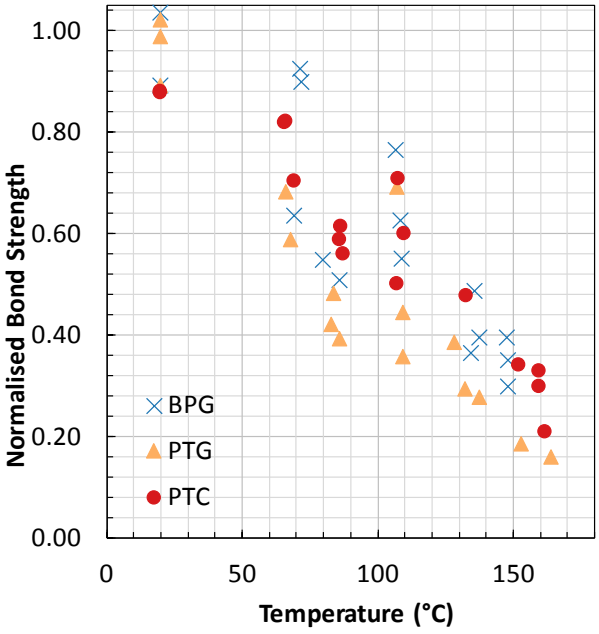

Figure 5-8 Normalised Bond Strength vs Temperature for all FRP bars

The previous figures show that bond is severely affected by softening of the polymer matrix, with all FRP bars, irrespective of fibre type losing between 70-80% of their bond strength by T_g *Tan*δ. This demonstrates good correlation with previous research

(Bank, Puterman, & Katz, 1998; A. Katz & Berman, 2000; Ammon Katz, Berman, & Bank, 1999). This is significant as it indicates that bond is critical even at lower temperatures, such as T_g *Onset.* At T_g *Onset* average bond strength loss of BPG and PTG bars was 34% and 57% respectively, in comparison to a 22% loss for PTC bars. Specifically for GFRP bars, this reinforces the requirement for cold anchorage, using techniques such as:

- cross-compartment continuous reinforcement;
- increased concrete cover; and/or
- bent FRP bars in anchorage.

During the bond pullout tests, and based on prior research involving bond pullout tests of FRP bars at ambient temperature, it was assumed that once the maximum average bond strength had been reached, during any given test, that a descending branch of the bond strength versus crosshead stroke response would be observed. However, during the testing, while there an initial "dip" in the average bond stress versus crosshead displacement curve, in some tests the load then continued to increase, albeit at a reduced stiffness (see Figure 5-9 as an example). This initial peak is reached where partial shearing of the resin coating has occurred, i.e. interfacial debonding (Chang, Yue, Lin, et al., 2010). As described previously, a bond breaker consisting of PVC tape was used to create a known bonded length of 40 mm within the bond pullout blocks, but it is hypothesised that this failed to perform precisely as intended once the FRP-concrete bond was initially lost (i.e. beyond the initial peak in the load versus crosshead displacement curves). In many of the bond pullout tests, final failure of the blocks occurred by lateral splitting of the concrete block (as depicted by the large drop in load in Figure 5-9), however this was at displacements well beyond the initial peak. As discussed in the literature review, Katz (1999) observed slip hardening whereby concrete became trapped between the coating and the core of the bar as it was pulled out. It is hypothesised that in these tests "bunching" of the top bond breaker (similar behaviour to that of the slip hardening phenomenon) occurred after the initial bond failure, and that this artificially

enhanced the load carrying ability of the specimens at large slip displacements by providing additional mechanical interlocking beyond the initial bond stress peak. A visual example of this, taken after splitting and failure of one of the PTG samples, shown in Figure 5-10Figure 5-11. The red de-bonding tape can be seen remaining in the concrete block after the FRP bar has been pulled out. By contrast the tape used as a bond breaker, at the bottom of the sample, has been pulled out with the bar.

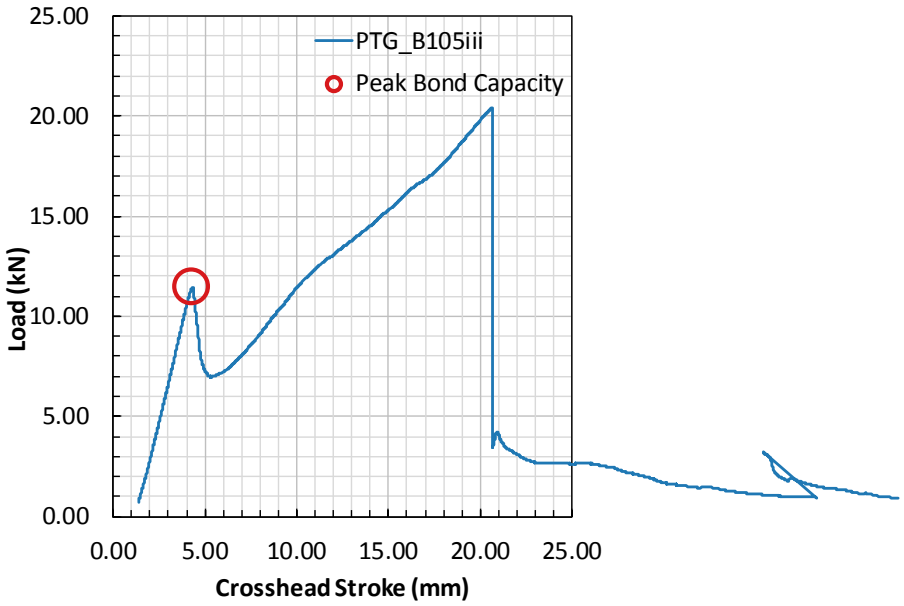

Figure 5-9: Typical Applied Load versus Crosshead Stroke Displacement Curve showing Peak Bond Capacity and Subsequent Increasing Load Thought to be Due to "Bunching" of the Bond Breaker

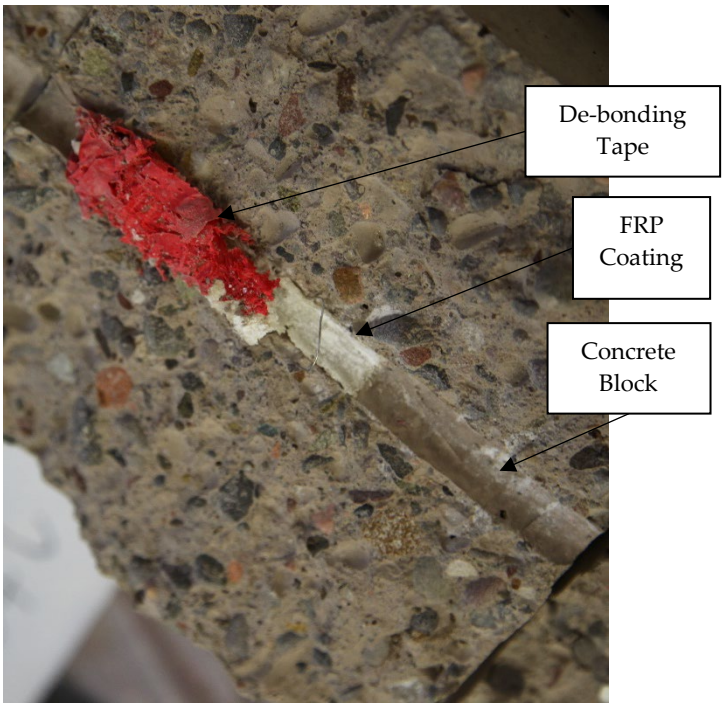

Figure 5-10 Post Testing Photo of Failed Sample PTG_B84ii as an example of Residual Bar Coating and "Bunching" of the Bond Breaker

Figure 5-11 Post Testing Photo of Bar PTG_B84ii showing Lower Bond Breaker

Load versus crosshead displacement for the initial five minutes of the testing (up to 10mm) for BPG, PTG and PTC bars are shown in Figure 5-12, Figure 5-13 and Figure 5-14 respectively. While final failure was typically as a result of concrete splitting, the increase in load carrying ability following the initial peak and dip, can be seen to decrease with increasing test temperature, (as shown in Figure 5-12, Figure 5-13 and Figure 5-14). Figure 5-15, Figure 5-16 and Figure 5-17 also show a visual representation of this, specifically in the case of the GFRP bars, more of the bar coating has been removed with increasing temperature, with complete interfacial debonding of the coating at the highest temperatures. Additionally the carbon bars, even at ambient, have lost a significant portion of the coating, whereby a comparatively low peak bond strength is achieved. As the tests are carried out under displacement control, the stress under any given strain, will be higher in the PTC (carbon) bars due to the higher modulus of elasticity, thus inducing higher interfacial shear stresses at the coating-bar core interface and subsequently causing the bond to fail at a lower load than that of the GFRP bars. The absolute bond strength potential of the bar's

coating may ultimately be inhibited by the stiffness of the FRP. As no transient tests were undertaken, no conclusions can be drawn on the impact of the modulus of elasticity on bond strength beyond these observations.

At the highest test temperature, the GFRP tests were terminated following complete pullout of the bars, and in contrast all of the final failures of the carbon (PTC) bars where by pullout instead of concrete splitting.

While BPG bars have a higher ambient temperature tensile capacity (1468MPa) than PTG bars (1093MPa), based on the testing data provided in Chapter 4, it appears that the visually coarser sand coating of the PTG bar yields superior average bond strength at all test temperatures. When normalised however, the percentage loss is comparable (see Figure 5-8). The PTC bars also have the coarser sand coating however as discussed the higher stiffness of the bars yields a lower bond strength due to the higher interfacial stresses.

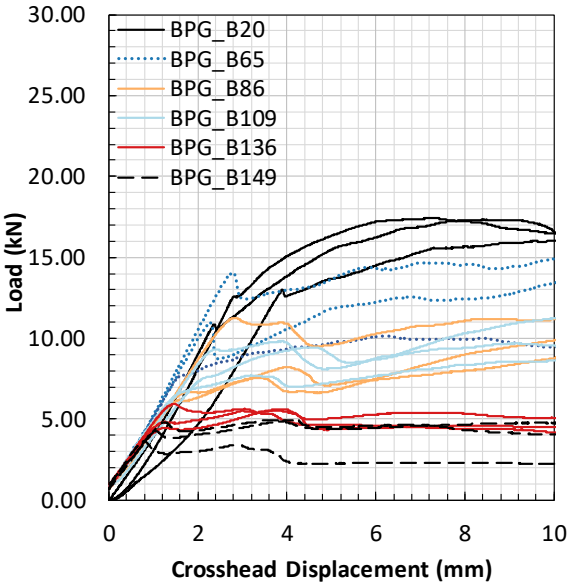

Figure 5-12 Load vs Crosshead Displacement for BPG Bars

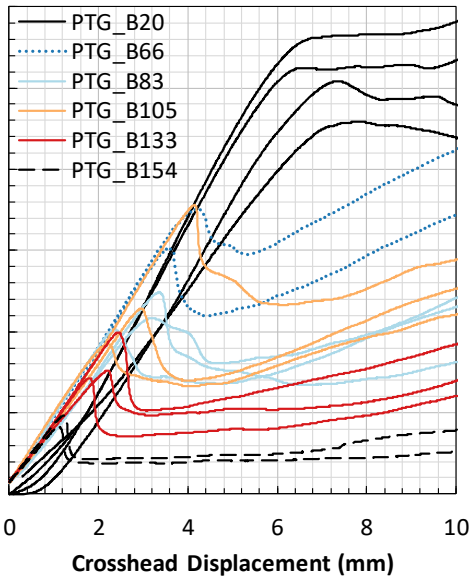

Figure 5-13 Load vs Crosshead Displacement for PTG Bars

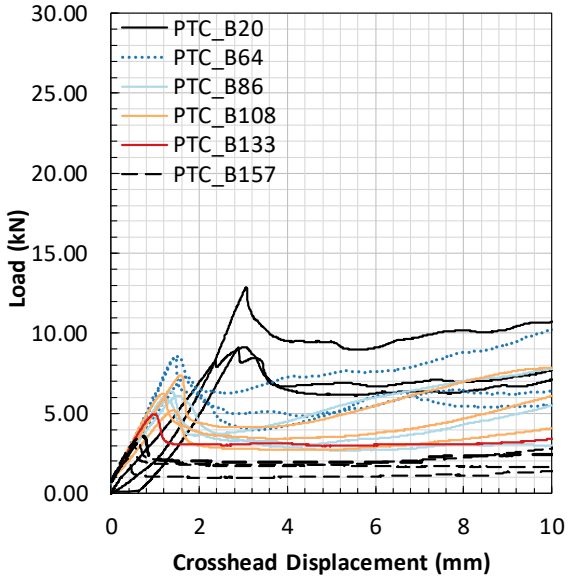

Figure 5-14 Load vs Crosshead Displacement for PTC Bars

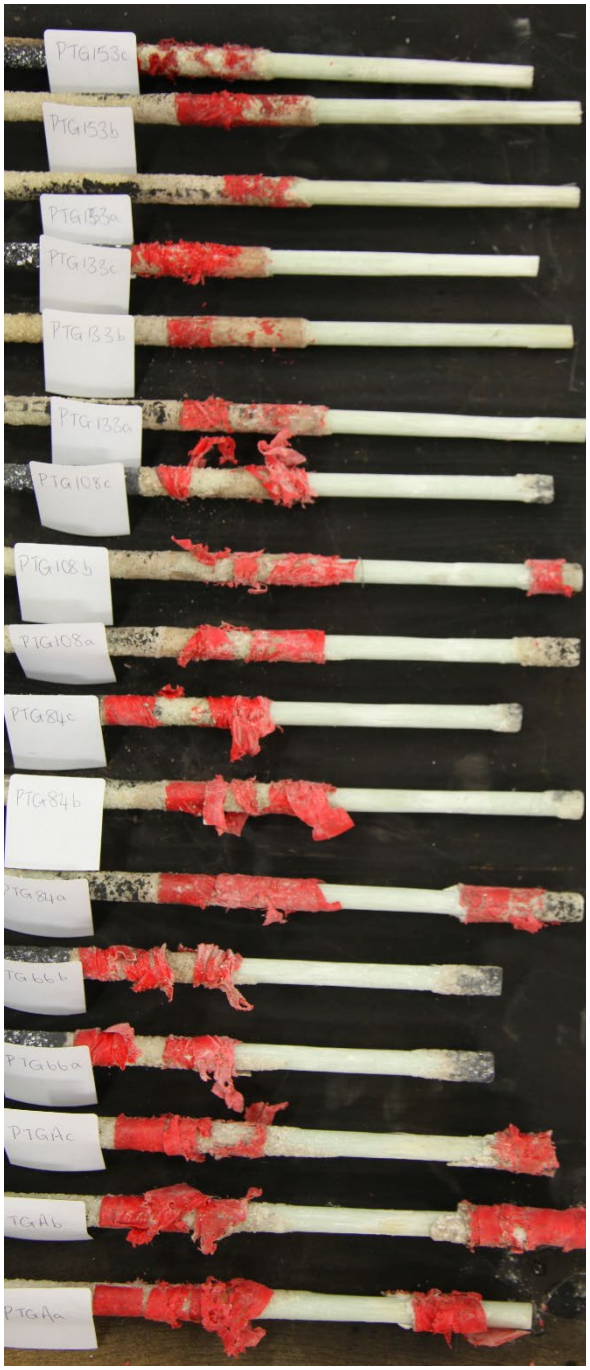

Figure 5-15: Typical Bond Failures for PTG Bars (Ambient – bottom to 154˚C - top)

Figure 5-16: Bond failures for BPG Bars (Ambient - bottom to 149˚C - top

Figure 5-17 Bond failures for PTC Bars (Ambient - bottom to 157˚C - top

5.4 BOND STRENGTH LOSS MODEL

It was observed during the bond pullout tests that failure of the specimens occurred in all cases due to separation of the bars' inner core from its surface sand coating, confirming that bond failure at elevated temperature was strongly dependent on the interfacial shear capacity of the resin close to the surface of the bar. Reductions in bond strength were thus observed to correlate reasonably well to the thermo-mechanical degradation of the polymer matrix; i.e. the softening of the polymer resin within the glass transition temperature range.

On the basis of the hypothesis that a correlation exists between bond strength reductions with increasing temperature and reductions in the FRPs' storage modulus (see Chapter 3) with increasing temperature, a minimum suite of tests is proposed herein to approximate the average bond strength loss for a pultruded FRP bar at elevated temperature. These are:

1. DMA testing to determine the storage modulus reduction with temperature, up to a temperature of twice T_g *Modulus*;
2. A minimum of two (preferably more) bond pullout tests on the FRP bar in question at a temperature in the range of T_g *Tanδ*, to define the residual bond strength above the glass transition; and
3. Where manufacturer specified average ultimate bond strength values at ambient temperature are not provided, a minimum of 2 to 3 bond pullout tests will also need to be carried out.

While bond strength models exist at ambient, limited models and no protocols have been established to determine bond strength loss at elevated temperature.

A semi-empirical model for average bond strength loss with increasing temperature is then described by the following equations:

$$\tau_T^* = \frac{\tau_T}{\tau_{amb}} = \alpha_g \qquad [5\text{-}2]$$

where τ_T is the ultimate average bond strength at temperature T and τ_{amb} is the ultimate bond strength at ambient temperature. The reduction of bond strength is assumed to be defined by the DMA storage modulus curve, which is given by:

$$\alpha_g\,(T) = \frac{E_T^* - E_g^*}{1 - E_g^*} \qquad [5\text{-}3]$$

where E_T^* and E_g^* are the normalised storage modulus values at temperature T and twice T_g *Modulus.* Given that the bond relies on chemical adhesion of the surface to the bar core, the DMA storage modulus curve has been modified such that it reduces to zero. The model therefore considers bond strength to be reduced to zero by 180°C. This was the maximum testing temperature during DMA, and is greater than T_g *Tanδ* for all of the FRP bars, therefore the polymer matrix will have softened and the interfacial shear stress capacity is effectively reduced to zero.

The predicted average ultimate bond strengths from the proposed model are shown in Figure 5-18, Figure 5-19 and Figure 5-20. The proposed model for GFRP bars overestimates the bond strength when compared against the average bond strengths obtained during the tests up until T_g *Modulus*, indicating that bond is susceptible at temperatures lower than the onset of the softening of the polymer resin. It is important to recognise that the thermal characterisation tests undertaken (i.e. DMA), were performed on core samples of the bar and therefore may not accurately reflect the behaviour of the polymer used in the secondary process of adhering the coating, perhaps accounting for the differences in the model versus the results. The adherence of the coating is applied in a secondary curing process (see section 2.3), and likely to not be cured to the same level as the core bar, reducing crosslinking of the polymer and ultimately meaning that the onset of the glass transition of the polymer occurs at a lower temperature. Additional DMA tests on the polymer coating would need to be performed to determine this. Unfortunately, due to the size of the bars, it was impossible to obtain a coating only sample of the bar.

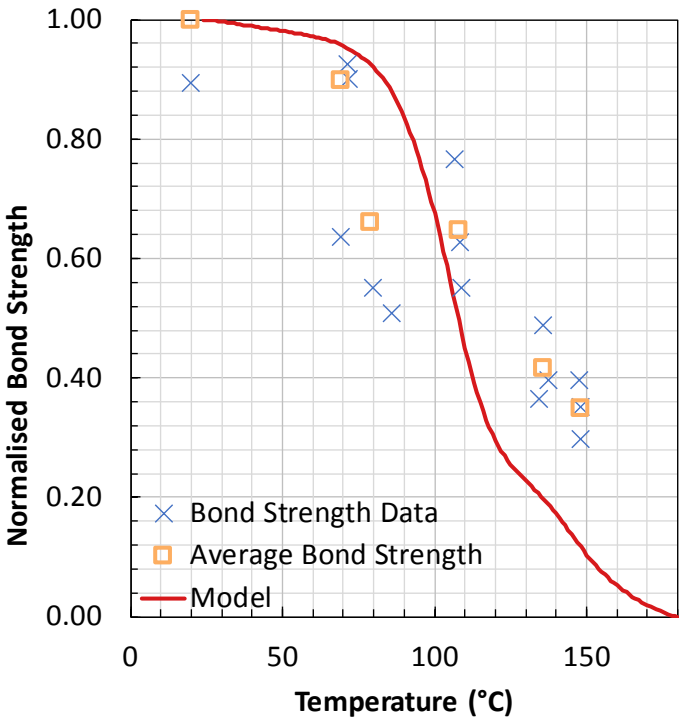

Figure 5-18: Comparison of model with bond pullout data for Bar BPG

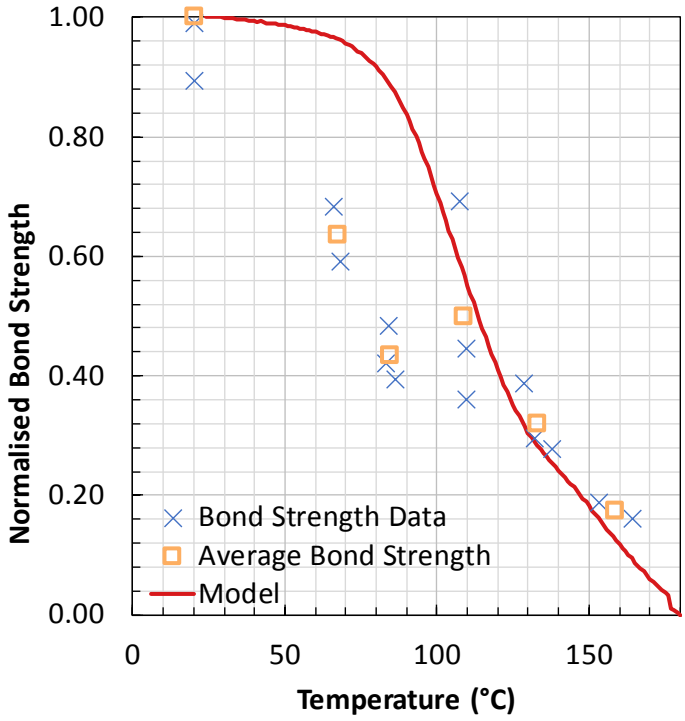

Figure 5-19: Comparison of model with direct tensile data for Bar PTG

Additionally the model assumes that zero bond strength is retained beyond $T_g\ Tan\delta$, whereas the test data indicates that there is some residual strength. Therefore the

model is conservative with respect to prediction of bond strength. It should be noted that in ACI 440-R1.15, no margin of safety has yet been determined for bond strength.

As this model only considers bond strength within the glass transition range, the model (Figure 5-20) does not account for bond strength loss beyond T_g $Tan\delta$ (108˚C for bar PTC). Similarly, the CFRP model overestimates the bond strength reduction at the lower temperatures. Beyond T_g $Tan\delta$, the model underestimates bond strength, potentially owing to the higher stiffness of the CFRP bars (as discussed previously).

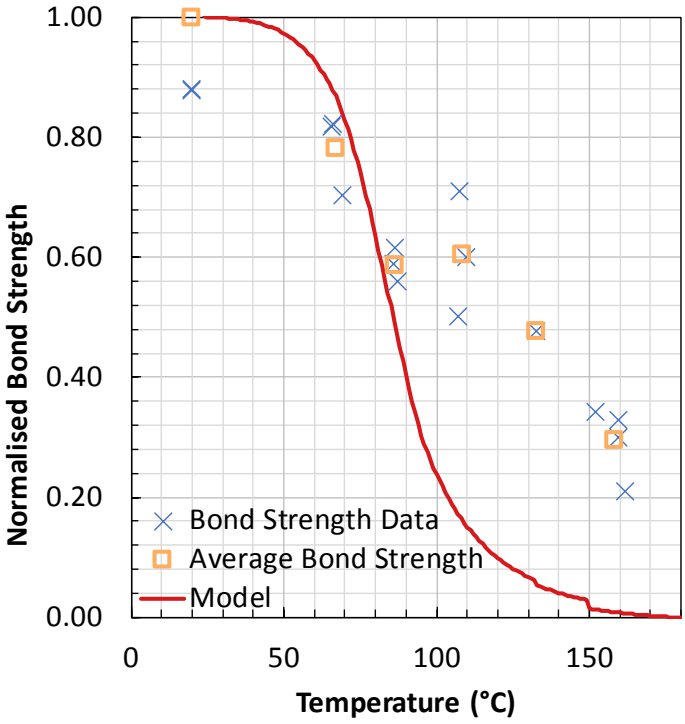

Figure 5-20: Comparison of model with direct tensile data for Bar PTC

It is acknowledged that this model is insufficient to predict bond strength loss at elevated temperature. In comparison to the model shown above, Rosa, Firmo, et al., (2018) have shown an unmodified DMA storage modulus curve against data from pullout curves, as shown in Figure 5-21.

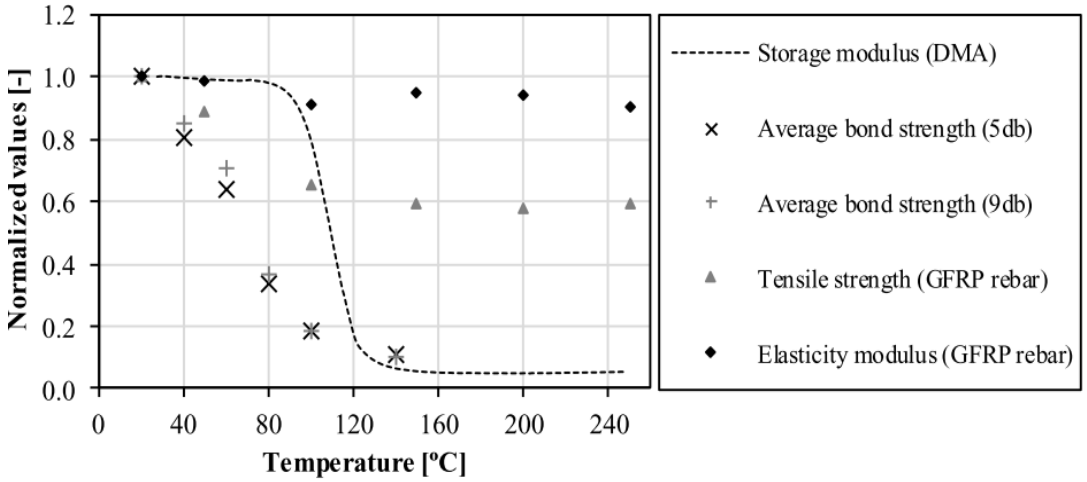

Figure 5-21 Normalized average values of bond strength, tensile strength, elasticity and storage modulus of the GFRP rebars, all as a function of temperature (Rosa, Firmo, Granadeiro, et al., 2018)

Similar to the test data presented herein, the onset of the glass transition occurs at higher temperatures than those at which bond strength is reduced.

The bond model produced by Katz & Berman (2000) was founded on the basis of a tanh function, with parametric analysis to determine the coefficients. These were based on the degree of crosslinking and glass transition temperature, as shown in Figure 5-22:

$$\tau^* = 0.5\left(1 - \tau_r^*\right) \tanh\left\{ -\frac{0.02}{\mathrm{Cr}}\left[T - k_1\left(T_g + \frac{k_1}{0.02}\mathrm{Cr}\right)\right]\right\} + 0.5\left(1 + \tau_r^*\right), \quad (10)$$

where

$$k_1 = \begin{cases} 1, & T_g \leqslant 80, \\ 1 - 0.025(T_g - 80), & 80 < T_g < 120, \\ 0, & T_g \geqslant 120. \end{cases}$$

Figure 5-22 Bond Strength loss model for FRP bars (Katz & Berman, 2000)

While this model shows good agreement with the data from the associated bond pullout tests (one example for a FRP bar similar to bar BPG is shown in Figure 5-23) this author acknowledges that the degree crosslinking must be known in order to

establish the bond loss curve. It was not possible to determine this for the FRP bars during this study.

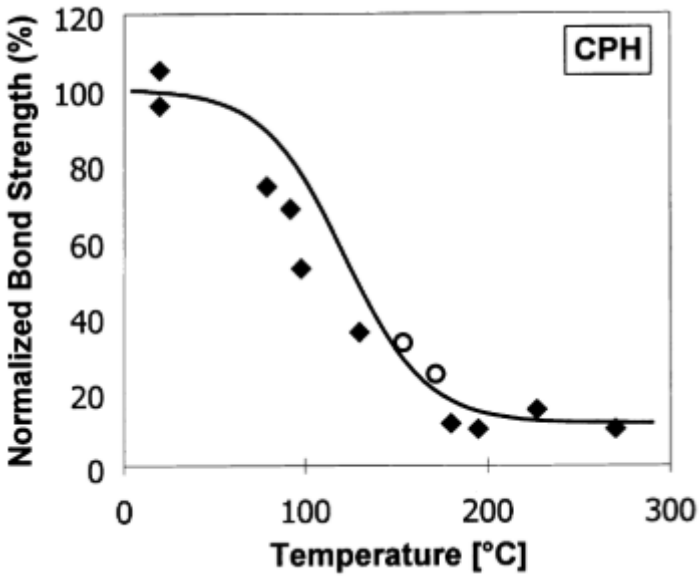

Figure 5-23 Comparison of experimental vs predicted results for bond strength loss for bar CPH (A. Katz & Berman, 2000)

Importantly the model has been related to the glass transition temperature though the author has not specified the method which must be used to define this, which could ultimately lead to more variability in the predicted results.

5.5 Further Work & Recommendations

The author acknowledges that lessons have been learned from these tests specifically with regard to the choice of bond breaker, which affected the post peak behaviour of the sample. Where possible the bond breaker should be prevented from "bunching", and providing additional resistance to pull out of the bar. As the bond breaker did not perform as required, further validation is required to confirm the results, though the tests have identified trends in the behaviour of the bond.

As examined in the literature review, there are limited tests on bond of FRP at elevated temperature and even fewer models, specifically with no clear evidence of alternative bond tests such as direct tensile pullout bond tests or eccentric pull out tests being carried out under fire conditions. It is recommended that alternate bond

pull out tests are undertaken, though consideration must be given to the appropriateness of the heating of the sample to ensure it is both comparable and realistic.

The tests presented in this chapter indicated that choice and application of surface treatment, as well as tensile stiffness may influence the behaviour of the bond. Additional research is required to understand these factors, specifically with DMA tests carried out on the surface polymer used to apply the coating.

Moving forward consideration should be given to the proprietary nature of the bars, which can be thermally characterised using bench scale analysis techniques such as DMA. As the temperatures defined note significant thermal events, (i.e. glass transition), then these should be used as testing temperatures. By undertaking future bond tests in this way, this would allow researchers to correlate trends in bond behaviour of bars.

Finally through the use of differential scanning calorimetry it would be possible to estimate the degree of crosslinking of the polymer bars, and subsequently compare the bond strength loss of the bars to the tanh model developed by Katz & Berman (2000). As a further development to this work, consideration should be given to the choice of T_g, with lower and upper bounds of the glass transition range used to capture the variability of bond strength loss at any given temperature.

5.6 Chapter Summary

Bond pullout tests have been undertaken for one CFRP and two GFRP bars embedded in concrete. While other bond tests were considered, they were not possible using the resources available at the University of Edinburgh. Steady state tests were performed at ambient and a range of temperatures, defined for the glass transition range, as set out in Chapter 3.

In agreement with previous researchers, the tests showed a significant loss of bond strength. The PTG bar yielded the highest ambient bond strength, though at T_g $Tan\delta$, the absolute values of bond strength were comparable across both the glass and the

carbon bars. The test results showed variability at similar test temperatures, which may be the result of a number of variables, e.g. type and application of surface treatment, and modulus of elasticity of the bars. Tape was used as a bond breaker, however post peak behaviour of the samples indicated that a more solid bond breaker was required, due to bunching of the tape.

A model has been produced based on a modified storage modulus curve (as defined by DMA, chapter 3) for each of the FRP bars. The predicted strength loss shows some correlation to the results, but ultimately do not accurately predict bond strength loss at elevated temperature. It is evident that the decrease in strength cannot be considered linear, based on the number of the samples tested, and the model presented by A. Katz & Berman (2000).

It is evident that the bond breaker is essential to the success of the bond pullout tests, though highlights that within a reinforced concrete element, a change in the linear profile of the reinforcement could provide additional bond resistance, e.g. bent bars at the anchorage. Interestingly for two FRP bars of the same coating, but different fibre type (PTG and PTC) they presented very different bond strength loss values and profiles. It is evident that with a higher stiffness bar, achieving the full potential of the coating (i.e. mechanical interlock), may ultimately be inhibited by the interfacial shear capacity at the coating-bar interface. The multi stage curing process of the FRP bars makes for a challenge in correlating bench scale behaviour to bond strength, specifically with regard to how polymer stiffness is affected by temperature, and in these tests the DMA results may not accurately reflect the part of the polymer (i.e. the coating) that is critical to maintaining the bond. As such, the bond strength model presented in this chapter, while providing some correlation, is insufficient to predict bond strength loss. Many more tests are required to build a bigger picture of bond strength loss within the glass transition range. The determination of bond strength loss at elevated temperature for FRP in concrete is significantly more challenging compared to that of steel (homogenous) due to the formulation of the bars and heterogeneous nature. However as agreed with other researchers, the overarching

conclusion is that cold anchorage is key to the maintaining structural fire resistance and preventing rebar pull out. As maintaining the bond between concrete and reinforcing material is critical to the stress transfer and performance of the reinforced concrete, the maximum temperatures of the reinforcing materials would need to be limited to at least T_g *Onset* if a cold anchorage zone cannot be maintained.

CHAPTER 6 FLEXURAL RESPONSE OF REINFORCED CONCRETE BEAMS AT ELEVATED TEMPERATURE

6.1 CHAPTER OVERVIEW

To understand the impact of tensile and bond strength loss on FRP reinforced concrete elements, this chapter presents results from 32 steel or FRP reinforced concrete (RC) beams in bending (eight beams per bar type). The beams were reinforced with a single FRP bar and tested in four-point bending using an ad-hoc non-standard fire testing approach, as alternative to standard fire testing. Additionally, the beams were fabricated with either continuous tension reinforcement or with a lap splice within the constant moment region near midspan. The beams were then tested under sustained loads considered to be representative of those that would be expected for comparable beams in an in-service condition, both at ambient temperature and under transient localised heating from below.

The tensile tests, presented in Chapter 4, have demonstrated that FRP bars can retain considerable (i.e. >50%) tensile strength at temperatures above T_g. As serviceability limits typically govern the design for both deflection (stiffness of FRP bars is typically less than that of steel reinforcing bars) and creep rupture, the FRP reinforcement is under-utilised in the ambient condition – unlike conventional steel RC which is typically under-reinforced, leading to a ductile failure. Due to FRP bars' high tensile strength at ambient temperature, and the fact that FRP reinforced concrete elements are often governed by serviceability considerations rather than ultimate strength, the absolute strength values of FRP bars at a given elevated temperature may actually be higher than for mild steel reinforcement at the same temperature. In certain applications, it may therefore be reasonable to assume that the critical temperature for FRP bars is significantly above T_g, provided that "cool" anchorage zones are maintained (recalling from Chapter 5 that bond strength is significantly reduced at temperatures above T_g). As discussed within the literature, two limiting temperatures should be considered for FRP reinforced concrete, related to bond strength and tensile loss (Weber, 2008b).

The intention of these tests was primarily demonstrative; considering the critical temperatures identified for tensile and bond identified in previous chapters, and also the impact of cold anchorage.

6.2 TESTING METHODOLOGY

6.2.1 Sample Preparation & Testing Procedure

The FRP reinforced concrete beam specimens were all designed in accordance (to the extent possible) with ACI 440.1 (ACI, 2006), whereas the steel reinforced beams were designed in accordance with ACI 318 (ACI, 2008).. The manufacturer specified properties for the FRP bars are shown in Table 6-1. Beam calculations are shown in the appendix B.

Table 6-1: Manufacturer Specified Properties

	BPG	**PTG**	**PTC**
Manufacturer	BP Composites Inc.*	Pultrall Inc.**	Pultrall Inc.
Bar #	3	3	3
Nominal Diameter (mm)	10	9.5	9.5
Fibre Type	Glass	Glass	Carbon
Fibre Content (% Wt.)	83.6	83	*-Not Specified-*
Resin	Vinyl Ester	Modified Vinyl Ester	Modified Vinyl Ester
Min. Tensile Strength (MPa)	1126	889	1431
Modulus of Elasticity (GPa)	63.2	53.4	120
Tensile Strain at Failure (%)	2.07	1.66	1.33

All 150mm square beams were reinforced with a single FRP/steel reinforcing bar and with a total length of 1450mm. Beams were cast with either continuous reinforcement or reinforcement which was lap spliced centered on midspan, with a splice length (overlap) of 420mm, as shown in Figure 6-1. The dimensions of the beams and the splice length chosen were essentially arbitrary, but dictated by the geometry of the loading and heating apparatus, as described in the following sections. The splice length in the BPG, PTG and PTC beams allowed 40%, 58% and 33% of the guaranteed tensile strength of FRP bar (f_{fu}*) (defined as mean tensile strength of sample of test

specimens minus three times standard deviation), to be developed. The developed tensile strength is above serviceability limits for both of the GFRP bars.

As beams were tested to failure in four point bending, steel shear reinforcement (6mm diameter square steel stirrups) was included outside the constant moment region (i.e. within the beams' shear spans). The concrete used had a 28-day cylinder compressive strength of 34MPa (standard deviation of 1.38MPa) and beams were cast from a single batch supplied by a local ready-mix concrete delivery company.

Sixteen of the 32 beams were tested using a transient thermal regime (i.e. load-then-heat), with the remaining beams tested in ambient conditions. The beams were loaded up to a pre-determined constant load (actually a pre-determined value of strain within the tensile flexural reinforcement, as described below), and this load level was held constant while the beams were heated until failure.

In the beams with continuous reinforcement a single strain gauge was placed on the tensile reinforcing bar at midspan so as to monitor the strain in the internal reinforcement during the loading stage of the tests (i.e. prior to heating). In the beams with spliced reinforcement, three strain gauges were placed evenly along one of the reinforcing bars within the midspan region. While strain gauges were used in the loading phase, it is acknowledged that during heating, they will fail, and the values were not considered once heating had commenced.

Linear potentiometers (LPs) were used to measure vertical displacements of the beams during both loading and heating phases of the tests, and reinforcing bar free end slips were also measured using LPs, as shown in Figure 6-2. An internal thermocouple (TC) tree with 5 TCs was cast into the concrete during fabrication of the beams. This was placed on the centerline of the each beam at midspan, allowing temperature measurements to be taken at depths of 0, 20, 30, 80 and 120mm from the heated face (i.e. the beams' soffit) (Figure 6-2), with a expected tolerance of +/- 2mm. Two additional TCs were installed, either at one end of the constant moment region (for the continuous reinforcement case) or at one end of the splice zone (for the spliced reinforcement beams), at both 0 and 20mm from the soffit.

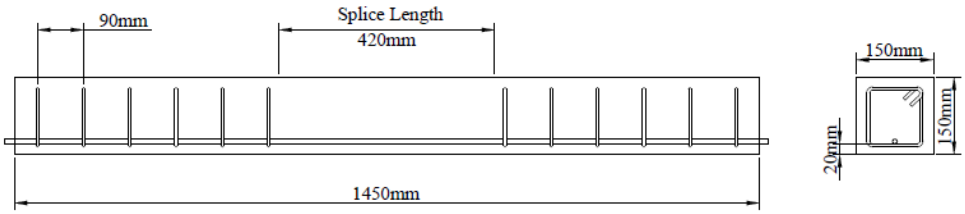

Figure 6-1: Steel or FRP Reinforced Concrete Beams – Dimensions and Reinforcement Detailing

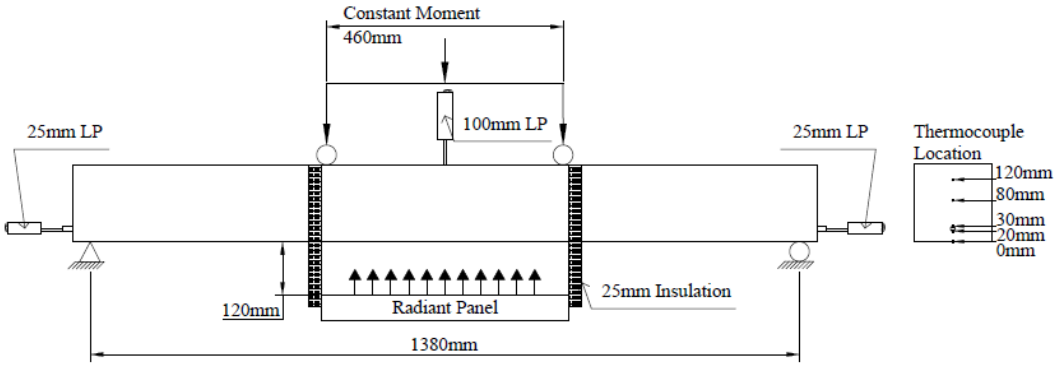

Figure 6-2: Schematic showing Test Setup for Steel/ FRP Reinforced Concrete Beams under Transient Heating

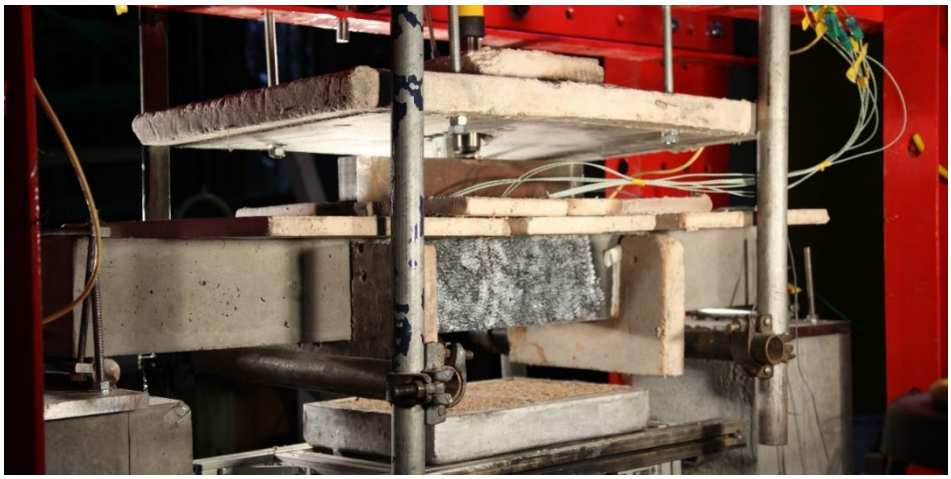

Figure 6-3: Photo showing Test Setup for Steel or FRP Reinforced Concrete Beams under Transient Localised Heating

All beams were tested in duplicate, either monotonically to failure at ambient temperature, or under sustained "service" loads with transient localised heating of the constant moment region (until failure or until the test was manually halted).

Tests at ambient temperature were performed under displacement control at a crosshead stroke rate of 2mm/min until failure. Transient thermal regime (i.e. fire)

tests were performed by loading the beams to above respective sustained service loads (based on creep rupture limit, 20% of guaranteed tensile strength for GFRP) and then heating them from below using a propane-fired radiant panel until failure (or for 90 minutes if no failure occurred).

The heated area in the transient tests was approximately controlled using ceramic fibre insulation boards, to ensure zones of cold anchorage for the flexural reinforcement located outside the heated zone (refer to Figure 6-2 and Figure 6-3). If no failure occurred during heating for 90 minutes, the beam was left to cool for 60 minutes under sustained load before the load was released. Beams that were intact after heating were cooled in ambient conditions, without any load applied, for a minimum of two weeks. Following cooling, residual monotonic testing to failure at ambient temperature, under displacement control at a crosshead displacement rate of 2mm/minute.

6.2.2 Testing Matrix for Reinforced Concrete Beam Tests

The testing matrix for the reinforced concrete beam tests is shown in Table 6-1. Thirty-two beams were tested in total; varied by reinforced, heating regime, and bar continuity conditions. All tests were performed in duplicate.

Table 6-2: Steel & FRP Reinforced Concrete Beam Testing Matrix

Reinforcing Materials	Specimen IDs		Testing Regime	Bar Diameter (mm)	Bar Continuity	# of Tests	Failure Mode
Steel	SAc1	SHc1	Ambient Temp.*	10	Continuous	2	Flexural
	SAc2	SHc2			Spliced	2	Flexural
	SAs1	SHs1	Transient Heating		Continuous	2	Steel Rupture
	SAs2	SHs2			Spliced	2	Steel Rupture
GFRP (BPG)	BPGAc1	BPGHc1	Ambient Temp.	10	Continuous	2	Flexural Shear
	BPGAc2	BPGHc2			Spliced	2	Flexural Shear
	BPGAs1	BPGHs1	Transient Heating		Continuous	2	Splice
	BPGAs2	BPGHs2			Spliced	2	Splice
GFRP (PTG)	PTGAc1	PTGHc1	Ambient Temp.	9.5	Continuous	2	Shear
	PTGAc2	PTGHc2			Spliced	2	Shear
	PTGAs1	PTGHs1	Transient Heating		Continuous	2	Splice
	PTGAs2	PTGHs2			Spliced	2	Splice
CFRP (PTC)	PTCAc1	PTCHc1	Ambient Temp.	9.5	Continuous	2	Shear
	PTCAc2	PTCHc2			Spliced	2	Shear
	PTCAs1	PTCHs1	Transient Heating		Continuous	2	Splice
	PTCAs2	PTCHs2			Spliced	2	Splice

*Ambient temperature of the lab typically fluctuated between 10˚C and 25˚C, although this is not thought to have significantly affected the experimental outcomes.

The unique identification for each test specimen is given herein in the form XXXTR1, where:

- "X" or "XXX" indicates the reinforcment type, i.e. S for steel or BPG, PTG, PTC,
- T indicates the test type; "A" for ambient and "H" for heated, i.e. transient thermal
- R indicates the continuity of the reinforcement; "C" for continuous and "S" for spliced
- "1" indicates the test repeat number for each set of variables.

For example, BPGAs2 is the second beam test at ambient with spliced BPG reinforcement.

6.3 RESULTS

Table 6-3 and Table 6-4 present selected test data for both the ambient and heated beam tests, respectively, along with beam designations based on the test variables. Figure 6-4, Figure 6-5, Figure 6-6, and Figure 6-7 show load vs central deflection for the ambient tests. Steel beams tested at ambient temperature, both continuous and spliced, experienced classical under-reinforced flexural failures, which occurred after large deformations and considerable yielding of the internal steel reinforcement. Spliced beams displayed a stiffening effect due to the presence of additional reinforcement in the midspan region (i.e. twice the reinforcement area within the splice region).

Both the PTG and BPG bar reinforced spliced beams tested at ambient temperature failed within the splice zone, coincident with concrete cover separation. Beams with continuous PTG and BPG bars failed due to tensile rupture of the FRP bars at the location of flexural shear cracks, along with localised concrete crushing close to the loading points. All PTC bar reinforced beams, whether with spliced or continuous bars, failed due to bond failure and slip of the CFRP bars within the anchorage zones, wherein interfacial separation of the bars' surface coating governed the behaviour and the bars slipped inside the beams. The strains in the respective reinforcing bars at peak loads are given in Table 6-3, and indicate the utilization of the various types of reinforcement at peak load during the ambient temperature beam tests.

Table 6-3: Ambient Beam Test Results

Name	Fibre Type	Bar Continuity	Peak Load (kN)	Strain in Bars at Peak Load (%)	FRP Bar Utilisation at Peak Load (%)[2]	Midspan Disp. at Peak Load (mm)	Failure Mode
SAc1	Steel	Continuous	22.4	-	-	46.0	Flexural
SAc2	Steel	Continuous	22.9	-	-	63.0	Flexural
SAs1	Steel	Spliced	24.4	-	-	22.2	Steel Rupture
SAs2	Steel	Spliced	26.2	-	-	39.9	Steel Rupture
BPGAc1	Glass	Continuous	34.8	1.43	69%	45.6	Flexural Shear
BPGAc2	Glass	Continuous	35.5	1.27	61%	30.3	Flexural Shear
BPGAs1	Glass	Spliced	36.7	1.28	62%	25.5	Splice
BPGAs2	Glass	Spliced	35.9	1.32	64%	26.4	Splice
PTGAc1	Glass	Continuous	30.6	1.06	64%	39.0	Shear
PTGAc2	Glass	Continuous	34.2	Failed Gauge	-	41.3	Shear
PTGAs1	Glass	Spliced	27.4	1.42	86%	24.6	Splice
PTGAs2	Glass	Spliced	27.8	1.29	78%	24.0	Splice
PTCAc1	Carbon	Continuous	39.8	0.81	61%	21.7	Shear
PTCAc2	Carbon	Continuous	37.4	>0.67[1]	-	21.0	Shear
PTCAs1	Carbon	Spliced	36.3	0.67	50%	15.7	Splice
PTCAs2	Carbon	Spliced	37.2	0.62	47%	17.6	Splice

[1] Indicates last recorded value as strain gauge failed 1 minute prior to failure of the beam.

[2] Based on manufacturer-specified tensile ultimate strain values (shown in Chapter 3)

Table 6-4: Heated Beam Test Results

Name	Fibre Type	Bar Continuity	Sustained Load (kN)	Bar Strain at Ignition[2] (%)	Time to Failure (min)	Peak Bar Temp.[3] (˚C)	Failure Mode	Residual Capacity (kN)
SHc1	Steel	Continuous	10.7	-	-	499[4]	-	25.0
SHc2	Steel	Continuous	10.9	-	-	475	-	25.0
SHs1	Steel	Spliced	10.9	-	-	474	-	21.7
SHs2	Steel	Spliced	10.8	-	-	498	-	17.6
BPGHc1	Glass	Continuous	13.3	27.2	63	499	Flexural/FRP Rupture	-
BPGHc2	Glass	Continuous	13.1	26.8	82	531	Flexural/FRP Rupture	-
BPGHs1	Glass	Spliced	13.0	26.7	11	181	Splice	-
BPGHs2	Glass	Spliced	13.1	26.8	11	167	Splice	-
PTGHc1	Glass	Continuous	10.6	31.7	-	566	-	10.7
PTGHc2	Glass	Continuous	10.6	31.4	-	526	-	15.7
PTGHs1	Glass	Spliced	10.6	31.8	16	260	Spice	-
PTGHs2	Glass	Spliced	10.6	31.8	17	249	Splice	-
PTCHc1	Carbon	Continuous	17.6	30.2	-	556	-	34.1
PTCHc2	Carbon	Continuous	17.6	30.0	-	560	-	30.7
PTCHs1	Carbon	Spliced	17.6	29.9	7	118[4]	Splice	-
PTCHs2	Carbon	Spliced	17.6	30.0	7	104	Splice	-

[2] As a percentage of the manufacturers' specified ultimate tensile strain (calculated from a plane section analysis under specified service load)

[3] Temperatures recorded from the lower surface of the reinforcing bars at midspan

[4] Measurement based on average data at underside of bar (20mm from soffit)

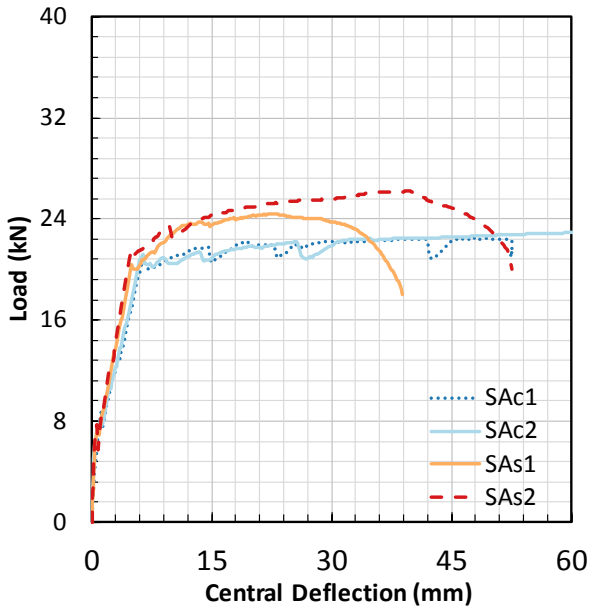

Figure 6-4 Ambient Temperature Load-Deflection Responses for Beams Reinforced with Steel

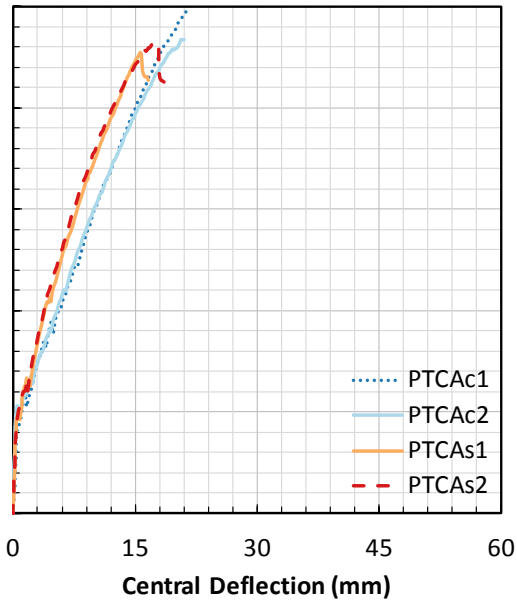

Figure 6-5Ambient Temperature Load-Deflection Responses for Beams Reinforced with PTC

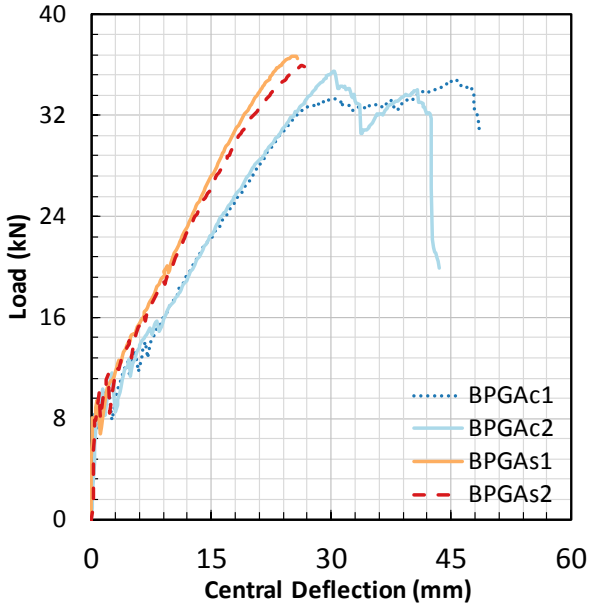

Figure 6-6 Ambient Temperature Load-Deflection Responses for Beams Reinforced with BPG

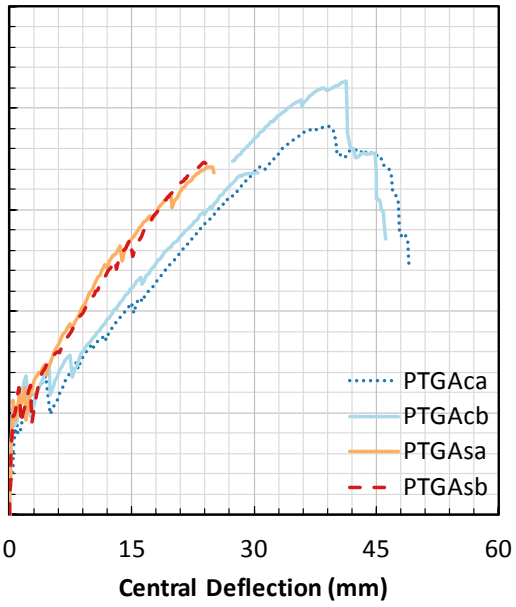

Figure 6-7 Ambient Temperature Load-Deflection Responses for Beams Reinforced with PTG

For the transient thermal tests, the placement of a thermocouple at the bottom of the beams allowed a determination of the typical temperature based exposure for the beams. Although it was not the intention to replicate the standard time-temperature curve, Figure 6-8 shows a comparison of the ISO 834 curve vs the soffit temperatures measured for all 16 reinforced beams heated under the transient thermal regime. The

curve for ISO 834 (European Committee for Standardization, 2001) given by Equation [6-1]:

$$T_{ISO} = 20 + 345log_{10}(8t + 1) \quad [6\text{-}1]$$

Where T_{ISO} is the temperature in °C and t is the time in minutes. In addition, the lower and upper bound values from the data set are shown in Figure 6-8. While the plateau temperatures are between 200°C and 300°C different, the initial stages of the heating are not dissimilar, in terms of rapid heating of the exposed element. It is noted also that the ISO 834 curve represents gas temperature within a furnace, while the data set depicts concrete temperature at the soffit, which will naturally be lower due to the thermal conductivity of the concrete being significantly less than that of air.

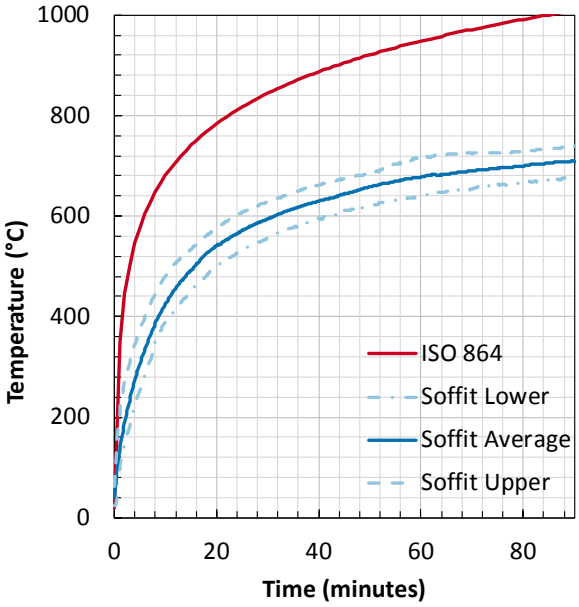

Figure 6-8 Comparison of ISO 834 vs Soffit Temperatures of Tested Beams

As reference, Table 6-5 shows the glass transition and decomposition temperatures defined in Chapter 3:

Table 6-5 Glass transition and decomposition temperatures for FRP bars

	BPG (°C)	PTG (°C)	PTC (°C)
T_g *Onset*	86	83	64
T_g *Modulus*	109	105	86
T_g *Tanδ*	136	154	108
T_d *Onset*	355	310	302
T_d *Peak*	414	384	377

Figure 6-9, Figure 6-10, Figure 6-11 and Figure 6-12 show the midspan deflections of the beams during the heated tests. Some beams (PTCHs1 & BPGHs1) are not shown due to malfunctioning of the deflection gauges during heating. Time zero in these plots is the onset of heating, which commenced after the beams had been loaded to the service loads given in Table 6-4, as already noted.

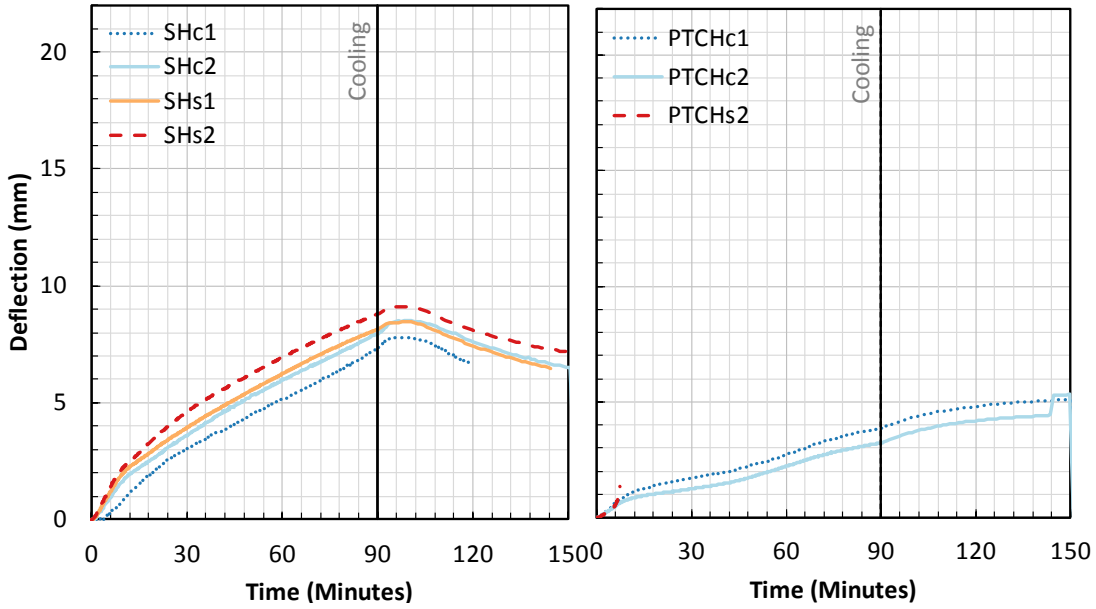

Figure 6-9 Heated Beam Deflections (from the Onset of Heating) for Beams Reinforced with Steel

Figure 6-10 Heated Beam Deflections (from the Onset of Heating) for Beams Reinforced with PTC

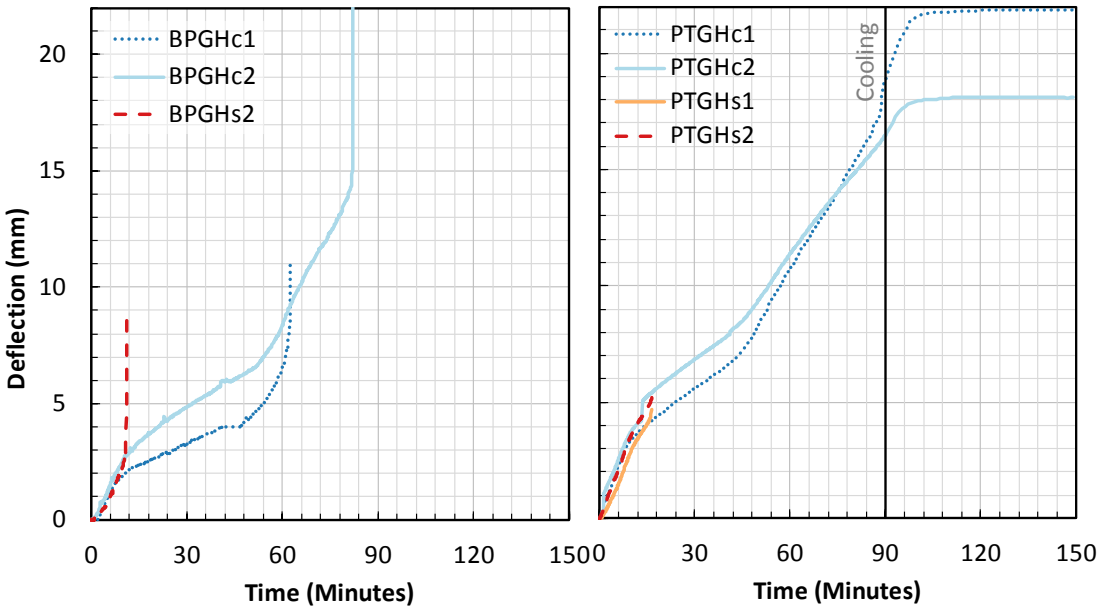

Figure 6-11 Heated Beam Deflections (from the Onset of Heating) for Beams Reinforced with BPG

Figure 6-12 Heated Beam Deflections (from the Onset of Heating) for Beams Reinforced with PTG

In all cases there is an increase in deflection during initial heating. This is due to thermal bowing of the beams resulting from the through thickness thermal gradients that are generated upon heating. This is followed by steady deflection increases, with differing responses depending on the reinforcement type and whether the reinforcement is continuous or spliced. Specifically for BPG and PTG beams (Figure 6-11 and Figure 6-12), the deflection increases again at approximately 48 and 45 minutes respectively. At this point in the heating, the temperatures at the underside of the rebars 448°C and 427°C for BPGHc1 and BPGHc2 respectively, and 422°C and 389°C for PTGHc1 and PTGHc2 respectively, have exceeded the peak decomposition temperature (Table 6-5) for each of the bars.

Additionally, as shown in Figure 6-13, flaming was observed at the central crack in the continuously reinforced concrete beams. It is understood that the crack was sufficiently wide enough to permit oxygen to interact with the decomposition of the polymer matrix and subsequently cause sustained flaming.

Figure 6-13 Sustained flaming at the centreline of PTGHc2 beam

By contrast the PTC continuously reinforced beams did not experience a secondary increase in deflection but rather continued deflected at the same rate, even when the radiant panels were switched off. The continuous deflection is presumably due to the thermal inertia within the beam and the sustained load which continued post heating for 60 minutes.

Steel reinforced beams (Figure 6-9) displayed steady deflection during heating but survived 90 minutes of heating, with decreases in deflection during cooling, as expected. Continuous PTC beams showed similar behaviour to steel beams, however deflections continued to increase, albeit at a lower rate, during cooling.

Figure 6-14 shows soffit and rebar temperatures (at the underside of the bars, 20mm from the soffit) experienced during the transient thermal regime. The beams, which failed during heating, have been shown on this figure also.

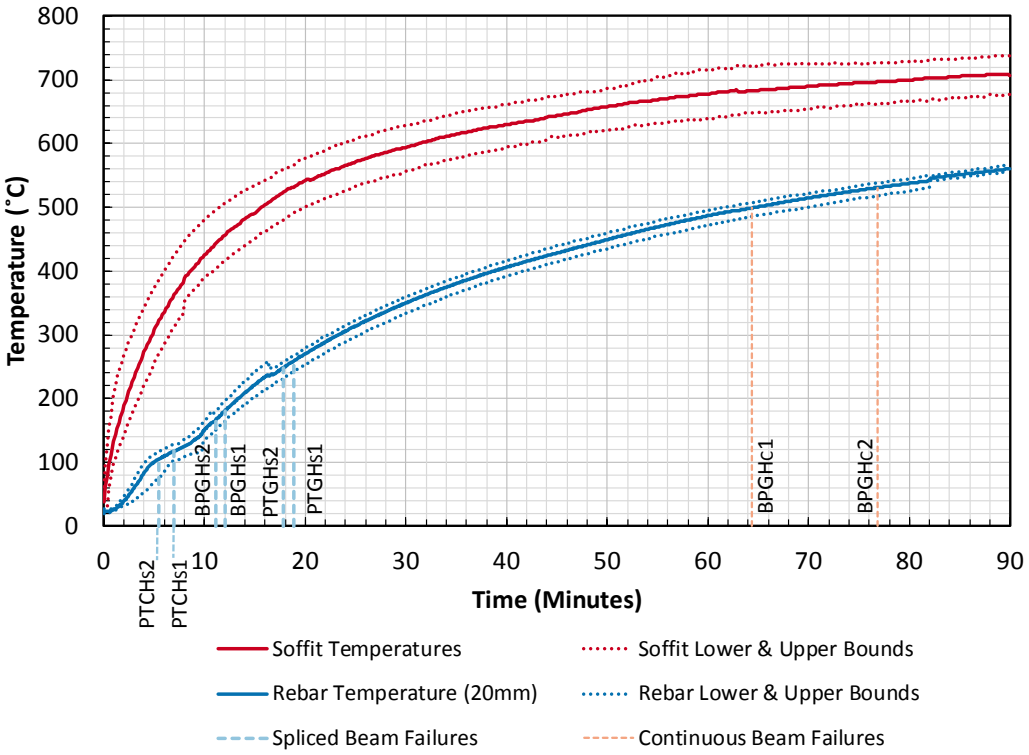

Figure 6-14 Plot showing soffit and rebar temperatures with beam failures indicated

Both continuously reinforced BPG beams failed by bar rupture in tension when the underside of the bar exceeded temperatures of 499˚C and 531˚C for BPGHc1 (see Figure 6-14 & Figure 6-15) and BPGHc2 respectively. Rebar temperatures at the top of the bar were 349˚C (Figure 6-15) and 418˚C for BPGHc1 and BPGHc2 respectively. All PTGHc beams survived the 90 minutes of heating, despite the bars experiencing temperatures of 566˚C and 526˚C for PTGHc1 and PTGHc2 (Figure 6-16) respectively. Rebar temperatures at the top of the bar were 453˚C and 423˚C for PTGHc1 and PTGHc2 (Figure 6-16) respectively. Both PTCHc beams did not fail during the heating phase with the rebar experiencing temperatures of 556˚C and 560˚C at the underside for PTCHc1 and PTCHc2 (Figure 6-17) respectively. Rebar temperatures at the top of the bar where 446˚C and 438˚C for the same beams respectively. Figure 6-15, Figure 6-16 and Figure 6-17 depict the temperature profiles for the concrete beams, with thermocouple placement as detailed in section 6.2.1. "Outside heated zone" refers to thermocouples placed at the end of the constant moment region (due to four point bending), which also coincided with being placed outside the vertical plane of the radiant panel used to heat the beams. Regardless of being *outside the*

heated zone, this part of the beam was exposed to both convective and radiative heat transfer. The temperatures shown in the following figures are as would be expected in a standard fire; causing compressive and tensile strength loss to both the concrete and the rebar respectively.

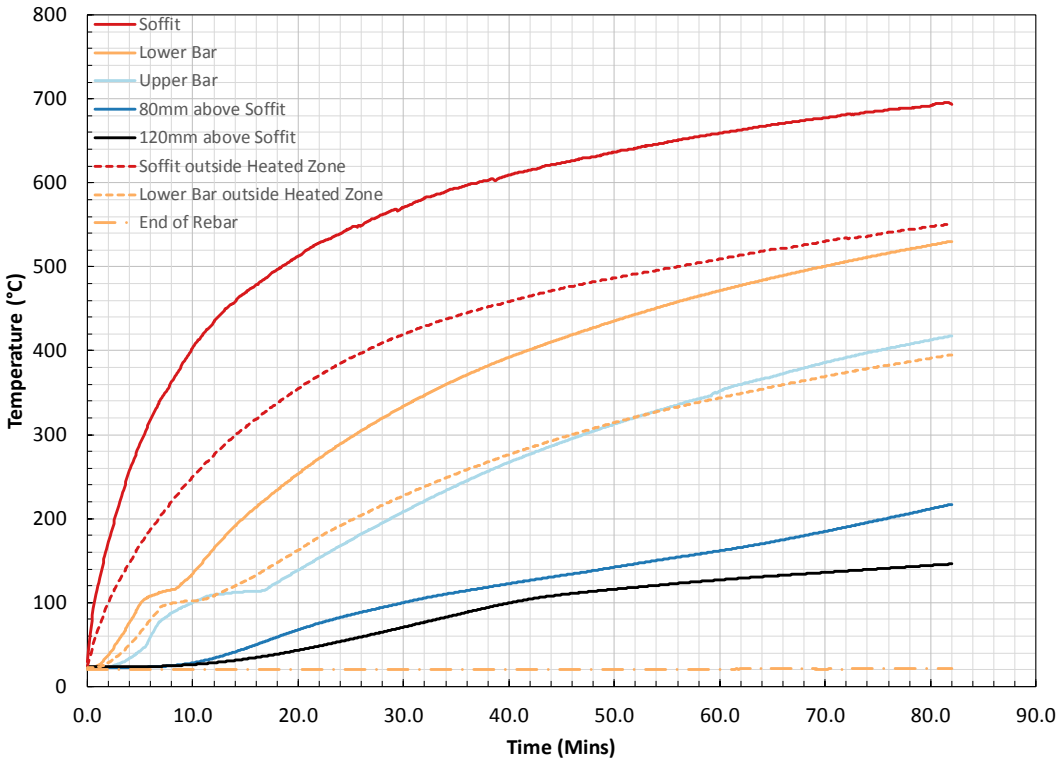

Figure 6-15 BPGHc1 Temperature Time Profiles

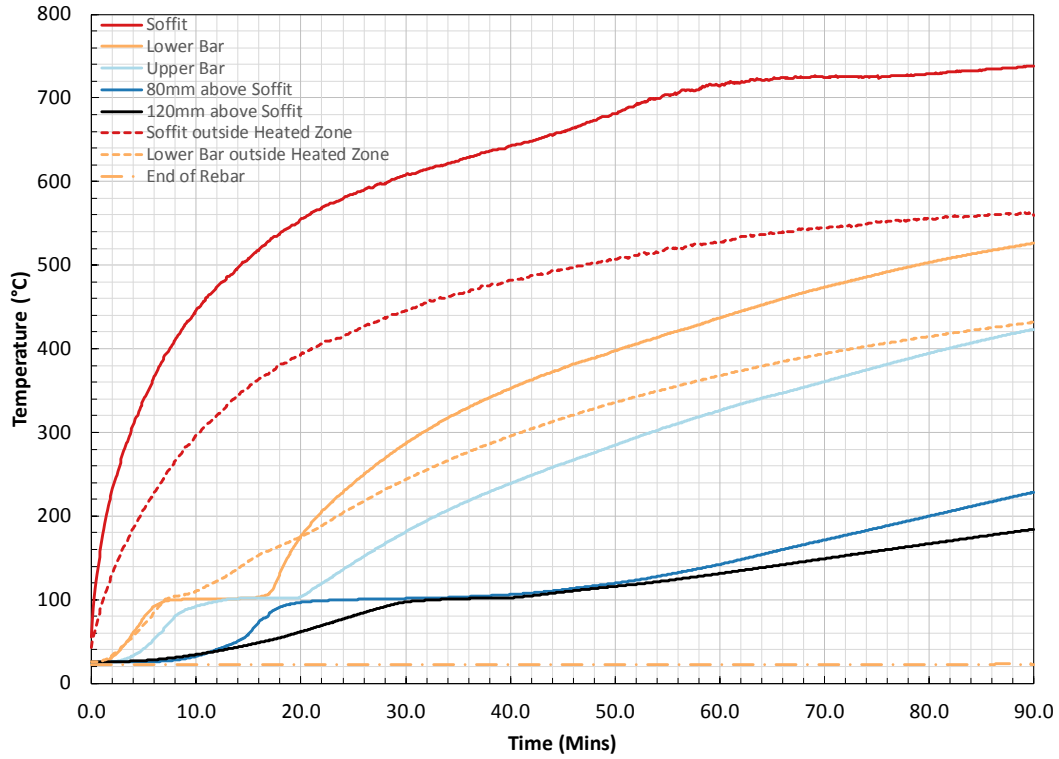

Figure 6-16 PTGHc2 Temperature Time Profiles

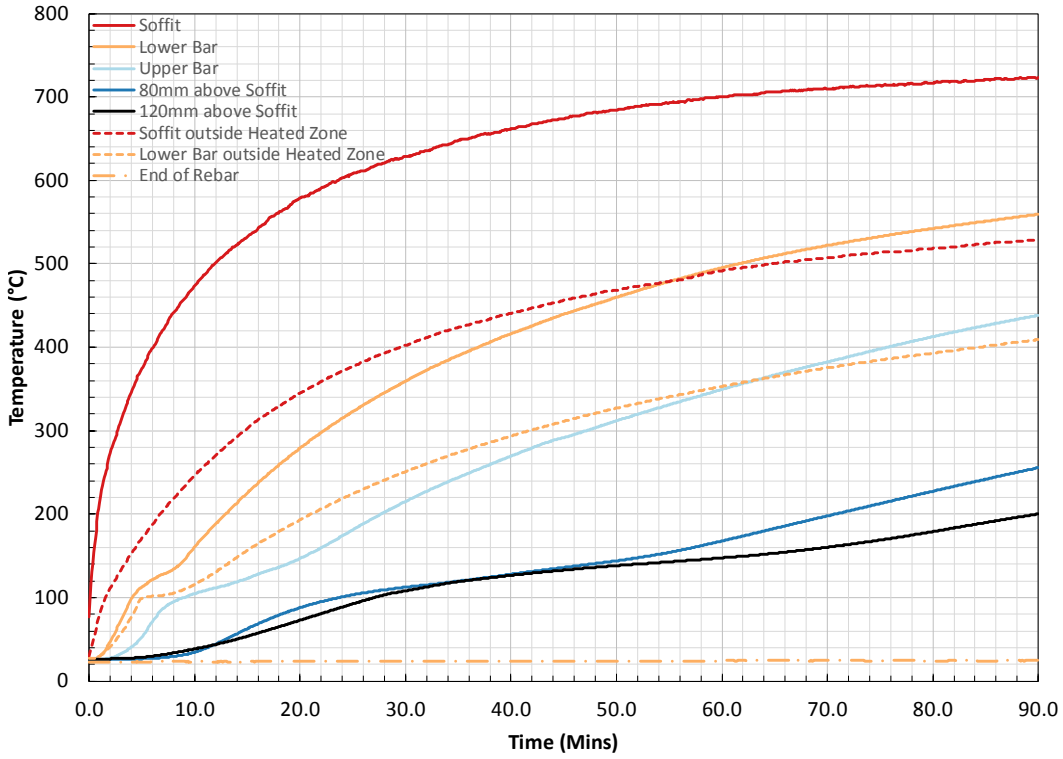

Figure 6-17 PTCHc2 Temperature Time Profiles

It is noted that even at the upper surface of the rebar, the failure temperatures are around the peak decomposition temperature for bar BPG and above $T_{d\ Peak}$ for bar PTG and PTC. This is a significant finding with respect to the temperatures that can be resisted with cold anchorage. Specifically for GFRP, this would therefore indicate that where FRP reinforcement is loaded to serviceability limits and cold anchorage is maintained, the reinforcement can still carry stress despite loss of interaction of the fibres due to decomposition of the matrix. While serviceability loads could not be attained (i.e. <55%) for the CFRP bars, during transient thermal heating, the positive impact of cold anchorage on performance of FRP at elevated temperature is evident even at loads of 30% f_{fu}.

As shown in Figure 6-15, Figure 6-16, Figure 6-17, temperature was not conducted along the bar based on placement of a thermocouple at the end of the reinforcement in the beam, which demonstrates that cold anchorage was maintained. It is also noted that there is a plateau at 100°C for the majority of the temperature measurements taken inside the beam, this is due the evaporation of moisture from the concrete (Kodur & Bisby, 2005). Figure 6-18 shows the temperatures profiles averaged for all the FRP continuous reinforced beams at 0, 30, 60 and 90 minutes of heating. They also show the lower and upper bounds for each of these profiles. Critically this demonstrates the relative consistency in heating across all the beam experiments.

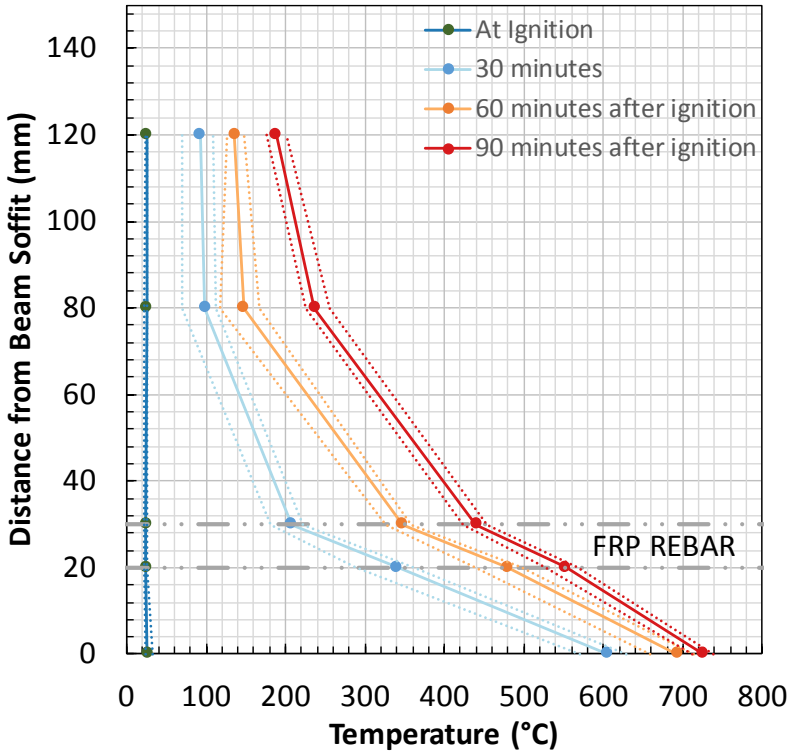

Figure 6-18 Average Temperature Profiles for Continuous Beams during Heating

As the temperature profiles of the beams are relatively consistent, as shown in Figure 6-18, a more detailed example (PTGHc1) is shown in Figure 6-19, for both heating and cooling of the reinforced beams using smaller time intervals.

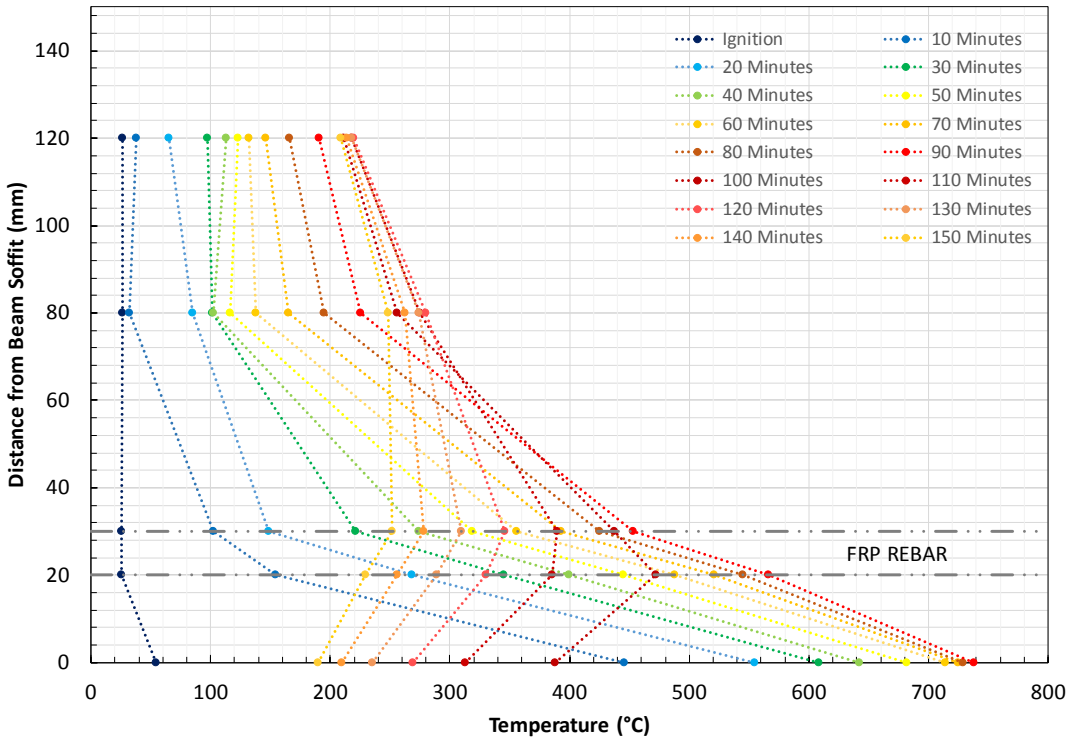

Figure 6-19 Time Temperature Variance through the Depth of the Concrete during Heating and Cooling (PTGHc1)

Beyond 20 minutes of heating, there is typically a difference of 120°C between the lower and upper surfaces of the FRP rebar, with an increasing differential between the soffit and upper most thermocouple (120mm above the soffit) up to 90 minutes of heating. The thermal inertia present in the concrete continues to maintain the temperature at the uppermost thermocouples during cooling. After 60 minutes of cooling, the soffit and lower bar temperatures are less than those observed at the uppermost thermocouple (120mm above the soffit).

As expected, given the known (and demonstrated in Chapter 5) bond criticality of FRP reinforcement at elevated temperature, all spliced FRP reinforced beams failed early in heating due to splice failure in the midspan region. Table 6-6 shows the temperatures, at the underside of the rebar both central and at the end of the splice region, at which the spliced beams failed. With reference to Table 6-5, it can be seen that in the central location (i.e. most exposed to fire conditions), the reinforcement temperature typically is greater than $T_g Tan\delta$. The temperature measured at the end of the splice varies between greater than $T_g Onset$ to $T_g Tan\delta$. The softening of the polymer

resin within the glass transition ranges ultimately leads to interfacial failure of the surface of the bar from the core.

Table 6-6 Rebar failure temperatures of spliced FRP beams

Specimen ID	Thermocouple Location			
	20mm (central, underside of rebar) (°C)		20mm (end of splice, underside of rebar) (°C)	
BPGHs1	181	>$T_g Tan\delta$	103	T_g *Modulus*-6°C
BPGHs2	167	>$T_g Tan\delta$	112	T_g *Modulus*+3°C
PTGHs1	259	>$T_g Tan\delta$	115	>T_g *Modulus*
PTGHs2	249	>$T_g Tan\delta$	149	$T_g Tan\delta$-5°C
PTCHs1	118	>$T_g Tan\delta$	102	$T_g Tan\delta$-6°C
PTCHs2	105	$T_g Tan\delta$-3°C	69	T_g*Onset*+5°C

As with the research presented by Nigro *et al.* (2011), the examination of bond strength loss in chapter 5 and the continuous FRP reinforced beams, the experiments demonstrate that cold anchorage is essential for FRP reinforced concrete to maintain load carrying capacity.

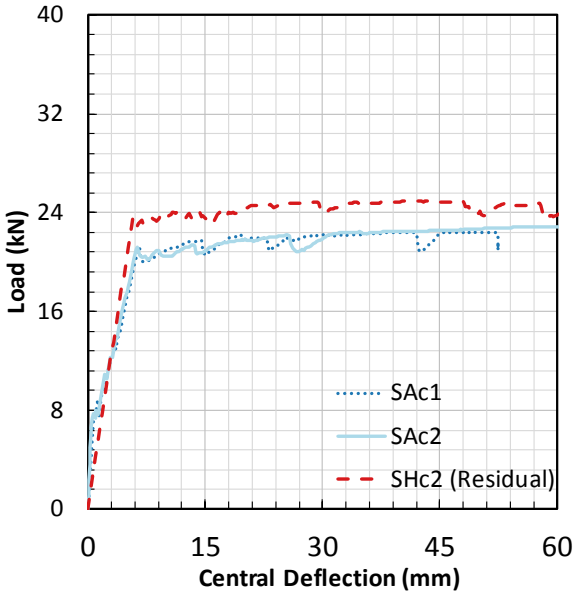

Figure 6-20 Load-deflection Responses for Ambient and Residually (Post-heating) Tested Steel Reinforced Beams

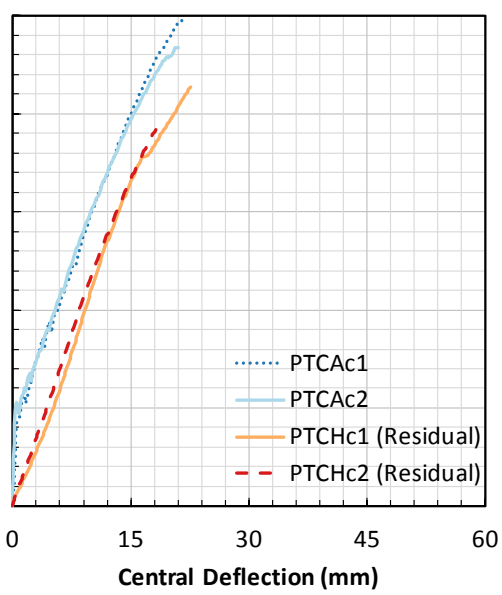

Figure 6-21 Load-deflection Responses for Ambient and Residually (Post-heating) Tested PTC Reinforced Beams

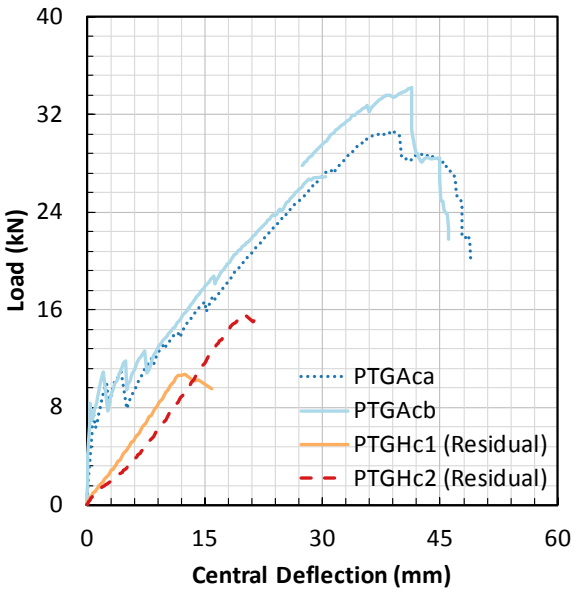

Figure 6-22 Load-deflection Responses for Ambient and Residually (Post-heating) Tested PTG Reinforced Beams

Figure 6-20, Figure 6-21 and Figure 6-22 show the post-cooling residual load versus midspan deflection responses of the beams that did not fail during heating. This figure shows that the steel reinforced beams experienced a mild increase in strength due to heating under sustained load, for reasons that remain unknown.

The residual capacity is seen to vary considerably between PTG and PTC beams, with the PTC bar reinforced beams experiencing only minor reductions in capacity after

heating and cooling, and indicating a possible influence of FRP fibre type on retention of load bearing capacity after exposure to heating. In both cases, the peak temperatures during heating exceeded the decomposition temperature of the poymer resin. The residual tests on continuous PTG reinforced beams retained 40-50% of their ambient capacity, while the continuous bar PTC beams retained more than 80% of their ambient strength. As during the ambient tests, the PTC continuous beams, failed due to slippage of the reinforcement, i.e. bond failure. As discussed in Chapter 5, it is hypothesised that the higher stiffness of the bars, is preventing the full bond potential of the surface treatment being reached, though more research is required to validate this theory.

6.4 DESIGN RECOMMENDATION

The following preliminary recommendations for FRP bars, can be made:

1. If cool anchorage of the tensile reinforcement cannot be provided, the limiting temperature should be conservatively taken as the lowest of the T_g values, $T_g Onset$. For the bars tested within this study, and based on the data presented in Chapter 3 of this thesis; these limiting temperatures would be 64°C, 86°C, and 83°C for the BPG, PTG, and PTC reinforcing bars, respectively.
2. Until more data is available, 'cool anchorage' should be defined as a length of reinforcement that can develop full ambient temperature capacity; this must be maintained below the limiting temperature noted in (1) above.
3. In cases where cool anchorage can be provided (as defined above and discussed within the literature review), and assuming that the sustained tensile stress in the FRP is less than 30% of ultimate (i.e. greater than serviceability limit for creep rupture of GFRP at 20%) at the onset of heating, the critical temperature for FRP bars may be defined based on the onset of decomposition of the polymer matrix, i.e. $T_d Onset$. This also implies the loss of interaction between FRP fibres and subsequently reduction in tensile strength of the bars. For the bars tested in the current study, and based on

the semi-empirical models presented in Chapter 4 of this thesis, conservative limiting temperatures (T_d *Onset*) would be 310˚C, 355˚C, and 302˚C for the BPG, PTG, and PTC reinforcing bars, respectively. Additional research is needed before this concept should be applied in design.

4. Surface treatment and secondary curing of the coating on FRP bars should be carefully considered both during manufacture and for the purposes of design, as shear capacity of the coating may impede FRP reinforcement being used to full effect, particularly in the case of higher stiffness bars such as CFRP.

This author acknowledges that CFRP was not tested to its full serviceability potential within this testing regime (due to restrictions on loading equipment) and thus additional testing on CFRP reinforced concrete is required to observe behaviour under more realistic service loads.

6.5 Chapter Summary

This chapter has presented tests at ambient temperature and under transient localised heating on 32 small-scale reinforced concrete beams reinforced with steel, CFRP, and 2 GFRP bars. The tests were intended to demonstrate the impact of tensile and bond strength loss at elevated temperature, discussed in chapter 4 and 5. Steel tests were carried out for comparison, and at ambient suffered classic under reinforced flexural failures, and furthermore retained considerable strength following the heated tests.

In conclusion, the beams confirmed the importance of cold anchorage in maintaining structural fire resistance of FRP reinforced concrete. Fundamentally and in agreement with prior research, two limiting temperatures have been set relating to bond and tensile strength. Conservatively, it has been proposed, that were cold anchorage cannot be maintained, i.e. bond will fail and the rebar will slip, T_g *Onset* should be the limiting temperature for the reinforcement. Moreover, where bond is not a factor, i.e. cold anchorage can be maintained, T_d *Onset* should be limiting temperature, where in the tensile tests, approximately 50% of tensile strength was retained for both CFRP

and GFRP bars. The continuous beam tests demonstrated that while the bars reached temperatures in excess of T_d *Onset* (700°C at the soffit), the majority of beams survived 90 minutes of heating.

By contrast the spliced beam tests demonstrated that bond failure was expected when the T_g range had been exceeded at the level of the FRP reinforcement. Temperatures at and in excess of $T_g Tan\delta$ were needed to cause failure of the spliced GFRP reinforced beams, likely due to the sustained strain in the FRP during heating being sufficiently low (30% of ultimate) allowing anchorage to be maintained for a short duration beyond the glass transition temperature range.

This is a significant demonstration of the viability of FRP reinforced concrete, with respect to fire, where it's use was previously seem to be limited by the softening of the polymer resin in the glass transition. The experiments have demonstrated the ability of the glass fibres to carry stress without the need for polymer interaction, where cold anchorage is achievable and serviceability limits are met.

CHAPTER 7 CONCLUSIONS

7.1 OVERVIEW

The main aim of this PhD research was to understand the response to fire of FRP reinforcing materials and FRP reinforced concrete in bending, and to determine a simplified approach that allows an evaluation of mechanical degradation of FRP at high temperature. The body of experimental work presented herein has adopted a multi-scale approach from bench scale characterisation tests to intermediate scale reinforced concrete beam experiments on three FRP bars, with an intent to correlate behaviour.

7.1.1 Key Findings

A substantial set of experiments on FRP internal reinforcement have been undertaken from bench scale thermal characterisation to intermediate scale FRP RC experiments. The work presented herein is unique in that the specific formulation of each tested FRP bar is taken into consideration throughout each set of tests, and correlations with tensile and bond behaviour at elevated temperature made on that basis.

Specifically the production of a novel predictive two step model, for tensile strength loss of FRP at elevated temperature, is an important advancement on the traditional one step loss, accounting for physical and thermal changes that FRP would undergo in a fire scenario. Crucially, instead of a generalized model, it can be readily adapted to each specific FRP formulation with a minimal suite of tests, acknowledging the proprietary nature of the FRP bars, the fundamental difference in comparison to steel reinforcement.

In the production of the model, thermal characterisation experiments have been undertaken with a view to demonstrating the range of temperatures assessed for both glass transition and decomposition of the polymer matrix. This research takes a step away from the approach of determining a single critical temperature without definition and basis of design. Instead an understanding of elemental structural response at elevated temperature has been developed, with critical temperatures based on both bond and tensile behaviour. Specifically for bond, cold anchorage is

crucial and where it cannot be maintained it is necessary to limit testing temperatures to T_g *Onset*. Whilst previous research has suggested limiting the temperature range for use of FRP to the glass transition range, this has never been clearly defined, as it has in this case. Where previous literature has limited the discussion to glass transition, this thesis has proven the value of understanding the decomposition of the polymer matrix, which is rarely discussed in literature. Considering decomposition and tensile capacity of FRP, where bond is not an issue, i.e. cold anchorage can be maintained, the limiting temperature has been recommended as T_d *Onset*. This is significantly higher than limiting temperatures stated within the literature (~300°C) and permits over 50% of tensile capacity to be retained (based on the 3 bars studied). Furthermore this has been demonstrated with confidence using FRP reinforced beams in four point bending, where reinforcement was exposed temperatures much greater than T_d *Onset* but yet did not fail during heating.

Conservative design recommendations have been made on the basis of experimental results that ultimately demonstrate the use of FRP as internal reinforcement in concrete as a potentially safe and viable alternative to steel in structural fire design.

7.1.2 Chapter 2: Literature Review

On review of the literature, it was evident that the mechanical properties of FRP reinforcement typically degrade with increasing temperature, particularly in the case of bond strength. While some models have been established, the great variability in the FRP bars requires testing of each FRP bar to determine loss of mechanical properties with high temperature, which has both significant time and cost implications. FRP has still to date been restricted in its use for structural fire design though steps have been taken to identify critical parameters that govern the thermal behaviour, such as concrete cover, aggregate type and reinforcement anchorage. These are reflected in the latest FRP guidance from the American Concrete Institute and the Canadian Standards Association, though substantial performance based analysis is required in the case of ACI 440.1R-15 heavily relying on is the rigor of the designer in understanding the latest research.

FRP is a material that is fundamentally different to that of steel reinforcement and therefore an evaluation of thermo-mechanical elemental behaviour must be undertaken. Experimentation and modelling has been undertaken for tensile strength loss at elevated temperature but with little regard to the specifics of the test temperatures and the range of test temperatures, which is considered by the research in this thesis, specific to the formulation of the FRP bar. To form an improved understanding of high temperature bond behaviour, more data is required considering different FRP fibre and coating types (set out experimentally in Chapter 5). While cold anchorage has been stated as important in the literature, few efforts have been made to demonstrate its requirement beyond bond pullout tests.

The research following the literature review chapter sought to bridge some of the gaps highlighted in our understanding of FRP as a reinforcing material in concrete.

7.1.3 Chapter 3: Bench Scale Thermal Characterisation of FRP bars

This chapter presents and discusses experimental work documenting thermal analysis on small samples taken from three different, commercially available FRP

bars; two manufactured from glass fibres and one from carbon fibres. A range of experiments was presented using dynamic mechanical analysis (DMA) and thermogravimetric analysis (TGA).

In contrast to previous literature, this author has presented glass transition temperatures as a range for each specific FRP encompassing multiple definitions of T_g. The range of values for any one bar has been demonstrated to vary by as much 80°C, and this is therefore significant in defining mechanical degradation.

As T_g is commonly seen as a limiting temperature, decomposition and oxidation of the polymer matrix is infrequently presented in the literature. On review of current research it is evident, that consideration of the placement of FRP reinforcement, i.e. cold anchorage, may present an opportunity for limiting temperatures to be higher than T_g. As such an evaluation of the thermal degradation of the sample through thermogravimetric analysis was undertaken to establish decomposition and oxidation temperatures, which are not typically reported in literature

This work forms the foundation for examining loss of mechanical properties at elevated temperature and the structural fire behaviour of FRP reinforced concrete. Moreover the work demonstrates the relatively straight forward and readily repeatable approach in using DMA and TGA to identify key thermal events that can be correlated to changes in mechanical behaviour

7.1.4 Chapter 4: Analysis of Tensile Strength Loss of FRP bars with Elevated Temperature

Steady state thermal regime tensile tests are presented on the three different FRP bars at elevated temperature. The selected testing temperatures are based on results from the bench scale thermal characterisation in Chapter 3. Also discussed is an anchorage technique was necessary to allow the FRP bars to be secured in a mechanical testing frame. A novel two-step model for reduction in tensile strength of FRP bars at elevated temperature has been presented, linking the bench scale behaviour to the observed tensile strength reductions at elevated temperature. Moreover, from the literature review, it was evident that tensile testing was an inefficient and costly

process. As such a minimum suite of tests necessary to predict tensile strength loss at elevated temperature, for any candidate FRP reinforcing bar, has been proposed.

This predictive tool has been demonstrated to be valid for various FRP bars and resin types, though limitations on its use for CFRP was acknowledged due to the influence of oxidation of the carbon fibres. Furthermore, T_g was typically seen as the limiting temperature for FRP bars, however the tensile tests demonstrated greater than 50% of their tensile strength was maintained beyond the T_g range to the onset of decomposition of the polymer matrix, $T_d\,Onset$.

7.1.5 Chapter 5: Analysis of Bond Strength Loss of FRP bars in concrete with Elevated Temperature

The bond behaviour of FRP reinforcing bars in concrete, being different to that of deformed steel reinforcing bars, is variable and depends on the surface coating applied to the FRP bars during manufacturing. Bond pullout tests are presented on FRP bars embedded in 150mm cubes of concrete to study and quantify the degradation of concrete FRP bond strength at temperatures within the glass transition temperature range. Crucially these experiments are carried out at temperatures within the glass transition range defined specifically for each bar in Chapter 3. This testing, alongside previous research, verified the requirement for cold anchorage of FRP reinforcement. A predictive model on the basis of modified DMA storage modulus curve (specific to each bar) was presented, however it cannot be relied on to accurately predict bond strength loss at elevated temperature. Lessons learned and further work required have been discussed to aid future research within this area.

The determination of bond strength loss at elevated temperature for FRP in concrete is significantly more challenging compared to that of steel (homogenous) due to the formulation of the bars and heterogeneous nature. However as agreed with other researchers, the overarching conclusion is that cold anchorage is key to the maintaining structural fire resistance and preventing rebar pull out.

7.1.6 Chapter 6: Analysis of FRP Reinforced Beams at Elevated Temperature

Tests on 32 FRP reinforced concrete beams tested in four-point bending under sustained load at elevated temperature have been presented with the intention of demonstrating the impact of tensile strength loss and bond critical applications. Through an examination of reinforcement temperatures, and general failure of the beams, it was possible to present a set of design recommendations:

1. If cool anchorage of the tensile reinforcement cannot be provided, the limiting temperature should be conservatively taken as the lowest of the T_g values, $T_g\,Onset$. For the bars tested within this study, and based on the data presented in Chapter 3 of this thesis; these limiting temperatures would be 64°C, 86°C, and 83°C for the BPG, PTG, and PTC reinforcing bars, respectively.
2. Until more data is available, 'cool anchorage' should be defined as a length of reinforcement that can develop full ambient temperature capacity; this must be maintained below the limiting temperature noted in (1) above.
3. In cases where cool anchorage can be provided, and assuming that the sustained tensile stress in the FRP is less than 30% of ultimate at the onset of heating, the critical temperature for FRP bars may be defined based on the onset of decomposition of the polymer matrix, i.e. $T_d\,Onset$. This also implies the loss of interaction between FRP fibres and subsequently reduction in tensile strength of the bars. For the bars tested in the current study, and based on the semi-empirical models presented in Chapter 4 of this thesis, conservative limiting temperatures ($T_d\,Onset$) would be 310°C, 355°C, and 302°C for the BPG, PTG, and PTC reinforcing bars, respectively. Additional research is needed before this concept should be applied in design.
4. Surface treatment and secondary curing of the coating on FRP bars should be carefully considered both during manufacture and for the purposes of design, as shear capacity of the coating may impede FRP reinforcement being used to full effect, particularly in the case of higher stiffness bars such as CFRP.

7.2 RECOMMENDATIONS

It is recommended that, in the first instance, temperatures, which are identified as "critical", should be clear in their definition and basis of design. This body of research has demonstrated the power of clearly relating thermal events to mechanical behaviour and subsequently establishing a predictive model. This analysis could be strengthened through testing on bars of alternate sizes, polymer and coating types, with consideration given to the relative curing through the diameter of the bar, specifically with regard to the secondary curing process of the coating.

As mentioned, spalling is a notable problem for concrete at elevated temperature, but beyond the scope of this thesis. Specifically direct flame impingement (exposure of the soffit due to spalling event) on the FRP reinforcement has not been researched. Given the propensity for FRP to be used in conjunction with high strength concrete, which is known to spall, this should form part of the ongoing research into FRP reinforcement. Equally, exposure of the FRP reinforcement raises an important question over toxicity of the bars during a fire and may be an appropriate research area to investigate.

In the development of models, it is imperative that these are validated against experiments. Strengthening the pool of data available for FRP tensile and bond tests can only seek to improve upon existing knowledge, allow for statistical analysis and validate the novel two-step model set out for tensile strength loss in this thesis.

In order to truly undertake a performance based design as required by ACI 440.1R-2015 for determining structural fire resistance of FRP reinforced concrete, a clear understanding of full structural interaction for FRP reinforced concrete in fire is required. As discussed in the literature review, the proprietary formulation of the FRP matrix makes for a considerable amount of variables in determining strength loss models; of which only a sample could be investigated in this thesis. A large data set would be required across multiple types of FRP bar to carry out a statistical analysis and provide valid inputs to a finite element model.

Much research has yet to be undertaken for FRP reinforced concrete at elevated temperature, with some general directions of study highlighted above. Fundamentally the researched presented herein seeks to competently contribute to this field of research.

CHAPTER 8 REFERENCES

Abbasi, A., & Hogg, P. J. (2005). Temperature and environmental effects on glass fibre rebar: Modulus, strength and interfacial bond strength with concrete. *Composites Part B: Engineering*, *36*, 394–404. https://doi.org/10.1016/j.compositesb.2005.01.006

Abbasi, A., & Hogg, P. J. (2006). Fire testing of concrete beams with fibre reinforced plastic rebar. *Composites Part A: Applied Science and Manufacturing*, *37*(8), 1142–1150. https://doi.org/10.1016/j.compositesa.2005.05.029

American Concrete Institute (ACI). (2006). Guide for the Design and Construction of Structural Concrete Reinforced with FRP Bars. In *ACI 440.1R-06*. https://doi.org/10.1061/40753(171)158

American Concrete Institute (ACI). (2008). Building Code Requirements for Structural Concrete and Commentary. In *ACI 318-08*. Michigan.

American Concrete Institute (ACI). (2015). Guide for the Design and Construction of Structural Concrete Reinforced with Fiber-Reinforced Polymer (FRP) Bars. In *440.1R-15*. Michigan.

American Society for Testing and Materials (ASTM). (2007). Standard Test Method for Glass Transition Temperature (DMA Tg) of Polymer Matrix Composites by Dynamic Mechanical Analysis (DMA). In *ASTM D7028*. https://doi.org/10.1520/D7028-07E01R15.2

American Society for Testing and Materials (ASTM). (2008). Tensile Properties of Pultruded Glass-Fiber-Reinforced Plastic Rod. In *ASTM D3916*. https://doi.org/10.1520/D3916-08.2

American Society for Testing and Materials (ASTM). (2018). Standard Test Methods for Fire Tests of Building Construction and Materials. In *ASTM E119*.

Bai, Y., & Keller, T. (2009). Modeling of Strength Degradation for Fiber-Reinforced Polymer Composites in Fire. *Journal of Composite Materials*, *43*, 2371–2385. https://doi.org/10.1177/0021998309344642

Bakis, C. E., Bank, L. C., Brown, V. L., Cosenza, E., Davalos, J. F., Lesko, J. J., … Triantafillou, T. C. (2002). Fiber-Reinforced Polymer Composites for Construction—State-of-the-Art Review. *Journal of Composites for Construction*, *6*(2), 73–87. https://doi.org/10.1061/(ASCE)1090-0268(2002)6:2(73)

Bakis, C. E., Lopez, M. M., & Witt, S. E. (2014). Interlaboratory Evaluation of Tg of Ambient-Cured Epoxies Used in Civil Infrastructure. *Proceedings of the 7th International Conference on FRP Composites in Civil Engineering (CICE 2014). August 20-22, 2014. Vancouver, Canada*, *440*, 1–6.

Bakis, C. E., Nanni, A., & Terosky, A. (1996). Smart pseudo-ductile, reinforcing rods for concrete: manufacture and test. *1st Int. Conf. on Composites in Infrastructures, ICCI 96*, 95–108. Tuscon, Arizona.

Bank, L. C., Puterman, M., & Katz, A. (1998). The Effect of Material Degradation on Bond Properties of Fiber Reinforced Plastic Reinforcing Bars in Concrete. *ACI Materials Journal*, Vol. 95, pp. 232–243.

Bisby, L. A. (2003). *Fire behaviour of fibre-reinforced polymer (FRP) reinforced or confined concrete* (Queen's University). https://doi.org/10.1021/ja067132y

Bisby, L. A. (2005). *Fire behaviour of fibre-reinforced polymer (FRP) reinforced or confined concrete*. 371.

Bisby, L. a., Green, M. F., & Kodur, V. K. R. (2005). Response to fire of concrete structures that incorporate FRP. *Progress in Structural Engineering and Materials*, *7*, 136–149. https://doi.org/10.1002/pse.198

Bisby, L. A., & Kodur, V. K. R. (2007). Evaluating the fire endurance of concrete slabs reinforced with FRP bars: Considerations for a holistic approach. *Composites Part B: Engineering*, *38*, 547–558. https://doi.org/10.1016/j.compositesb.2006.07.013

Bisby, L. A., & Stratford, T. (2012). Opportunities for PerformanceBased Fire Resistance Design of FRP Reinforced Concrete Slabs. *Proceedings of the 6th International Conference on FRP Composites in Civil Engineering (CICE 2012). June*

13-15, 2012., 1–8. Rome, Italy.

Brannigan, V. M. (2008). The Regulation of Technological Innovation: The Special Problem of Fire Safety Standards. *Proceedings for Fire Safety Engineering Applied to (FireSEAT) Fire and Building Safety in the Single European Market November 12*, 20–33. Edinburgh, Scotland.

Burgoyne, C., & Balafas, I. (2007). Why is FRP not a Financial Success? *Proc. 8th Intl. Conf. on FRP …*, 1–10. Retrieved from http://www-civ.eng.cam.ac.uk/cjb/papers/cp74.pdf

Callister, J. W. D. (2007). *Materials Science and Engineering: An Introduction* (7th ed.). John Wiley & Sons, Ltd.

Canadian Standards Association. (2012). Design and construction of building structures with fibre-reinforced polymers. *CSA S806-12*, pp. 1–206. Mississauga, Ontario.

Chana, P. S. (1990). A Test Method to Establish Realistic Bond Stresses. *Magazine of Concrete Research*, *42*(151), 83–90.

Chang, X., Yue, G., Lin, H., & Tang, C. (2010). Modeling the pullout behavior of fiber reinforced polymer bars from concrete. *Construction and Building Materials*, *24*(4), 431–437. https://doi.org/10.1016/j.conbuildmat.2009.10.020

Chapman, C. B. (1974). *Fibres*. Butterworth& Co Ltd.

Clarke, J. (1993). Alternative Materials for Reinforcement and Prestressing of Concrete. In *Blackie Academic and Professional*. Glasgow, UK.

Correia, J. R., Gomes, M. M., Pires, J. M., & Branco, F. a. (2013). Mechanical behaviour of pultruded glass fibre reinforced polymer composites at elevated temperature: Experiments and model assessment. *Composite Structures*, *98*, 303–313. https://doi.org/10.1016/j.compstruct.2012.10.051

Dimitrienko, Y. I. (1997). Thermomechanical behaviour of composite materials and

structures under high temperatures: 1. Materials. *Composites Part A: Applied Science and Manufacturing*, *28*(5), 453–461. https://doi.org/10.1016/S1359-835X(96)00144-3

Dimitrienko, Y. I. (1999). *Thermomechanics of Composites under High Temperatures.* London: Klewer Academic Publishers.

Elbadry, M., & Elzaroug, O. (2004). Control of cracking due to temperature in structural concrete reinforced with CFRP bars. *Composite Structures*, *64*, 37–45. https://doi.org/10.1016/S0263-8223(03)00211-3

Eligehausen, R., Popov, E. P., & Bertero, V. V. (1982). Local Bond Stress-Slip relationships of Deformed Bars under Generalised Excitations. In *Proceedings of the 7th European Conference on Earthquake Engineering* (Vol. 4, pp. 69–80). https://doi.org/http://dx.doi.org/10.18419/opus-415

Erki, M. A., & Rizkalla, S. H. (1993). Anchorages For FRP Reinforcement. *Concrete International*, *15*(6), 54–59.

European Committee for Standardization. (2001). Fire resistance tests – general requirements. In *EN 1363-1:2001*.

European Committee for Standardization. (2010). Eurocode 2: Design of concrete structures. Part 1-2: General Rules - Structural fire design. *BS EN 1992-1-2:2004 (Incorporating Corrigendum July 2008)*.

Foster, S. K., & Bisby, L. A. (2008). Fire Survivability of Externally Bonded FRP Strengthening Systems. *Journal of Composites for Construction*, *12*(5), 553–561. https://doi.org/10.1061/(ASCE)1090-0268(2008)12:5(553)

Galati, N., Nanni, A., Dharani, L. R., Focacci, F., & Aiello, M. A. (2006). Thermal effects on bond between FRP rebars and concrete. *Composites Part A: Applied Science and Manufacturing*, *37*(8), 1223–1230. https://doi.org/10.1016/j.compositesa.2005.05.043

Garlock, M., Paya-Zaforteza, I., Kodur, V., & Gu, L. (2012). Fire hazard in bridges:

Review, assessment and repair strategies. *Engineering Structures*, *35*, 89–98. https://doi.org/10.1016/j.engstruct.2011.11.002

German Institue for Standardization. (1999). Aerospace - Fiber reinforced materials - Determination of glass transition of fiber composites under dynamic load. In *DIN 65583:1999-04*. Berlin.

Hajiloo, H., Gales, J., Noël, M., & Green, M. F. (2015). Material Characteristics of Glass Fibre Reinforced Polymer (GFRP) Bars at High Temperature. In V. K. R. Kodur & N. Banthia (Eds.), *Response of Structures Under Extreme Loading: Proceedings of the Fifth International Workshop on Performance, Protection & Strengthening of Structures under Extreme Loading (PROTECT 2015). June 28-30, 2015. East Lansing, MI, USA.*

Hollaway, L. C. (2003). The evolution of and the way forward for advanced polymer composites in the civil infrastructure. *Construction and Building Materials*, *17*(03), 365–378. https://doi.org/10.1016/S0950-0618(03)00038-2

Ibell, T., Darby, A., & Denton, S. (2009). Research issues related to the appropriate use of FRP in concrete structures. *Construction and Building Materials*, *23*(4), 1521–1528. https://doi.org/10.1016/j.conbuildmat.2008.05.011

Ilg, P., Hoehne, C., & Guenther, E. (2016). High-performance materials in infrastructure: A review of applied life cycle costing and its drivers - The case of fiber-reinforced composites. *Journal of Cleaner Production*, *112*, 926–945. https://doi.org/10.1016/j.jclepro.2015.07.051

ISIS Canada Corporation. (2006). Reinforcing Concrete Structures with Fibre Reinforced Polymers. In L. G. Jaeger (Technical Editor) (Ed.), *Design Manual 3 Version 2* (Design Man).

Kashwani, G. A., & Al-Tamimi, A. K. (2014). Evaluation of FRP bars performance under high temperature. *Physics Procedia*, *55*, 296–300. https://doi.org/10.1016/j.phpro.2014.07.043

Katz, A. (1999). Bond mechanism of FRP rebars to concrete. *Materials and Structures*, *32*(December), 761–768. Retrieved from http://www.springerlink.com/index/q0614kp713208743.pdf

Katz, A., & Berman, N. (2000). Modeling the effect of high temperature on the bond of FRP reinforcing bars to concrete. *Cement and Concrete Composites*, *22*, 433–443.

Katz, A., Berman, N., & Bank, L. C. (1999). Effect of High Temperature on Bond Strength of FRP Rebars. *Journal of Composites for Construction*, *3*(2), 73–81. https://doi.org/10.1061/(ASCE)1090-0268(1999)3:2(73)

Kodur, V. K. R., & Baingo, D. (1998). *Fire Resistance of FRP Reinforced Concrete Slabs*. Institute for Research in Construction, National Research Council Canada.

Kodur, V. K. R., & Bisby, L. A. (2005). Evaluation of Fire Endurance of Concrete Slabs Reinforced with Fiber-Reinforced Polymer Bars. *Journal of Structural Engineering*, *131*(January), 34–43. https://doi.org/10.1061/(ASCE)0733-9445(2005)131:1(34)

Kumahara, S., Masuda, Y., Tanano, H., & Shimizu, A. (1993). Tensile Strength of Continuous Fiber Bar Under High Temperature. In A. Nanni & C. W. Dolan (Eds.), *Fibre-Reinforced-Plastic Reinforcement for Concrete Structures: An International Symposium* (pp. 731–742). Detroit, Michigan: American Concrete Institue.

Lattimer, B. Y., & Ouellette, J. (2006). Properties of composite materials for thermal analysis involving fires. *Composites Part A: Applied Science and Manufacturing*, *37*(7), 1068–1081. https://doi.org/10.1016/j.compositesa.2005.01.029

Maranan, G. B., Manalo, A. C., Karunasena, W., Benmokrane, B., & Lutze, D. (2014). Flexural behaviour of glass fibre reinforced polymer (GFRP) bars subjected to elevated temperature. *23rd Australasian Conference on the Mechanics of Strcutures and Materials (ACMSM23)*, *I*, 187–192. Byron Bay, NSW: Southern Cross University, Lismore.

Masmoudi, R., Zaidi, A., & Gérard, P. (2005). Transverse Thermal Expansion of FRP

Bars Embedded in Concrete. *Journal of Composites for Construction*, *9*(5), 377–387. https://doi.org/10.1061/(ASCE)1090-0268(2005)9:5(377)

MatWeb. (2019). Steels, General Properties. Retrieved January 2, 2019, from http://www.matweb.com/search/datasheet.aspx?matguid=10e1c14130cd4ed6ae64b85723be53af&n=1&ckck=1

McIntyre, E. R. E., Bilotta, A., Bisby, L. A., & Nigro, E. (2014). Mechanical Properties of Fibre Reinforced Polymer Reinforcement for Concrete at High Temperature. In G.-Q. Li, S.-C. Jiang, S.-W. Chen, V. K. R. Kodur, J. Jiang, & G.-B. Lou (Eds.), *Progress in Structural Safety: Proceedings of the Eighth International Conference on Structures in Fire (SiF 2014). June 11-13, 2014. Shanghai, China* (pp. 1227–1234). Shanghai: Tongji University Press.

Micelli, F., & Nanni, a. (2003). Tensile characterization of FRP rods for reinforced concrete structures. *Mechanics of Composite Materials*, *39*(4), 293–304. https://doi.org/10.1023/A:1025638310194

Michels, J., Widmann, R., Czaderski, C., Allahvirdizadeh, R., & Motavalli, M. (2015). Glass transition evaluation of commercially available epoxy resins used for civil engineering applications. *Composites Part B: Engineering*, *77*, 484–493. https://doi.org/10.1016/j.compositesb.2015.03.053

Nanni, A. (1993). Flexural Behaviour and Design of RC Members using FRP Reinforcement. *Journal of Structural Engineering*, *119*(11), 3344–3359.

Neale, K. W., & Labossiere, P. (1991). *Advanced Composite Materials with Applications to Bridges*. Montreal, Canada.

Nigro, E., Cefarelli, G., Bilotta, A., Manfredi, G., & Cosenza, E. (2011). Fire resistance of concrete slabs reinforced with FRP bars. Part I: Experimental investigations on the mechanical behavior. *Composites Part B: Engineering*, *42*(6), 1739–1750. https://doi.org/10.1016/j.compositesb.2011.02.025

Nigro, E., Cefarelli, G., Bilotta, A., Manfredi, G., & Cosenza, E. (2013). Adhesion at

high temperature of FRP bars straight or bent at the end of concrete slabs. *Journal of Structural Engineering*, *4*(2), 71–86.

Orangun, C., Jirsa, J. O., & Breen, J. E. (1977). A Reevaluation of Test Data on Development Length and Splices. *ACI Journal Proceedings*, *74*(3), 114–122.

PerkinElmer. (2008). *Dynamic Mechanical Analysis (DMA) A Beginner's Guide*.

Pultrall. (2005). *Case Study: Laurier-Tache Parking Garage*. Retrieved from http://www.vrodcanada.com/sites/default/files/Project_Report/Case Study for Laurier Tache.pdf

Regnier, N., & Mortaigne, B. (1995). Analysis by pyrolysis/gas chromatography/mass spectrometry of glass fibre/vinylester thermal degradation products. *Polymer Degradation and Stability*, *49*(95), 419–428. https://doi.org/10.1016/0141-3910(95)00129-A

Rehm, G., & Franke, L. (1979). Kunstharzgebundene Glasfaserstabe als Bewehrung im Betonbau Deutscher Ausschuss fur Stahlbeton. *Heft 304*.

RILEM-CEB. (1983). *Recommendation RC 6: Bond test reinforcement steel - PULL-OUT TEST* (Concrete Reinforcement Technology, Ed.). Paris: Georgi Publishing Company.

Robert, M., & Benmokrane, B. (2010a). Behavior of GFRP Reinforcing Bars Subjected to Extreme Temperatures. *Journal of Composites for Construction*, *14*(August), 353–360. https://doi.org/10.1061/(ASCE)CC.1943-5614.0000092

Robert, M., & Benmokrane, B. (2010b). Behavior of GFRP Reinforcing Bars Subjected to Extreme Temperatures. *Journal of Composites for Construction*, *14*(4), 353–360.

Robert, M., Cousin, P., & Benmokrane, B. (2009). Durability of GFRP Reinforcing Bars Embedded in Moist Concrete. *Journal of Composites for Construction*, *13*(2), 66–73. https://doi.org/10.1061/(ASCE)1090-0268(2009)13:2(66)

Rosa, I. C., Firmo, J. P., Granadeiro, L., & Correia, J. R. (2018). Effect of High

Temperatures on the Bond Performance of GFRP Bars to Concrete. *9th Internation Conference on Fibre-Reinforced Polymer (FRP) Composites in Civil Engineering (CICE 2018)*, (July). https://doi.org/10.3151/jact.16.75

Rosa, I. C., Firmo, J. P., Santos, P., Arruda, M. R. T., & Correia, J. R. (2018). Fire Behaviour of GFRP-Reinforced Concrete Slab Strips: Fire Resistance Tests and Numerical Modelling. *9th Internation Conference on Fibre-Reinforced Polymer (FRP) Composites in Civil Engineering (CICE 2018)*, (July). Paris.

Rostasy, F. S. (1992). Fiber Composite Elements and Techniques as Non-Metallic Reinforcement of Concrete. *Brite Project 4142/BREU – CT 91 0515, Evaluation of Potentials and Production Techniques of FRP, Technical Report Task 1.*

Saafi, M. (2002). Effect of fire on FRP reinforced concrete members. *Composite Structures*, *58*, 11–20. https://doi.org/10.1016/S0263-8223(02)00045-4

Scottish Government. (2017). Technical Handbook - Non-Domestic. In *NDTH*. https://doi.org/10.1105/tpc.112.099721

Sen, R., Mariscal, D., & Shahawy, M. (1993). Durability of Fiberglass Prestensioned Beams. *ACI Structural Journal*, *90*(5), 525–533.

Sumida, A., Fujisaki, T., Watanabe, K., & Kato, T. (2001). Heat Resistance of Continuous Fiber Reinforced Plastic Rods. In C. J. Burgoyne (Ed.), *The Fifth Annual Symposium on Fibre-Reinforced-Plastic Reinforcement for Concrete Structures (FRPRCS-5)* (pp. 557–565). London: Thomas Telford.

Tanano, H., Masuda, Y., Kage, T., Fukuyama, H., Nishida, I., & Hashimoto, T. (1995). Fire Resistance of Continuous Fibre Reinforced Concrete. In L. Taerwe (Ed.), *Non-metallic (FRP) Reinforcement for Concrete Structures* (pp. 368–375). London, UK: E&FN Spon.

Tanano, H., Masuda, Y., Sakashita, M., Oono, Y., Nonomura, K., & Satake, K. (1997). Tensile Properties of High Temperatures of Continuous Fiber Bars and Deflections of Continuous Fiber Reinforced Concrete Beams under High-

Temperature Loading. *Non-Metallic (FRP) Reinforcement for Concrete Structures*, 43–50. Sapporo: Japan Concrete Institute.

Tastani, S. P., & Pantazopoulou, S. J. (2006). Bond of GFRP Bars in Concrete : Experimental Study. *Journal of Composites for Construction*, *10*(5), 381–391. https://doi.org/10.1061/(ASCE)1090-0268(2006)10:5(381)

Wagner, M. (2009). Thermal Analysis in Practice. In *Collected Applications Thermal Analysis*. Mettler Toledo.

Wambeke, B., & Shield, C. (2006). Development Length of Glass Fiber Reinforced Polymer Bars in Concrete. *ACI Structural Journal*, *103*(1), 11–17.

Wang, Y. C., Wong, P. M. H., & Kodur, V. (2007). An experimental study of the mechanical properties of fibre reinforced polymer (FRP) and steel reinforcing bars at elevated temperatures. *Composite Structures*, *80*, 131–140. https://doi.org/10.1016/j.compstruct.2006.04.069

Wang, Y. C., Wong, P. M. H., & Kodur, V. K. R. (2003). Mechanical Properties of Fibre Reinforced Polymer Reinforcing Bars at Elevated Temperatures. *ASCE/SFPE Conference on Designing Structures for Fire.*, 183–192. Baltimore: Society of Fire Protection Engineers.

Weber, A. (2008a). Fire-resistance tests on composite rebars. *Fourth International Conference of FRP Composites in Civil Engineering (CICE 2008)*, 22–24. Retrieved from http://www.iifc-hq.org/proceedings/CICE_2008/papers/2.D.1.pdf

Weber, A. (2008b). Fire-resistance tests on composite rebars. In M. Motavalli (Ed.), *Fourth International Conference of FRP Composites in Civil Engineering (CICE 2008)* (pp. 22–24). Retrieved from http://www.iifc-hq.org/proceedings/CICE_2008/papers/2.D.1.pdf

APPENDICES

A. CHAPTER 3 APPENDICES

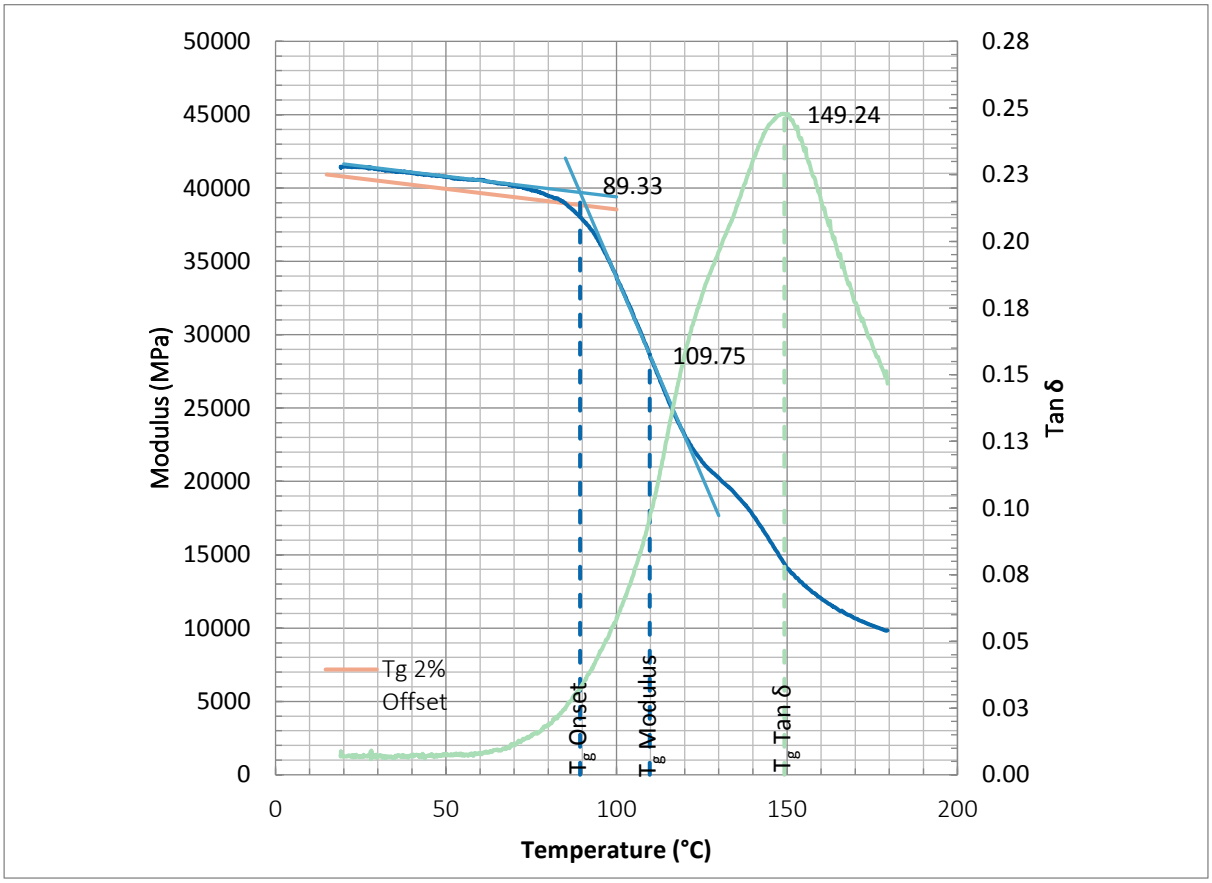

Appendix Figure 1 DMA BPGi plot

Tg Tan	Peak Tan δ	0.2479	x	y		
	T_g Tan δ	149.24	149.24	0		
			149.24	0.2479		
		Min. Value Deriv.	Temp. (x)	Modulus (y)	Y-intercept	
Tg Modulus	USM Deriv.	-4745	100.10	33866	508868	
	USM Smoothed Derivative (40)	-688	99.90	34056	102791	
	USM Smoothed Derivative (50)	-680	109.75	28650	103288	
	SM Deriv	-665	100.00	-640	65814	
	SM Smoothed Derivative (10)	-633	109.75	-531	68895	
	SM Smoothed Derivative (25)	-602	109.49	-519	65385	
	Tg Modulus	109.75	x	y		
			109.75	0		
			109.75	28650		
Tg Onset	*Approx location of tangents to determine grad & slope*		x	y		
	Modulus Gradient	-542	85	42042	*98*	*35000*
	Y-intercept	88083	130	17667	*110*	*28500*
	Initial Gradient	-28	20	41640	*25*	*41500*
	Y-intercept	42200	100	39400	*50*	*40800*
	Tg Onset	89.33	89.33	0		
			89.33	39699		
Tg Loss	Loss Modulus	4092.51	138.68	0		
			138.68	4093		
Tg Offset	98% Storage Modulus	40570.23	56.44	0		
			56.44	40570		
	Tg Onset - 50°c	39.33	41061.58	40240.3455		
Tg Offset	98% Initial Y-Intercept	41341	*15*	*40927*		
	Initial Gradient	-28	*100*	*38541449*		
	Gradient (Trendline Modulus Data)	-197.03623				
	Y-Intercept (Trendline Modulus Data)	55,688.13	84.87	0		
	Tg 2% Offset (Trendline equation)	84.87342535	84.87	38996		
	Plot between (based on Tg graph)	84	&	88		

Appendix Figure 2 BPGi, Tg values determined from DMA analysis

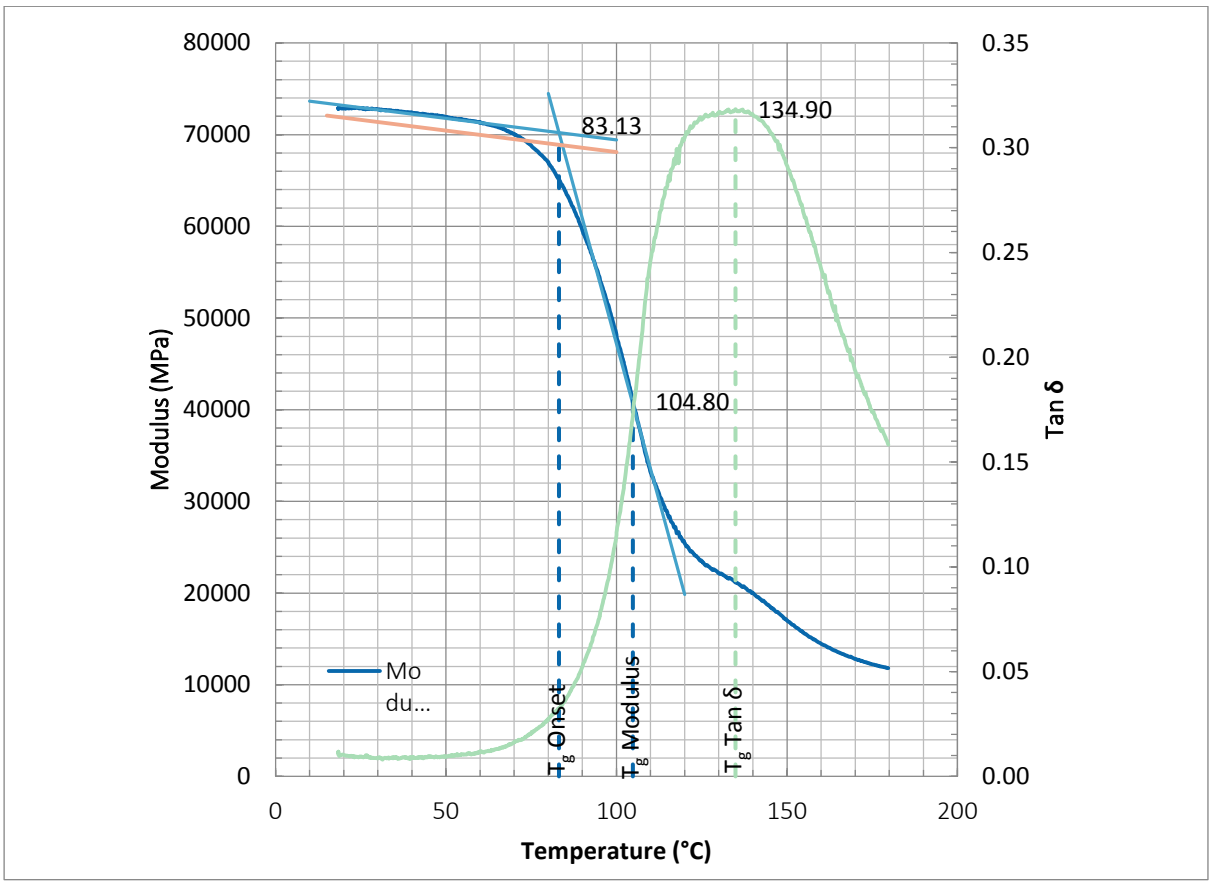

Appendix Figure 3 DMA BPGii plot

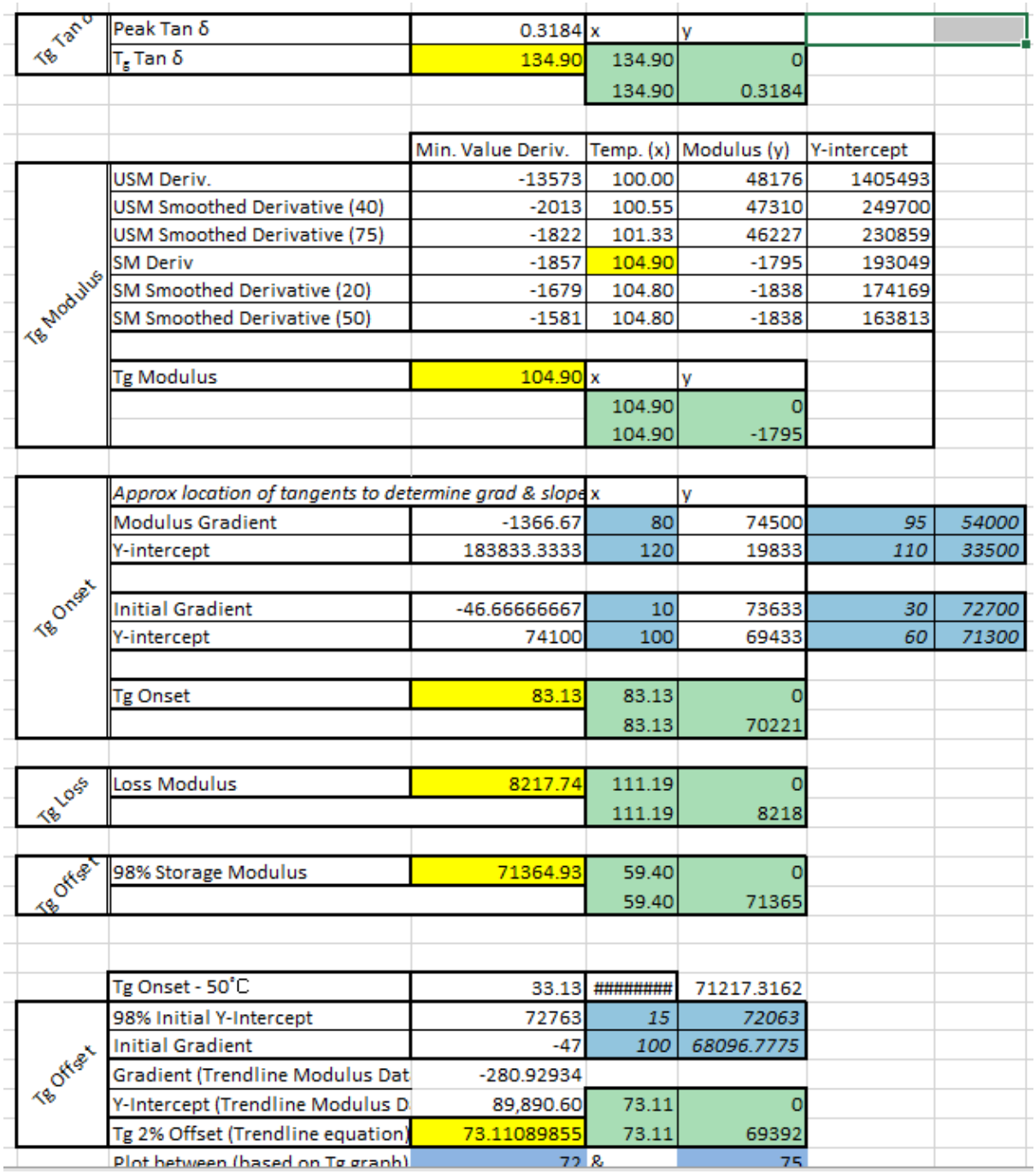

Tg Tan δ	Peak Tan δ	0.3184	x	y		
	T_g Tan δ	134.90	134.90	0		
			134.90	0.3184		
		Min. Value Deriv.	Temp. (x)	Modulus (y)	Y-intercept	
Tg Modulus	USM Deriv.	-13573	100.00	48176	1405493	
	USM Smoothed Derivative (40)	-2013	100.55	47310	249700	
	USM Smoothed Derivative (75)	-1822	101.33	46227	230859	
	SM Deriv	-1857	104.90	-1795	193049	
	SM Smoothed Derivative (20)	-1679	104.80	-1838	174169	
	SM Smoothed Derivative (50)	-1581	104.80	-1838	163813	
	Tg Modulus	104.90	x	y		
			104.90	0		
			104.90	-1795		
Tg Onset	*Approx location of tangents to determine grad & slope*		x	y		
	Modulus Gradient	-1366.67	80	74500	*95*	*54000*
	Y-intercept	183833.3333	120	19833	*110*	*33500*
	Initial Gradient	-46.66666667	10	73633	*30*	*72700*
	Y-intercept	74100	100	69433	*60*	*71300*
	Tg Onset	83.13	83.13	0		
			83.13	70221		
Tg Loss	Loss Modulus	8217.74	111.19	0		
			111.19	8218		
Tg Offset	98% Storage Modulus	71364.93	59.40	0		
			59.40	71365		
	Tg Onset - 50˚C	33.13	#########	71217.3162		
Tg Offset	98% Initial Y-Intercept	72763	*15*	*72063*		
	Initial Gradient	-47	*100*	*68096.7775*		
	Gradient (Trendline Modulus Dat	-280.92934				
	Y-Intercept (Trendline Modulus D	89,890.60	73.11	0		
	Tg 2% Offset (Trendline equation)	73.11089855	73.11	69392		
	Plot between (based on Tg graph)	72	&	75		

Appendix Figure 4 BPGii, Tg values determined from DMA analysis

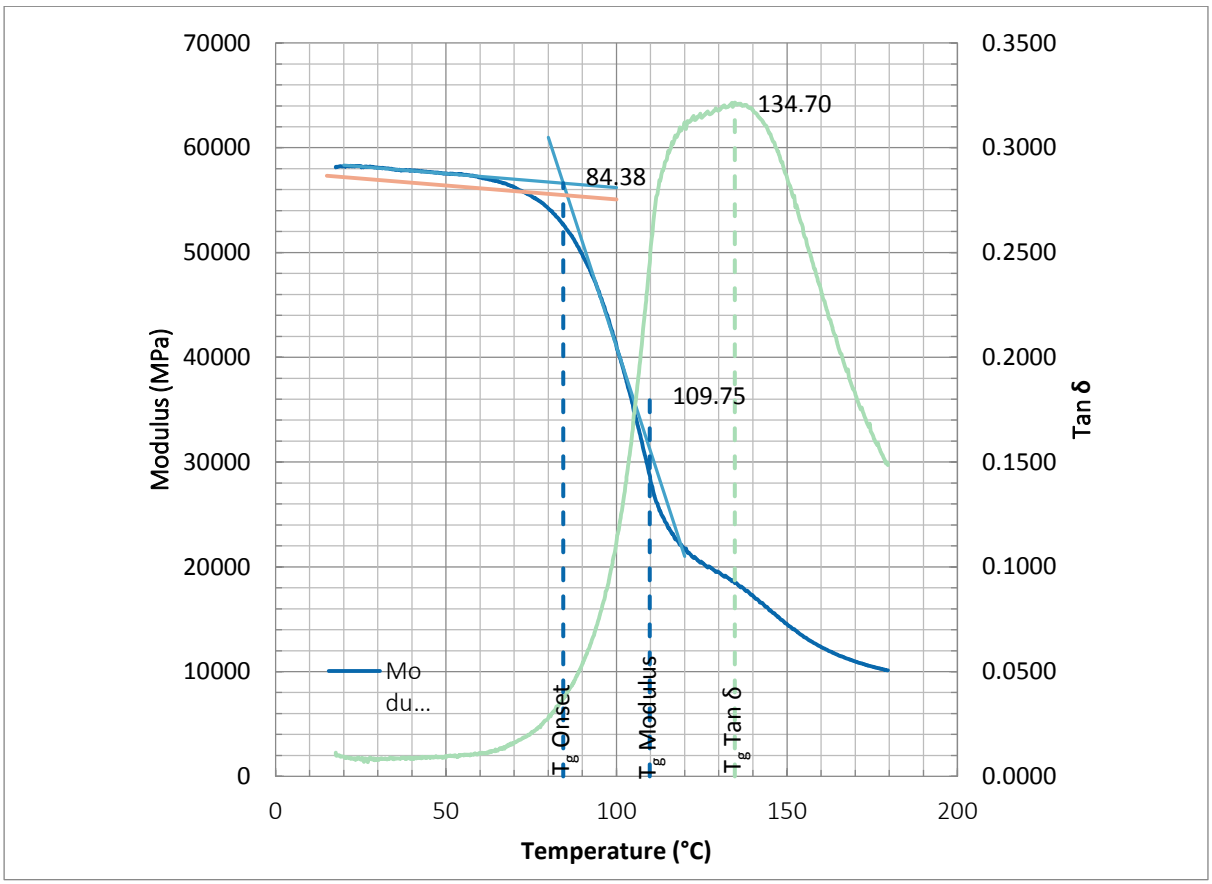

Appendix Figure 5 DMA BPGiii plot

Tg Tan δ	Peak Tan δ	0.3215	x	y		
	T_g Tan δ	134.70	134.70	0		
			134.70	0.3215		
		Min. Value Deriv.	Temp. (x)	Modulus (y)	Y-intercept	
Tg Modulus	USM Deriv.	-9424	102.90	37800	1007511	
	USM Smoothed Derivative (40)	-1633	103.41	37110	205949	
	USM Smoothed Derivative (50)	-1569	104.00	36400	199529	
	SM Deriv	-1498	109.75	-1039	163344	
	SM Smoothed Derivative (10)	-1458	109.75	-1039	158934	
	SM Smoothed Derivative (25)	-1402	109.40	-1480	151863	
	Tg Modulus	109.75	x	y		
			109.75	0		
			109.75	36400		
Tg Onset	*Approx location of tangents to determine grad & slope*		x	y		
	Modulus Gradient	-1000	80	61000	*93*	*48000*
	Y-intercept	141000	120	21000	*100*	*41000*
	Initial Gradient	-26.66666667	20	58333	*25*	*58200*
	Y-intercept	58866.66667	100	56200	*55*	*57400*
	Tg Onset	84.38	84.38	0		
			84.38	56616		
Tg Loss	Loss Modulus	7241.81	111.60	0		
			111.60	7242		
Tg Offset	98% Storage Modulus	56960.78	63.30	0		
			63.30	56961		
	Tg Onset - 50˚C	34.38	########	56816.7308		
Tg Offset	98% Initial Y-Intercept	57734	*15*	*57334*		
	Initial Gradient	-27	*100*	*55066.9591*		
	Gradient (Trendline Modulus Dat	-163.57619				
	Y-Intercept (Trendline Modulus D	67,677.48	72.63	0		
	Tg 2% Offset (Trendline equation)	72.63083418	72.63	55806		
	Plot between (based on Tg graph)	71	&	75		

Appendix Figure 6 BPGiii, Tg values determined from DMA analysis

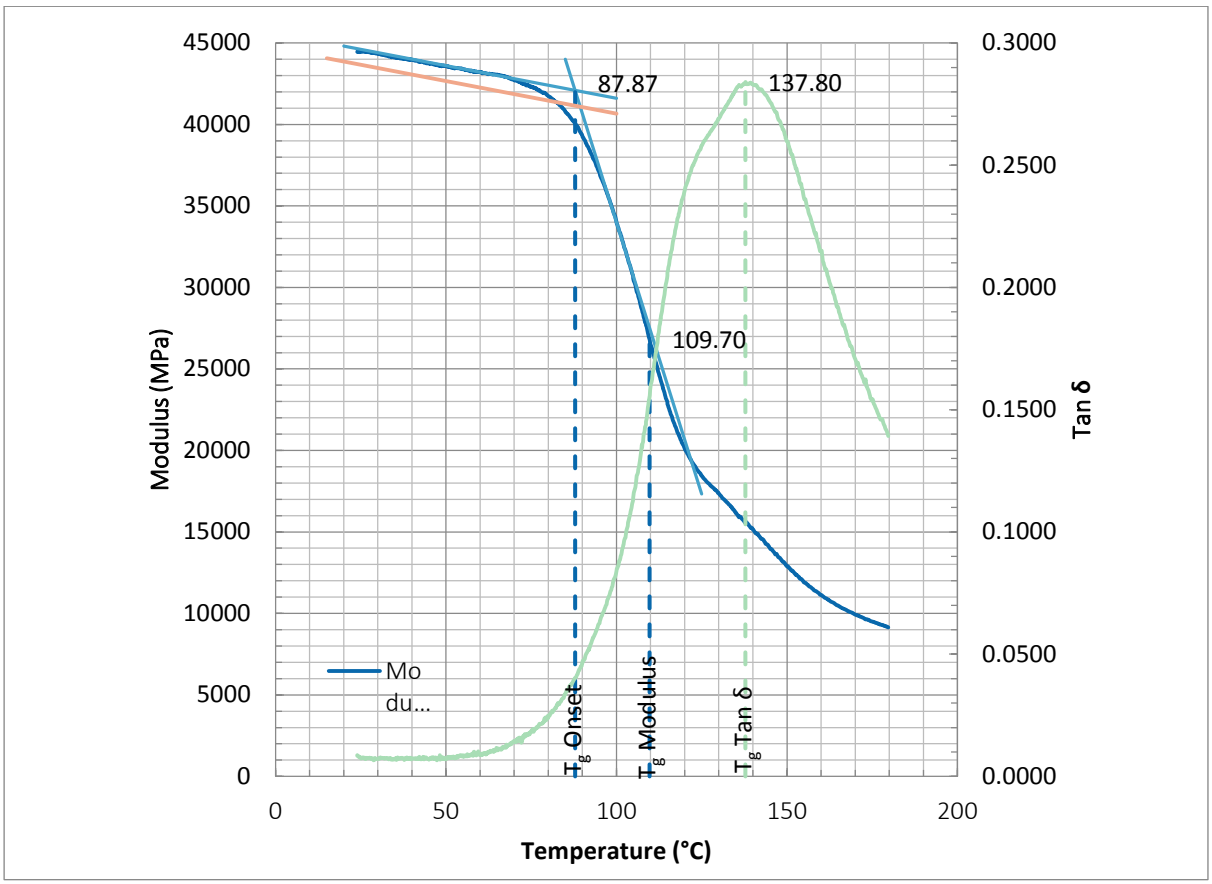

Appendix Figure 7 DMA BPGiv plot

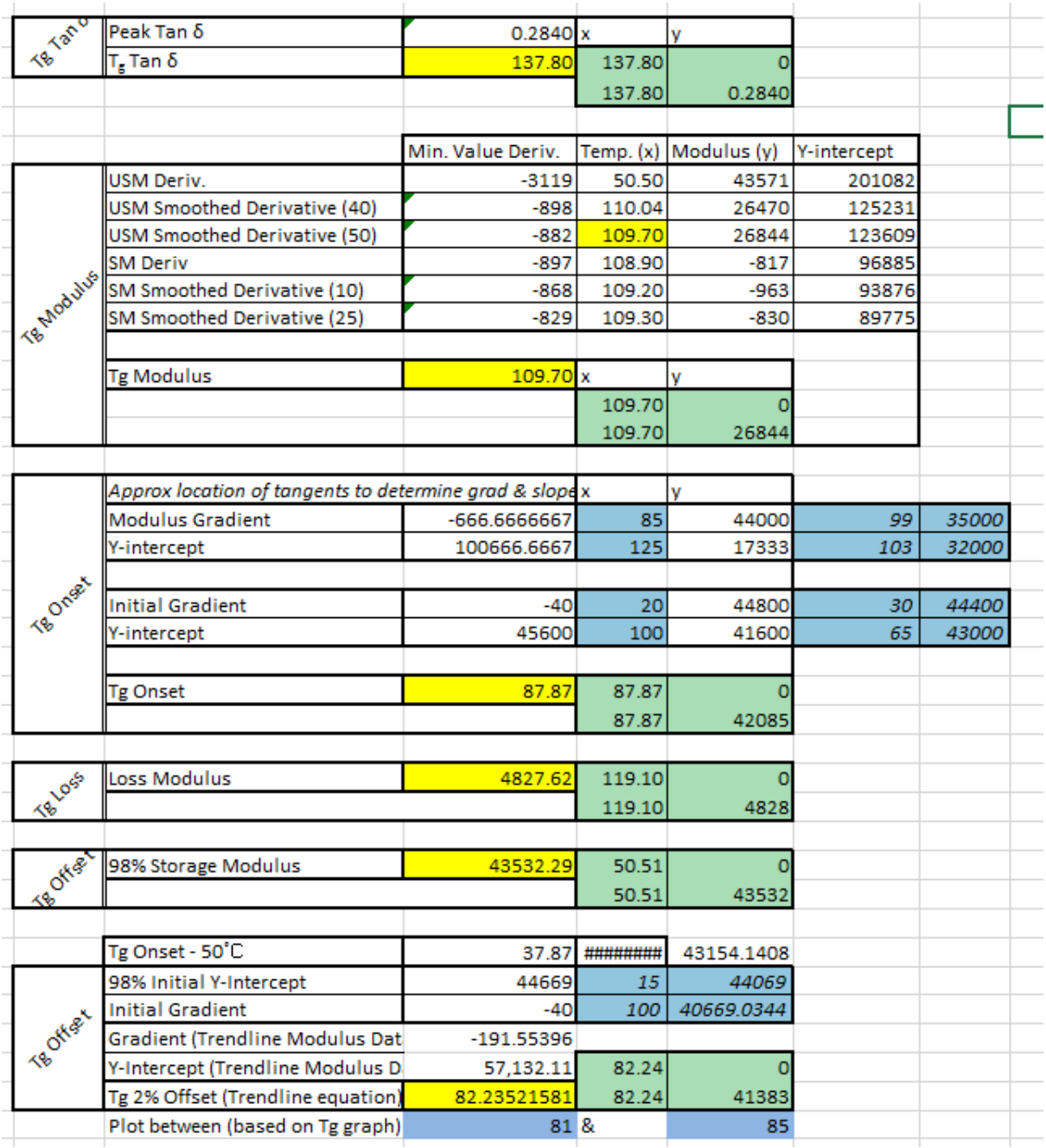

Tg Tan δ	Peak Tan δ	0.2840	x	y		
	T_g Tan δ	137.80	137.80	0		
			137.80	0.2840		
		Min. Value Deriv.	Temp. (x)	Modulus (y)	Y-intercept	
Tg Modulus	USM Deriv.	-3119	50.50	43571	201082	
	USM Smoothed Derivative (40)	-898	110.04	26470	125231	
	USM Smoothed Derivative (50)	-882	109.70	26844	123609	
	SM Deriv	-897	108.90	-817	96885	
	SM Smoothed Derivative (10)	-868	109.20	-963	93876	
	SM Smoothed Derivative (25)	-829	109.30	-830	89775	
	Tg Modulus	109.70	x	y		
			109.70	0		
			109.70	26844		
Tg Onset	*Approx location of tangents to determine grad & slope*		x	y		
	Modulus Gradient	-666.6666667	85	44000	*99*	*35000*
	Y-intercept	100666.6667	125	17333	*103*	*32000*
	Initial Gradient	-40	20	44800	*30*	*44400*
	Y-intercept	45600	100	41600	*65*	*43000*
	Tg Onset	87.87	87.87	0		
			87.87	42085		
Tg Loss	Loss Modulus	4827.62	119.10	0		
			119.10	4828		
Tg Offset	98% Storage Modulus	43532.29	50.51	0		
			50.51	43532		
	Tg Onset - 50°C	37.87	########	43154.1408		
Tg Offset	98% Initial Y-Intercept	44669	*15*	*44069*		
	Initial Gradient	-40	*100*	*40669.0344*		
	Gradient (Trendline Modulus Dat	-191.55396				
	Y-Intercept (Trendline Modulus D	57,132.11	82.24	0		
	Tg 2% Offset (Trendline equation)	82.23521581	82.24	41383		
	Plot between (based on Tg graph)	81	&	85		

Appendix Figure 8 BPGiv, Tg values determined from DMA analysis

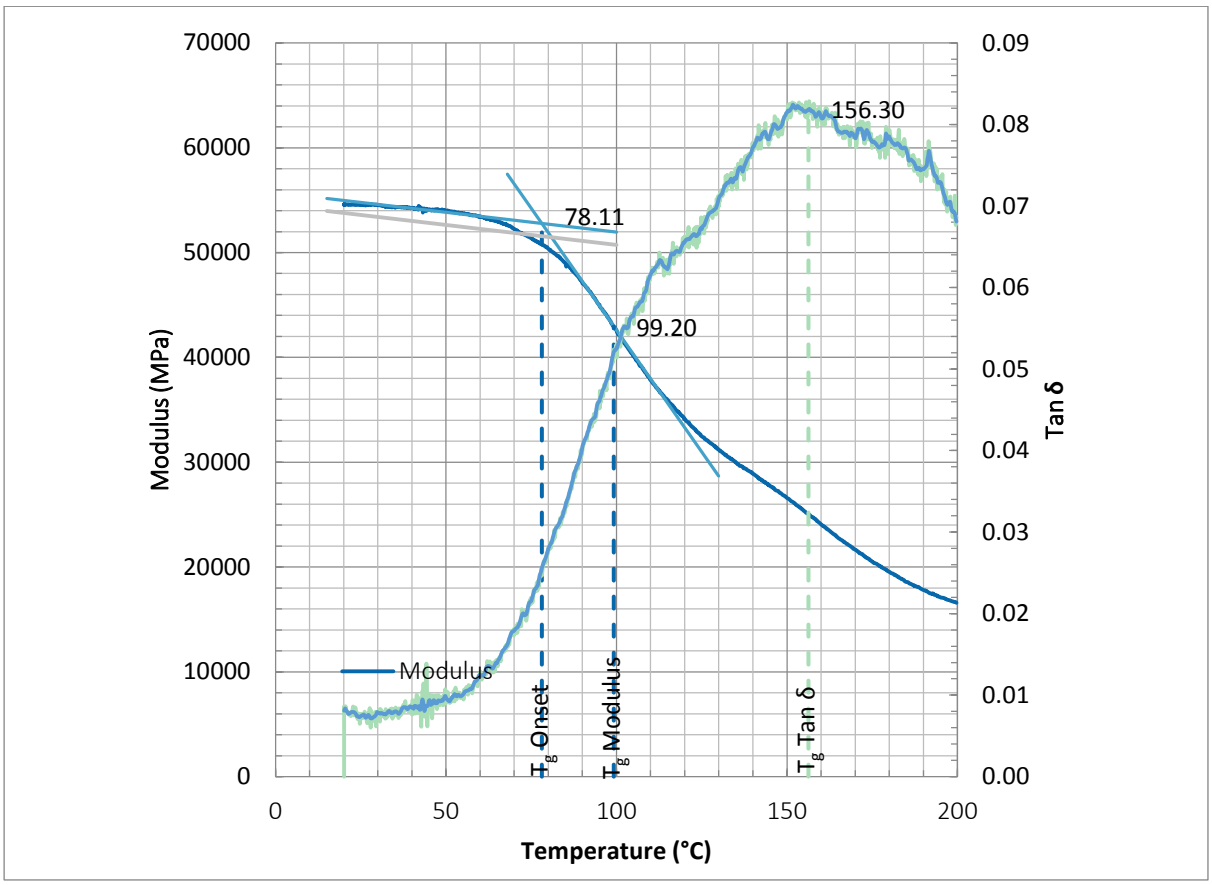

Appendix Figure 9 DMA PTGi plot

Smoothed Tg Tan δ	Smoothed Peak Tan δ	0.0824				
	Smoothed T_g Tan δ	151.70				
Tg Tan	Peak Tan δ	0.0829	x	y		
	T_g Tan δ	156.30	156.30	0		
			156.30	0.0818		
		Min. Value Deriv.	Temp. (x)	Modulus (y)	Y-intercept	
Tg Modulus	USM Deriv.	-3598	43.10	54188	209243	
	USM Smoothed Derivative (40)	-660	99.20	42945	108418	
	USM Smoothed Derivative (50)	-638	99.20	42945	106263	
	SM Deriv	-594	100.00	-626	58776	
	SM Smoothed Derivative (10)	-574	100.10	-626	56862	
	SM Smoothed Derivative (25)	-526	100.60	-611	52334	
	Tg Modulus	99.20	x	y		
			99.20	0		
			99.20	42945		
Tg Onset	*Approx location of tangents to determine grad & y*		x	y		
	Modulus Gradient	-465	68	57471	*90*	*47250*
	Y-intercept	89063	130	28667	*114*	*36100*
	Initial Gradient	-37.93103448	15	55169	*30*	*54600*
	Y-intercept	55737.93103	100	51945	*59*	*53500*
	Tg Onset	78.11	78.11	0		
			78.11	52775		
Tg Loss	Loss Modulus	2368.17	112.60	0		
			112.60	2368		
Tg Offset	98% Storage Modulus	53508.37	59.10	0		
			59.10	54587		
		98% Tangent	0	53508.37		
			100	53508.37		
		100% Tangent	0	54587		
			100	54587		
	Tg Onset - 50°c	28.11	54551.11	53460.0839		
Tg Offset	98% Initial Y-Intercept	54526	*15*	*53957*		
	Initial Gradient	-38	*100*	*50733.111*		
	Gradient (Trendline Modulus Da	-174.21336				
	Y-Intercept (Trendline Modulus	64,423.66	72.62	0		
	Tg 2% Offset (Trendline equatio	72.62457566	72.62	51764		
	Plot between (based on Tg grap	70	&	76		

Appendix Figure 10 PTGi, Tg values determined from DMA analysis

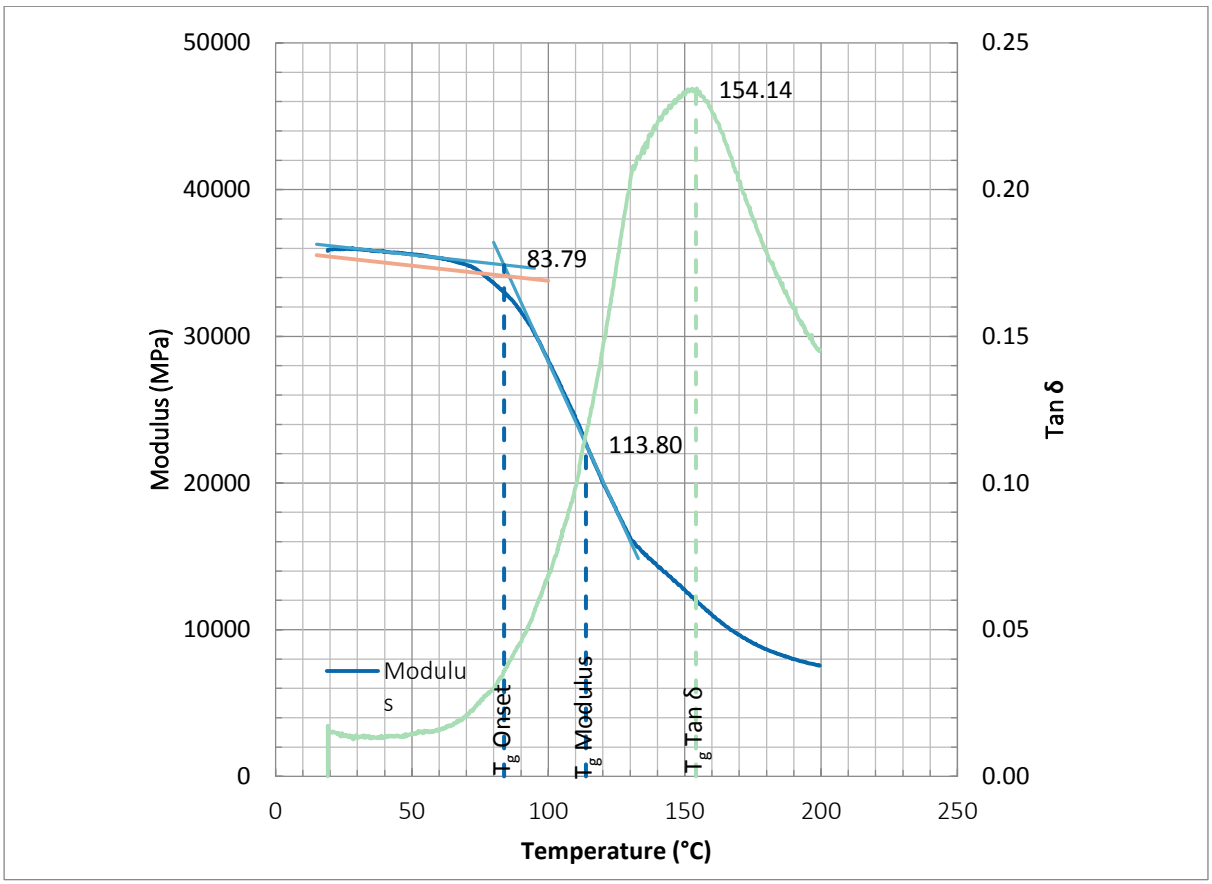

Appendix Figure 11 DMA PTGii plot

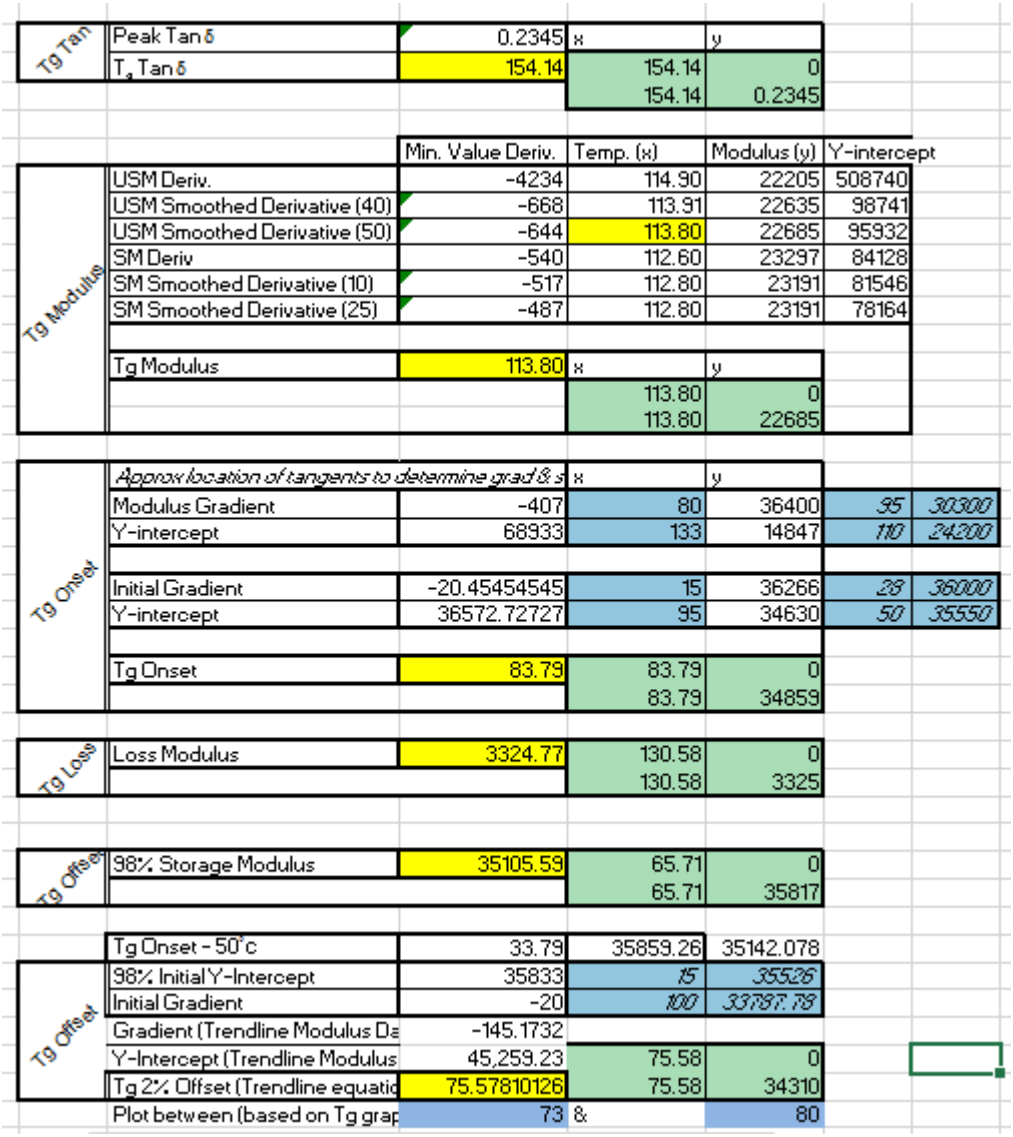

Tg Tan	Peak Tan δ	0.2345	x	y		
	T_g Tan δ	154.14	154.14	0		
			154.14	0.2345		
		Min. Value Deriv.	Temp. (x)	Modulus (y)	Y-intercept	
Tg Modulus	USM Deriv.	-4234	114.90	22205	508740	
	USM Smoothed Derivative (40)	-668	113.91	22635	98741	
	USM Smoothed Derivative (50)	-644	113.80	22685	95932	
	SM Deriv	-540	112.60	23297	84128	
	SM Smoothed Derivative (10)	-517	112.80	23191	81546	
	SM Smoothed Derivative (25)	-487	112.80	23191	78164	
	Tg Modulus	113.80	x	y		
			113.80	0		
			113.80	22685		
Tg Onset	*Approx location of tangents to determine grad & s*		x	y		
	Modulus Gradient	-407	80	36400	*95*	*30300*
	Y-intercept	68933	133	14847	*110*	*24200*
	Initial Gradient	-20.45454545	15	36266	*28*	*36000*
	Y-intercept	36572.72727	95	34630	*50*	*35550*
	Tg Onset	83.79	83.79	0		
			83.79	34859		
Tg Loss	Loss Modulus	3324.77	130.58	0		
			130.58	3325		
Tg Offset	98% Storage Modulus	35105.59	65.71	0		
			65.71	35817		
	Tg Onset - 50°c	33.79	35859.26	35142.078		
Tg Offset	98% Initial Y-Intercept	35833	*15*	*35526*		
	Initial Gradient	-20	*100*	*33787.78*		
	Gradient (Trendline Modulus Da	-145.1732				
	Y-Intercept (Trendline Modulus	45,259.23	75.58	0		
	Tg 2% Offset (Trendline equatio	75.57810126	75.58	34310		
	Plot between (based on Tg grap	73	&	80		

Appendix Figure 12 PTGii, Tg values determined from DMA analysis

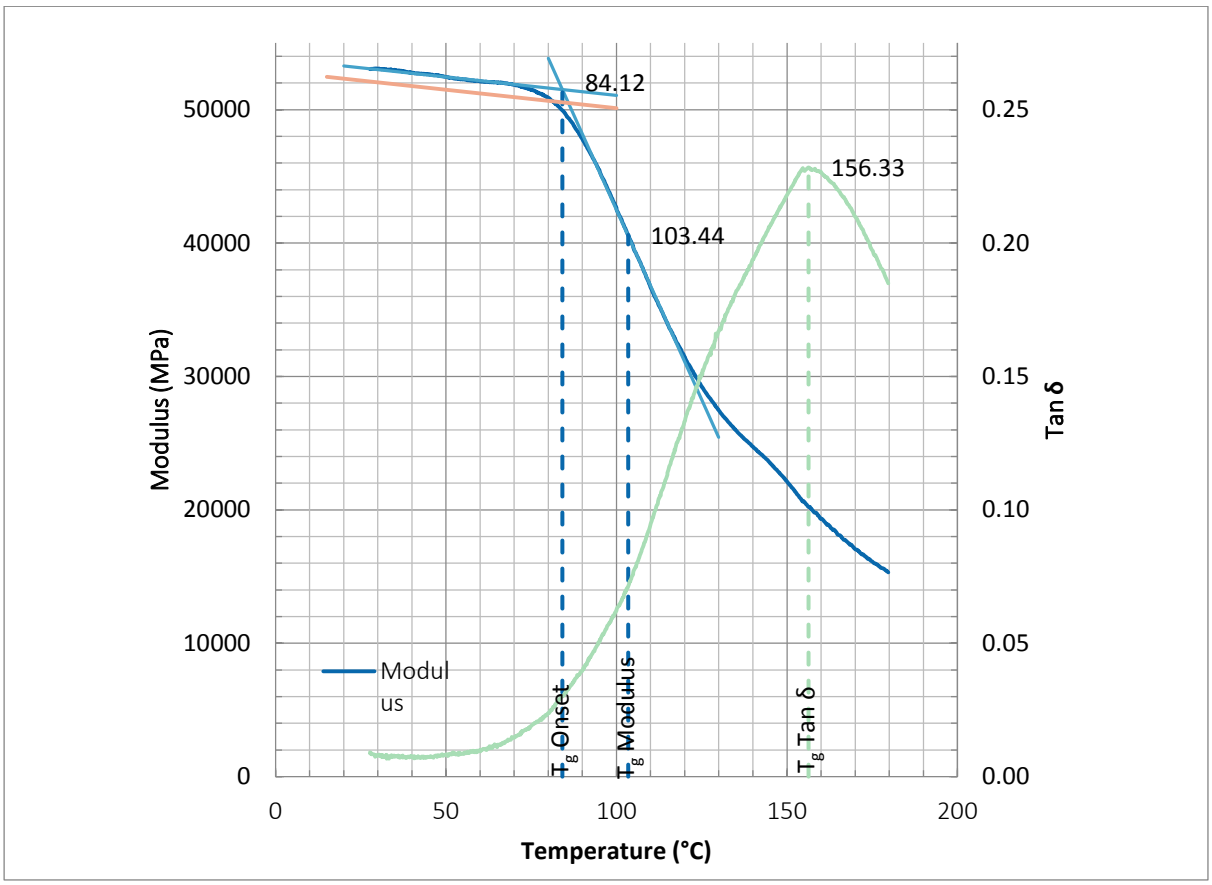

Appendix Figure 13 DMA PTGiii plot

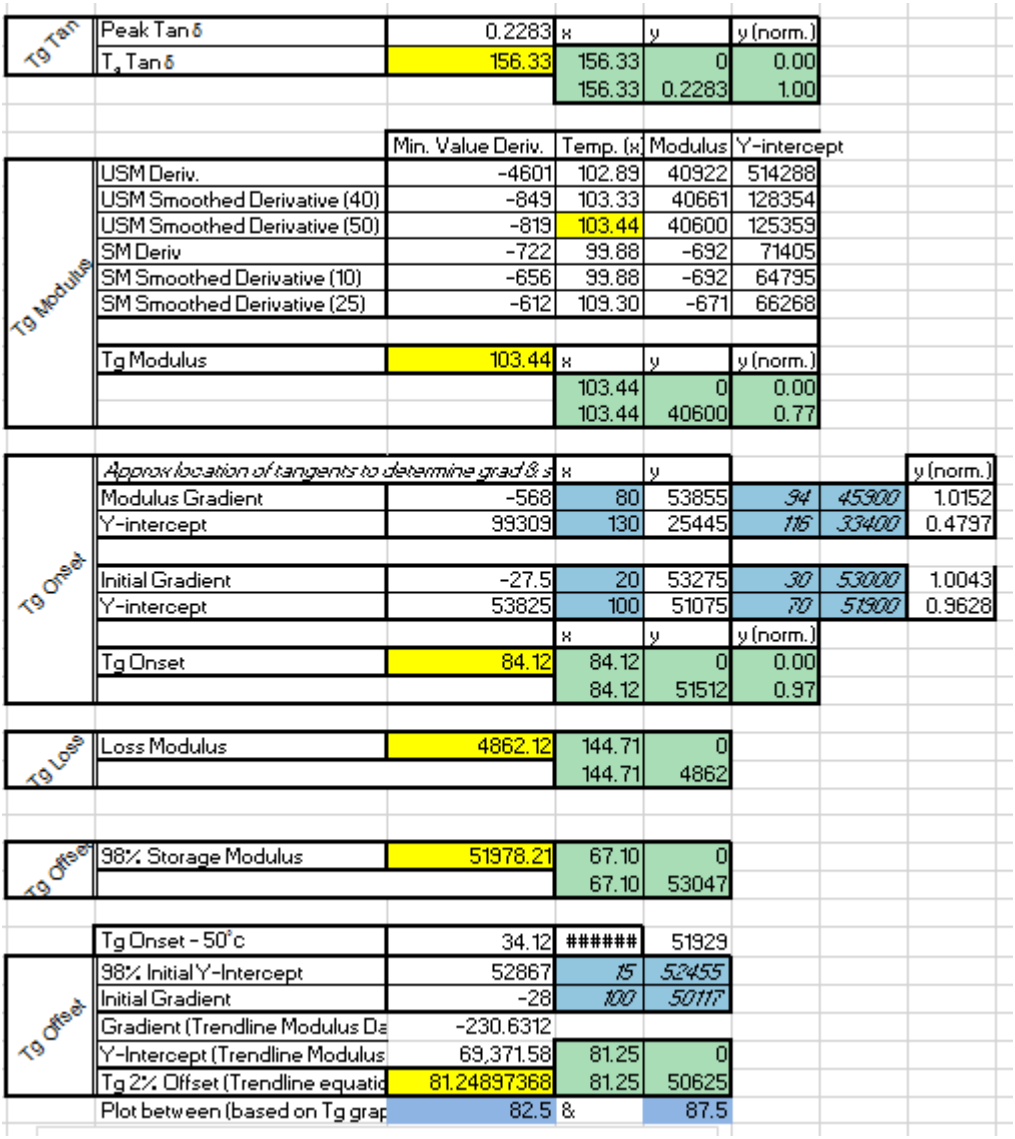

Tg Tan	Peak Tan δ	0.2283	x	y	y (norm.)			
	T_g Tan δ	156.33	156.33	0	0.00			
			156.33	0.2283	1.00			
		Min. Value Deriv.	Temp. (x	Modulus	Y-intercept			
Tg Modulus	USM Deriv.	-4601	102.89	40922	514288			
	USM Smoothed Derivative (40)	-849	103.33	40661	128354			
	USM Smoothed Derivative (50)	-819	103.44	40600	125359			
	SM Deriv	-722	99.88	-692	71405			
	SM Smoothed Derivative (10)	-656	99.88	-692	64795			
	SM Smoothed Derivative (25)	-612	109.30	-671	66268			
	Tg Modulus	103.44	x	y	y (norm.)			
			103.44	0	0.00			
			103.44	40600	0.77			
Tg Onset	*Approx location of tangents to determine grad & s*		x	y				y (norm.)
	Modulus Gradient	-568	80	53855	*94*	*45900*		1.0152
	Y-intercept	99309	130	25445	*116*	*33400*		0.4797
	Initial Gradient	-27.5	20	53275	*30*	*53000*		1.0043
	Y-intercept	53825	100	51075	*70*	*51300*		0.9628
			x	y	y (norm.)			
	Tg Onset	84.12	84.12	0	0.00			
			84.12	51512	0.97			
Tg Loss	Loss Modulus	4862.12	144.71	0				
			144.71	4862				
Tg Offset	98% Storage Modulus	51978.21	67.10	0				
			67.10	53047				
	Tg Onset - 50°c	34.12	######	51929				
Tg Offset	98% Initial Y-Intercept	52867	*15*	*52455*				
	Initial Gradient	-28	*100*	*50117*				
	Gradient (Trendline Modulus Da	-230.6312						
	Y-Intercept (Trendline Modulus	69,371.58	81.25	0				
	Tg 2% Offset (Trendline equatio	81.24897368	81.25	50625				
	Plot between (based on Tg grap	82.5	&	87.5				

Appendix Figure 14 PTGiii, Tg values determined from DMA analysis

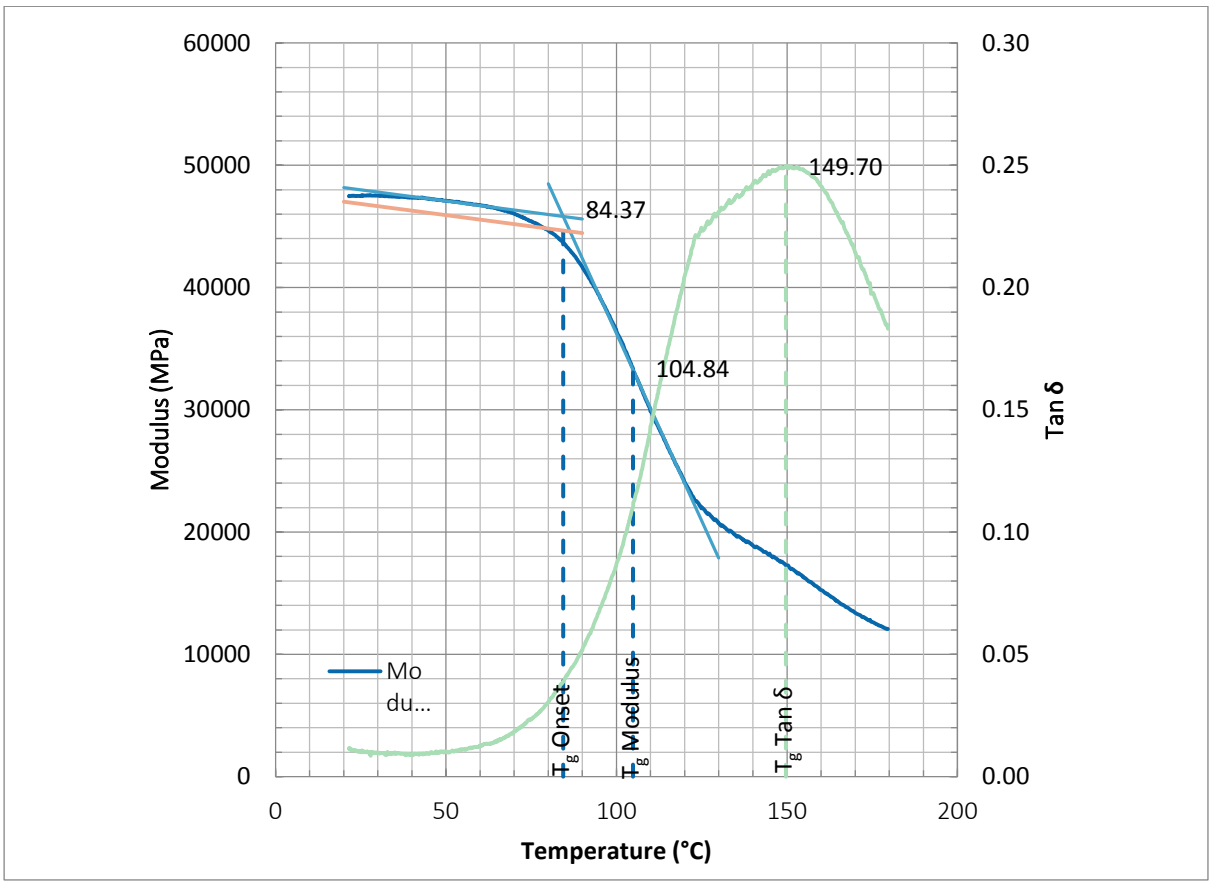

Appendix Figure 15 DMA PTGiv plot

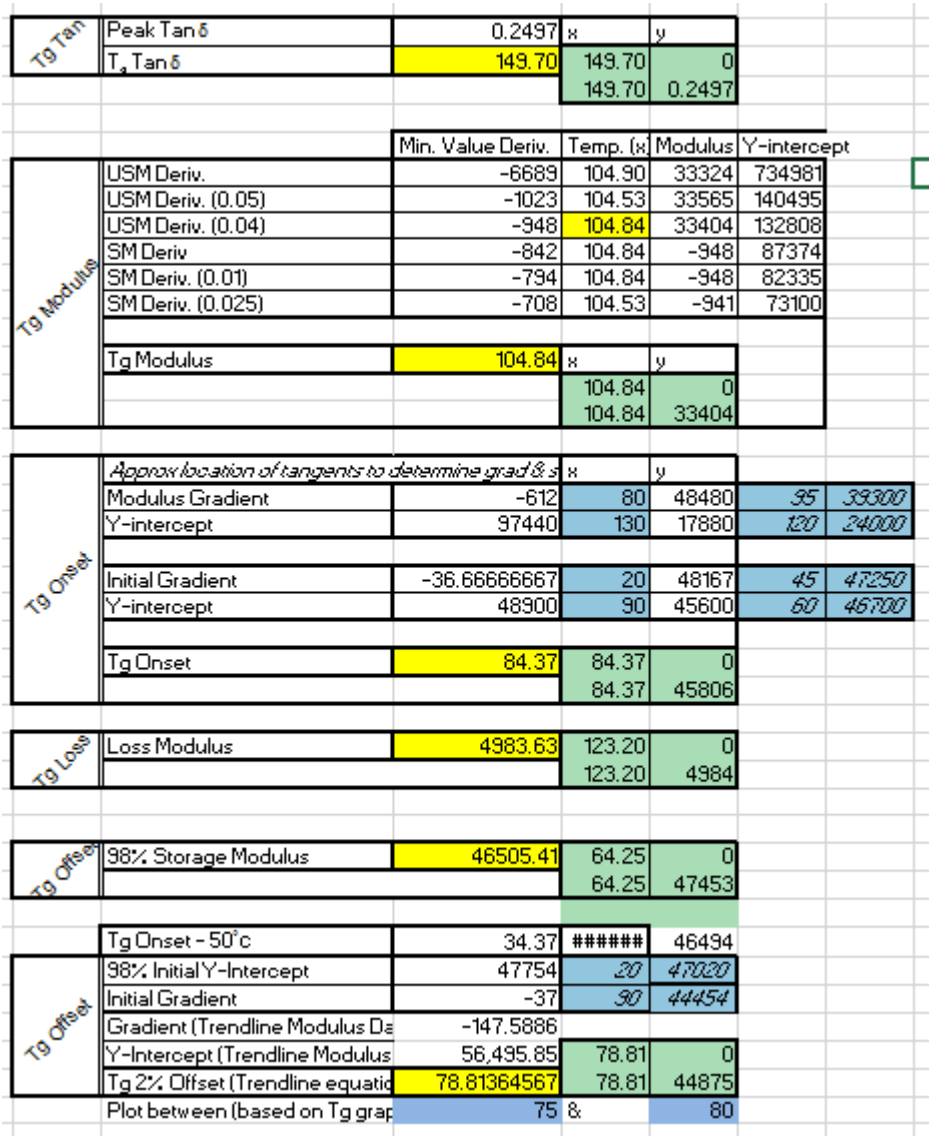

Tg Tan	Peak Tan δ	0.2497	x	y		
	T_g Tan δ	149.70	149.70	0		
			149.70	0.2497		
		Min. Value Deriv.	Temp. (x)	Modulus	Y-intercept	
Tg Modulus	USM Deriv.	-6689	104.90	33324	734981	
	USM Deriv. (0.05)	-1023	104.53	33565	140495	
	USM Deriv. (0.04)	-948	104.84	33404	132808	
	SM Deriv	-842	104.84	-948	87374	
	SM Deriv. (0.01)	-794	104.84	-948	82335	
	SM Deriv. (0.025)	-708	104.53	-941	73100	
	Tg Modulus	104.84	x	y		
			104.84	0		
			104.84	33404		
Tg Onset	*Approx location of tangents to determine grad & s*		x	y		
	Modulus Gradient	-612	80	48480	*35*	*39300*
	Y-intercept	97440	130	17880	*120*	*24000*
	Initial Gradient	-36.66666667	20	48167	*45*	*47250*
	Y-intercept	48900	90	45600	*60*	*46700*
	Tg Onset	84.37	84.37	0		
			84.37	45806		
Tg Loss	Loss Modulus	4983.63	123.20	0		
			123.20	4984		
Tg Offset	98% Storage Modulus	46505.41	64.25	0		
			64.25	47453		
	Tg Onset - 50°c	34.37	######	46494		
Tg Offset	98% Initial Y-Intercept	47754	*20*	*47020*		
	Initial Gradient	-37	*90*	*44454*		
	Gradient (Trendline Modulus Da	-147.5886				
	Y-Intercept (Trendline Modulus	56,495.85	78.81	0		
	Tg 2% Offset (Trendline equatio	78.81364567	78.81	44875		
	Plot between (based on Tg grap	75	&	80		

Appendix Figure 16 PTGiv, Tg values determined from DMA analysis

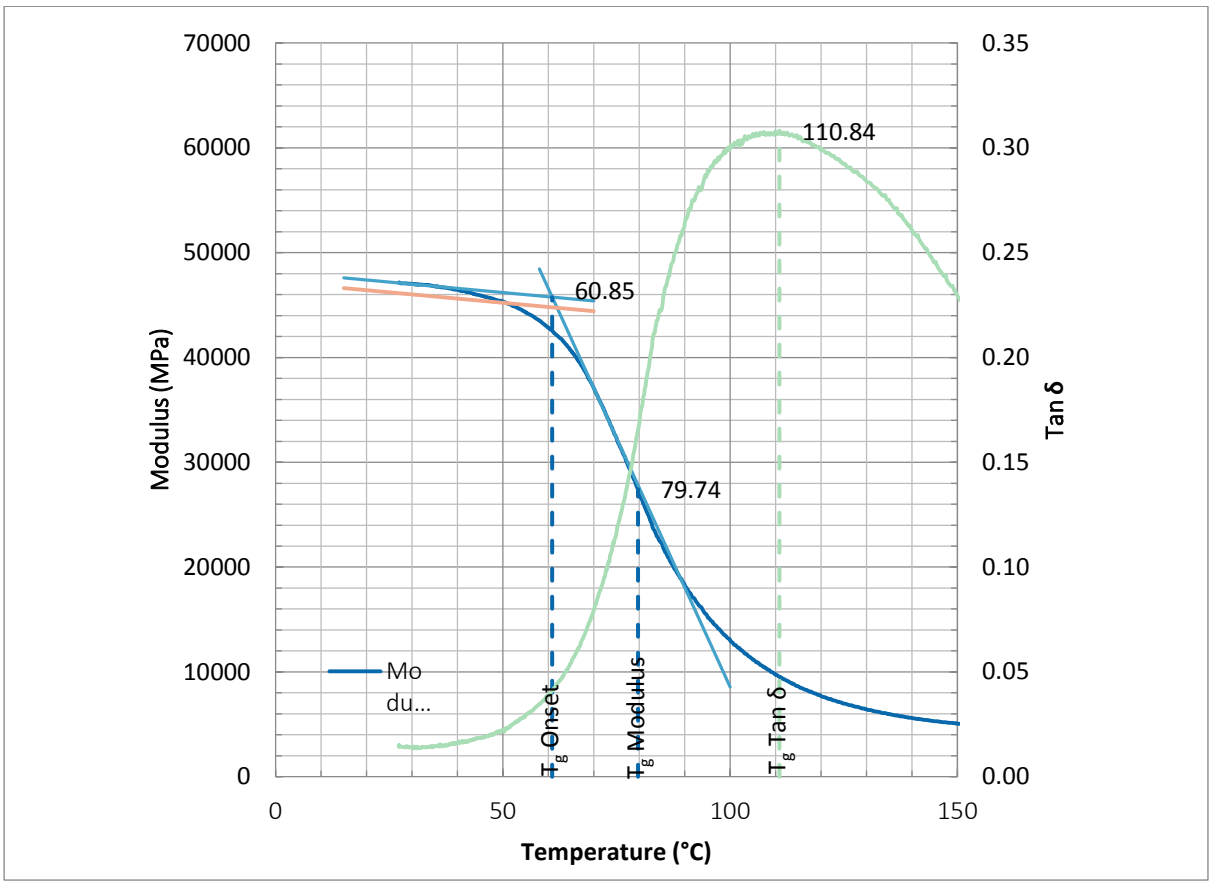

Appendix Figure 17 DMA PTCi plot

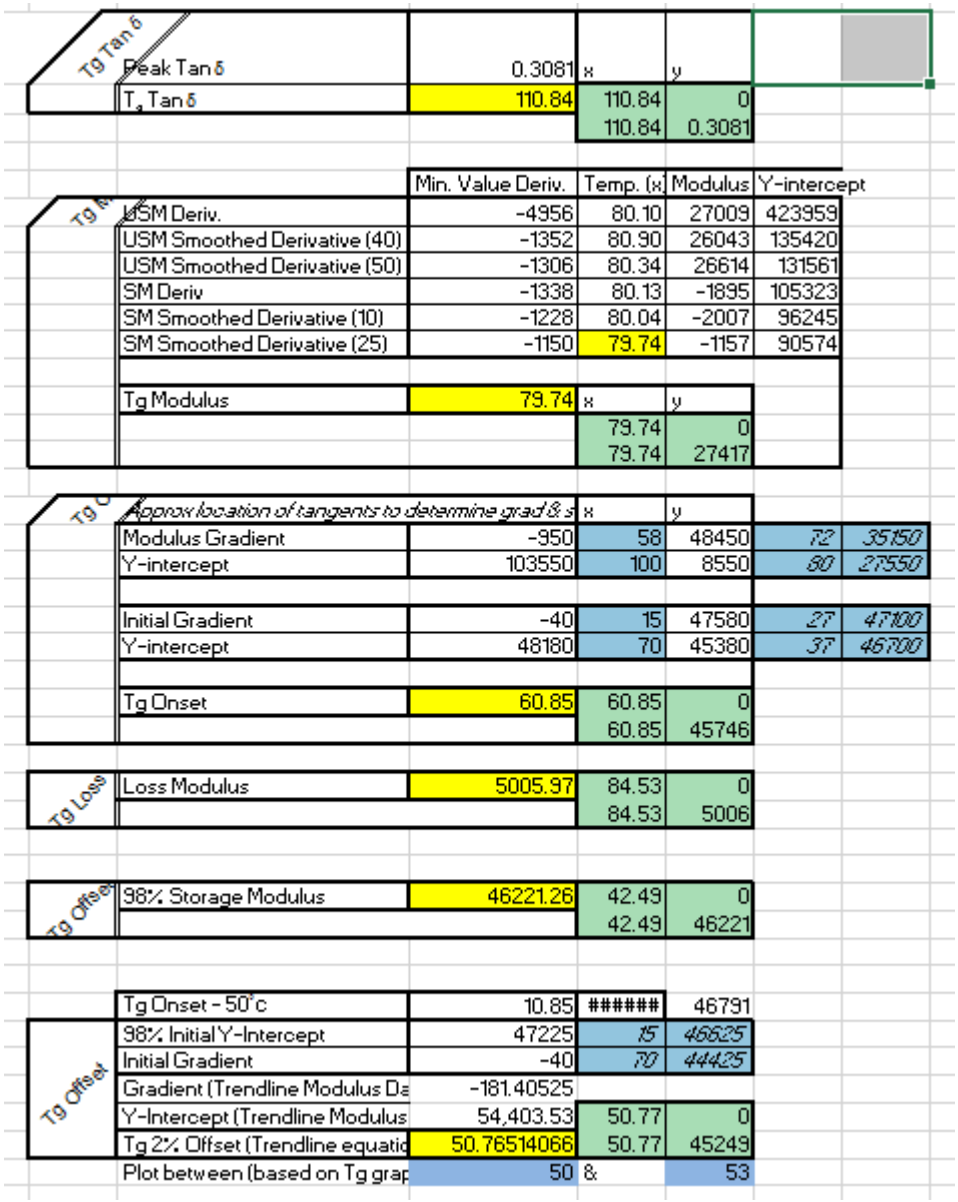

Tg Tan δ						
	Peak Tan δ	0.3081	x	y		
	T_g Tan δ	110.84	110.84	0		
			110.84	0.3081		
		Min. Value Deriv.	Temp. (x)	Modulus	Y-intercept	
Tg M	USM Deriv.	-4956	80.10	27009	423959	
	USM Smoothed Derivative (40)	-1352	80.90	26043	135420	
	USM Smoothed Derivative (50)	-1306	80.34	26614	131561	
	SM Deriv	-1338	80.13	-1895	105323	
	SM Smoothed Derivative (10)	-1228	80.04	-2007	96245	
	SM Smoothed Derivative (25)	-1150	79.74	-1157	90574	
	Tg Modulus	79.74	x	y		
			79.74	0		
			79.74	27417		
Tg O	*Approx location of tangents to determine grad & i*		x	y		
	Modulus Gradient	-950	58	48450	*72*	*35150*
	Y-intercept	103550	100	8550	*80*	*27550*
	Initial Gradient	-40	15	47580	*27*	*47100*
	Y-intercept	48180	70	45380	*37*	*46700*
	Tg Onset	60.85	60.85	0		
			60.85	45746		
Tg Loss	Loss Modulus	5005.97	84.53	0		
			84.53	5006		
Tg Offset	98% Storage Modulus	46221.26	42.49	0		
			42.49	46221		
	Tg Onset - 50°c	10.85	######	46791		
Tg Offset	98% Initial Y-Intercept	47225	*15*	*46525*		
	Initial Gradient	-40	*70*	*44425*		
	Gradient (Trendline Modulus Da	-181.40525				
	Y-Intercept (Trendline Modulus	54,403.53	50.77	0		
	Tg 2% Offset (Trendline equatio	50.76514066	50.77	45249		
	Plot between (based on Tg grap	50	&	53		

Appendix Figure 18 PTCi, Tg values determined from DMA analysis

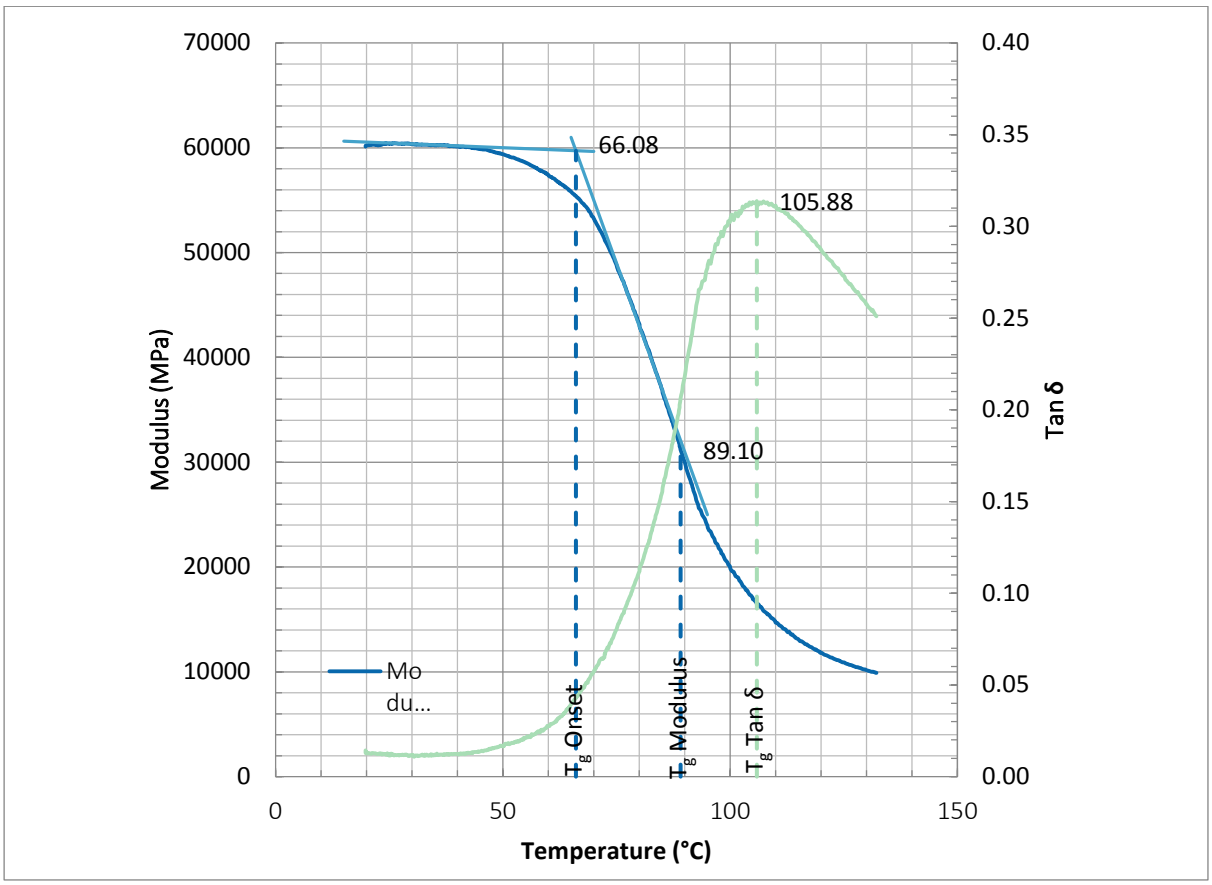

Appendix Figure 19 DMA PTCii plot

Tg Tan δ						
	Peak Tan δ	0.3138	x	y		
	T_g Tan δ	105.88	105.88	0		
			105.88	0.3138		
		Min. Value Deriv.	Temp. (x	Modulus	Y-intercept	
Tg M	USM Deriv.	-5095	98.00	21434	520749	
	USM Smoothed Derivative (40)	-1648	89.04	31378	178138	
	USM Smoothed Derivative (50)	-1613	88.40	32369	174922	
	SM Deriv	-1642	88.90	-1131	144841	
	SM Smoothed Derivative (10)	-1572	88.90	-1131	138577	
	SM Smoothed Derivative (25)	-1463	89.10	-1182	129186	
	Tg Modulus	89.10	x	y		
			89.10	0		
			89.10	31183		
Tg O	Approx location of tangents to determine grad & s		x	y		
	Modulus Gradient	-1200	65	61000	76	47800
	Y-intercept	139000	95	25000	84	38200
	Initial Gradient	-18	15	60628	26	60430
	Y-intercept	60898	70	59638	36	60250
	Tg Onset	66.08	66.08	0		
			66.08	59709		
Tg Loss	Loss Modulus	6797.50	93.10	0		
			93.10	6797		
Tg Offset	98% Storage Modulus	58909.65	53.10	0		
			53.10	58910		
	Tg Onset - 50°c	16.08	######	59396		
Tg Offset	98% Initial Y-Intercept	59686	15	59416		
	Initial Gradient	-18	70	59426		
	Gradient (Trendline Modulus Da	-178.6116				
	Y-Intercept (Trendline Modulus	68,406.66	54.30	0		
	Tg 2% Offset (Trendline equatio	54.29763572	54.30	58725		
	Plot between (based on Tg grap	52	&	56		

Appendix Figure 20 PTCii, Tg values determined from DMA analysis

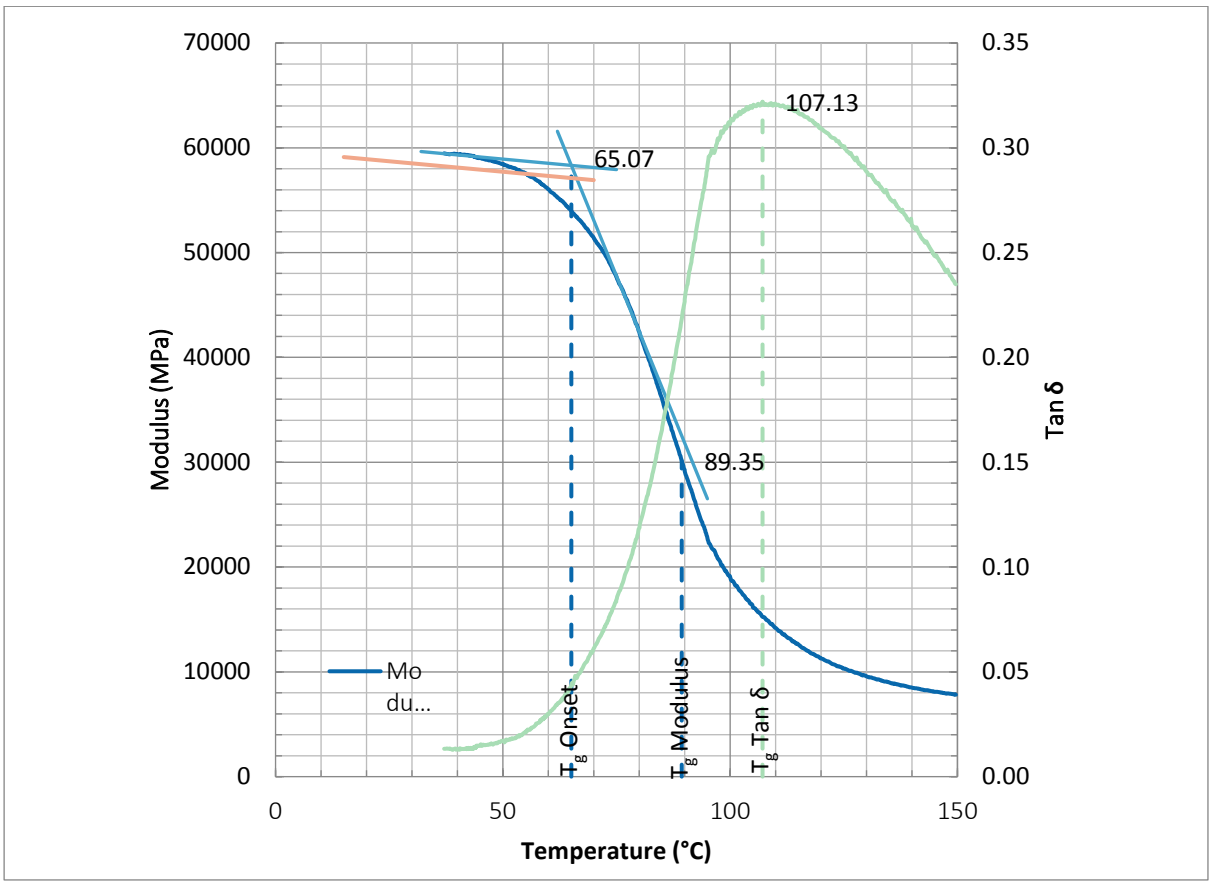

Appendix Figure 21 DMA PTCiii plot

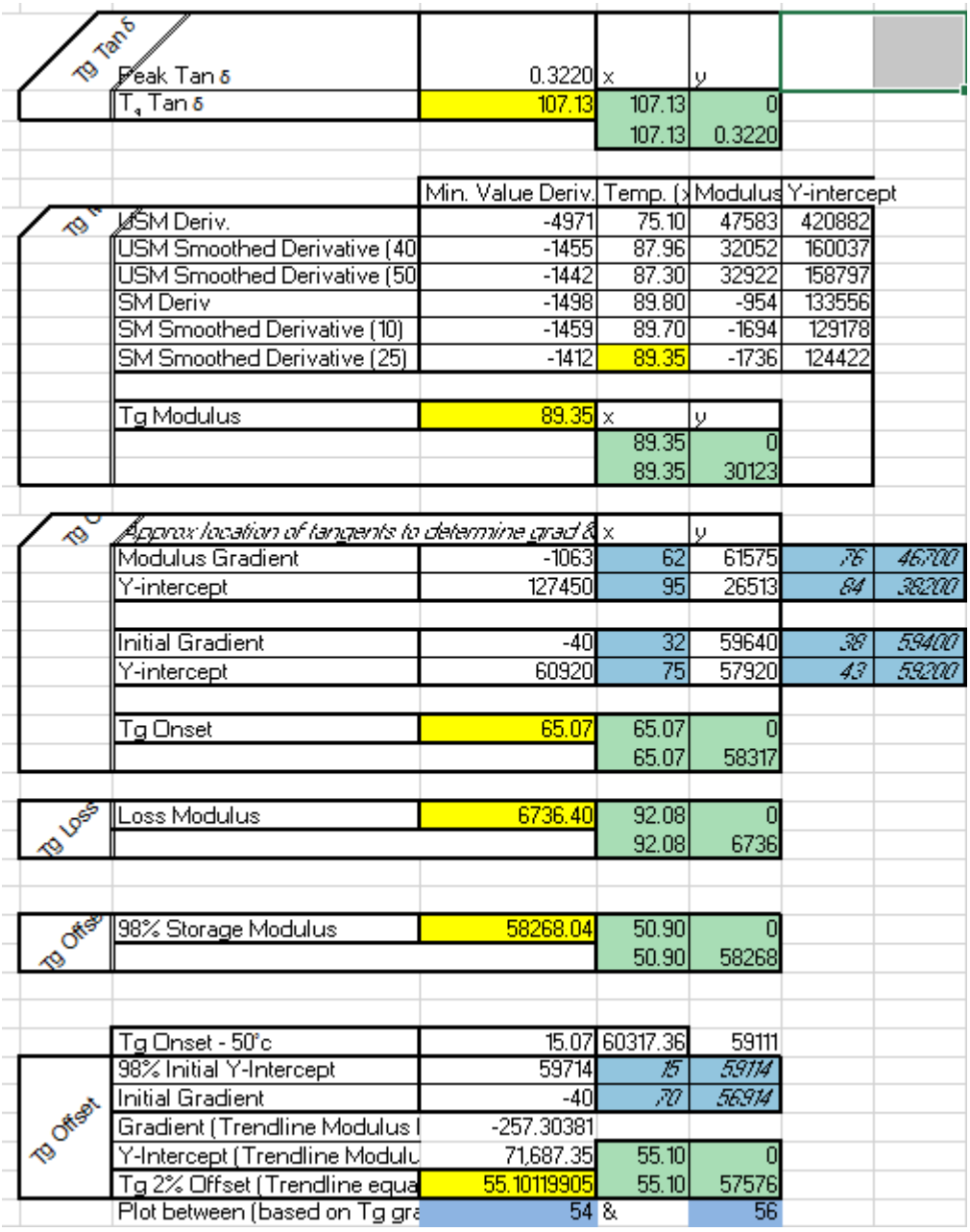

Tg Tan δ	Peak Tan δ	0.3220	x	y		
	T_g Tan δ	107.13	107.13	0		
			107.13	0.3220		
		Min. Value Deriv.	Temp. (x	Modulus	Y-intercept	
Tg M	USM Deriv.	-4971	75.10	47583	420882	
	USM Smoothed Derivative (40	-1455	87.96	32052	160037	
	USM Smoothed Derivative (50	-1442	87.30	32922	158797	
	SM Deriv	-1498	89.80	-954	133556	
	SM Smoothed Derivative (10)	-1459	89.70	-1694	129178	
	SM Smoothed Derivative (25)	-1412	89.35	-1736	124422	
	Tg Modulus	89.35	x	y		
			89.35	0		
			89.35	30123		
Tg O	Approx location of tangents to determine grad &		x	y		
	Modulus Gradient	-1063	62	61575	76	46700
	Y-intercept	127450	95	26513	84	38200
	Initial Gradient	-40	32	59640	38	59400
	Y-intercept	60920	75	57920	43	59200
	Tg Onset	65.07	65.07	0		
			65.07	58317		
Tg Loss	Loss Modulus	6736.40	92.08	0		
			92.08	6736		
Tg Offset	98% Storage Modulus	58268.04	50.90	0		
			50.90	58268		
	Tg Onset - 50°c	15.07	60317.36	59111		
Tg Offset	98% Initial Y-Intercept	59714	15	59114		
	Initial Gradient	-40	70	56914		
	Gradient (Trendline Modulus I	-257.30381				
	Y-Intercept (Trendline Modulu	71,687.35	55.10	0		
	Tg 2% Offset (Trendline equa	55.10119905	55.10	57576		
	Plot between (based on Tg gra	54	&	56		

Appendix Figure 22 PTCiii, Tg values determined from DMA analysis

B. CHAPTER 6 APPENDICES

Calculations for Steel Reinforced Beams:

FRP Factors			
$f_{u,ave}$			
f_{yk}	500	MPa	Eqn 7-1
e_{fu}	0.0025		Eqn 7-2
E_F	200000	**MPa**	

Concrete Factors			
Concrete Class	35/45		
f_{cu}	45	MPa	
f_{ck}	35	MPa	(f'c)
$f_{ck\,(psi)}$	5076	psi	
f_{cd}	19.83	MPa	
f_{ctm}	3.2	MPa	
E_{cm}	34000	MPa	
f_{ctk}	2.24	MPa	
f_{ctd}	2.8	MPa	
b1	0.8		
e_{cu}	0.30%		

1Bar

Slab Dimensions		
Breadth	150	mm
Depth	150	mm
Number of bars	1	
Diameter	10	mm
X-Sect Area	78.53981634	mm^2
Abars	78.53981634	
Cover Depth	20	mm
Effective Depth	125	mm

FRP Reinforcement Ratio, r_f	0.00418879		
Balanced Reinforcement Ratio, r_{fb}	0.025963636		
Is $r_f < r_{fb}$?	yes		
	Steel Yield		
$F_{concrete}$ (in terms of x)	3570	x	
F_{steel}	39270	N	
x	11.00	mm	
M_{ult}	4.74E+06	Nmm	
$A_{s,min}$	66.56	mm^2	Eqn 10-3
$A_{s,min}$	63.00	mm^2	
# of Steel Bars	0.85		

Length	1450	mm	
Min req'd Thickness	80.78571429		Table 9-5(a)

I_g	4.22E+07	mm4			
n_f	0.17				
neutral axis to reinforcement depth ratio, k	0.04		ACI440 Eqn 8-12		
I_{cr}	1.98E+05		ACI440 Eqn 8-11		
M_{cr}	1.80E+06	Nmm	Eqn9-9		
	1.80	kNm			
Sagging Moment at SLS	2.37E+06		*from FTool*	*based on*	4.42 *kN point lo*
I_e	1.86E+07		Eqn 8-13a	Total Load	8.84 kN
Is $I_e < I_g$?	Yes		Eqn 8-13a		

Change Ig to Ie where Ma>Mcr, do two/three iterations to find deflection

Shear Capacity			
Vc	18858	N	Eqn11-3
without shear stirrups, Vs=0			
Vn	18858	kN	

devolopment length			
fye	521.7982369	MPa	
ld	420	mm	12.2.2

splice strength is the development length based on steel yield strength

Calculations for PTC Reinforced Beams:

FRP Factors			
$f_{u,ave}$			
f_{fu}*	1596	MPa	
C_E	1		Table 7.1
f_{fu}	1596	MPa	Eqn 7-1
$f_{fu\ (psi)}$	231483.84	psi	
e_{fu}*	0.0133		
e_{fu}	0.0133		Eqn 7-2
E_F	120000	MPa	

Beam Length	1.5	m
Estimated depth	150	mm
Estimated width	150	mm
Estimated cover	20	mm

1mm=	0.04	inches
1inch=	25.4	mm
$1inch^2$=	645	mm^2
1MPa=	145	psi

Concrete Factors			
Concrete Class	35/45		
f_{cu}	45	MPa	
f_{ck}	35	MPa	(f'c)
$f_{ck\ (psi)}$	5076	psi	
f_{cd}	19.83	MPa	
f_{ctm}	3.2	MPa	
E_{cm}	34000	MPa	
f_{ctk}	2.24	MPa	
f_{ctd}	2.8	MPa	
b_1	0.8		1-3 Notation
e_{cu}	0.003		

f_{fu}	1596		
E_f			

1Bar

Slab Dimensions				
Breadth	150	mm	5.91	in
Depth	150	mm	5.91	in
Number of bars	1			
Diameter	9.5	mm		
X-Sect Area	71.3	mm^2		
Abars	71.3			
Cover Depth	20	mm		
Effective Depth	125.25	mm	4.93	in

FRP Reinforcement Ratio, r_f	0.003795077		Eqn 8-2		
Balanced Reinforcement Ratio, r_{fb}	0.002744592		Eqn 8-3		
Is $r_f < r_{fb}$?	no				
	Concrete Crushing				
Is $r_f < 1.4r_{fb}$?	yes				
Strength Reduction Factor, F	0.65		Eqn 8-7, Fig 8.3		
f_f	1333.30	Mpa	Eqn 8-4d		
Is $f_{fu} > f_f$?	Yes				
a	21.30	mm	Eqn 8-4b		
neutral axis, c	26.63	mm			
Nominal Flexural Strength, M_n	10894192	Nmm	Eqn 8-4a	*based on*	22.56 *kN point loads*
	10.89	kNm		Total Load	45.12 kN
Design Flexural Strength, FM_n	7.03	kNm	Eqn 8-1		
Design flexural strength should be ≥ the factored moment			Eqn 8-1		

Min Reinf. req'd to prevent failure upon concrete failure			8.2.4
Min FRP Reinforcement, $A_{f,min}$	0.04	inches2	Eqn 8-8
Min FRP Reinforcement, $A_{f,min}$	0.04	inches2	
Is it > $(330b_wd)/f_{fu}$	Yes		
Req'd min reinforcement	0.04	inches2	
Req'd min reinforcement	28.33	mm2	
# of FRP bars	0.40		
Is req'd bars <design bars	Yes		
If no then need to increase # of bars			

k_b	1.4		8.3.1
b	1.25		8.3.1.
Cover Depth to Centre of Bar, d_c	24.75	mm	
Spacing between Bars	0	mm	
Creep Rupture Stress Limit	55%		
Calculated Max Crack Width, w	0.63	mm	Eqn 8-9
Max Allowable Crack Width (Code)	0.7	mm	8.3.1
Allowable Crack Width	0.63	mm	

Recommended Min Thickness	150	mm	Table 8.2

I_g	4.22E+07	mm4	
n_f	0.28		
neutral axis to reinforcement depth ratio, k	0.05		Eqn 8-12
I_{cr}	2.98E+05		Eqn 8-11
M_{cr}	1.80E+06	Nmm	ACI318-08 Eqn9-9

		1.80	kNm			
b_d		0.28		Eqn 8-13b		
is b_d<1?	Yes			Eqn 8-13b		
Sagging Moment at SLS		2808000		*from FTool*	*based on*	5.35 *kN point loads*
I_e		3.29E+06		Eqn 8-13a	Total Load	10.7 kN
Is I_e<I_g?	Yes			Eqn 8-13a		

Change Ig to Ie where Ma>Mcr, do two/three iterations to find deflection

Creep Rupture Stress Limit			
CFRP	319.20	Mpa	Table 8.3
Sagging, $f_{f,s}$	319.26	MPa	Eqn 8-16

At Creep Rupture, Max Shear	4.494	kN	*from FTool*
At Ult, Max Shear	20.84	kN	

Shear Capacity			ACI440.1R-06
neutral axis depth, c=kd	5.675220796		
Concrete Shear Capacity, V_c	2.01	kN	Eqn 9-1
without shear Stirrups, Vs=0			
Vn	2.01	kN	

Shear Capacity			ACI318R-08
Vc	4.15	kN	Eqn11-3
without shear stirrups, Vs=0			
Vn	4.15	kN	

Shear Capacity			CNR-DT 203/2006
Es	200000	MPa	Eqn4.13
Is $1.3(Ef/Es)^{1/2}$<1	0.25819889		
t_{Rd}	0.7		
k	1.47475		
r_1	0.003795077		
$V_{Rd,ct}$	6.77	kN	

Shear Stirrup Design			ACI318R-08
Vs required	21	kN	Eqn11-15
f_{yt}	420	Mpa	
f_{yt}	60916.8	psi	
Spacing, s	90	mm	
Spacing, s	3.54	in	
A_v	0.25	in^2	
A_v	159.81	mm^2	
# of stirrups	1		
To put across shear area require	*6*	*stirrups each sid*	
A_v	1711.2	mm^2	
A_v	2.65	in^2	
Vs	224856	N	

devolopment length			
a	1		11.1.1
C	24.75	mm	
f_{fe}	319.20		
l_e	181.76		
Min embeddment length to reach creep rupture			
Length of FRP required for continous	1490	mm	(1486mm)
Midspan Length	725		
f_{fe}	774		Eqn11-3
% of Ffu	48.51%		
% of creep rupture	242.55%		
Minimum embeddment length is 20db, i.e. 190mm			
Overlap	420	mm	
Length of FRP required for splice	955.00	mm	
Max achievable strength at mid span	567	Mpa	
f_{fe}	519	Mpa	
% of Ffu	32.50%		

Calculations for BPG Reinforced Beams:

FRP Factors			
$f_{u,ave}$			
f_{fu}*	1299	MPa	
C_E	1		Table 7.1
f_{fu}	1299	MPa	Eqn 7-1
$f_{fu\ (psi)}$	188406.96	psi	
e_{fu}*	0.0207		
e_{fu}	0.0207		Eqn 7-2
E_F	63200	MPa	

Beam Length	1.5	m
Estimated depth	150	mm
Estimated width	150	mm
Estimated cover	20	mm

1mm=	0.04	inches
1inch=	25.4	mm
$1inch^2$=	645	mm^2
1MPa=	145	psi

Concrete Factors			
Concrete Class	35/45		
f_{cu}	45	MPa	
f_{ck}	35	MPa	(f'c)
$f_{ck\ (psi)}$	5076	psi	
f_{cd}	19.83	MPa	
f_{ctm}	3.2	MPa	
E_{cm}	34000	MPa	
f_{ctk}	2.24	MPa	
f_{ctd}	2.8	MPa	
b_1	0.8		1-3 Notation
e_{cu}	0.003		

f_{fu}	1299
E_f	

1Bar	***Slab Dimensions***			
	Breadth	150	mm	5.91 in
	Depth	150	mm	5.91 in
	Number of bars	1		
	Diameter	9.5	mm	
	X-Sect Area	71.3	mm^2	
	Abars	71.3		
	Cover Depth	20	mm	
	Effective Depth	125.25	mm	4.93 in

FRP Reinforcement Ratio, r_f	0.003795077		Eqn 8-2
Balanced Reinforcement Ratio, r_{fb}	0.002333609		Eqn 8-3
Is $r_f < r_{fb}$?	no		
	Concrete Crushing		
Is $r_f < 1.4r_{fb}$?	no		
Strength Reduction Factor, F	0.65		Eqn 8-7, Fig 8.3
f_f	999.74	Mpa	Eqn 8-4d
Is $f_{fu}>f_f$?	Yes		
a	15.97	mm	Eqn 8-4b
neutral axis, c	19.97	mm	
Nominal Flexural Strength, M_n	8358714	Nmm	Eqn 8-4a
	8.36	kNm	
Design Flexural Strength, FM_n	5.43	kNm	Eqn 8-1
Design flexural strength should be ≥ the factored moment			Eqn 8-1

equivalent	20	kN point loads	
Total Load	40	kN	
based on	17.16	*kN point loads*	
Total Load	34.32	kN	

Min Reinf. req'd to prevent failure upon concrete failure			8.2.4
Min FRP Reinforcement, $A_{f,min}$	0.05	inches2	Eqn 8-8
Min FRP Reinforcement, $A_{f,min}$	0.05	inches2	
Is it > $(330b_wd)/f_{fu}$	Yes		
Req'd min reinforcement	0.05	inches2	
Req'd min reinforcement	34.81	mm2	
# of FRP bars	0.49		
Is req'd bars <design bars	Yes		
If no then need to increase # of bars			

k_b	1.4		8.3.1
b	1.24		8.3.1.
Cover Depth to Centre of Bar, d_c	24.75	mm	
Spacing between Bars	0	mm	
Creep Rupture Stress Limit	20%		
Calculated Max Crack Width, w	0.35	mm	Eqn 8-9
Max Allowable Crack Width (Code)	0.7	mm	8.3.1
Allowable Crack Width	0.35	mm	

Recommended Min Thickness	150	mm	Table 8.2

I_g	4.22E+07	mm4	
n_f	0.54		
neutral axis to reinforcement depth ratio, k	0.06		Eqn 8-12
I_{cr}	5.53E+05		Eqn 8-11
M_{cr}	1.80E+06	Nmm	ACI318-08 Eqn9-9
	1.80	kNm	
b_d	0.33		Eqn 8-13b
is b_d<1?	Yes		Eqn 8-13b

Sagging Moment at SLS	2.2730E+06		*from FTool*	*based on*	4.21 *kN point loads*
I_e	7.09E+06		Eqn 8-13a	Total Load	8.42 kN
Is I_e<I_g?	Yes		Eqn 8-13a		

Change Ig to Ie where Ma>Mcr, do two/three iterations to find deflection

Creep Rupture Stress Limit				
GFRP	259.80	Mpa	Table 8.3	3.64
Sagging, $f_{f,s}$	259.89	MPa	Eqn 8-16	

At Creep Rupture, Max Shear	4.494	kN	*from FTool*
At Ult, Max Shear	20.84	kN	

Shear Capacity			ACI440.1R-06
neutral axis depth, c=kd	7.75		
Concrete Shear Capacity, V_c	2.75	kN	Eqn 9-1
without shear Stirrups, Vs=0			
Vn	2.75	kN	

Shear Capacity			ACI318R-08
Vc	4149.45	lb	Eqn11-3
without shear stirrups, Vs=0			18895.21932
Vn	4149.45	kN	

Shear Capacity			CNR-DT 203/2006
Es	200000	MPa	Eqn4.13
Is $1.3(Ef/Es)^{1/2} \leq 1$	0.187379591		
t_{Rd}	0.7		
k	1.47475		
r_1	0.003795077		
$V_{Rd,ct}$	4.91	kN	

devolopment length			
a	1		11.1.1
C	24.75	mm	
f_{fe}	259.80		
l_e	110.85		
Min embeddment length to reach creep rupture			
Length of FRP required for continous	1490	mm	(1486mm)
Midspan Length	725		
f_{fe}	774		Eqn11-3
% of Ffu	59.60%		
% of creep rupture	298.01%		
Minimum embeddment length is 20db, i.e. 190mm			
Overlap	420	mm	
Length of FRP required for splice	955.00	mm	
Max achievable strength at mid span of FRP	567	Mpa	
f_{fe}	519	Mpa	
% of Ffu	39.93%		

Shear Stirrup Design			ACI318R-08
Vs required	21	kN	Eqn11-15
f_{yt}	420	Mpa	
f_{yt}	60916.8	psi	
Spacing, s	90	mm	
Spacing, s	3.54	in	
A_v	0.25	in^2	
A_v	159.81	mm^2	
# of stirrups	1		
To put across shear area require	*6*	*stirrups each sid*	
A_v	1711.2	mm^2	
A_v	2.65	in^2	
Vs	224856	N	

Calculations for PTG Reinforced Beams:

FRP Factors				
$f_{u,ave}$				
f_{fu}*	899	MPa		
C_E	1		Table 7.1	
f_{fu}	899	MPa	Eqn 7-1	
$f_{fu\ (psi)}$	130390.96	psi		
e_{fu}*	0.0166			
e_{fu}	0.0166		Eqn 7-2	
E_F	53400	MPa		

Beam Length	1.5	m		
Estimated depth	150	mm		
Estimated width	150	mm		
Estimated cover	20	mm		
1mm=	0.04	inches		
1inch=	25.4	mm		
$1inch^2$=	645	mm^2		
1MPa=	145	psi		

Concrete Factors				
Concrete Class	35/45			
f_{cu}	45	MPa		
f_{ck}	35	MPa	(f'c)	
$f_{ck\ (psi)}$	5076	psi		
f_{cd}	19.83	MPa		
f_{ctm}	3.2	MPa		
E_{cm}	34000	MPa		
f_{ctk}	2.24	MPa		
f_{ctd}	2.8	MPa		
b_1	0.8		1-3 Notation	
e_{cu}	0.003			

f_{fu}	899				
E_f					

1Bar	***Slab Dimensions***					
	Breadth	150	mm	5.91	in	
	Depth	150	mm	5.91	in	
	Number of bars	1				
	Diameter	9.5	mm			
	X-Sect Area	71.3	mm^2			
	Abars	71.3				
	Cover Depth	20	mm			
	Effective Depth	125.25	mm	4.93	in	

FRP Reinforcement Ratio, r_f	0.003795077		Eqn 8-2			
Balanced Reinforcement Ratio, r_{fb}	0.004004071		Eqn 8-3			
Is $r_f < r_{fb}$?	yes					
	FRP Rupture Failure					
Strength Reduction Factor, F	0.55		Eqn 8-7, Fig 8.3			
Neutral axis, c	17.95	mm				
Nominal Flexural Strength, M_n	7568010	Nmm	Eqn 8-4a	*based on*	15.48	*kN point loads*
	7.57	kNm		Total Load	30.96	kN
Design Flexural Strength, FM_n	4.16	kNm	Eqn 8-1			
Design flexural strength should be ≥ the factored moment			Eqn 8-1			

Min Reinf. req'd to prevent failure upon concrete failure			8.2.4
Min FRP Reinforcement, $A_{f,min}$	0.08	inches2	Eqn 8-8
Min FRP Reinforcement, $A_{f,min}$	0.07	inches2	
Is it > $(330b_wd)/f_{fu}$	Yes		
Req'd min reinforcement	0.08	inches2	
Req'd min reinforcement	50.30	mm2	
# of FRP bars	0.71		
Is req'd bars <design bars	Yes		
If no then need to increase # of bars			

k_b	0.8		8.3.1
b	1.23		8.3.1.
Cover Depth to Centre of Bar, d_c	24.75	mm	
Spacing between Bars	0	mm	
Creep Rupture Stress Limit	20%		
Calculated Max Crack Width, w	0.16	mm	Eqn 8-9
Max Allowable Crack Width (Code)	0.7	mm	8.3.1
Allowable Crack Width	0.16	mm	

Recommended Min Thickness	150	mm	Table 8.2

I_g	4.22E+07	mm4	
n_f	0.64		
neutral axis to reinforcement depth ratio, k	0.07		Eqn 8-12
I_{cr}	6.49E+05		Eqn 8-11
M_{cr}	1.80E+06	Nmm	ACI318-08 Eqn9-9
	1.80	kNm	
b_d	0.19		Eqn 8-13b
is b_d<1?	Yes		Eqn 8-13b
Sagging Moment at SLS	1.5702E+06		*from FTool*

I_e	1.17E+07		Eqn 8-13a		
Is $I_e<I_g$?	Yes		Eqn 8-13a	*based on*	2.716 *kN point loads*
Change Ig to Ie where Ma>Mcr, do two/three iterations to find deflection				Total Load	5.432 kN

Creep Rupture Stress Limit			
GFRP	179.80	Mpa	Table 8.3
Sagging, $f_{f,s}$	179.85	MPa	Eqn 8-16

At Creep Rupture, Max Shear	4.494	kN	*from FTool*
At Ult, Max Shear	20.84	kN	

Shear Capacity			ACI440.1R-06
neutral axis depth, c=kd	8.409677411		
Concrete Shear Capacity, V_c	2.99	kN	Eqn 9-1
without shear Stirrups, Vs=0			
Vn	2.99	kN	

Shear Capacity			ACI318R-08
Vc	18895.22	kN	Eqn11-3
without shear stirrups, Vs=0			
Vn	18895.22	kN	

Shear Capacity			CNR-DT 203/2006
Es	200000	MPa	Eqn4.13
Is $1.3(Ef/Es)^{1/2}\leq 1$	0.172240142		
t_{Rd}	0.7		
k	1.47475		
r_1	0.003795077		
$V_{Rd,ct}$	4.52	kN	

devolopment length			
a	1		11.1.1
C	24.75	mm	
f_{fe}	179.80		
l_e	15.34		
Min embeddment length to reach creep rupture			
Length of FRP required for continous	1490	mm	(1486mm)
Midspan Length	725		
f_{fe}	774		Eqn11-3
% of Ffu	86.12%		
% of creep rupture	430.60%		
Minimum embeddment length is 20db, i.e. 190mm			
Overlap	420	mm	
Length of FRP required for splice	955.00	mm	
Max achievable strength at mid span	567	Mpa	
f_{fe}	519	Mpa	
% of Ffu	57.70%		

Shear Stirrup Design			ACI318R-08
Vs required	21	kN	Eqn11-15
f_{yt}	420	Mpa	
f_{yt}	60916.8	psi	
Spacing, s	90	mm	
Spacing, s	3.54	in	
A_v	0.25	in^2	
A_v	159.81	mm^2	
# of stirrups	1		
To put across shear area require	*6*		*stirrups each si*
A_v	1711.2	mm^2	
A_v	2.65	in^2	
Vs	224856	N	